

1. Report No. TX-01/7-3925-1		2. Government Accession No.		3. Recipient's Catalog No.	
4. Title and Subtitle EVALUATION OF THE PERFORMANCE OF TEXAS PAVEMENTS MADE WITH DIFFERENT COARSE AGGREGATES				5. Report Date September 1998/Revised June 1999/ Revised October 2000	
				6. Performing Organization Code	
7. Author(s) B. Frank McCullough, Dan Zollinger, and Terry Dossey				8. Performing Organization Report No. 7-3925-1	
9. Performing Organization Name and Address Center for Transportation Research Texas Transportation Institute The University of Texas at Austin The Texas A&M University System 3208 Red River, Suite 200 College Station, TX 77843 Austin, TX 78705-2650				10. Work Unit No. (TRAIS)	
				11. Contract or Grant No. 7-3925	
12. Sponsoring Agency Name and Address Texas Department of Transportation Research and Technology Transfer Section/Construction Division P.O. Box 5080 Austin, TX 78763-5080				13. Type of Report and Period Covered Research Report (9/96 — 8/97)	
				14. Sponsoring Agency Code	
15. Supplementary Notes Project conducted in cooperation with the Texas Department of Transportation.					
16. Abstract This report summarizes 23 years of work undertaken in Texas to understand the reasons for significant performance differences found in pavements placed around the state. To a significant degree, pavement performance can be predicted based on the concrete material properties, on the environmental conditions prevailing when the pavement was placed, and on the pavement type.					
17. Key Words Coarse aggregates, continuously reinforced concrete pavement (CRCP), portland cement concrete			18. Distribution Statement No restrictions. This document is available to the public through the National Technical Information Service, Springfield, Virginia 22161.		
19. Security Classif. (of report) Unclassified	20. Security Classif. (of this page) Unclassified	21. No. of pages 274	22. Price		

**EVALUATION OF THE PERFORMANCE OF TEXAS PAVEMENTS MADE WITH
DIFFERENT COARSE AGGREGATES**

by

B. Frank McCullough,

Dan Zollinger,

and

Terry Dossey

Research Report Number 3925-1

Project No. 7-3925

*Evaluation of the Performance of Texas Pavements Made with Different Coarse
Aggregates*

Conducted for the

TEXAS DEPARTMENT OF TRANSPORTATION

in cooperation with the

**U.S. DEPARTMENT OF TRANSPORTATION
Federal Highway Administration**

by the

**CENTER FOR TRANSPORTATION RESEARCH
Bureau of Engineering Research
THE UNIVERSITY OF TEXAS AT AUSTIN**

and the

**TEXAS TRANSPORTATION INSTITUTE
TEXAS A&M UNIVERSITY SYSTEM**

September 1998

Revised: June 1999

Revised: October 2000

IMPLEMENTATION STATEMENT

The observations and recommendations developed in this report provide an excellent starting point for an improvement program. Using this information the key elements for an implementation plan are provided in Chapter 9 in terms of specific recommendations for developing a high performance pavement (HPCP) that encompasses design, construction, specifications, and testing. The objective of this program is to eliminate or minimize the instances in which PCC pavement failures cause CRC pavement sections to fall far short of their predicted life. Thus, results from the implementation plan should provide PCC pavements that serve for 25 to 40 years on high-volume facilities with minimum maintenance.

The reader is referred to Chapter 9 for the 55 specific recommendations in five basic areas discussed in the following sections (number of implementation items shown in parenthesis):

- (9.2) Improving pavement performance (17)
- (9.3) Guidelines for selecting PCC coarse aggregate (2)
- (9.4) Developing concrete pavement placement guidelines (10)
- (9.5) Improving and refining CRCP design models (14)
- (9.6) General PCC pavement developments (12)

These items represent a continuous improvement program in each of these areas that may be achieved over the next five years. The intent is to avoid moving too rapidly (i.e., in a way that invites controversy and minimizes acceptance) yet providing a series of progressive steps that will lead to an incremental evolution toward HPCP.

DISCLAIMERS

The contents of this report reflect the views of the authors, who are responsible for the facts and the accuracy of the data presented herein. The contents do not necessarily reflect the official views or policies of the Federal Highway Administration or the Texas Department of Transportation. This report does not constitute a standard, specification, or regulation.

There was no invention or discovery conceived or first actually reduced to practice in the course of or under this contract, including any art, method, process, machine, manufacture, design or composition of matter, or any new and useful improvement thereof, or any variety of plant, which is or may be patentable under the patent laws of the United States of America or any foreign country.

NOT INTENDED FOR CONSTRUCTION, BIDDING, OR PERMIT PURPOSES

B. Frank McCullough, P.E. (Texas No. 19924)
and
Dan Zollinger, P.E.
Research Supervisors

ACKNOWLEDGMENTS

The authors would like to thank Mr. Steve Simmons of the Houston District for his invaluable assistance in coordinating this project with TxDOT. Appreciation is also expressed to Mr. Rick Nelson, who contributed some of the material contained herein in the form of his Master's thesis. Finally, we acknowledge the contributions of the other members of the project monitoring committee, which included J. Nichols (FHWA), W. Torres (HOU), and A. Wimsatt (FTW).

Research performed in cooperation with the Texas Department of Transportation and the U.S. Department of Transportation, Federal Highway Administration.

TABLE OF CONTENTS

CHAPTER 1. INTRODUCTION	1
1.1 BACKGROUND.....	1
1.2 HISTORICAL DEVELOPMENT.....	2
1.3 COARSE AGGREGATE STUDIES OVERVIEW	5
Research Study 422.....	5
Research Study 1244.....	7
Field Test in Friendswood, Texas (Project 6)	9
Field Test in Cypress, Texas (Project 7)	12
Summary of Findings from 422 and 1244	16
1.4 RESEARCH STUDY 7-3925	19
1.5 REPORT OBJECTIVES AND SCOPE.....	22
CHAPTER 2. FIELD EXPERIMENTS AND MONITORING.....	25
2.1 EXPERIMENTAL VARIABLES.....	25
Monitoring Performance Indicators	26
Crack Spacing — Distribution and Average.....	26
Crack Width	30
Crack Spalling	30
Crack Randomness	31
2.2 EVAPORATION-INDUCED STRENGTH LOSS	34
Conceptual Strength Loss Mechanism Hypothesis.....	35
Conceptual Results from Hypothesis	37

2.3 PERFORMANCE VARIABLES	38
2.4 SUMMARY	40
CHAPTER 3. CYPRESS AND FRIENDSWOOD FIELD SITES	41
3.1 EXPERIMENTAL PAVEMENT SECTIONS TO IMPROVE	
CRACK PATTERNS	41
Field Test in Friendswood, Texas (Project 6)	42
Field Observation of Cracking	42
Strain Measurement.....	48
Field Test in Cypress, Texas (Project 7)	51
Crack Control Sections.....	54
Measured Crack Widths	62
Consideration of Pavement Temperature and Relative Humidity	63
Concrete Strength Gain	73
3.2 CONCLUSIONS	75
CHAPTER 4. OBSERVATIONS FROM HOUSTON AND HEMPSTEAD TEST	
 SECTIONS.....	77
4.1 CRACK SPACING	77
Crack Development over Time	77
Placement Time and Season.....	78
Placement Temperature.....	83
Steel Percentage	84
Skewed Steel	86
Aggregate Type.....	87
Blended Aggregate.....	89
Summary	90
4.2 CRACK WIDTH.....	90
Early-Age Cracking.....	90
Placement Season.....	91
Reinforcing Steel.....	91

Aggregate Type	92
Pavement Thickness	92
Summary	92
4.3 RANDOMNESS INDEX (RI)	92
4.4 DELAMINATION SPALLING.....	95
Spalling over Time	95
Placement Season	95
Placement Time	96
Aggregate Type	97
Alternate Curing Techniques	97
Summary	97
4.5 EVAPORATION-INDUCED STRENGTH LOSS	98
Field Data	98
4.6 SUMMARY	101
CHAPTER 5. CHARACTERIZATION OF DELAMINATION SPALLING.....	105
5.1 INTRODUCTION.....	105
5.2 OVERVIEW.....	105
Stresses Due to Temperature Variation.....	106
Stresses Due to Moisture Variation.....	106
Stresses Due to Combined Temperature and Moisture Variation.....	107
5.3 SPALLING MECHANISM.....	107
Delamination Formation	107
Delamination Extension	109
Spall Development	109
Summary	110
CHAPTER 6. THERMAL COEFFICIENT OF CONCRETE.....	113
6.1 FACTORS AFFECTING CTE	113
Cement Paste	113

Aggregates.....	114
6.2 THERMAL COEFFICIENT PREDICTION	115
From Components	115
From Chemical Testing.....	115
6.3 SUMMARY	117
CHAPTER 7. VALIDATION OF CRCP-8	119
7.1 CRACK SPACING.....	119
Crack Distribution.....	119
Mean Crack Spacing	119
7.2 SUMMARY	123
CHAPTER 8. IMPLICATIONS OF STUDY.....	125
8.1 IMPROVING PAVEMENT PERFORMANCE.....	125
General Discussion.....	125
Establishing Significant Factors.....	127
8.2 CONCRETE PAVEMENT PLACEMENT GUIDELINES	129
Concrete Temperature	129
Evaporation	136
8.3 GUIDELINES FOR COARSE AGGREGATE.....	140
Guideline to Achieve Equal Performance.....	141
Quantification of Design Factors	142
Method of Construction	142
8.4 PREDICTING PAVEMENT PERFORMANCE.....	143
Steel Stress	144
Crack Width	144
Bond Development Length	145
Summary	147
8.5 FUTURE PROGRAM DEVELOPMENTS.....	147
Enhancements.....	147

Additional Program Developments.....	149
8.6 GENERAL PCC PAVEMENT DEVELOPMENTS	150
Database Additions	151
Criteria Development	151
Design Development.....	151
Performance-Related Specification Developments.....	152
CHAPTER 9. CONCLUSIONS AND RECOMMENDATIONS	155
9.1 INTRODUCTION.....	155
9.2 IMPROVING PAVEMENT PERFORMANCE.....	155
9.3 GUIDELINES FOR SELECTING PCC COARSE AGGREGATE.....	158
9.4 CONCRETE PAVEMENT PLACEMENT GUIDELINES	159
9.5 IMPROVING AND REFINING CRCP DESIGN MODELS	161
9.6 GENERAL PCC PAVEMENT DEVELOPMENTS	163
REFERENCES.....	167
APPENDIX A	171
APPENDIX B.....	201
APPENDIX C	207
APPENDIX D	213
APPENDIX E.....	217

LIST OF TABLES

Table 1.1 Four mix designs used in the Cypress test section.....	16
Table 2.1 Factorial of variables for Projects 1–8 developed in Projects 0-1244 and 7-3925.....	25
Table 2.2 Number of condition surveys taken on each project since the initial construction	27
Table 3.1 Crack survey data for sawcut section TS2 (1 ft=0.30 m).....	45
Table 3.2 Deviate distances of cores from original places of inducers.....	46
Table 3.3 List of Cypress crack control sections	55
Table 3.4 Percentage of cracks initiated at a crack inducer	58
Table 3.5 Flexural strengths (psi) of concrete for the four mix designs	73
Table 5.1 Description of qualitative curing conditions.....	108
Table 8.1 Significance ranking of performance indicators and variables studied in Projects 1–8.....	129
Table 8.2 Recommended evaporation controls.....	140

LIST OF FIGURES

Figure 1.1 Historical development of the coarse aggregate evaluation project	3
Figure 1.2 Development of failures in SRG vs. LS pavements	4
Figure 1.3 Distribution of crack spacing in SRG and LS pavements (1 ft=0.30 m).....	5
Figure 1.4 Map of test sections from Projects 422 and 1244 (Ref 7)	8
Figure 1.5 Typical experimental factorial and test section layout for Projects 1–4.....	9
Figure 1.6 Layout of test sections for Project 6 — FM 528 Friendswood site	10
Figure 1.7 Type I crack inducer located in TS1	11
Figure 1.8 Type III crack inducer located in TS3	11
Figure 1.9 Layout of test sections for Project 7 US 290 Cypress site.....	12
Figure 1.10 Location of four mix designs for part I-A shown in Figure 1.9.....	14
Figure 1.11 Curing methods used in part I-A.....	15
Figure 1.12 Metallic crack inducer located on top of longitudinal rebar	15
Figure 1.13 Test sections in Hempstead, Texas (Project 8).....	21
Figure 1.14 Test section layout — Westbound lanes.....	22
Figure 1.15 Test section layout — Eastbound lanes	22
Figure 2.1 Conceptual phases in the life of a CRCP illustrating the reduction in mean crack spacing over time.....	28
Figure 2.2 Conceptual crack spacing distributions	29
Figure 2.3 Example of deep delamination spalling.....	31
Figure 2.4 Typical types of cracking (Ref 10)	32
Figure 2.5 Definition of terms used to determine R.....	32
Figure 2.6 Definition of N for use in the randomness index equation and typical examples (Eq 2.1).....	34
Figure 2.7 Effects of a different evaporation rates on concrete slabs	36
Figure 2.8 Effect of a low evaporation rate on relative humidity of a slab.....	36
Figure 2.9 Cumulative strength distribution of the top part of concrete cores.....	36
Figure 2.10 Cumulative strength distribution of the bottom part of concrete cores	37
Figure 2.11 Example of a cumulative strength distribution plot.....	38
Figure 2.12 Typical cumulative strength distribution	39
Figure 3.1 Percentage of cracks occurring at Type I inducers with or without a transverse sawcut.....	44
Figure 3.2 Cores from nonsawcut part in subsection 1 where Type I crack inducer was located	44
Figure 3.3 Cores from nonsawcut part in TS3 where Type III crack inducer was located	46
Figure 3.4 Percentage of cracks occurring at Type III inducers with or without notches	47
Figure 3.5 Layout of extensometers in Friendswood investigation section.....	50

Figure 3.6 Extensometers as placed before casting of concrete.....	50
Figure 3.7a Cypress weather conditions during early-aged crack development.....	52
Figure 3.7b Early-aged crack development as affected by aggregate blends at Cypress —Part 1-A	52
Figure 3.8 Uncontrolled cracking test sections placed in morning hours	53
Figure 3.9 Uncontrolled cracking test sections placed in afternoon hours	53
Figure 3.10 Type III crack inducer located on the top of longitudinal rebar— Part IV ...	55
Figure 3. 11 Cracking development at sawcut locations.....	58
Figure 3.12 Longitudinal sawcutting using the early-entry method	59
Figure 3.13 Type III crack inducer— single-layer configuration	59
Figure 3.14 Percentage of cracks occurring at the rebar in the Cypress section.....	60
Figure 3.15 Percentage of cracks occurring at the rebar in the LaPorte section	61
Figure 3.16 Crack width variation with method of curing and coarse aggregate blend ...	62
Figure 3.17 Ambient temperature and RH in Cypress from August 25 through August 30, 1992.....	64
Figure 3.18 Ambient temperature and solar radiation in Cypress from August 25 through August 30, 1992	65
Figure 3.19 Typical temperature variation with time.....	65
Figure 3.20 Typical temperature distribution with depth (morning)	66
Figure 3.21 Typical temperature distribution with depth (afternoon).....	66
Figure 3.22 Temperature variation in the section with different curing methods.....	67
Figure 3.23 A specially designed device for measuring RH in concrete pavement.....	68
Figure 3.24 Measurement of RH in the field	68
Figure 3.25 Typical RH variation with time	69
Figure 3.26 Typical RH distribution with depth (1 day).....	69
Figure 3.27 Typical RH distribution with depth (5 days)	70
Figure 3.28 RH in section cured by polyethylene sheet.....	71
Figure 3.29 Effect of curing method on RH in concrete pavement	72
Figure 3.30 Linseed oil and water-based curing compound curing experiment	72
Figure 3.31 Comparison of curing compound performance relative to cracking density	73
Figure 3.32 Effect of curing method on RH in concrete pavement	74
Figure 3.33 Percentage of cracks at different times	75
Figure 4.1 Typical formation of the crack distribution over time for an SRG section paved at night (Project 8 — Section 23E).....	78
Figure 4.2 Crack spacing for the 10th, 50th, and 90th percentile over time (Project 8 — Section 23E)	79
Figure 4.3 Percentage of cracks spaced less than 3 ft (0.91 m) apart over time (Project 8 — Section 23E)	79

Figure 4.4 Typical formation of the crack distribution over time for an SRG section paved during day (Project 8 — Section 28E).....	80
Figure 4.5 Typical formation of the crack distribution over time for an SRG section paved during winter (Project 1 — Section A).....	81
Figure 4.6 Typical formation of the crack distribution over time for an SRG section paved during summer (Project 2 — Section A)	81
Figure 4.7 Percentage of cracks spaced less than 3 ft (914.4 mm) apart over time (Projects 1, 2, and 8) for the SRG combinations.....	82
Figure 4.8 Crack distribution for sections with summer and winter paving at ages of 2,600 to 2,800 days (Projects 1 and 2 — Sections B and D)	83
Figure 4.9 Comparison of crack spacing vs. steel percentage at 2,700 days (Project 3 Sections A–C)	85
Figure 4.10 Effect of bar size on crack spacing at 2,400 days (Project 4 — Sections E and G)	86
Figure 4.11 Crack spacing comparison for skewed vs. normal transverse steel at 100 days for SRG sections (Project 8).....	87
Figure 4.12 Crack spacing comparison for skewed vs. normal transverse steel at 640 days for SRG sections (Project 8).....	87
Figure 4.13 Comparison of crack distribution for SRG and LS at 640 days (Project 8) ..	88
Figure 4.14 Percentage of cracks less than 3 ft (0.91 m) apart (Projects 1–4, and 8).....	89
Figure 4.15 Comparison of crack spacing distributions for LS, SRG, and blended coarse aggregate at 640 days (Project 8)	90
Figure 4.16 Randomness index (RI) distribution by section for the Project 8 test section.....	94
Figure 4.17 Average RI for Projects 1– 4 and 8.....	94
Figure 4.18 Spalling in Projects 1 and 2 (top left — LS summer, top right — LS winter, bottom left — SRG summer, bottom right — SRG winter)	96
Figure 4.19 Cumulative strength distribution for siliceous river gravel (SRG) aggregate, Project 8.....	98
Figure 4.20 Cumulative strength distribution for limestone aggregate, Project 8	99
Figure 4.21 Cumulative strength distribution from Las Vegas at low evaporation rates, but delayed application of the curing compound.....	100
Figure 4.22 Cumulative strength distribution from Las Vegas at high evaporation rate.....	101
Figure 4.23 Cumulative strength distribution from Las Vegas for the top layers.....	102
Figure 4.24 Cumulative strength distribution from Las Vegas for the bottom layers	103
Figure 5.1 Typical example of spalling.....	106
Figure 5.2 Conceptual illustration of relative moisture loss and stresses due to different curing conditions	108
Figure 5.3 Conceptual illustration of the delamination mechanism and	

the relative impact of different curing conditions	110
Figure 5.4 Historical development of spalling as a function of evaporation rate	111
Figure 6.1 CTE for SRG and LS aggregates	114
Figure 6.2 Effect of CaO on the CTE of aggregates	116
Figure 6.3 Effect of SiO ₂ on CTE of aggregates.....	116
Figure 7.1 Comparison of predicted to actual crackspacing at 640 days for LS Day (Project 8 — Section 31W).....	120
Figure 7.2 Comparison of predicted to actual crack spacing at 640 days for LS Night (Project 8 — Section 21W)	121
Figure 7.3 Comparison of predicted to actual crack spacing at 640 days for SRG Day (Project 8 — Section 31E).....	121
Figure 7.4 Comparison of predicted to actual crack spacing at 640 days for SRG Night (Project 8 — Section 24E).....	122
Figure 7.5 Comparison of predicted to actual crack spacing at 640 days for blend Day (Project 8 — Section 21E).....	122
Figure 7.6 Predicted versus actual mean crack spacing ($r^2=0.71$)	123
Figure 8.1 Maturity meter (records concrete temperature)	130
Figure 8.2 Weather station (records temperature, humidity, and wind speed)	131
Figure 8.3 Effect of curing temperature on heat of hydration (140°F = 60°C).....	131
Figure 8.4 Relationship of air and concrete temperatures to stress.....	133
Figure 8.5 Typical air and concrete temperatures during winter placement.....	133
Figure 8.6 Typical air and concrete temperatures during summer placement	134
Figure 8.7 Influence of placement time on longitudinal cracking (SRG).....	135
Figure 8.8 Influence of placement time on longitudinal cracking (LS).....	135
Figure 8.9 Pavement failure as a function of temperature at placement.....	135
Figure 8.10 Factors influencing evaporation rate.....	136
Figure 8.11 Monitoring evaporation to select curing treatment.....	137
Figure 8.12 Effect of high evaporation rate on spalling development (BW-8)	
Figure 8.13 Differential tensile strength on BW-8 Project.....	138
Figure 8.14 Relative effectiveness of curing methods	139
Figure 8.15 Water loss in El Paso	139
Figure 8.16 Maximum steel stress calculated for Projects 1-4 and 8 (CRCP-8).....	145
Figure 8.17 Crack width calculated at the minimum design temperature of 20°F using CRCP-8 for Projects 1-4 and 8 (0.01 in. =0.25 mm)	146
Figure 8.18 Bond development length calculated using CRCP-8 for Projects 1-4 and 8 (0.01 in. = 0.25 mm).....	146
Figure 8.19 Conceptual flow of the analysis program CRCP-8.....	148
Figure 8.20 Conceptual flow for the CRCPAV (design) program.....	149
Figure 8.21 Exponential effect of humidity in maturity equation.....	154

CHAPTER 1. INTRODUCTION

This report summarizes 23 years of work undertaken in Texas to understand the reasons for significant performance differences found in pavements placed around the state. To a significant degree, pavement performance can be predicted based on the concrete material properties, on the environmental conditions prevailing when the pavement was placed, and on the pavement type.

1.1 BACKGROUND

Continuously reinforced concrete (CRC) pavements are characterized by the presence of longitudinal reinforcing steel placed continuously throughout their length. Technically speaking, CRC pavements have no intentionally placed transverse joints other than construction joints in the pavement. However, the continuity of the concrete in the pavement is interrupted by a great number of transverse cracks caused by volumetric changes in the concrete that are a result of shrinkage and temperature changes. When a transverse crack occurs, the stress distributions in concrete and the reinforcing rebar change greatly from point to point in the pavement. Experience has indicated that pavement performance is significantly linked to the resulting transverse crack pattern (or postcracking) behavior of CRC pavement. For example, short crack spacings coupled with pavement locations where poor support conditions exist have shown a strong correlation with a high frequency of punchout distress. On the other hand, long crack spacings can lead to large crack openings that can result in crack spalling, steel rupture, and poor load transfer efficiency. Once load transfer has diminished to a certain extent, punchout distress or faulting may be evident, particularly where loss of support exists under the pavement.

In the 1986/1993 AASHTO *Guide for Design of Pavement Structures*, a procedure was set forth that considers crack spacing, crack width, and steel stress at a crack in the design of CRC pavement. The design percentage of longitudinal steel is selected in such a way that the results from the analysis satisfy the desired range in crack spacing, allowable steel stress, and crack width. This analysis is a function of such predetermined parameters as concrete tensile strength, thermal coefficients of steel and concrete, rebar diameter, concrete tensile stress generated by wheel load, concrete shrinkage, and design temperature drop

based upon predictive formulas. This design method suggests providing an appropriate percentage of steel reinforcement to distribute transverse cracks, so that instead of a few wide cracks, there are numerous cracks consisting of small widths.

During construction, it is expected that the final crack spacing will fall into the desirable range as a result of the above-mentioned design parameters. Unfortunately, it is difficult to eliminate “Y” cracks and other defects (such as closely spaced transverse cracks) by adjusting only the amount of longitudinal steel, primarily because of the variability of material properties, construction factors, and environmental conditions that are to some extent outside the contractor’s control. Moreover, the early-aged cracking behavior of CRC pavements is affected not only by the previously noted design parameters, but also by the vertical location of the longitudinal and transverse steel reinforcement, coarse aggregate type, and ambient temperature conditions at the time of paving. This has been a concern for some time, and efforts were undertaken to develop a greater knowledge base of these factors and their influence on CRC pavement performance during construction. A primary focus of the test sections constructed in these projects was on investigating the influence of the above factors (under field conditions) on crack development in CRC pavement, and on developing construction guidelines that consider these factors in providing and advancing new concepts in the technology of CRC pavement construction. The sections that follow will describe these efforts, along with some of the experiments conducted to better understand and improve CRC pavement performance.

1.2 HISTORICAL DEVELOPMENT

Beginning in 1974, the Texas State Department of Highways and Public Transportation (now the Texas Department of Transportation, or TxDOT) initiated research that looked for ways to improve the performance of concrete pavements. The first step in the process was to survey every mile of portland cement concrete (PCC) pavement in the state for rehabilitation prioritization (Figure 1.1). When performance differences were noted in the sections, TxDOT decided to continue periodically surveying the continuously reinforced concrete pavement (CRCP) sections and to establish a database. The objectives of the database were to provide performance data for developing design methods, construction specifications, maintenance effects, and a comparison of pavement types (Ref 1).

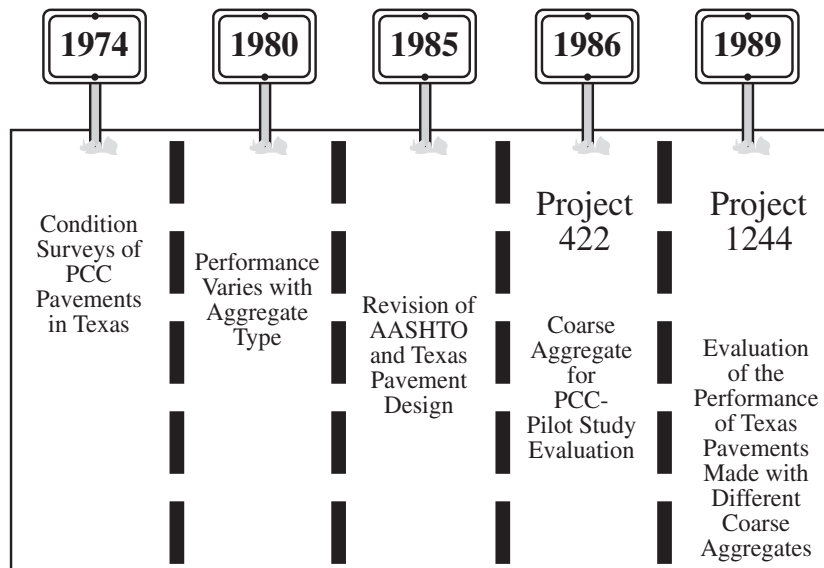


Figure 1.1 Historical development of the coarse aggregate evaluation project

Using the database, researchers were able to look at the data to find performance differences in similar pavements. After performance differences were found, the Center for Transportation Research (CTR) at The University of Texas at Austin began to investigate what caused the differences, with the goal of producing improved pavement performance.

One of the primary original findings of the pavement surveys was that the concrete coarse aggregate type was a significant factor in pavement performance (Ref 11). This finding was so important that when the AASHTO and Texas Pavement Designs were modified in 1985, they reflected the differences in performance that were found (Figure 1.1).

Figure 1.2 shows the difference in performance between pavements constructed with siliceous river gravel (SRG) and limestone (LS) aggregates. The curves in the figure were fit to the 20-year performance histories in the rigid pavement (RP) database and, thus, represent the average rate of failure development for limestone and river gravel pavements with and without swelling subgrades. Again using the RP database, Figure 1.3 was prepared, showing the significant difference between LS and SRG in terms of crack spacings — LS pavements

tending to stabilize at a crack spacing of around 6 ft (1.83 m) vs. a much lower spacing of 2–3 ft (0.61–0.91 m) for SRG pavements. The closer crack spacing for the SRG pavements greatly increases the probability of a longitudinal crack intersecting two transverse cracks, ultimately resulting in a greater number of failures per mile (1 mile= 1.6 km), as observed in the preceding figure.

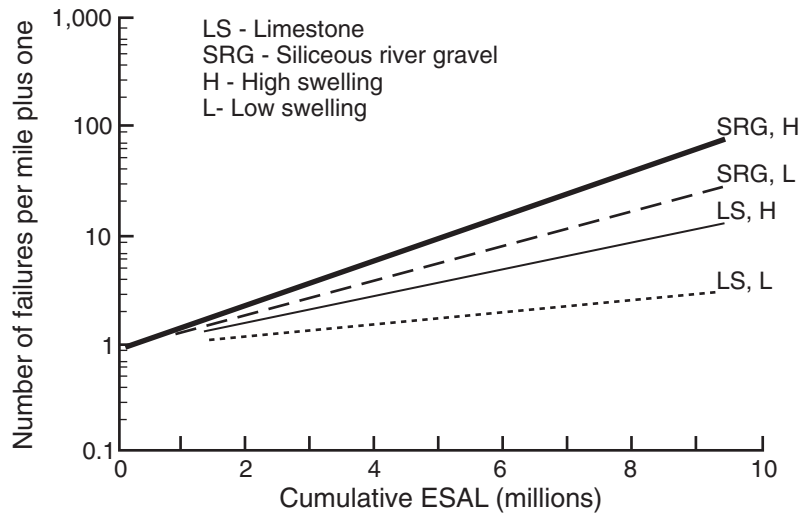


Figure 1.2 Development of failures in SRG vs. LS pavements

After finding the differences in pavement performance based on aggregate type, it was important to understand the material properties causing the differences, and to then evaluate ways to improve concrete pavement performance through a controlled study. With this purpose in mind, TxDOT commissioned a series of coarse aggregate studies that looked at the differences in pavement performance considering coarse aggregate type and other factors.

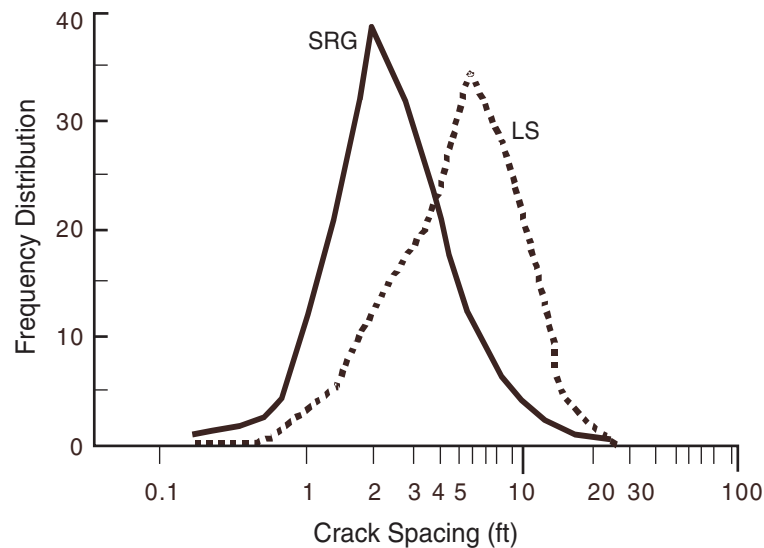


Figure 1.3 Distribution of crack spacing in SRG and LS pavements (1 ft=0.30 m)

1.3 COARSE AGGREGATE STUDIES OVERVIEW

As these studies began, the primary objective was to evaluate concrete with different coarse aggregates using laboratory and field methods. The laboratory work began first, with the results of the laboratory work leading to guidelines for the design of the field test sections. Eight different sets of test sections were placed in the Houston, Texas area to study ways to improve concrete performance. In each project, a number of pavement conditions were varied to better understand their effects on pavement performance. Monitoring the performance of these test sections over the years has led to improved design and construction procedures.

RESEARCH STUDY 422

Three major areas of concentration were chosen for Research Study 422. The first part of the project involved a laboratory study on concrete properties. Following the laboratory study, a design study was conducted. Finally, the results of the first two parts of the project were applied by placing four test sections in and around Houston.

The purpose of the laboratory study was to analyze concrete mix properties using mix designs that were being used around Texas at the time. Concrete specimens were cast in the laboratory using both limestone and siliceous river gravel coarse aggregates; the specimens were then tested for fundamental concrete properties, such as Young's modulus (E), shrinkage, thermal coefficient, freeze-thaw resistance, flexural strength, compressive strength, and tensile strength (Ref 11). The laboratory results revealed that the concrete's shrinkage, thermal coefficient, and Young's modulus were significantly different for the two aggregate types. Specifically, the ratios of tensile strength, thermal coefficient, and elastic modulus for SRG to limestone were 0.96, 1.57, and 1.14, where $Z_{SRG}/Z_{LS} \geq 0.96$, $\alpha_{SRG}/\alpha_{LS} \geq 1.57$, and $E_{SRG}/E_{LS} \geq 1.14$, respectively. The strength values were very similar, but this was as expected since the mix designs were intended to meet a minimum specified strength. The results of the laboratory study were then applied to a design study.

The design study focused on setting up a procedure to compare the effects of coarse aggregates on the design of CRC pavements. The report on Phase II concluded that aggregate type cannot be ignored in the design of CRC pavements. It was also determined that two distinct steel reinforcement designs should be produced to accommodate the differences in aggregate type (Ref 12). The third phase of Research Study 422 was a field study that applied the principles learned from the first two parts of the project. Four series of test sections, referred to as Projects 1–4 in this report, were placed in Houston to conduct this part of the study. The locations of these projects are shown on the Houston area map presented in Figure 1.4.

The primary factors evaluated in each series of test sections were aggregate type, steel percentage, and bar size, as shown in Figure 1.5; pavement thickness was considered between projects. Note in Figure 1.5 that the medium steel percentage was considered to be the optimal steel percentage; the high and low steel percentages are approximately 0.10% above and below the medium steel percentage. Also note that the steel percentage varied based on aggregate type. Because the pavement thickness varied among the projects, the steel percentages also changed slightly among projects. Owing to construction delays, an additional variable was introduced, namely, placement season. The construction delays

actually were helpful; because they led to the finding that placement season has a very large effect on pavement performance.

The findings from the test sections developed in Research Study 422 were very encouraging and were reported in connection with the Research Study 422 reports (Refs 8, 12, 13). Some of the findings determined that placement season; placement time and temperature, steel percentage, and aggregate type are all strong factors contributing to crack spacing. These findings will be discussed in more detail in conjunction with the data obtained from subsequent projects in Chapters 7 and 8, which speak to design validation and the implication of the study results, respectively.

RESEARCH STUDY 1244

The results obtained from Research Study 422 prompted a need to construct additional test sections to evaluate the effects of curing types and to investigate crack control methods to eliminate very close crack spacing. Accordingly, four more locations were chosen for placement of test sections in the Houston area (Figure 1.4, Projects 5–8).

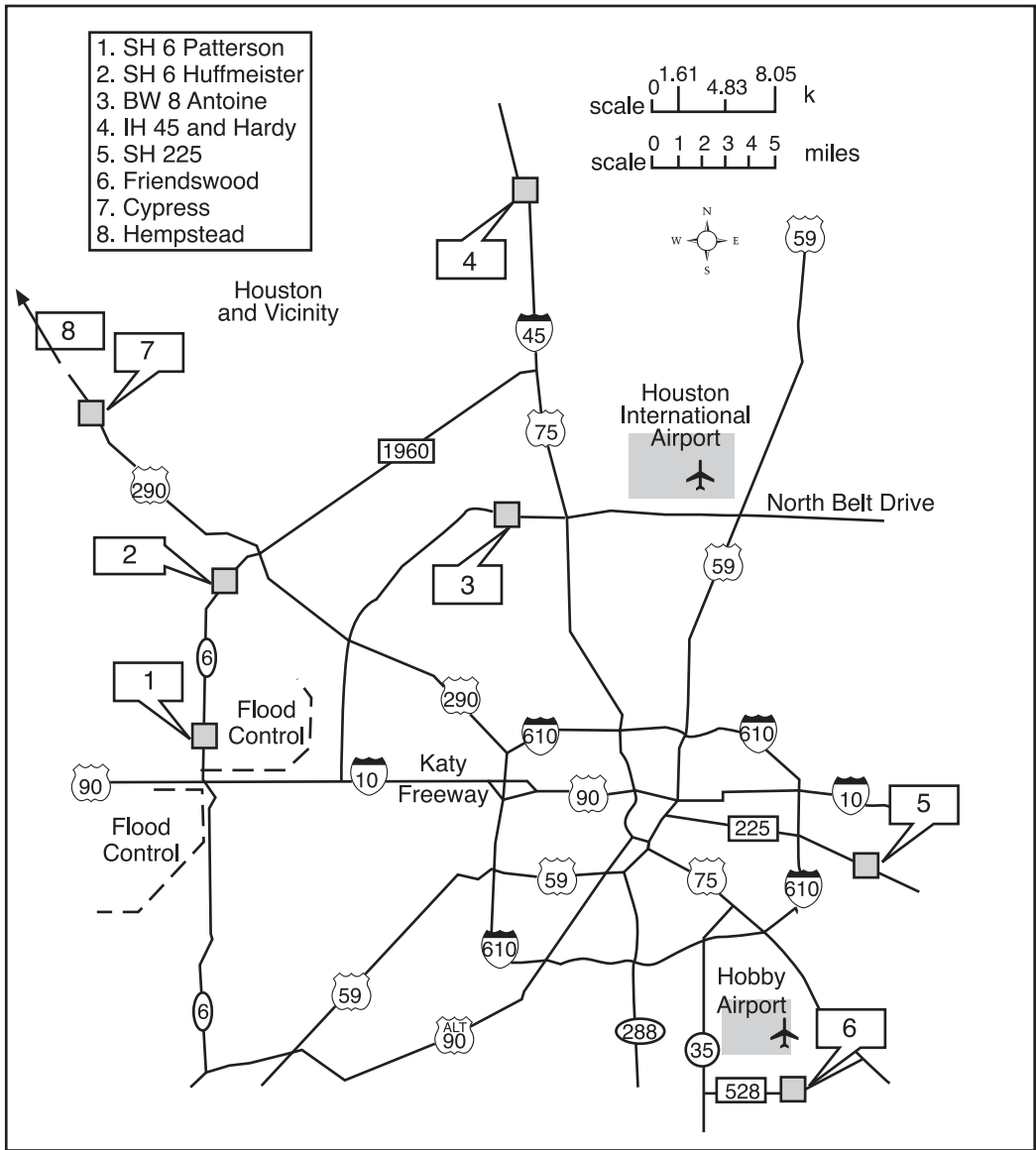


Figure 1.4 Map of test sections from Projects 422 and 1244 (Ref 7)

While the results from Project 5 “SH 225” have been previously reported, the results from Projects #6, “Friendswood,” and #7, “SH 290-Cypress,” were not reported as part of Project 1244. Therefore, they have been included in this report. First, the nature of the experiment for these two projects is described in the following subsections, with the results described in Chapter 3. Project 8, relating to the Hempstead bypass, did not begin on time owing to construction delays; subsequently it was constructed and monitored under TxDOT

Research Study 3925. The experimental nature of the test sections is described in a subsequent section entitled “Research Study 3925,” while the observations and results are presented in Chapter 4.

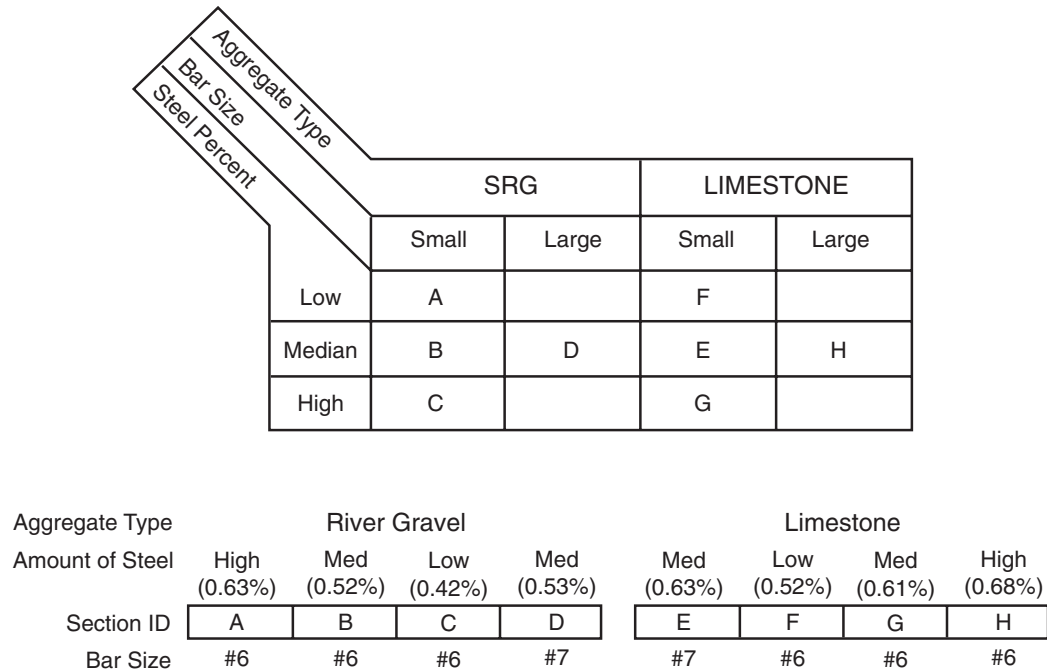


Figure 1.5 Typical experimental factorial and test section layout for Projects 1–4

FIELD TEST IN FRIENDSWOOD, TEXAS (PROJECT 6)

The CRC pavement test section on FM 528 in Friendswood, Texas, was constructed in November 1993 with the specific purpose of determining the best method to synthetically control the crack pattern in CRC pavement under cool weather paving conditions using river gravel coarse aggregate. Figure 1.6 shows the layout of the test section in Friendswood, which was constructed with a pavement thickness of 10 in. (25.4 cm). The section consists of four different crack control sections. The first section (TS1) and the third section (TS3) consisted of a specially made crack inducer section, whereas section two (TS2) and section four (TS4) consisted of regular transverse steel. The paving started on the morning of November 2, 1993, toward IH-45. For mechanical reasons, the paving machine stopped after

placing 25 ft (7.62 m) of concrete. Paving restarted the next day at 7:00 a.m. on November 4, 1993. In TS1, the Type I crack inducer that consisted of an L-shaped angled metal sheet placed at 5 ft (1.52 m) intervals also served as a support for the longitudinal reinforcing steel that eliminated the need for transverse rebars (Figure 1.7) placed at 5 ft (1.52 m) intervals. Transverse sawcut notches were aligned with some of the Type I crack inducers at both 5 ft (1.52 m) and 2.5 ft (0.76 m) intervals (about 7 hours after paving). In Sections 2–4, transverse rebar was used to support longitudinal steel at the standard 30 in. (76.2 cm) intervals. In Section TS3, Type III crack inducers that consisted of corrugated sheets and metal were placed on the top of and aligned with the longitudinal and transverse reinforcement. The transverse crack inducers were placed at 5 ft (1.52 m) intervals, coinciding with alternating transverse rebars (Figure 1.8). Sections TS2 and TS4 were identical except for the plastic debonding inserts, described in detail in Chapter 3, that were used in TS2. Sections TS2 and TS4 contain transverse sawcuts as crack initiators that were aligned both with the transverse steel and in between the reinforcement.

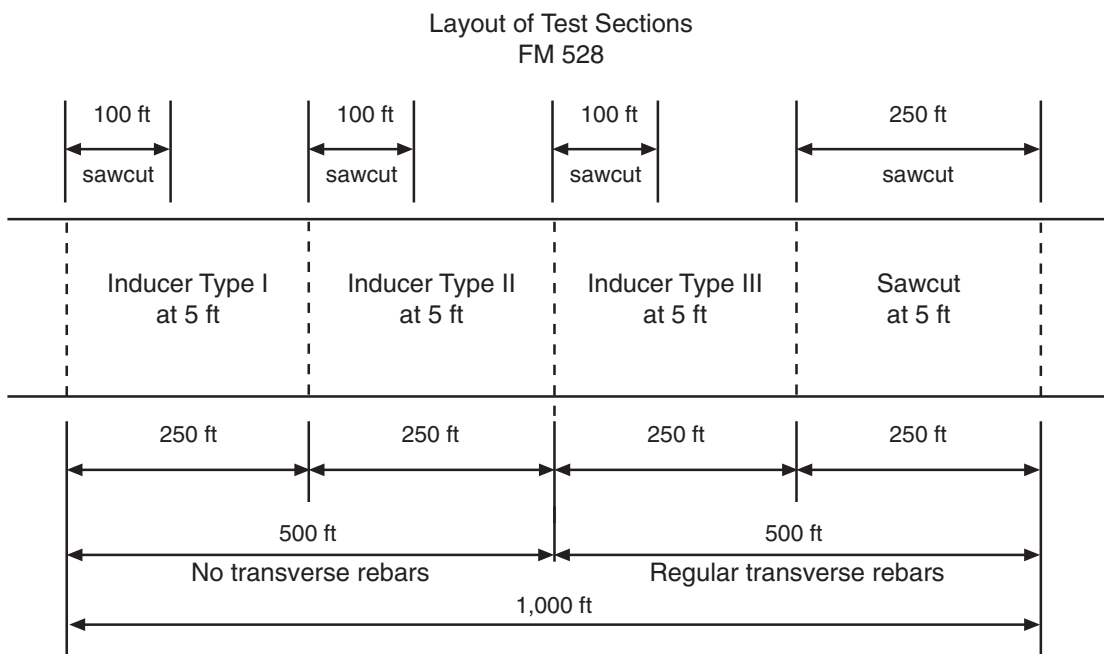


Figure 1.6 Layout of test sections for Project 6 — FM 528 Friendswood site
(1 ft = 0.30 m)



Figure 1.7 Type I crack inducer located in TS1



Figure 1.8 Type III crack inducer located in TS3

As the above description indicates, this experimental section included several different combinations of crack initiation techniques, such as Type I inducers coinciding with transverse sawcuts at 5 ft (1.52 m) and 2.5 ft (0.76 m) intervals (a sawcut placed between the notches), Type III inducer and transverse rebar at 10 ft (1.52 m) intervals coinciding with surface cuts and with sawcut placed out 2.5 ft (0.76 m) intervals between the inducers, and the standard transverse rebar at 2.5 ft (0.76 m) intervals with a surface cut at 5 ft (1.52 m) and 2.5 ft (0.76 m) intervals.

FIELD TEST IN CYPRESS, TEXAS (PROJECT 7)

The layout of the CRC pavement investigation site constructed on SH 290 in Cypress, Texas, is shown in Figure 1.9. This pavement section consisted of a 13 in. (33.02 cm) pavement thickness and a double layer of steel reinforcement in either a stacked or staggered configuration. Four different concrete mix designs (summarized in Table 1.1) with different types or amounts of coarse aggregates were used. They were systematically sequenced in two separate areas of the investigation section, as illustrated in Figure 1.10.

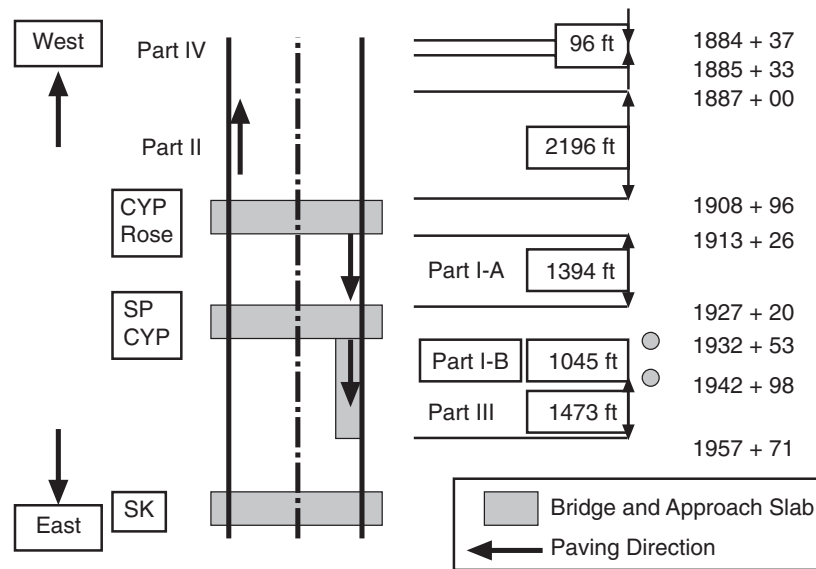


Figure 1.9 Layout of test sections for Project 7 US 290 Cypress site (1 ft = 0.30 m)

The Cypress test section also included three different curing mediums (polyethylene film, a double coat of waxed-based membrane curing compound, and a single coat of waxed-based membrane curing compound) (Figure 1.11). All experimental crack control and early-aged sawcutting techniques were employed in specially designated Test Areas I-B and III to induce pavement cracking at 3 ft (0.91 m), with a combination of 4 ft (1.21 m) and 5 ft (1.52 m) pairs, 5.9 ft (1.82 m), and 8.9 ft (2.74 m) crack spacings. Metallic crack inducers, also called Type III inducers (Figure 1.12), were placed in Test Area III in both single and stacked double layer configurations and were anchored to the double layer of longitudinal reinforcement to provide support against the flow of the fresh concrete during the paving operations. The locations of transverse rebar and crack inducers were recorded before the concrete pavement was placed. These inducers were placed in a variety of configurations and patterns. Gages of various types were installed in the test section to instrument the test pavements for temperature, moisture, and shrinkage variations as a function of the curing conditions. These devices consisted of thermocouples, monitoring points for specially modified relative humidity (RH) sensors, and Demac points for measuring the surface movement of the slab (these were embedded in the pavement section while the concrete was in a fresh state). Immediately after paving, field measurements and crack surveys were conducted by personnel from both the Texas Transportation Institute (TTI) at Texas A&M University and the Center for Transportation Research (CTR) at The University of Texas at Austin.

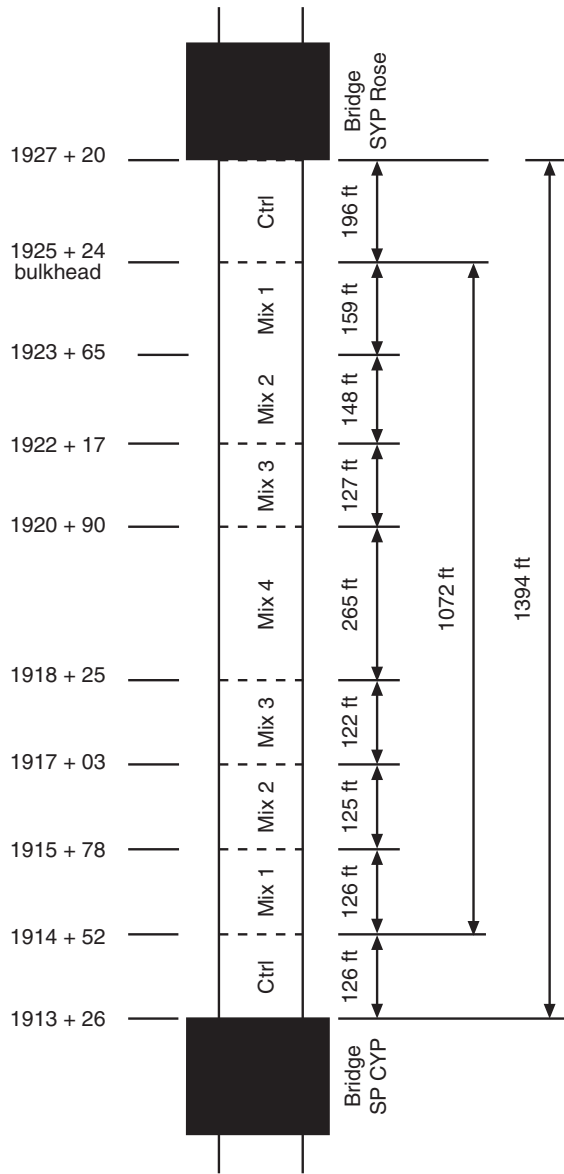
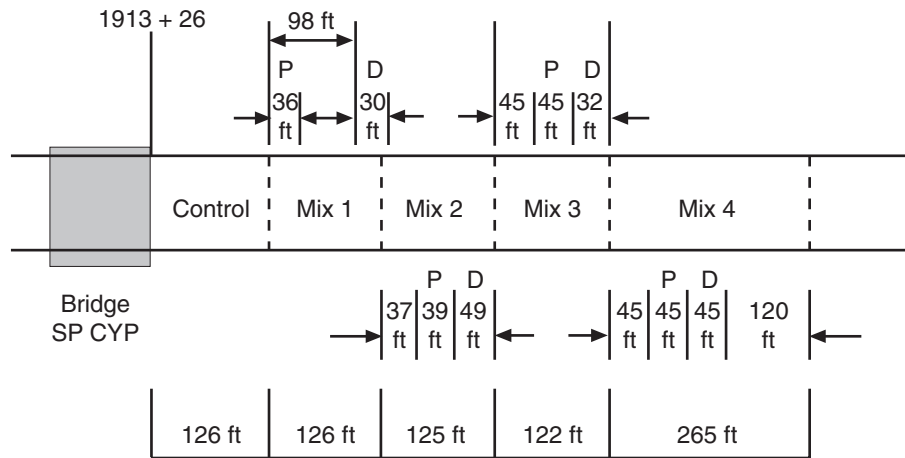


Figure 1.10 Location of four mix designs for part I-A shown in Figure 1.9 (1 ft = 0.30 m)



P = Polyethelene film covered D = Double coat of curing compound
 Single coat of curing compound elsewhere in Part I-A

Figure 1.11 Curing methods used in part I-A (1 ft = 0.30 m)



Figure 1.12 Metallic crack inducer located on top of longitudinal rebar

A portable weather station was placed near the job site before construction commenced. The ambient temperature and relative humidity, solar radiation, and wind speed were recorded from August 19 to October 4, 1992, at half-hour intervals. The maximum daily temperature difference (between maximum and minimum temperatures) ranged between -20°F to -30°F (-6.66°C to -1.11°C), while the maximum ambient temperature was about 90°F (32.2°C). The minimum daily relative humidity ranged between 30–50%.

Table 1.1 Four mix designs used in the Cypress test section

Composition LB per cubic foot	Mix 1 100% LS	Mix 2 67% LS 33% RG	Mix 3 67% RG 33% LS	Mix 4 100% RG
Coarse Aggregate	277	185.7/96.4	195.8/91.5	292.2
Water	35	35	35	35
Cement	65.8	65.8	65.8	65.8
Fly Ash	23	23.1	23.1	23.1
Fine Aggregate	233	232	232	231
Entrained Air	4.5%	6.4%	5.5%	4.6%
W/C Ratio	0.53	0.53	0.53	0.53
Cement Factor	6	6	6	6
CAF	0.652	0.652	0.652	0.652
Max. CA Size (cm)	3.81	3.81/3.81	3.81/3.81	3.81

SUMMARY OF FINDINGS FROM 422 AND 1244

Research Studies 422 and 1244 produced some very important findings and led to some new hypotheses regarding concrete performance with different coarse aggregate types. The major finding from the variables directly considered was that a large part of the performance differences in concrete pavements could be directly attributed to the coarse aggregate used in the concrete. The steel percentages, which ranged from low to high value, i.e., a difference of approximately 0.2%, used on these test sections did not have a significant effect on the performance of the pavement. This could be attributed to the fact that all the steel percentages are acceptable values for the Houston area. Indirectly, it was also found that high placement temperatures, e.g., ambient temperatures above 90°F (32.2°C), could lead to a very erratic crack pattern and, consequently, poor performance. These conditions led to

PCC temperatures in the 140°F to 150°F (60°C to 65.55°C) range and rapid decreases in temperature during the first 24 hours when the concrete is relatively weak. This difference is the single most important factor controlling early-aged crack development and the primary cause of the difference in performance in pavements made with either aggregate. It was found that the high temperature conditions overwhelm all other variables considered. For example, no steel combinations can offset this phenomenon, but unfortunately when the cause of the problem was not fully understood in the past, the longitudinal steel percentages were arbitrarily increased over the years. Thus, original steel percentages that were providing acceptable design conditions were increased to offset problems caused by other phenomena. It should also be pointed out that although early-aged concrete strength is relatively low, the bond strength of concrete with limestone aggregate is significantly greater than that of concrete with SRG coarse aggregate.

Failure models for siliceous river gravel and limestone aggregates were developed; since portland cement concrete fails primarily in tension, the effects of tension on concrete were the focus of the failure model development.

A variety of techniques were developed for improving pavement performance, including night placement, saw cutting of the fresh concrete to control crack development, aggregate blends, and various curing techniques; methods to improve base materials were also developed. The projects showed that night placement gave better results than day placement. By using saw cutting, the cracks in the pavement became much straighter, thus reducing the randomness that sometimes leads to punchouts. Such curing techniques as polyethylene sheeting and double membrane curing were used to reduce the pavement evaporation rate; these in turn helped to control future spalling and reduced the number of cracks that occur very early in the pavement life.

The projects also were used to produce design aids for concrete pavement design. The *CHEM2* computer program was developed to provide the designer with a preliminary estimate of the fundamental concrete properties using simple chemical tests of the coarse aggregate (Ref 14). *CHEM2* uses the chemical constituents of the coarse aggregate, which can be obtained relatively cheaply through oxide residue testing, to predict its mineral composition. Based on the aggregate's mineral composition, the program predicts fundamental concrete properties, such as the coefficient of thermal expansion.

These studies have provided continuing development of a mechanistic empirical program, dubbed *CRCP-8* that has been calibrated and validated using empirical data obtained from the rigid pavement database. The first version of the program dates back to 1974 (Ref 16), with a series of modifications based on the latest research introduced thereafter. The data from these projects were used to further calibrate the crack width and the performance curves. In this program, the concrete properties (e.g., tensile strength) and aggregate properties (e.g., coefficient of thermal expansion) must be input. The expected air temperatures, steel percentage, and loading conditions must also be provided. From that information, crack spacing distributions and mean crack spacing are computed along with the mean crack width and maximum steel stress. In addition, a cumulative failure development as a function of time is computed. This program provides a performance prediction for a specific design and is especially valuable in comparing and evaluating several different possible pavement designs and construction conditions, as well as for use in diagnostic studies.

Another computer program developed from these projects was the design aid *CRCPAV*, which can be used to find CRCP steel percentages based on the highway geometric properties, other material properties, and acceptable levels of crack width, steel stress, aggregate properties, and crack spacing (Ref 9). Since *CRCP-8* is a predictive program for a specific design, numerous program solutions were investigated for use in developing a regression model. This model then permitted the *CRCPAV* program to be developed, which allows the desired performance to be input and then solves for the design parameters, i.e., a design program. Once the properties are given as input into the program, the program showing the optimal steel range produces a graph.

Another important development of Research Study 422 was the CRCP89 Steel Standard. CRCP89 is a newer steel design standard that varies the steel in the section based on the coarse aggregate type. The purpose of the standard was to develop similar crack patterns in concrete made from either siliceous river gravel or limestone aggregate. Although the standard is no longer in use, it was the first attempt to obtain equal and adequate performance from the two aggregates.

Other findings of the projects dealt with the testing of such concrete properties as strength. A large number of specimens were compared using tensile, flexural, and

compression testing. The results showed that flexural and tensile strengths have a reasonable correlation across all aggregate types. However, poor correlations were found between tensile and compressive strengths, unless the aggregate type was taken into account. It should be noted that SRG mixtures have a greater thermal coefficient of expansion than mixtures with limestone aggregates.

Since compression test results do not have a reliable correlation to the tensile strength of the concrete when comparing concrete made from different aggregates, care should be taken when evaluating results from compression tests. If results from compression testing are compared directly, erroneous conclusions could be made about a specimen's resistance to cracking. Therefore, tension testing was used in these test sections to avoid this problem and, more importantly, because concrete fails in tension. A special test procedure was also developed to measure aggregate bond strength.

Recommendations that can be used to improve pavement performance were provided based on the results obtained from Research Studies 422 and 1244. Night placement and the use of blended aggregates have been recommended, insofar as they seem to overcome some of the differences in siliceous river gravel and limestone performance. Since numerous key hypotheses were developed from these two projects, more research was needed to validate the previous findings.

1.4 RESEARCH STUDY 7-3925

The primary objective of designing and constructing the Hempstead sections was to validate hypotheses from previous experiments, and to determine feasible sawcutting requirements for SRG CRC pavements. Some specific objectives were to perform early-age and later-life condition surveys of the test sections, to monitor performance based on coarse aggregate type, to refine thermal coefficient(α_c) testing and crack control techniques for SRG CRC pavement, to develop a spalling model, and to support the Quality Control/Quality Assurance (QC/QA) Specification development. The purpose behind each of these objectives is discussed below.

Coarse aggregate type relative to bond strength, shrinkage, and thermal coefficient of expansion was identified from the beginning of the study as a very important factor in

predicting pavement performance; indeed, these are the strongest factors in determining a pavement's performance, given that coarse aggregates form such a large percentage of the concrete's volume and, consequently, are the dominant factors relative to aggregate type selection and specification.

Since these factors are so important for concrete exposed to large environmental stresses at both early and late ages (as are pavements), testing has focused on developing equipment that can measure the coefficient of thermal expansion and the bond strength of the coarse aggregate in a simple and direct procedure using a water bath for the thermal coefficient at expansion and split tensile test specimen for the aggregate bond strength. Pavement designs could easily be changed to account for differences in aggregate properties using tests.

A major objective of this project was also to develop and identify the spalling mechanism for future use in a spalling model. Spalling occurs in concrete mixtures having relatively high shrinkage stresses and low aggregate bond strengths. A spalling model would be useful in identifying such combinations, since spalling is one of the significant distresses that CRC pavements experience. If such information can be developed to decrease spalling in concrete pavements, the life-cycle cost of CRC pavements could be significantly reduced.

The final objective of Research Study 7-3925 was to support QC/QA specification development. All findings from this project are being shared directly with the QC/QA specification development team, so that improvements in concrete pavement performance can be incorporated as quickly as possible.

With these objectives in mind, the final test sections were placed in Hempstead, Texas (Project 8), which is located near Houston (Figure 1.13). These sections are part of the new US 290 Hempstead bypass. The layout developed for Hempstead called for twenty-two test sections, with each about 1,200 ft (365.76 m) long, as shown in Figures 1.14 and 1.15. Figure 1.14 shows the layout for the westbound lanes (WBL), with crushed limestone aggregate (LS) used exclusively on this half of the project. The numbers shown in Figure 1.14 represent the variables evaluated in the WBL; an explanation of the numbers as to the variable considered are presented in the key. As shown in Figure 1.14, the effects of time of placement (i.e., night or day), longitudinal saw cuts, and varying steel percentages were investigated.

Figure 1.15 shows the layout for the eastbound lanes (EBL), with siliceous river gravel (SRG) used primarily in these test sections. However, two sections, 20E and 21E, were placed using a 50–50 aggregate blend of siliceous river gravel and crushed limestone. The purpose of these sections was to establish placement characteristics of blended mixtures and to determine if the crack patterns of the blended sections would fall between those of the SRG and LS sections, as was the case for the properties of the lab specimens prepared in Research Study 1244 (Ref 2). The variables in the eastbound section included time of placement; saw cuts (transverse and longitudinal), steel percentages, skewed steel, and curing technique.

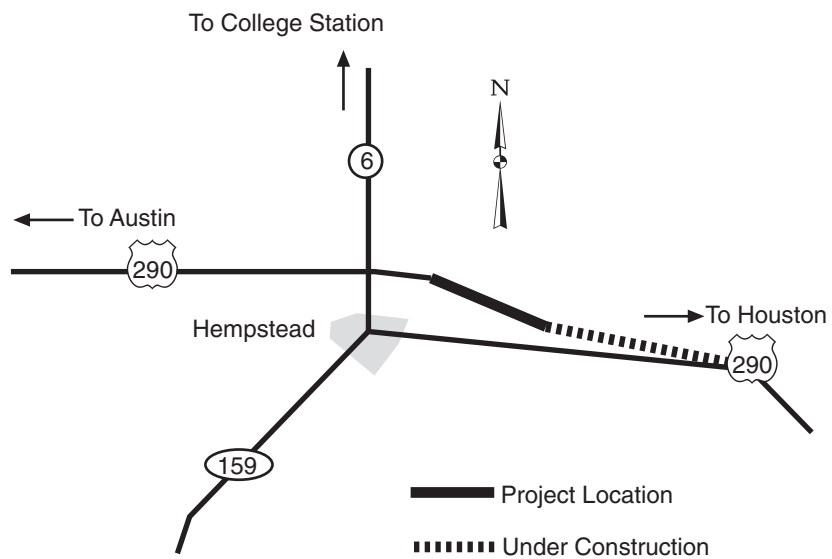


Figure 1.13 Test sections in Hempstead, Texas (Project 8)

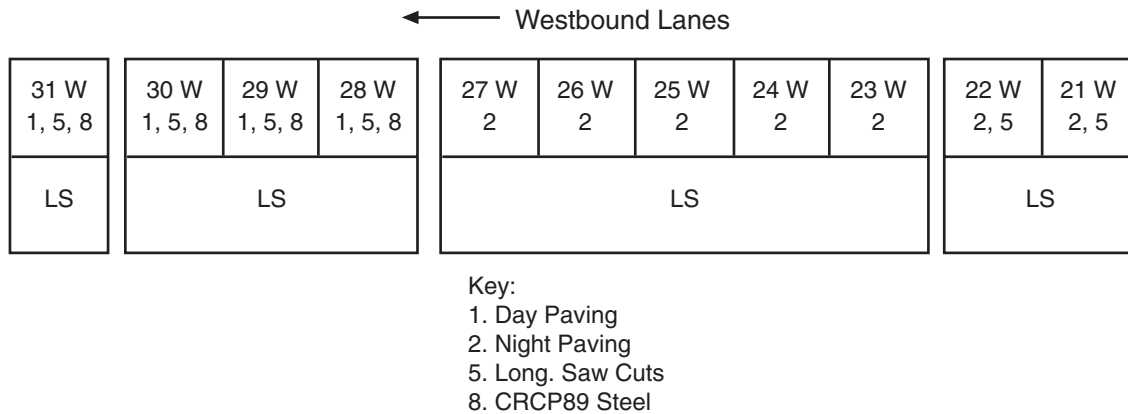


Figure 1.14 Test section layout — Westbound lanes

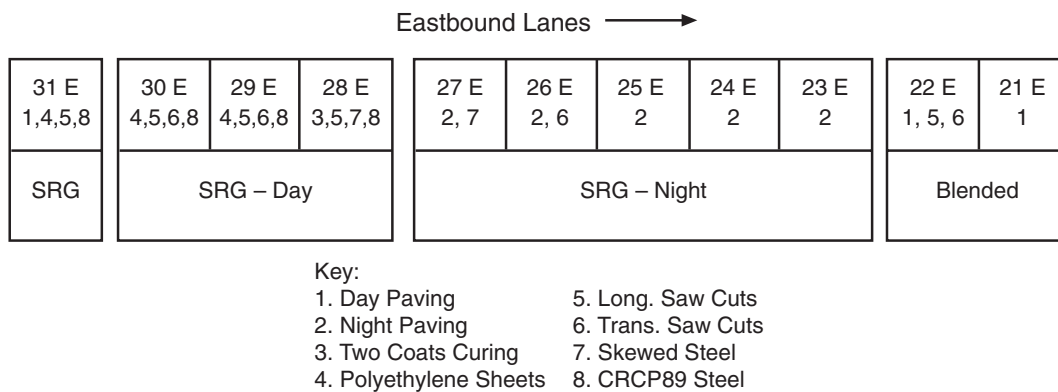


Figure 1.15 Test section layout — Eastbound lanes

1.5 REPORT OBJECTIVES AND SCOPE

The overall objective of this report is to summarize all the findings, data, conclusions, and recommendations developed not only in Projects 1–8 (shown in Figure 1.4), but through other previous experience as well. By combining all the available data, a summary of the most current understanding on how to improve the performance of concrete pavements, especially CRCP, should be developed. More specifically, the report subobjectives are to:

1. Discuss the findings of each project considering such performance indicators as crack spacing, crack width, crack control, spalling, crack randomness, and evaporation-rate-induced strength loss, with such discussion focused on improving pavement performance.
2. Develop concrete pavement placement guidelines that may be utilized to improve the long-term performance of CRCP.
3. Develop guidelines for selecting coarse aggregates.
4. Use the observed performance indicators and variables to validate the CRCP-8 program and to improve its capability of predicting performance to aid in design, construction, specifications, and diagnostic work.
5. Identify the spalling mechanism and then model it.
6. Support the present efforts in developing a performance-oriented QC/QA specification for PCC and provide future guidelines for modifications.

The overall scope of this report is to summarize the observations, trends, conclusions, and recommendations developed in connection with Projects 1–8. Thus, the material will be documented for use in planning, designing, and constructing CRC pavements.

Chapter 2 compares and contrasts the experiments and monitoring procedures used for each project. The normal performance indicators, such as crack spacing, crack width, and spalling, are described and new ones, such as crack randomness and tensile strength distribution vertically through the slab, are added.

Chapter 3 describes the results and findings obtained from the Cypress (Project 7) and Friendswood (Project 8) field test sections. These studies predate the Hempstead field testing and helped to set the parameters for that later experiment.

Chapter 4 discusses observations of the trends in the performance indicators relative to the performance variables. Chapter 5 then conceptually describes the spalling mechanism and the variables affecting the development. Chapter 6 describes the coefficient of thermal expansion (CTE) and the procedures for measuring it in general and specific terms.

Chapter 7 presents the validation of the CRCP-8 crack spacing and distribution algorithms using the data from Projects 1–4 and 8. Chapter 8 discusses the results in terms of improving performance and predicting performance; areas needing additional developments

are also identified. Chapter 9 presents the conclusions and recommendations developed in this project. Appendix A then presents the crack distribution over time for Projects 1–4 and 8. Appendix B compares crack distribution for the test sections with variable steel percentage for Projects 1–4. Appendix C compares crack distribution for test sections with varied reinforcement bar diameters for Projects 1–4. Appendix D compares crack distributions for test sections with different placement seasons for Projects 1–4. Finally, Appendix E presents the spalling model.

CHAPTER 2. FIELD EXPERIMENTS AND MONITORING

In order to evaluate performance differences, it is important to decide which variables may be important to pavement performance and to then find methods to monitor differences in those variables. In this chapter, the projects discussed in Chapter 1 will first be discussed in terms of the experimental variables that affect performance. Then, the methods used to evaluate performance differences will be discussed (i.e., performance indicators). Finally, the chapter provides the fundamental properties of the performance variables that are used to define performance differences.

2.1 EXPERIMENTAL VARIABLES

Nine experimental variables evolved directly (controlled) or indirectly (uncontrolled) over time for these eight projects. Table 2.1 shows the variables evaluated in Projects 1–8 (Ref 3). Notice that not all the variables were evaluated in each project. For example, in Project 1–6, the standard curing technique was not varied. The paving dates reveal the projects represent ages from 2 to 8 years old at the time of data analysis for this report.

Table 2.1 Factorial of variables for Projects 1–8 developed in Projects 0-1244 and 7-3925 (Note: 1 in. =2.54 cm)

Factor	Level	Project							
		1 Patterson	2 Huffmeister	3 BW-8	4 IH-45	5 SH 225	6 Friendwood	7 Cypress	8 Hempstead
Aggregate Type	SRG	Yes	Yes	Yes	Yes	Yes	Yes	Yes	Yes
	LS	Yes	Yes	Yes	Yes	No	No	Yes	Yes
	Blended	No	No	No	No	No	No	Yes	Yes
No. of Diff. Steel Percentages		3 per Aggregate	3 per Aggregate	3 per Aggregate	3 per Aggregate	Not Varied	Not Varied	Not Varied	1 per Aggregate
Bar Size		#6 and #7	#6 and #7	6 and #7	#6 and #7	Not Varied	Not Varied	Not Varied	Not Varied
No. of Steel Mats		1	1	1	1	1	1	2	2
Curing Types	Standard	Yes	Yes	Yes	Yes	Yes	Yes	Yes	Yes
	2 Coats Curing	No	No	No	No	No	No	Yes	Yes
	Poly Sheets	No	No	No	No	No	No	Yes	Yes
Saw Cuts		No	No	No	No	Yes	Yes	Yes	Yes
Skewed Steel		No	No	No	No	Yes	No	No	No
Thickness		11"	11"	10"	15"	13"	10"	13"	—
Paving Time		Day	Day	Day	Day	Day	Day	Day	Day/Night
Paving Date		Jan 90	June 89	Nov 89	Jan 90	Nov 92	Nov 93	Aug 92	95
Paving Season		Winter	Summer	Fall	Winter	Fall	Fall	Summer	Summer

MONITORING PERFORMANCE INDICATORS

Since the initiation of the CRCP condition surveys and the development of the CRCP programs (Refs 11 and 16), the important performance indicators considered have been:

1. Average crack spacing
2. Average crack width
3. Steel and concrete stress
4. Punchouts
5. Spalling

With time, it has been found that the crack spacing distribution must be included, since small crack spacing eventually lead to punchouts. In addition, studies have also shown that the nature of crack randomness and intersections also leads to punchouts (Ref 10). Finally, the vertical distribution of tensile strength also leads to spalling, thus, it is also a performance indicator (Refs 18, 19). All of the performance indicators with the exception of steel stress and punchouts were used on these projects. The project budget did not permit the installation of strain gauges and punchouts have not occurred at the time of this report.

To characterize the results of the experiments, five performance indicators were used: crack spacing distributions, crack width measurements, crack spalling, Crack Randomness Index (Ref 10), and the vertical profile of tensile strength. Using these indicators, Projects I8 were surveyed periodically to view trends in the pavement condition (Ref 7).

CRACK SPACING — DISTRIBUTION AND AVERAGE

In CRC pavements, cracks are allowed to develop randomly over time. However, the pavement is designed to produce a stable crack spacing after a year or two that generally has a mean value between 3 ft (0.91 m) and 8 ft (2.43 m). If a high percentage of the cracks are less than 3 ft (0.91 m) apart, punchouts can become a severe problem with time. Conversely, if the crack spacing is too large, the stress in the steel can become large enough to cause yielding.

The test section crack spacing was surveyed frequently as shown in Table 2.2. Previous studies have shown that crack spacings generally change rapidly during the initial period, then stabilize after one year and hold relatively constant until pavement wear out phase is experienced as shown in Figure 2.1 (Ref 15). Thus, all the crack patterns at the time of this report should be considered as stable, and all observations or conclusions relative to

crack spacing could be considered as long term. For example, Project 4 has been surveyed sixteen times since it was constructed. In Table 2.2 the number of surveys has been divided into two categories. The first category gives the number of surveys taken during the first year, while the second category contains the number of condition surveys that were taken after the pavement was 1 year old.

Table 2.2 Number of condition surveys taken on each project since the initial construction

Project	Project Age	Condition Surveys		
		First Year	After First Year	Total
1 – Patterson	7 Years	8	4	12
2 – Huffmeister	8 Years	7	5	12
3 – BW-8	8 Years	9	5	14
4 – IH-45	7 Years	12	4	16
5 – SH 225	5 Years	NA	1	1
6 – Friendswood	4 Years	5	1	6
7 – Cypress	5 Years	8	2	10
8 – Hempstead	2 Years	6	2	8

The crack spacing surveys are important during both early and late pavement life, because at these times trends can be established as to the formation of cracks. For example, in Project 8 some test sections were placed during the day, while others were placed at night. Cracks formed much more quickly in the sections that were placed during the day. For summer placements, studies in connection with Project 2 found that concrete pavements placed in the middle of the day have more erratic crack patterns; accordingly, a random index factor was developed as explained in a following section of this chapter (Ref 6).

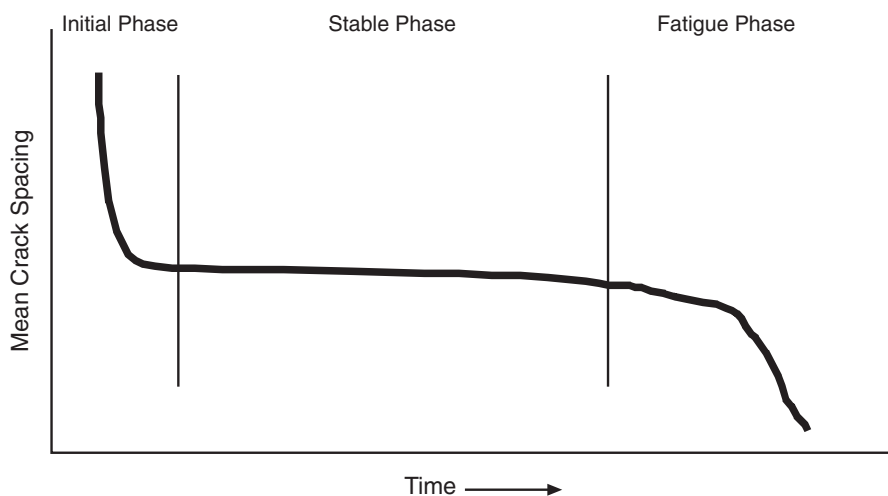


Figure 2.1 Conceptual phases in the life of a CRCP illustrating the reduction in mean crack spacing over time

Crack spacing is important in the design of CRC pavements. By monitoring the rate of cracking over time, the percentage of cracks that are likely to cause failures in the pavement can be determined. This is done primarily by looking at the percentage of cracks that are less than 3 ft (0.91 m) apart. Although the number has been set at 3 ft (0.91 m) from experience, the primary criterion is that the minimum spacing be twice the bond development length of the bar. With values less than this, the continuity of the pavement is lost.

The cracks that are less than 3 ft (0.91 m) apart are often associated with punchout failures; the condition for future punchouts is established when transverse cracks or meandering cracks are very close together. Longitudinal cracks form, with traffic applications, when transverse cracks are close together, creating a lack of bonding and producing a condition of low-load transfer across the crack. Once two longitudinal cracks form between transverse cracks, a block of concrete can become isolated from the slab, i.e., a punchout. The only thing that prevents the block from moving independently from the slab is the aggregate interlock between the newly formed block and the remainder of the slab. As the crack widths increase over time, the block becomes free to move independently from the rest of the slab. When loads are repetitively applied to the block, it is pushed down into the

subgrade. After repeated loading, the block no longer provides continuity with the rest of the slab, leading to increased stress, failures in the surrounding concrete, and an uncomfortable ride.

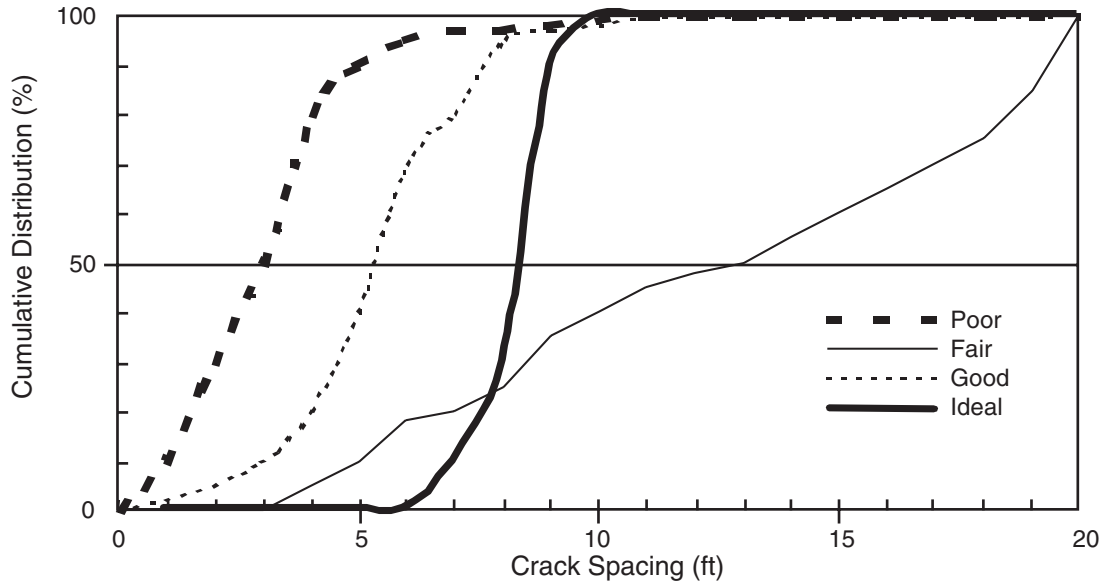


Figure 2.2 Conceptual crack spacing distributions

Crack spacing is, therefore, monitored in an attempt to predict punchout failures. Figure 2.2 shows four conceptual crack spacing distributions to demonstrate the range of conditions found in the field. Notice that the “ideal” crack spacing has all cracks at a uniform spacing between 5 ft (1.52 cm) and 8 ft (2.43 cm) apart. The “poor” distribution results when punchouts are likely to occur due to a large number of small crack spacings, e.g., 50% of the spacings are less than 3 ft (0.91 cm) for the illustration. The exact percentage has not been established at the present time, but should be the objective of future studies. The “fair” distribution has a small number of crack spacings less than 3 ft (0.91 cm), but may not be desirable because the steel stress may become too high since the cracks are very far apart, especially with SRG coarse aggregates. The “good” distribution represents realistic acceptable crack spacing because only 10% of the cracks are less than 3 ft (0.91 cm) apart.

The focus of this research has been to produce crack spacing distributions that are as close to an ideal distribution as possible. Efforts have been focused in altering the steel

percentage, reinforcement bar size, placement season, placement temperature, and aggregate type to accomplish that goal.

CRACK WIDTH

The pavement's crack width is important in CRC pavements, and generally should be no more than 0.025 in. (0.63 mm) at 32°F (zero degrees centigrade), i.e., the freezing point of water. Steel is, therefore, used in CRC pavement to resist the concrete contraction so that the crack widths will remain small. By so doing, water will not penetrate the pavement and load transfer is maximized. As the crack width increases the load transfer due to aggregate interlock is reduced. Eventually, deflection spalling will occur at the cracks.

For design temperatures below freezing, the crack widths may be more than 0.025 in. (0.63 mm), since the frozen conditions will not permit penetration of water. If the cracks are larger than 0.025 in. (0.63 mm) and material enters into them, crushing or other distresses of the pavement can result as the cracks attempt to close when hot or moist conditions prevail. If that occurs, the pavement can no longer function as it was designed.

CRACK SPALLING

Spalling occurs when small pieces of concrete are sheared off from the main concrete slab in the area of cracks or joints. The two major forms of spalling are called "deflection spalling" due to traffic load and frequency, and "delamination spalling." Deflection spalling occurs at the cracks, while delamination spalling generally starts at the crack and progresses away from cracks for some distance.

The distress caused by delamination spalling is related to the evaporation rate at the time of pavement construction. Delamination spalling is caused by a rapid change in the concrete moisture content near the surface of the pavement and, consequently, leads to differential moisture induced stresses in the pavement. The pavement then develops horizontal cracks below its surface. Although not apparent at the time of construction, the material above the horizontal cracks will shear out and will produce a surface indentation as shown in Figure 2.5.

If the evaporation rate is low, the delamination is likely to occur near the surface. As the evaporation rate increases, the rapid change in the moisture content will occur lower

down in the pavement. Therefore, when the pavement begins to spall, the spall depth will be greater in pavements with a high evaporation rate.

When shallow delamination spalling occurs, only the surface of the concrete is affected. Therefore, it is not as significant a distress to the pavement. Deep spalling, however, is often a much greater concern in pavement performance since it is usually 10 in. (2.54 cm) to 25 in. (6.35 cm) deep. With severe spalls, rehabilitative steps are often necessary because severe spalling produces a poor riding quality. Design and construction steps were taken in several of the test sections on Projects 7 and 8 to reduce spalling. Their effectiveness is evaluated based on the amount of spalling in the test sections.



Figure 2.3 Example of deep delamination spalling

CRACK RANDOMNESS

Cracks that meander to an extreme degree are more likely to be involved in a punchout. In fact, punchout pavement failures are invariably associated with very closely spaced cracks, generally, less than 2 ft (0.60 m) apart, or meandering cracks (Ref 4). Secondary cracks often form near meandering primary cracks that come close together, while relatively straight cracks do not often have many secondary cracks unless they are very close

to other cracks or a joint (Figure 2.4). Once the secondary cracks form, punchouts will follow.

It is often difficult to characterize the extent to which cracks meander when conducting a condition survey, since cracks are more easily described qualitatively than quantitatively. Attempting to overcome this difficulty, several methods have been proposed to quantify the variability of cracks. The measure of crack variability chosen for use on these projects was the Crack Randomness Index (Ref 10).

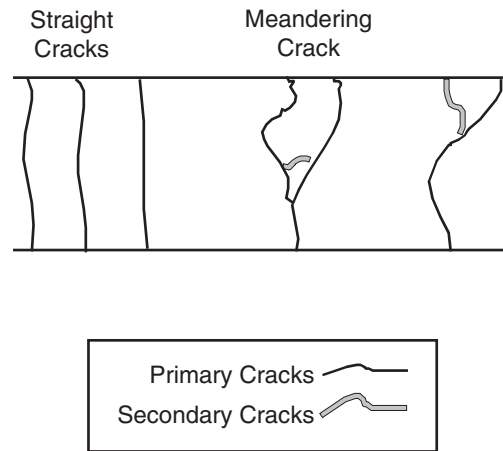


Figure 2.4 Typical types of cracking (Ref 10)



Figure 2.5 Definition of terms used to determine R

The Crack Randomness Index uses two quantitative aspects of a crack to evaluate its variability (Eq. 2.1). The first part of the randomness index is the crack length. The crack length (L) is measured by following the crack along its length across a lane using a distance-measuring wheel such as a Roll-A-Tape (Figure 2.5). Then the lane width (W) is measured. The crack length (L) divided by the lane width (W) gives the term “R” used in Equation 2.1.

$$RI = \frac{5.463}{(R+1)^{0.259}(N+1)^{0.510}} \quad (2.1)$$

where

$$R = \frac{L-W}{W} \times 100\% ,$$

L = length of the crack measured along the crack (Figure 2.3),

W = lane width (Figure 2.4), and

N = number of blocks of concrete that are enclosed by joints, edges, or cracks (Figure 2.6).

After finding the value of the two terms, Equation 2.1 can be used to calculate the randomness index for the crack. The equations yield values of randomness from 0 to 5.46. (A perfectly straight line has a value of 5.46.)

The equation for randomness index places a very large emphasis on the “N” factor. Mildly meandering cracks can still score fairly high on the Randomness Index (RI) if the cracks do not intersect other cracks ($N=0$). This is due to the fact that the randomness index is used as a guide to predict punchouts. Punchouts are usually concentrated in an area with intersecting cracks or “Y” shaped cracks.

The second term in the equation describes the likelihood that the crack will form a punchout based on its shape. This term is called “N.” It stands for the number of concrete blocks that are enclosed by discontinuities such as cracks, joints, or the pavement edge as shown in left side of Figure 2.6 (Ref 5). Notice that a “Y” crack has an “N” value of 1, while an “X” crack has an “N” value of 2. On the right side of Figure 2.6, typical values of RI are shown for a range of cases. The RIs at the top are for straight lines at various angles only, whereas in the lower part of the figure one block is assumed to be present. The range of RI

goes from 3.20 to 5.96 in this example, thus, one should remember that values of 3.0 are low. Note that values lower than 3.0 are possible, only if “X” cracking is present.

Using the information from Figure 2.6, a quantitative scale can be established to determine the quality of a crack based on the RI. The upper end of the poor range was set with extreme meandering and one block. The upper end of the fair section was set at the value where an occasional block crack appears. The remainder of the scale was divided between good and excellent. This method will be further illustrated in Chapter 4.

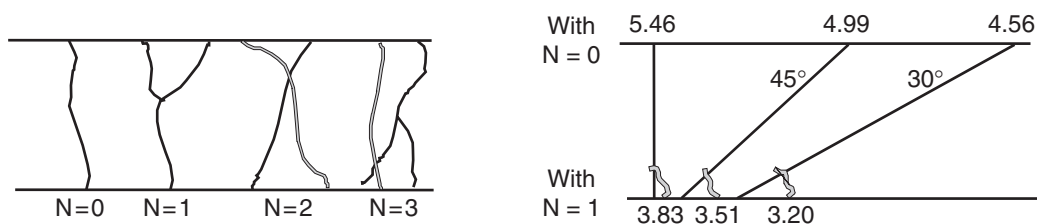


Figure 2.6 Definition of N for use in the randomness index equation and typical examples (Eq 2.1)

2.2 EVAPORATION-INDUCED STRENGTH LOSS

The final part of monitoring that will be discussed is the relationship between concrete’s evaporation rate and tensile strength. The relationship between concrete evaporation rate and early-age plastic shrinkage cracking is well documented (Ref 17). (Early-age plastic shrinkage cracking in concrete is closely related to high evaporation rates.) However, the relationship between concrete’s evaporation rate and tensile strength distribution is not as thoroughly understood at the present time. However, the premature occurrence of distress types such as spalling and punchouts generally attributed in a gross way to construction “problems” or “deficiencies” may be directly related to this phenomenon. Thus, in the following subsections, a hypothesis conceptual strength loss mechanism occurring vertically through the pavement is described. This is followed by a conceptual discussion of how the results from field-testing would look are discussed. Not stated or investigated is the extension of the hypothesis that these vertical variations will lead to significant variations by location in the slab.

CONCEPTUAL STRENGTH LOSS MECHANISM HYPOTHESIS

Whenever the evaporation rate is high enough to pull water from the surface of the concrete faster than the bleed water can replace it, damage will occur to the concrete. That damage may be in the form of plastic shrinkage cracking or strength loss. Both of these factors may lead to delamination spalling or premature failure.

Experience has shown that concrete specimens have reduced tensile strength when exposed to high evaporation rates. The reason for the difference is based on the effect produced by water leaving the concrete at different evaporation rates. If the evaporation rate is low, the bleed water reaches the surface faster than it evaporates; consequently, no strength loss occurs.

As the evaporation rate increases, the surface becomes dry, and water normally used for the hydration process is pulled from the top layer of the slab (Figure 2.7). Figure 2.8 shows this same concept from a different perspective. Considering the slab's relative humidity, notice that it stabilizes very quickly when the evaporation rate is low to moderate. Therefore, the upper concrete is much more significantly affected by the moisture differential than the lower concrete.

As the evaporation rate continues to increase, the upper part of the slab becomes so dry that the water that would normally be used for hydration is pulled from successively lower layers of the slab. So when the evaporation rate is high, the relative humidity of the slab drops throughout the slab (Figure 2.9). Obviously, the moisture loss in the top will always exceed the moisture loss in the lower portions of the slab. Any evaporation rate greater than 0.2 lb/ft²/hr (0.976 kg/m²/hr) is high enough to consider delaying placement until the evaporation rate drops (Ref 17).

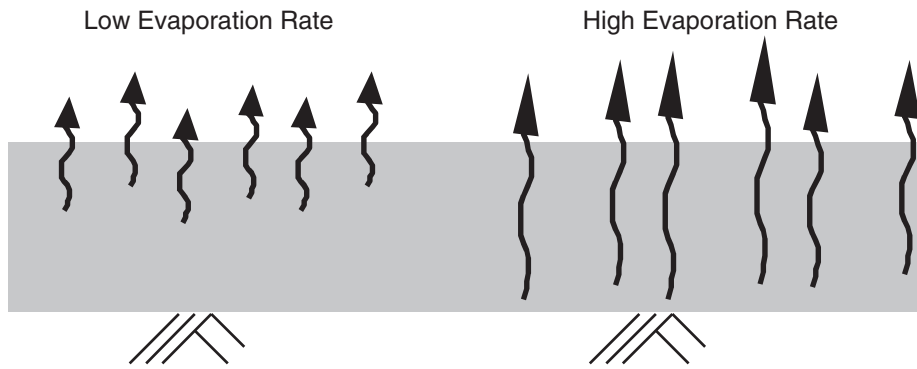


Figure 2.7 Effects of a different evaporation rates on concrete slabs

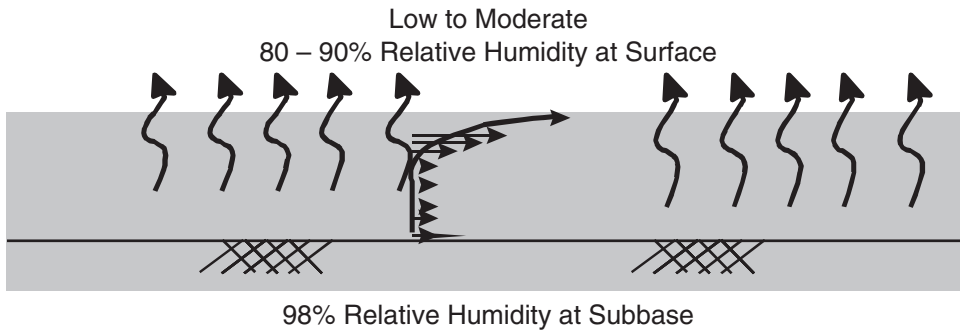


Figure 2.8 Effect of a low evaporation rate on relative humidity of a slab

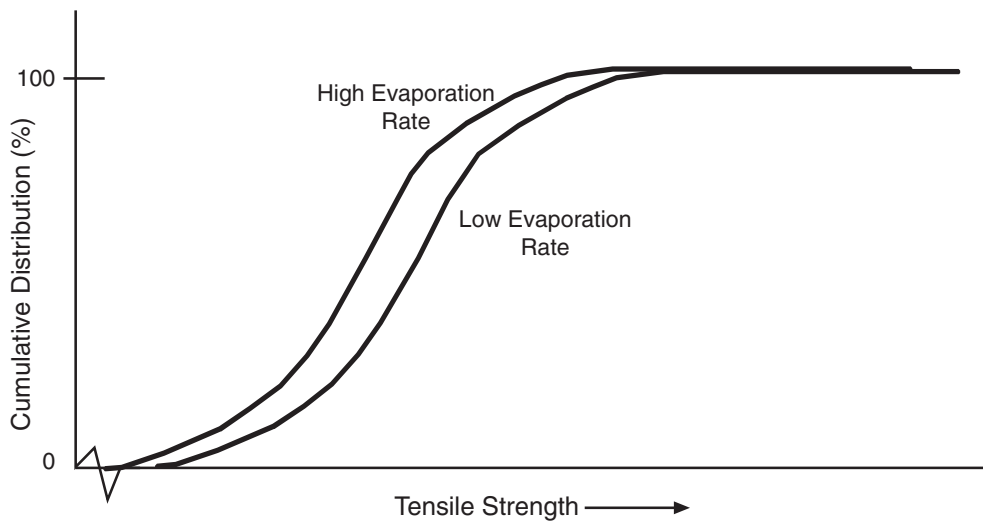


Figure 2.9 Cumulative strength distribution of the top part of concrete cores

CONCEPTUAL RESULTS FROM HYPOTHESIS

The hypothesis can be verified by testing concrete cores at different layers. The results can then be compared with evaporation rates to determine if evaporation rates have a significant effect on core strength.

The next step is to determine an effective way to view and compare the results. If several cores are taken in concrete poured at times of high and low evaporation rates, a cumulative strength distribution can be used to show the effects of evaporation rate on tensile strength. The strength of the upper layers can then be compared directly at different evaporation rates. Figure 2.10 shows how these results should appear. The strength distributions should be similar in the upper layers for both high and low evaporation rates.

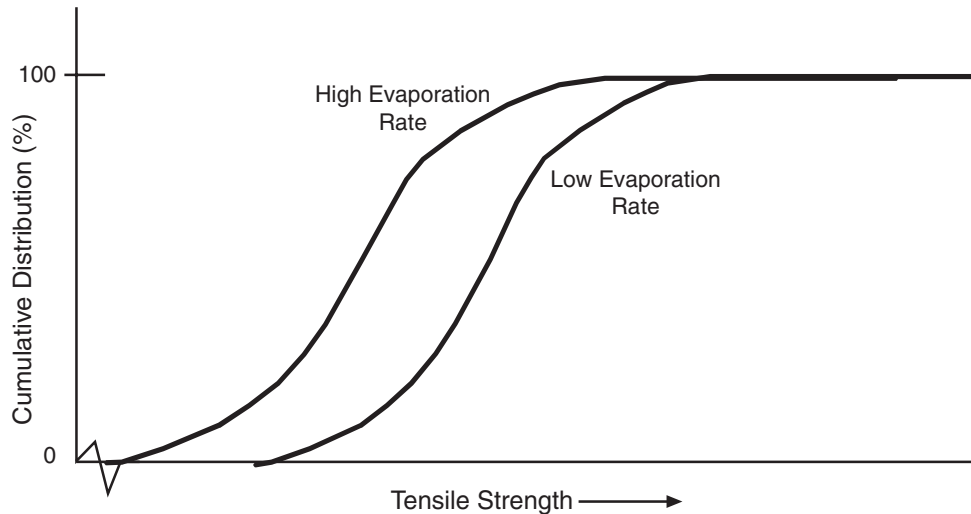


Figure 2.10 Cumulative strength distribution of the bottom part of concrete cores

In the lower layers, the strength distribution should not be so uniform. The strength at the bottom should be significantly different for high and low evaporation rates in the lower concrete layers (Figure 2.11). Notice that the low evaporation rate does not significantly affect the strength of the bottom layer of concrete. However, the high evaporation rate can

produce a strength drop all the way through the pavement. Field data will be introduced in Chapter 4 to evaluate this hypothesis.

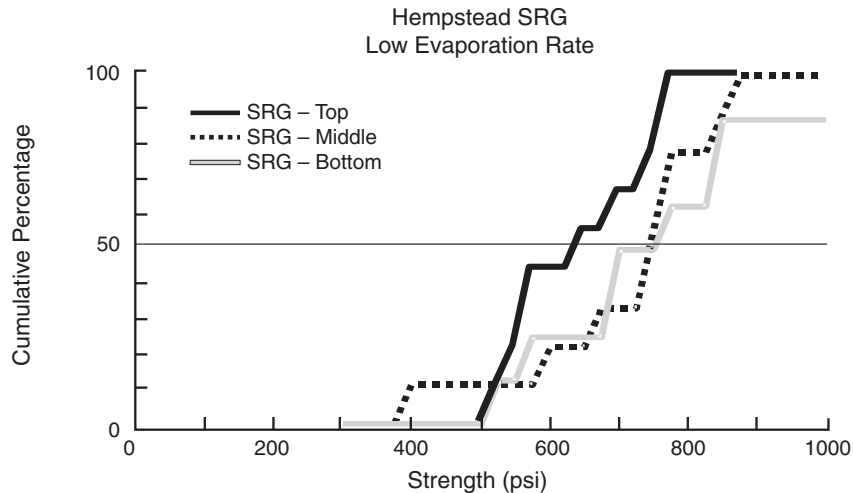


Figure 2.11 Example of a cumulative strength distribution plot

2.3 PERFORMANCE VARIABLES

After deciding what tests should be used to monitor the pavements, it is important to look at how the concrete should be characterized. It is usually considered best to characterize materials by their fundamental properties; that is, by looking at strength or other such material properties. These properties are called *performance variables* because they affect the performance of the concrete. The performance variables monitored in these projects include factors relating to concrete properties and environmental conditions at the time of paving.

The performance variables related to concrete properties that were monitored in this experiment are strength (mean and strength profiles), strain, shrinkage, modulus of elasticity, and coefficient of thermal expansion. The factors monitored related to paving conditions were concrete and ambient temperature during construction, concrete evaporation rate, solar radiation, and humidity. These variables were monitored because they were deemed important to pavement performance.

Concrete strength is widely recognized as an important factor in pavement performance. Since concrete fails primarily in tension, tensile strength was monitored in this

experiment. Several samples were tested for each test section so the results could be analyzed to compare different test sections. The results from this experiment have been analyzed by comparing both the mean strength and the cumulative strength distribution. The cumulative strength distribution was used to analyze the data because it shows all the data points, not just the mean. Figure 2.12 shows a typical cumulative strength distribution plot.

Using the cumulative strength distribution plot, the maximum, minimum and median values can easily be determined. Different sections can also be compared using cumulative strength distributions.

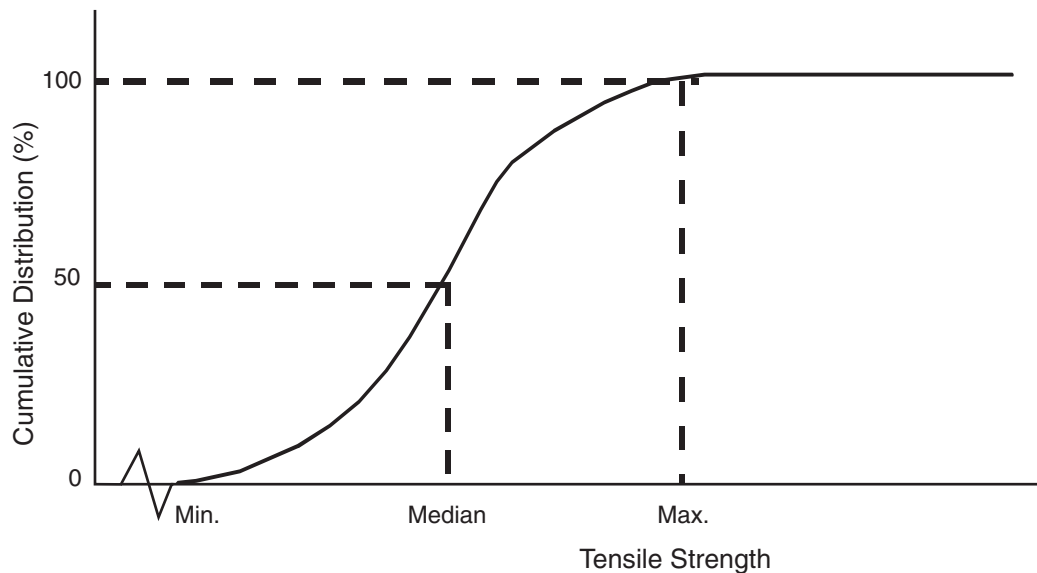


Figure 2.12 Typical cumulative strength distribution

It is also important to monitor the strain in the pavement because strain and strength are essential to predicting crack development. Strain can be induced by a variety of factors, including shrinkage, moisture, thermal, and load-related effects.

To be able to evaluate the stress in the pavement, some appropriate coefficients must be known. For example, stress is often caused by a combination of factors. The stress may be induced by load and thermal changes. If the modulus of elasticity and coefficient of thermal expansion are known, the stress condition can be determined.

The environmental conditions during paving are also important when evaluating a pavement's behavior and performance. If the evaporation rate is high, the pavement will experience both vertical and horizontal plastic shrinkage cracking more than pavements placed when a low evaporation rate is present.

Factors affecting the concrete evaporation rate include the air and concrete temperatures, the humidity, and wind speed. Curing techniques can be used to control the concrete evaporation rate such as curing compounds, cotton mats, paper, or water.

2.4 SUMMARY

The studies represented by Projects 1–8 considered a large number of experimental variables that were known to affect pavement performance. The pavement performance was evaluated by monitoring the performance indicators of crack spacing, crack width, crack spalling, crack randomness, and vertical strength loss. Fundamental properties that relate to pavement performance are called *performance variables*. Performance variables studied in this project include strength, concrete constituent properties (e.g., coefficient of thermal expansion), and environmental variables (e.g., evaporation rates around the time of paving).

CHAPTER 3. CYPRESS AND FRIENDSWOOD FIELD SITES

The focus of the field investigations was (1) to make observations on how coarse aggregate type affects pavement performance at an early age during construction, and (2) to examine methods to ensure that the final crack spacing will fall into a desirable range suitable for optimizing the performance of the pavement system. It was determined during field investigations that it is difficult to eliminate “Y” cracks and other defects (e.g., closely spaced transverse cracks) by adjusting only the amount of longitudinal steel. The difficulty in eliminating these defects is primarily to the variability of material properties, construction factors, and environmental conditions that are to some extent outside a contractor's control. Moreover, the early-aged cracking behavior of CRC pavements is affected significantly by coarse aggregate type and by ambient temperature conditions at the time of paving. Because this has been a concern for some time, efforts were undertaken to better understand these factors and their influence on CRC performance during construction.

In presenting data obtained from project test sections, this chapter summarizes the influence of the above factors on crack development in CRC pavements under field conditions. This information has played a key role in developing construction guidelines that can enhance CRC pavement performance. The sections that follow will describe these efforts and some of the experiments conducted to better understand and improve the performance of CRC pavements.

3.1 EXPERIMENTAL PAVEMENT SECTIONS TO IMPROVE CRACK PATTERNS

CRC pavement test sections examining coarse aggregate effects on pavement crack patterns in light of different crack control and curing methods were constructed on Highway 290 in Cypress and in Friendswood, Texas. The information obtained from these sections provides a basis for suggesting specifications for the construction of CRC pavement using different coarse aggregate types. Although discussed in greater detail later, the Cypress test section was useful in examining the factors that affect cracking behavior of CRC pavement under hot weather conditions (given that the construction took place in August 1992). These

test sections included a variety of methods deployed to control transverse cracking in CRC pavements under field conditions. These methods involved:

- shallow transverse sawcuts in the pavement surface,
- metallic crack inducers placed in various configurations, and
- transverse reinforcement.

Sawcutting techniques and crack inducers were used to control, on an experimental basis, the transverse crack locations at prescribed intervals. Transverse rebar and inducer locations were documented prior to initiating concrete paving operations.

FIELD TEST IN FRIENDSWOOD, TEXAS (PROJECT 6)

As previously noted, the CRC pavement test section on FM 528 in Friendswood, Texas, was constructed in November 1993 under cool weather construction conditions. This test section consisted of special crack control sections that were developed as a result of experimental crack sections constructed in the Cypress project described later in this chapter.

FIELD OBSERVATION OF CRACKING

To observe the formation of cracking, the entire experimental section in Friendswood was surveyed for transverse cracks on November 11, 18, and 25; on December 8, 1993; and on February 4, 1994. The primary results are summarized below in Figure 3. 1, which shows the percentage of transverse cracks that occurred at specifically located Type I crack inducers (previously described in Chapter 1 and shown in Figure 3.2) with and without transverse sawcuts in TS 1. These crack inducers were affixed to the subbase and supported the longitudinal steel at 5 ft (1.5 m) intervals. The sawcut notches were aligned either with the inducer or between the inducers. In some cases the sawcuts were located at 5 ft (1.5 m) or 2.5 ft (0.8 m) intervals. The field observations indicated that it took 7 days or less for 100% of the cracks to be initiated by the Type I crack inducers without a sawcut notch. It took approximately 21 days for 100% of the cracks to be initiated by the combination of Type I crack inducers and sawcut notches. This may indicate that a Type I crack inducer may be more efficient in crack initiation than sawcuts under cool weather construction conditions. It is interesting to note that in the areas where the sawcut spacing was 2.5 ft (0.8 m), most

cracks occurred at 5 ft (1.5 m) intervals, except for two locations at 2.5 ft (0.8 m) intervals. No uncontrolled cracks were found in this section within the first four months after paving. On February 4, 1994, eleven concrete cores were taken with the assistance of personnel from the Houston District. Four cores were taken from the nonsawcut portion TS 1, which included twelve Type I crack inducers.

In TS2 (which was nearly identical to TS4), 6 in. (150 mm) plastic sleeves were centered at the cross points between the longitudinal and transverse steel to intentionally eliminate the bond between the concrete and the longitudinal reinforcement 3 in. (75 mm) in both directions from the transverse rebar, and to help initiate cracking at the transverse reinforcement. However, crack survey results indicated that the plastic sleeve did not function as a crack inducer. It seemed that there was very little difference between TS2 and TS4 in terms of crack pattern development for nonsawcut pavement sections. Table 3.1 shows that portion of crack survey data pertaining to the sawcut segment located in TS2. The length of this segment was approximately 100 ft (30.5 m) and contained eleven sawcut notches.

One of the sawcuts were made at 5 ft (1.5 m) intervals and five were made at 2.5 ft (0.8 m) intervals (for eleven total sawcuts). One random crack developed between two sawcuts spaced on 2.5 ft (0.8 m) intervals, which coincided with an existing transverse crack in the adjacent lane. It seems that a high potential of irregular cracking existed where the sawcut portion ended and the nonsawcut portion began, and between segments of different sawcut intervals. However, most random cracking, where it developed, occurred between sawcut notches. Some of these cracks were induced by existing cracks in the adjacent lane.

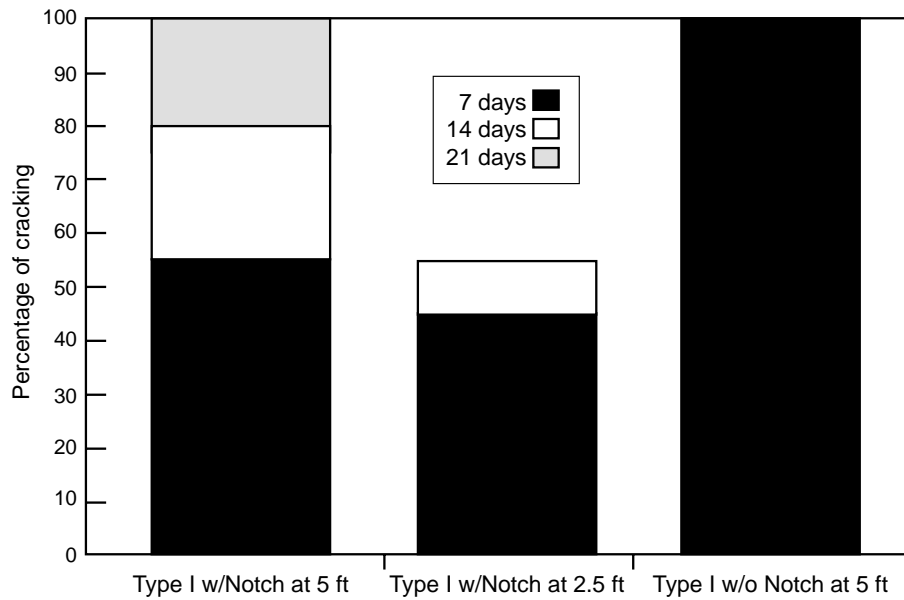


Figure 3.1 Percentage of cracks occurring at Type I inducers with or without a transverse sawcut (1 ft = 0.30 m)



Figure 3.2 Cores from nonsawcut part in subsection 1 where Type I crack inducer was located

Table 3.1 Crack survey data for sawcut section TS2 (1 ft=0.30 m)

Station No. (ft)	Distance from pts to pts	Notch (N) Rebar (R) Inducer	Date of Crack Survey					Remarks
			Nov. 11	Nov. 18	Nov. 25	Dec. 8	Feb. 4	
153+75	3.5	R						
	10	N+R	X					d
	5	N+R	X					d
	5	N+R	X					d
154+00	5	N+R						
	5	N+R	X					d
	5	N+R	X					d
	2.5	N+R						
	2.5	N+R						
	2.5	N+R						
	2.5	N+R						
	1				X			*see note
	1.5	N+R						
154+25	5	R						

On TS3, Type III crack inducers were used at 5 ft (1.5 m) intervals with and without notches at 2.5 ft (0.8 m) intervals. In the nonsawcut areas, it was found 7 days after paving that 100% of the cracks occurred consistently on one side of the inducers anywhere from 2 to 11 in. (50 to 280 mm) away from the original inducer location, which was apparently related to the direction of paving. Since the Type III crack inducers were located on the top of the longitudinal rebar, there was some concern that the crack inducers were disturbed by the placing operations.

On February 4, 1994, seven cores were taken from the nonsawcut part in TS 3 (which included fourteen Type III crack inducers). The distances between the centers of the cores and the original centerlines of crack inducers are listed in Table 3.2. The results of the core drilling (represented in Figure 3.3) verified that: (1) the locations of Type III crack inducers were disturbed by the paving machine and (2) the crack inducer did initiate transverse cracks.

Table 3.2 Deviate distances of cores from original places of inducers

Core No.	1	2	3	4	5	6	7
Deviate Distance	4.5"	4.0"	8.5"	11.0"	2.5"	2.0"	2.0"

Note: 1 in. = 25.4 mm



Figure 3.3 Cores from nonsawcut part in TS3 where Type III crack inducer was located

Figure 3.4 shows the percentage of cracks that occurred through Type III crack inducers with or without a sawcut notch in TS3, where Type III crack inducers were located on the top of transverse rebar at 5 ft (1.5 m) intervals. The transverse notches were also vertically located with inducers at 5 ft (1.5 m) intervals or between the inducers, but located

with the transverse rebar at 2.5 ft (0.8 m) intervals. We noted that it took 7 days or less for 100% of the cracks to be initiated by Type III crack inducers without sawcut notches. It took 21 days or less for 95% of the cracks to be initiated by a combination of Type III crack inducers and notches. Again, this finding verifies the conclusions that under cool weather paving conditions Type III crack inducers may be more efficient than surface notching for crack initiation purposes. Approximately 50% of the cracks occurred at 5 ft (1.5 m) intervals even in the subsection where the notch spacing was at 2.5 ft (0.8 m) intervals.

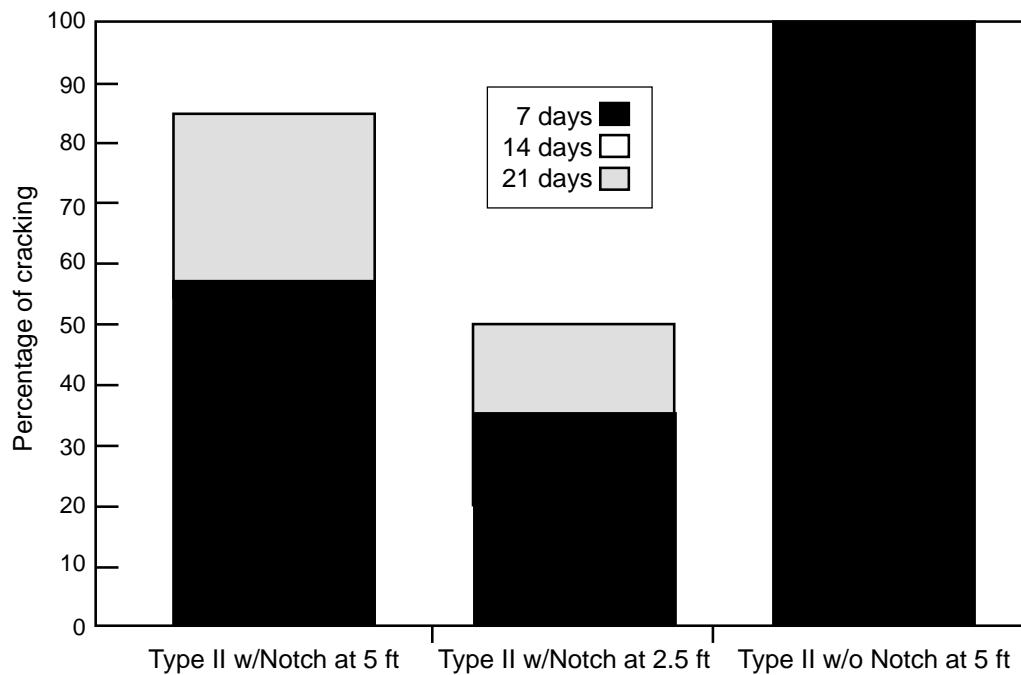


Figure 3.4 Percentage of cracks occurring at Type III inducers with or without notches (1 ft=0.30 m)

All of the cracking in the section of TS4 that consisted of transverse sawcut notches located or aligned with the location of the transverse reinforcement was controlled at 5 ft (1.5 m) intervals. This combination also appears to be acceptable for cool weather placement. It should also be pointed out that the complete surface crack pattern in the base was recorded on October 21 and 28, 1993. It was determined that no cracks were reflected from the existing cracks in the base, since none of the cracks in the slab matched those noted in the base.

STRAIN MEASUREMENT

After analyzing various possible strain measurement methods for concrete, vibrating wire strain gauges or extensometers were selected to obtain strain and temperature data associated with the curing process. The vibrating wire principle of strain measurement is very simple and well known. The strain experienced by the gauge changes the tension of the steel wire and, therefore, its natural frequency. The relation governing tension with frequency is:

$$f = \frac{1}{2l} \sqrt{\frac{TG}{m}} \quad (3.1)$$

where f is the natural frequency (Hz), l is the length of the wire between anchorages (m), T is its tension (Kg), m is its mass per unit length (kg/m), and G is the gravitational constant (m/sec²). Equation (3.1) can be rewritten to give the relationship between strain (ϵ) and frequency:

$$\epsilon = Qf^2 \quad (3.2)$$

where Q is the gauge constant $4l^2m/EGA$ (sec²), A is the cross section of the wire (m²), and E is Young's modulus for steel (N/ m²).

The strain gauge consisted of a thin steel wire held in tension between two anchorages. The wire is set into transverse vibration by exciting it with a short pulse of current passed through the coil of an electromagnet positioned near the midpoint of the wire. The same coil is then used to detect the frequency of the vibrating wire. When the distance between the anchorages changes, the tension of the wire and its natural frequency also change. This type of strain gauge has been used successfully to investigate not only the thermal strain of concrete at early ages, but also the long-term drying shrinkage strain of concrete.

Eight IRAD vibrating wire extensometers, EM-5 (commercially available), were used in TS4 to measure concrete strains and temperature. The layout of the embedded extensometers in the concrete pavement and the locations of the eight extensometers in the test section are shown in Figure 3.5. Three extensometers, EM-5 (3, 4, and 7) were placed longitudinally at different distances from the center of two adjacent notches to detect the

longitudinal variation of concrete strain after cracks occurred at the notches. Extensometers 2 and 3, and 5, 6, and 7 were stacked vertically to measure the vertical strain gradients near the notch (or crack) and at the center of the span, respectively. Extensometers 1 and 8 were placed at the edge of the lane longitudinally and at the center of the span in transverse direction, respectively. Figure 3.6 shows the photograph of the extensometers as fixed to the reinforcing rebars prior to casting. In order to prevent any random cracking between the two notches, the center transverse rebar at 2.5 ft (0.8 m) interval was removed and a specially designed device for measuring internal relative humidity was placed in the adjacent transverse rebar interval (see the white PVC pipe in Figure 3.6).

The Cypress test section consisted of a 13 in. (330 mm) thick pavement and contained a double layer of steel reinforcement. Since the paving for the Cypress project was performed during the month of August (under temperatures that ranged from 90 to 100°F [32 to 38°C]), the findings obtained from the Cypress section are relevant to concrete pavement construction under hot weather conditions as they would occur in areas of Texas. An important aspect of this field section was the development of a better understanding of crack development and the effect that curing has upon the spalling mechanism. Since aggregate bond strength plays a key role in the development of spalling, four different aggregate combinations (noted in Figure 3.7a and b) were used in the Cypress test site in the form of four different concrete mix designs. Since curing effectiveness also plays an important role in the development of spalling (along with development of the crack pattern), different curing methods were used within the test site to investigate the effect of curing method or type on CRC pavement crack performance. The effect of curing during placement in terms of the concrete temperature and relative humidity were measured by thermocouples and specially modified (commercially available) humidity sensors.

between the top and the middle of the pavement section, which is consistent with strain patterns that result in spalling distress.

FIELD TEST IN CYPRESS, TEXAS (PROJECT 7)

Transverse cracks were allowed to occur randomly — especially in parts I-A and II — or were controlled by inducers at prearranged locations in part III. Parts I-A and II were paved with four different types of mixtures and were allowed to develop random cracking patterns. In part I-A, which consisted of the uncontrolled cracking section, four mix designs were included. Mix designs 1 to 4 contained 100% limestone, 67% limestone and 33% river gravel, 67% river gravel and 33% limestone, and 100% river gravel, respectively, as previously indicated. Paving at the Cypress test section started in the early morning of August 20th. The crack patterns are characterized in Figure 3.7b relative to the number of transverse cracks per foot. Generally, the greater the siliceous river gravel content, the shorter the cracking interval and the greater the cracking density. The crack densities dropped off in placements made in the afternoon owing to lower paving and setting temperatures that develop at the end of the day.

Figures 3.8 and 3.9 show the crack spacing variation in each mix design as a function of the time of placement (morning versus afternoon). Not only was the time of initial crack occurrence delayed, but also initial crack spacing was reduced for all mix designs when paving occurred in the afternoon before 4 p.m. Concrete having more river gravel as its coarse aggregate had fewer uniformly distributed cracks and smaller average crack spacing than did concrete having more limestone. More cracks tended to occur at early ages in concrete having river gravel than was the case in concrete that used limestone as the coarse aggregate.

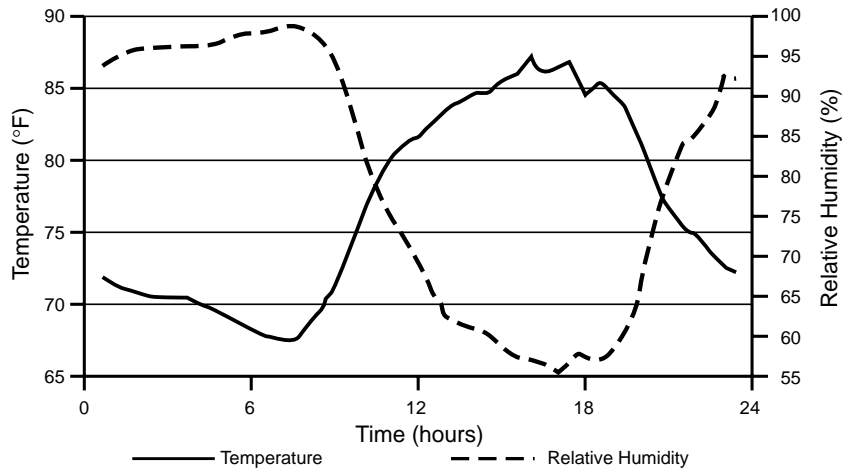


Figure 3.7a Cypress weather conditions during early-aged crack development

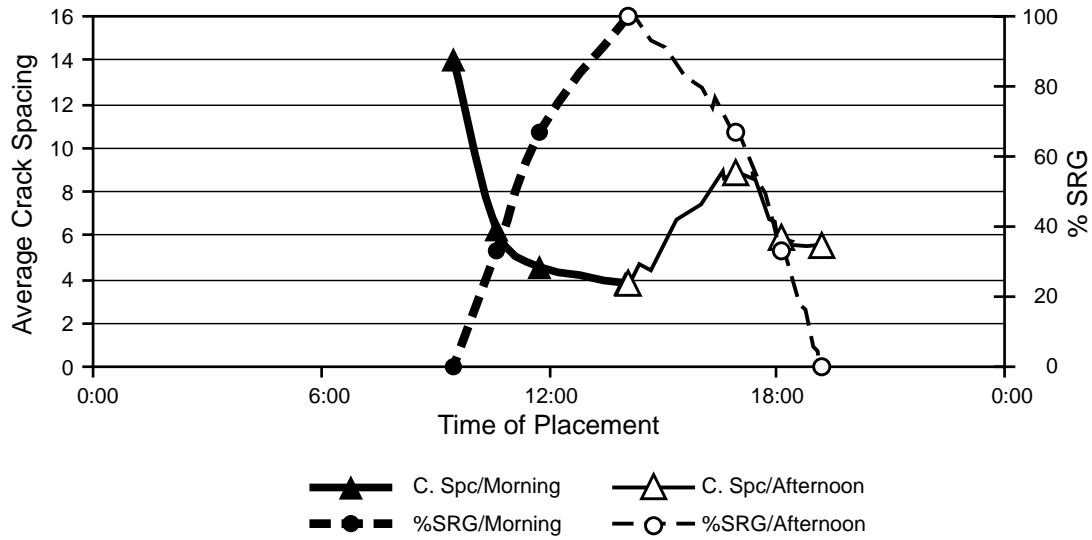


Figure 3.7b Early-aged crack development as affected by aggregate blends at Cypress — Part 1-A

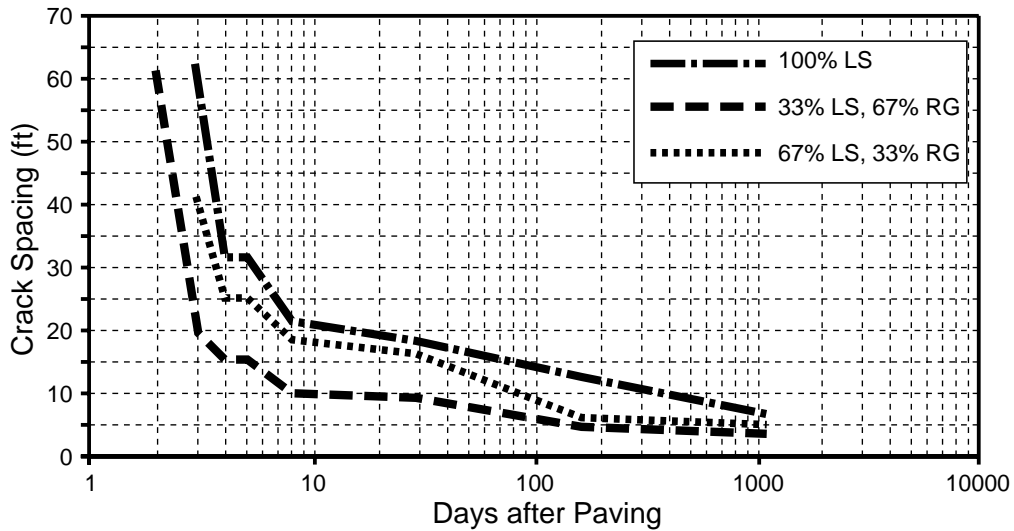


Figure 3.8 Uncontrolled cracking test sections placed in morning hours

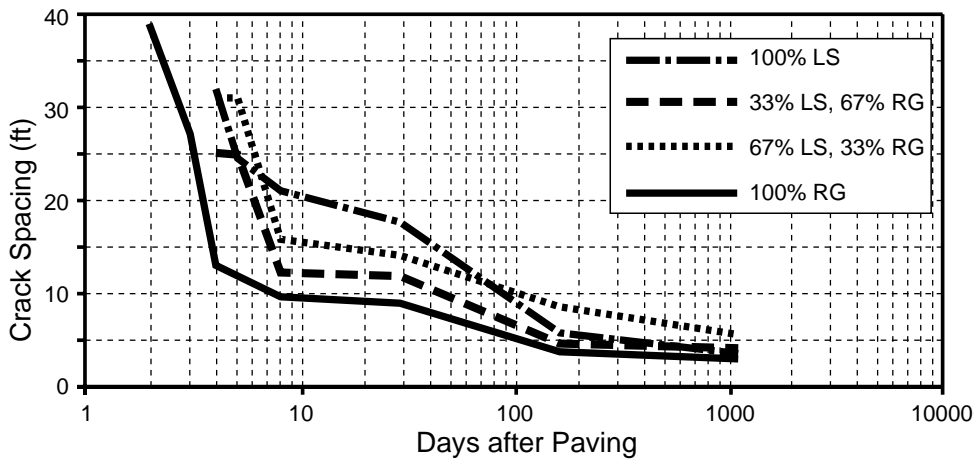


Figure 3.9 Uncontrolled cracking test sections placed in afternoon hours

The field results indicated that under the same environmental conditions, CRC pavement using limestone as the coarse aggregate had a larger average crack spacing than did CRC pavement that used river gravel as the coarse aggregate. Typically, the crack spacing ranged from 5 to 37 ft (1.5 to 11.2 m), with an average of 12 ft (3.6 m) for limestone concrete and a range of 2 to 10 ft (0.6 m to 3 m) (average of 4 ft [1.2 m]) for river gravel concrete. A design sawcut interval of 8 or 12 ft (2.4 or 3.6 m) may be achieved in concrete pavement

with limestone under some conditions, but it may not be achieved in concrete pavement with river gravel, particularly if constructed during the summer months.

It was found that the visible depth of most initial vertical cracks observed from the edge of the pavement was more than $4/5$ the pavement's thickness when they were first observed on the early morning of the third or fourth days after paving. The widths of early developing cracks (all were less than 0.38 mm [15 mil]) were larger than the widths of later developing cracks. This finding indicates that the history of crack formation development may affect the structural responses of CRC pavements and their associated long-term performance.

CRACK CONTROL SECTIONS

Crack induction was achieved by the use of shallow sawcut notches in the surface of the pavement or by the use of specially made and placed metallic crack inducers previously described. A layout of crack control methods and type of curing is provided in Table 3.3. Each of these methods consisted of Type III induction devices placed between the transverse reinforcing steel (whether it was in a staggered or stacked configuration), either in a single or double layer. A method of crack control included in Table 3.3 that was placed in part IV is shown in Figure 3.10.

Table 3.3 List of Cypress crack control sections

Location	Type of Crack Control	Spacing	Curing
Part I-B	Sawcut w/rebar	3, 6, and 9 ft	Type II, Linseed Oil
Part I-B	Sawcut between rebar and w/skewed steel	3, 6, and 9 ft	Type II, Linseed Oil, and Water-Based Compound
Part III-B1	Single and Double w/stacked rebar	4/5 ft	Type I, II
Part III-B2	Single and Double w/stacked rebar	6 ft	Type II
Part III-B3	Single and Double w/stacked rebar	9 ft	Type II
Part III-C1	Single and Double w/staggered rebar	4/5 ft	Type II
Part III-C2	Single and Double w/staggered rebar	6 ft	Type II
Part III-C3	Single and Double w/staggered rebar	9 ft	Type II
Part IV	Single between stacked rebar	3 ft	Type II

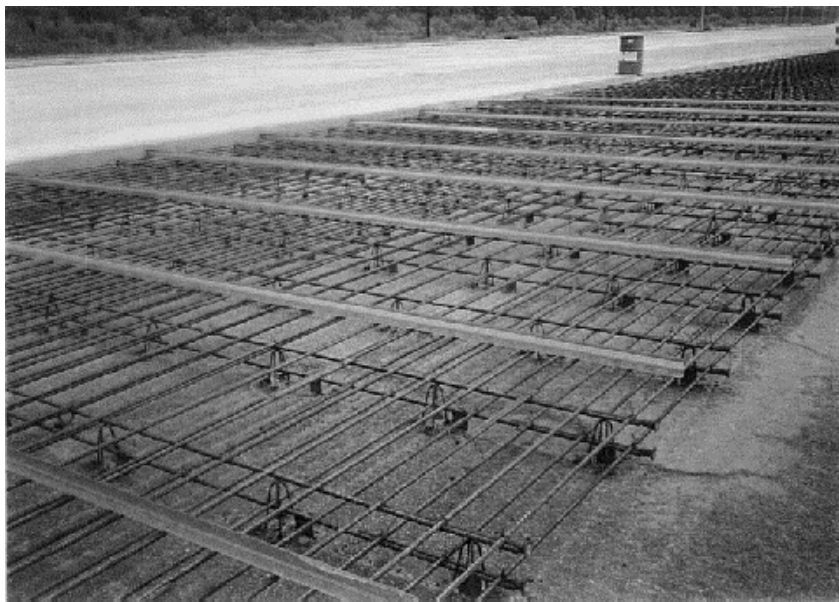


Figure 3.10 Type III crack inducer located on the top of longitudinal rebar— Part IV

In each of these placements it was of interest to observe if the Type III inducers could divert the crack location away from the location of the transverse reinforcement. It was interesting to note that several cracks were unintentionally controlled by the transverse reinforcement that is typically placed as part of normal pavement reinforcement to support the longitudinal reinforcement in position. A section in part I-B was placed with skewed transverse steel with reduced crack initiation on the transverse bar by approximately 50%.

Consequently, two methods were considered in the test sections constructed at the Cypress site for initiating cracks in CRC pavements. Early-aged sawcutting techniques were used (a Soff-cut® portable saw machine was employed) for surface notching, while the second method consisted of Type III crack inducers placed to initiate cracking at the interior of the pavement thickness. The length of the transverse crack control section was approximately 1,200 ft (365.8 m). Early-aged sawcuts were made about 4 hours later after placement with 3 ft (0.9 m) and 4/5 ft (1.2/1.5 m) combinations, and with 6 ft (1.8 m) and 9 ft (2.7 m) intervals.

Experience with early-aged sawcutting has indicated that notches should be made between the initial and final setting of the concrete. Timing is a very important factor in achieving the goal of artificial crack induction, particularly at shallow notch depths. Results from crack surveys conducted on these test sections have indicated that surface notches placed early (shortly after initial set has occurred) show very positive results, and that transverse cracking can be controlled by this technique. Comparisons illustrated in Figure 3.11 show that nearly 100% cracking occurred in the notches spaced at 3 ft (0.9 m) and at 4/5 ft (1.2/1.5 m) notch combinations approximately three days after paving the Cypress test sections. However, in the 6 ft (1.8 m) and 9 ft (2.7 m) sawcut interval sections, it took six days to reach 100% cracking at the notches after placement. As noted in Figure 3.11, secondary cracking occurred (after day 20) in the 9 ft (2.7 m) sawcut interval sections. A similar pattern was noted in the internally induced crack control sections that were similarly spaced. This finding may indicate that either the length of the sawcut interval should be increased for these conditions, or the design percent of steel reinforcement should be reduced to balance construction cost versus performance (as long as the desired crack widths are maintained). It should be noted that a 10% reduction in steel content offsets the cost of the

sawcutting. If the above-mentioned results are compared with the uncontrolled cracking in the Cypress sections, it can be found that it took several months to reach an average crack spacing of 6 ft (1.8 m) or even longer to reach an average crack spacing of 3 ft (0.9 m). The longitudinal contraction joint was also cut using the early-aged sawing method to a nominal depth of 1 in. (25.4 mm) in selected paving segments, as shown in Figure 3.12.

Unlike the notching technique that was used to initiate cracking on the surface of the pavement, crack inducers were used to initiate cracking from interior portions of the pavement. A variety of crack inducer configurations was installed in the Cypress section, part III. A sample of one of the configurations is illustrated in Figure 3.13. The performance of the Type III inducers is summarized in Table 3.4; it is noted that a greater percentage of cracks occurred at the double crack inducers than at the single crack inducers. However, the incidence of cracks that occurred at the Type III crack inducers is much less than that for the early-aged surface notches. Under the paving and weather conditions that prevailed during the placing of the Cypress test sections, there appeared to be a number of cracks that were not controlled by the Type III crack inducers; in addition, it was apparent that the early-aged sawcuts were more effective in controlling crack location in hot weather paving conditions. It was interesting to note that several cracks, in both the LaPorte (Project 5) and the Cypress test sections, were found to coincide with the location of the transverse reinforcement. Thus, it may be possible for the design engineer to take advantage of the positioning of the transverse steel in the control of transverse cracking in conjunction with early-age sawcutting. It is anticipated that if Type III crack inducers are embedded closer to the surface of the pavement (and if corrosion potential is not a concern). The majority of the cracks will form at the inducers where the stress is greater and the concrete is weakest.

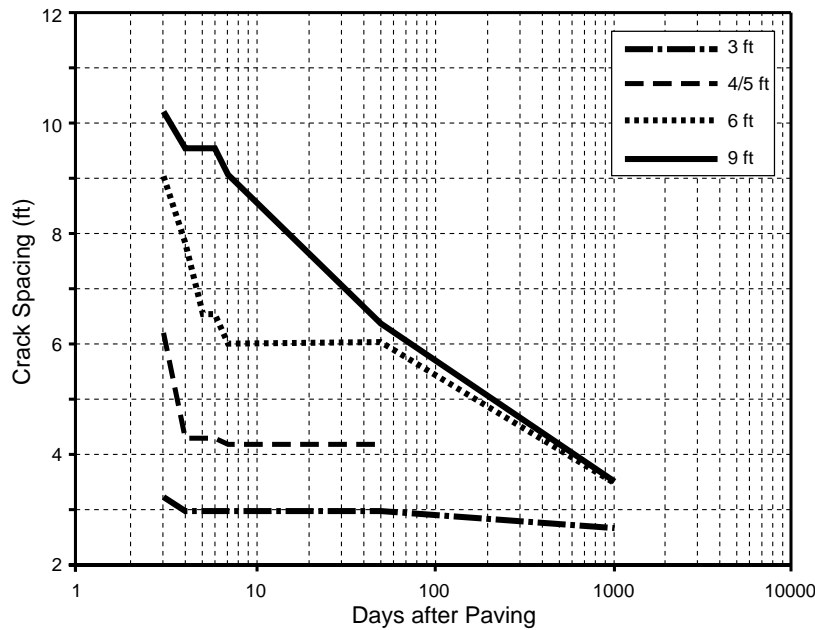


Figure 3. 11 Cracking development at sawcut locations

Table 3.4 Percentage of cracks initiated at a crack inducer

Location	No of Coatings	Spacing	Total No. of Cracks	No. of Cracks at Inducers	Total %
Part III B1	Double	4'5'	14	8	57.14
	Single	4'5'	15	6	40.00
Part III B2	Double	6'	17	8	47.06
	Single	6'	14	6	42.85
Part III B3	Double	9'	15	6	40.00
	Single	9'	25	-	-

As previously discussed, transverse rebar in CRC pavements is used (1) to support the longitudinal steel reinforcement at the desired vertical location during the construction process, and (2) to maintain the spacing of the longitudinal steel during placing operations. However, field surveys of the test sections undertaken during the first 30 days found that there are a certain percentage of cracks initiated by the transverse reinforcement, as previously noted. These surveys have indicated that the percentage of cracks initiated by the transverse rebar is about 50%; the percentage is even greater in concrete pavements

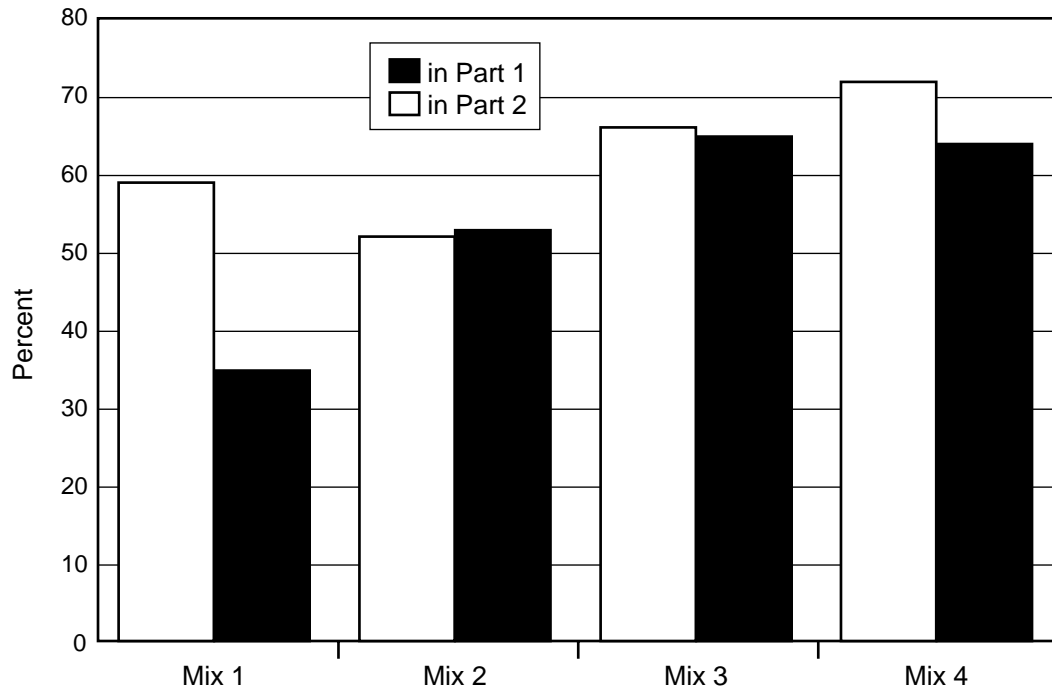


Figure 3.14 Percentage of cracks occurring at the rebar in the Cypress section

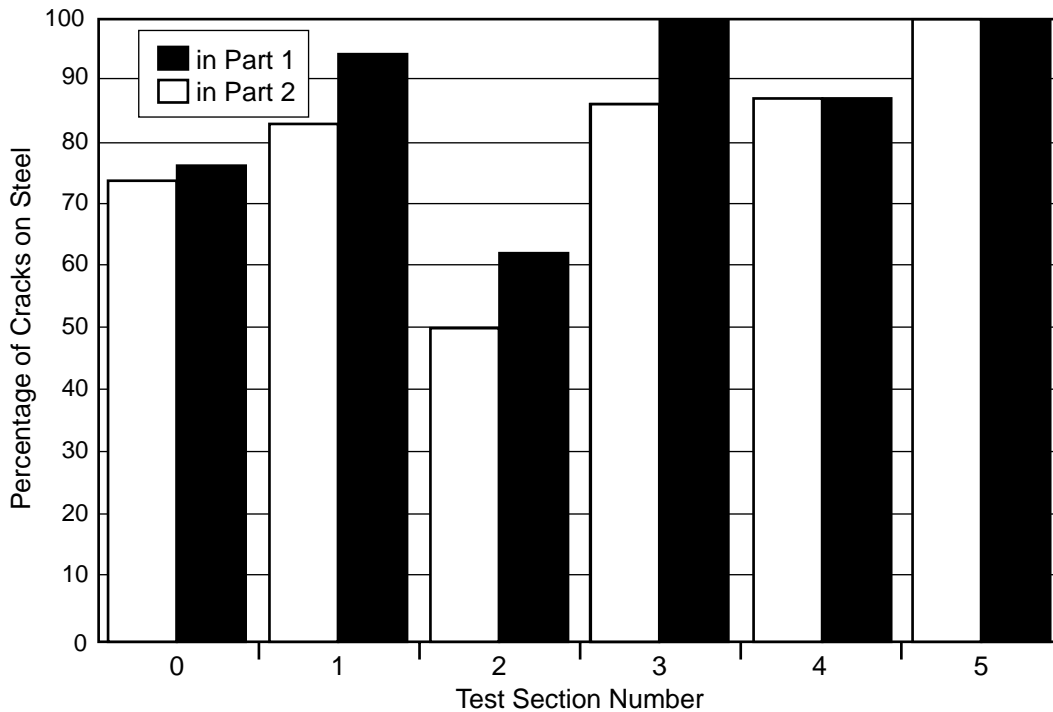


Figure 3.15 Percentage of cracks occurring at the rebar in the LaPorte section

Based on our limited observations, it is somewhat apparent that surface crack initiation (i.e., early-aged notching techniques) under the prevailing temperature and moisture paving conditions is more effective than interior crack initiation (i.e., crack inducer or transverse reinforcement). Usually, the notch width is larger than an initial random crack opening, which may suggest that the notches should be sealed after sawcutting to reduce the possibility of spalling around the notches (though spalling of this nature has not been observed in the early-aged sawcuts). Whether the transverse crack is initiated by crack inducers or by notches, it is expected that crack width or the crack opening could be minimized through this process.

In any case, longitudinal reinforcement is currently designed in CRC pavements so that the resulting crack spacings and widths are limited to certain ranges. Although the objective of longitudinal reinforcement in concrete pavement is to maintain tightly closed transverse crack widths, current construction methods could be modified to adopt early-aged cutting to actively or positively induce cracks at more favorable intervals — particularly in

pavements constructed with river gravel aggregates. But it is worth noting that the location of early-aged cracks cannot be completely controlled by longitudinal reinforcement alone because of the propensity of early-aged cracks to initiate at the pavement surface or at the transverse steel location, particularly when placement is performed under summer or hot weather conditions. Another factor worth considering is the vertical position of the steel reinforcement that may affect the transverse crack spacing and, in turn, the crack width.

MEASURED CRACK WIDTHS

Crack width measurements were made on cracks in sections of various curing and cracking combinations. The width of transverse cracks in CRC pavements is critical to quality performance because the cracks control the degree of load transfer from one slab to the other as the load moves across the crack. Figure 3.16 illustrates crack width measurements taken in PSart I-A over a variety of curing methods and coarse aggregate blends. The figure indicates that wider crack widths result from a lower quality of curing. This may be due to a greater amount of drying shrinkage at the surface of the pavement, which results in the transverse cracks opening to a larger degree. Interestingly, Figure 3.16 shows that wider crack widths are associated with more SRG, i.e., higher thermal coefficient, even though shorter crack spacings are experienced. This again indicates that the thermal coefficient is a very significant factor. The double membrane curing tended to perform as expected for shorter crack spacing that may have counteracted the effects of drying shrinkage.

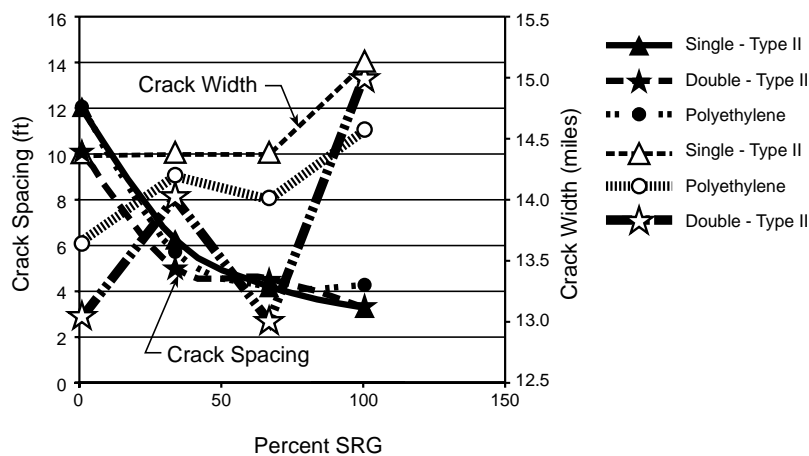


Figure 3.16 Crack width variation with method of curing and coarse aggregate blend

CONSIDERATION OF PAVEMENT TEMPERATURE AND RELATIVE HUMIDITY

Previous field studies of CRC performance in Texas concluded that the formation of transverse cracks results from a drop in pavement temperature following the rise in temperature owing to the evolution of the heat of hydration. However, at this very early age, it is expected that both pavement temperature and moisture changes affect the development of transverse cracking, particularly at the pavement surface, where a certain amount of shrinkage due to moisture loss, combined with the temperature effects in the concrete close to the surface of the pavement, may be the primary factors that initiate cracks at the pavement surface. After the concrete material achieves a level of maturity and strength, the drying shrinkage may make less of a contribution to later transverse crack development (which continues for a year or more after placement of the pavement). Typically, 80 to 90% of the transverse crack develops during the first 180 days after paving.

Figure 3.17 shows hourly ambient temperature and relative humidity data from August 25 to August 30, 1992, with such data representative of the weather conditions prevailing during placement and curing of the pavement section. The solar radiation data from August 25 to August 30, 1992, are shown in Figure 3.18. As seen in the figures, the maximum daily temperature difference during those 6 days ranged between 11 (20) to 16.7EC (30EF), and the maximum ambient temperature was about 32.2EC (90EF). The minimum daily relative humidity ranged between 30% and 50%. Pavement temperatures were measured and recorded by both manual and automatic means using embedded thermocouples. A typical temperature distribution with depth in the concrete pavement at early ages shown in Figure 3.19 indicates that the temperature variation at the pavement surface is larger than that at the pavement bottom. A maximum pavement temperature condition occurred, in this instance, during day 2 and day 3 after paving. It is seen in Figures 3.20 and 3.21 that the maximum temperature difference between the top and the bottom of pavement ($T_{\text{TOP}} - T_{\text{BOTTOM}}$) was a minus 20°F (-6.68°C), which occurred at 7 a.m. in the morning, and a plus 22°F (-5.67°C) at 4 p.m. in the afternoon, respectively, on day 2 after paving. However, the maximum temperature difference over the period from day 2 to day 4 was 42°F (23°C) at the pavement surface, and WC 28°F (-2.22°C) at the bottom of the pavement.

The effects of different curing methods and coarse aggregate types on pavement temperature development are shown in Figure 3.22. The newly placed concrete pavements covered by polyethylene sheeting developed greater maximum temperatures than pavement sections cured by a single or double coat of Type II curing compound. Figure 3.22 also shows that the temperatures in the sections with mix designs 2 and 3, which contain 33% and 67% river gravel as the coarse aggregate, respectively, are greater than those in the control sections, which contain 100% limestone as the coarse aggregate.

In order to account for the effects of curing methods and moisture variation on cracking behavior in concrete pavement, the bulk polymer resistive relative humidity sensor was used to measure pore relative humidities internal to the concrete placed in the field test section. To ensure the accuracy of the concrete materials' relative humidity measurements made with these (especially at high humidity range), a chilled mirror optical dewpoint meter was used to calibrate the resistive-type relative humidity (RH) sensors.

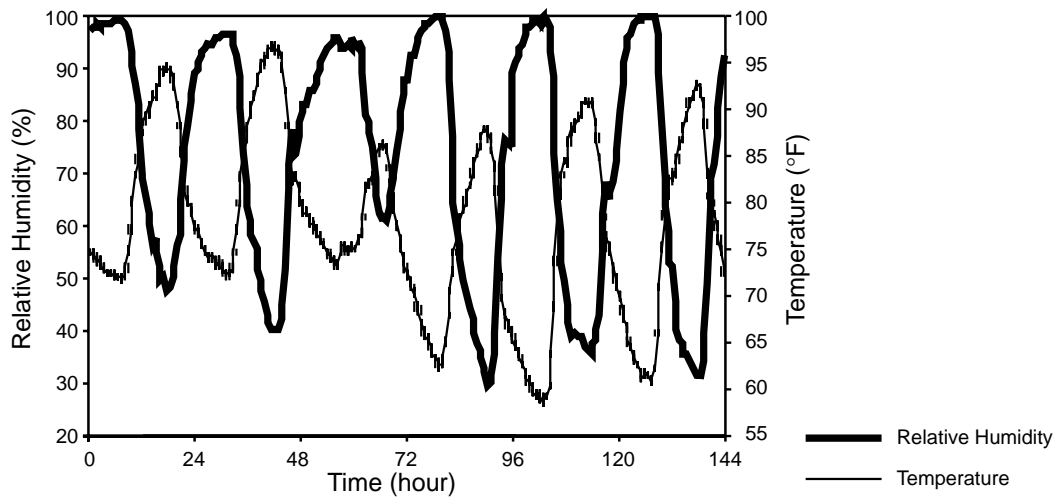


Figure 3.17 Ambient temperature and RH in Cypress from August 25 through August 30, 1992

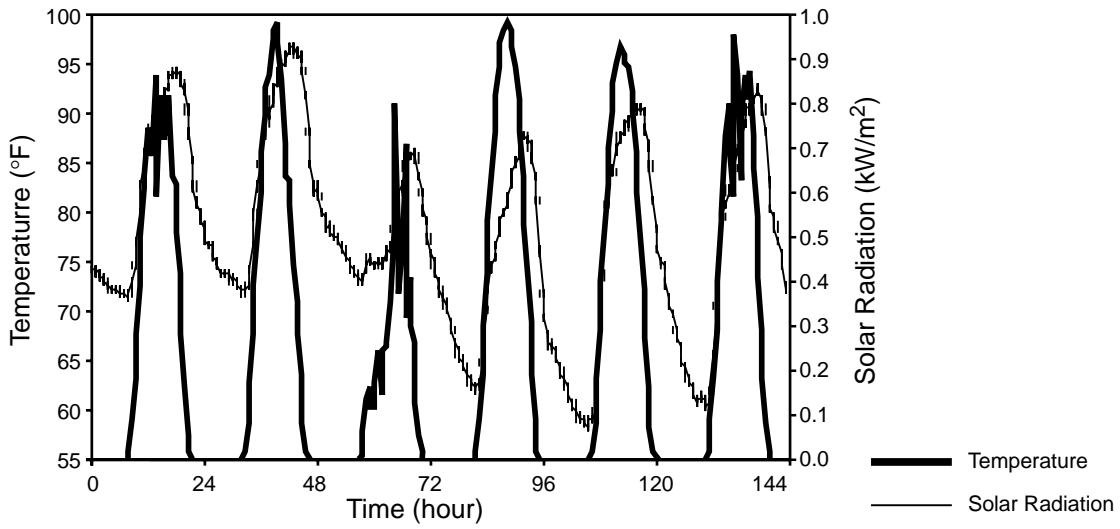


Figure 3.18 Ambient temperature and solar radiation in Cypress from August 25 through August 30, 1992

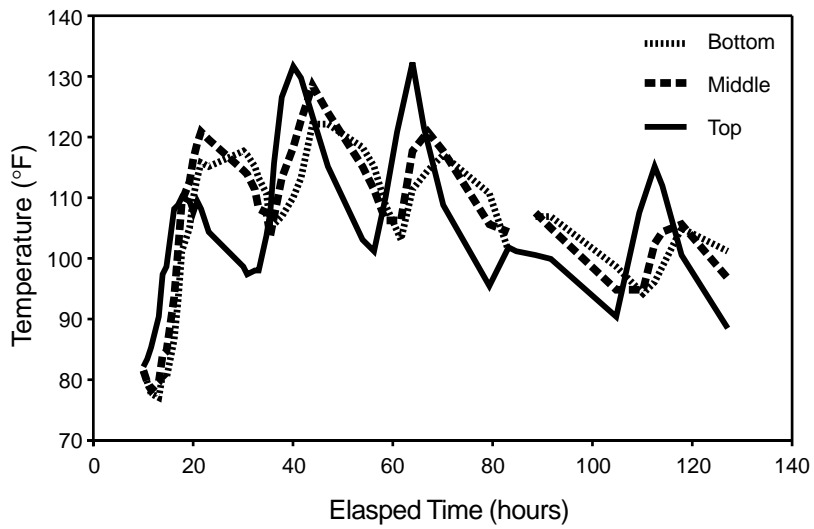


Figure 3.19 Typical temperature variation with time

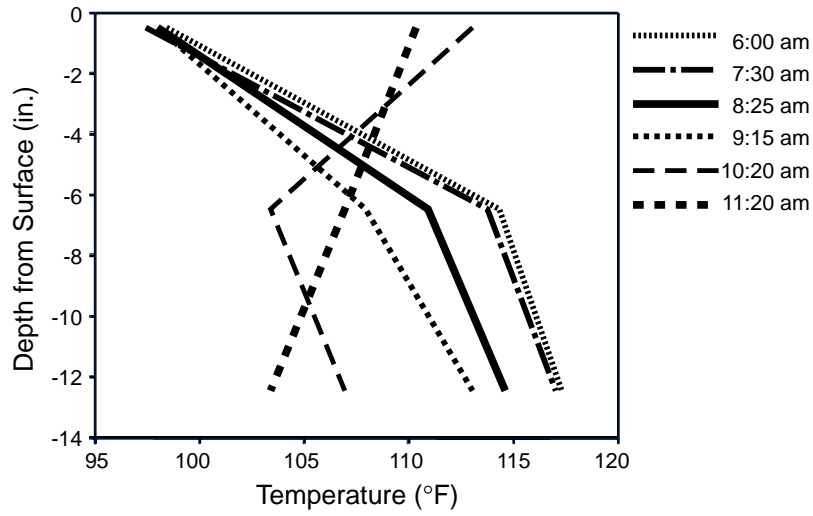


Figure 3.20 Typical temperature distribution with depth (morning)

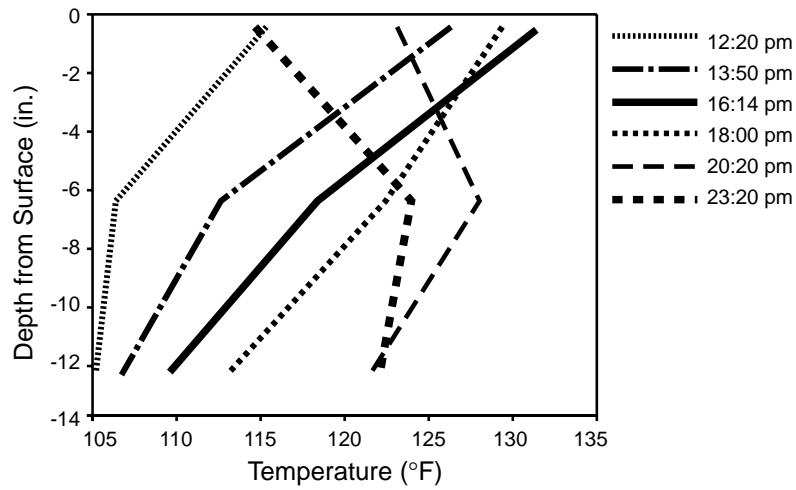


Figure 3.21 Typical temperature distribution with depth (afternoon)

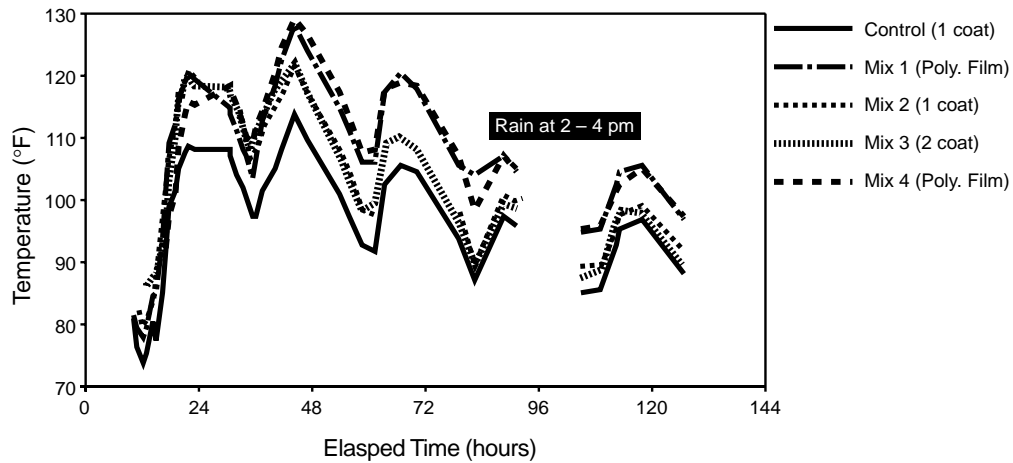


Figure 3.22 Temperature variation in the section with different curing methods

A specially designed device for measuring internal relative humidity in field concrete was developed at TTI for field installations (Figure 3.23). Figure 3.24 shows how relative humidity in concrete was measured using the RH sensors after the device was embedded in the concrete pavement. Relative humidity measurements were taken at depths from the pavement surface ranging from 0.5 in. (12.5 mm) to 11.5 in. (292 mm) at 2.5 in. (63.5 mm) intervals. The field installation was configured to protect the sensors while monitoring hardening concrete. A rubber stopper sealed each sensor position when a sensor was not in place to maintain the relative humidity under in situ drying conditions. With the use of the specially prepared RH sensors and protective insertion devices discussed previously, the interior relative humidity in the concrete pavement was successfully measured. Several observations were noted with respect to the variation in relative humidity within the pavement section. Typical relative humidity variation as measured from the Cypress test section is shown in Figure 3.25. The moisture profiles in the second day and first 5 days after paving of the Cypress test section are shown in Figures 3.26 and 3.27, respectively. The interior relative humidity in concrete pavements tends to vary with daily temperature variation.

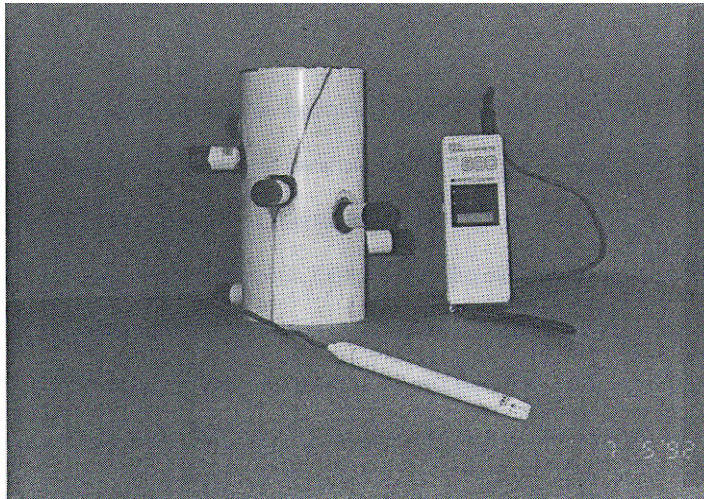


Figure 3.23 A specially designed device for measuring RH in concrete pavement



Figure 3.24 Measurement of RH in the field

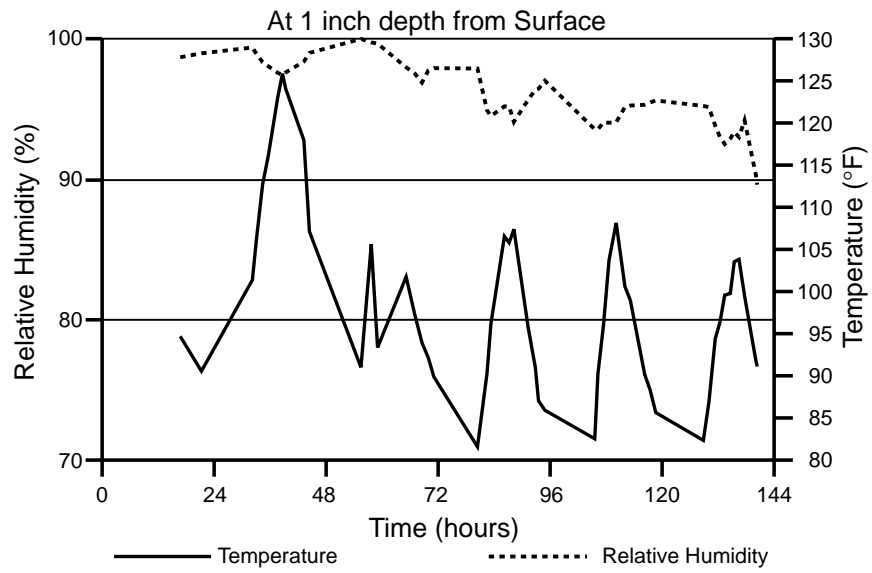


Figure 3.25 Typical RH variation with time

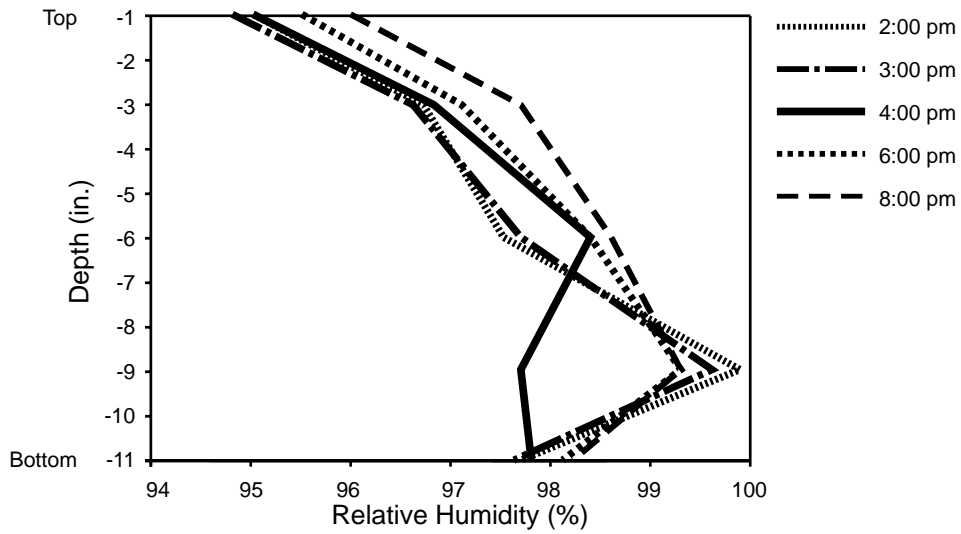


Figure 3.26 Typical RH distribution with depth (1 day)

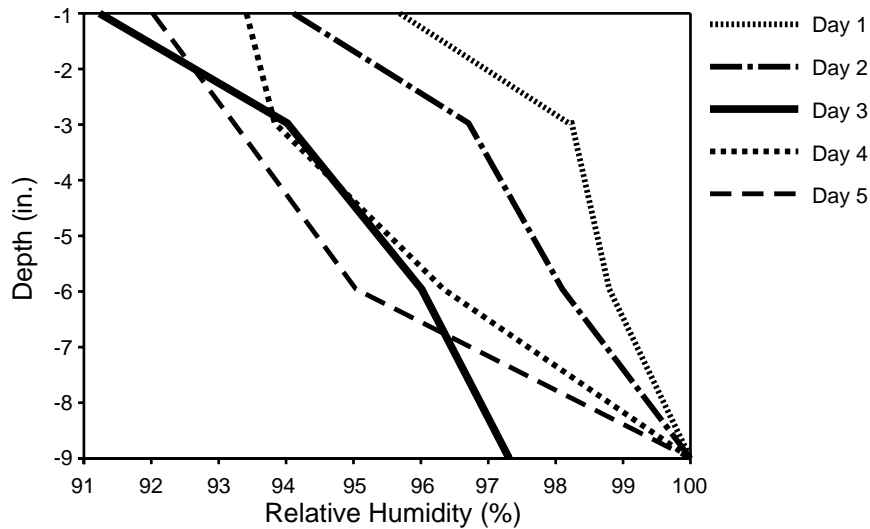


Figure 3.27 Typical RH distribution with depth (5 days)

In other words, when temperature increases the relative humidity decreases and vice versa. This indicates that the interior relative humidity in concrete is a function of interior concrete temperature. However, during the hardening process, the overall tendency of relative humidity variation was to decrease with time. A similar characteristic was not as evident in pavement sections cured by polyethylene sheeting (Figure 3.28), in comparison with sections cured by a single coating of Type II curing compound (Figure 3.25). Polyethylene sheeting curing also affects the initial pavement temperatures, particularly under hot paving conditions, as illustrated in Figure 3.22. Figure 3.29 shows the effect of different curing methods on interior relative humidity in concrete measured on day 29 (single: one coat Type II curing compound; double: two coats Type II curing compound; Poly Cure: polyethylene sheeting). It should be noted that the polyethylene sheets covered the surface of pavement for about two weeks. From the viewpoint of preventing moisture loss, polyethylene film is more effective than a double coating of Type II curing compound at early ages. However, during the later stages of curing, a double coating of Type II curing compound appeared to be equivalent to the effectiveness provided by the polyethylene film. Both are more effective than a single coat of Type Id curing compound.

In contrast to temperature variation at the pavement surface, the loss of relative humidity at the surface is larger than that at the bottom of the pavement. With respect to the combined effects of moisture and temperature, no pavement cracking was observed in the Cypress crack control sections until the morning of the third or fourth day after placement of the pavement. The noted variation in temperature and moisture with time and with depth apparently must achieve a certain level prior to crack initiation, since transverse cracks did not occur (in the crack control section) until the early morning of day 3.

As a final note on the curing effectiveness of different curing compounds, an interesting curing experiment was conducted using linseed oil and a water-based curing compound in part I-B (Figure 3.30).

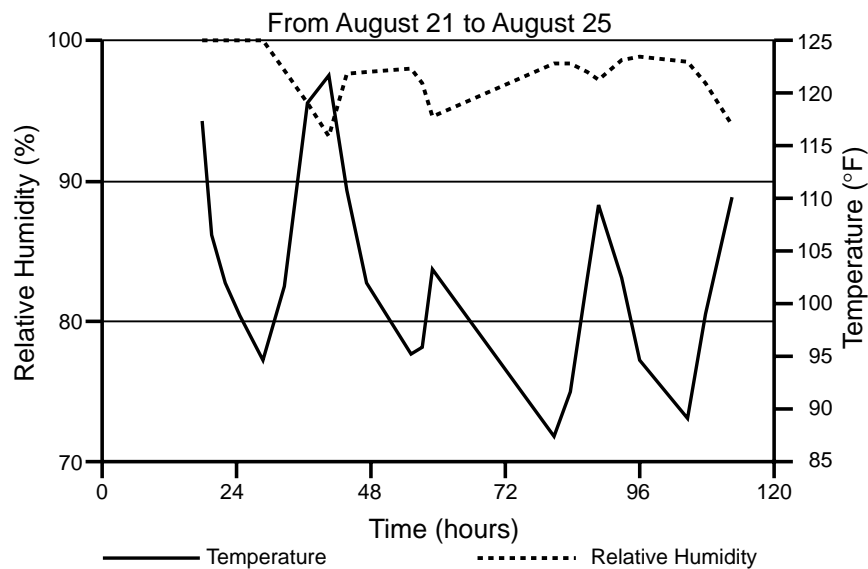


Figure 3.28 RH in section cured by polyethylene sheet

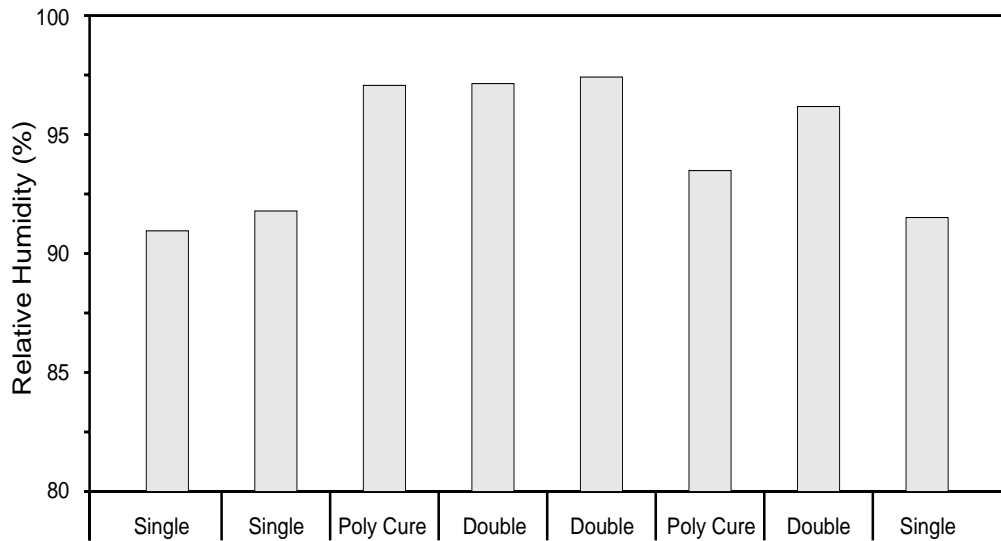


Figure 3.29 Effect of curing method on RH in concrete pavement



Figure 3.30 Linseed oil and water-based curing compound curing experiment

Portions of part I-B were sawcut at 3 ft (0.9 m) intervals in each of these curing sections and compared with the same pattern of sawcuts in a section cured with Type II curing compound. Figure 3.31 illustrates the performance difference in the curing medium in terms of cracking density. It is clear that crack control was much more difficult to achieve in

sections cured by the linseed oil and water-based curing compound. This suggests that too much drying shrinkage can lead to excessive and uncontrolled cracking.

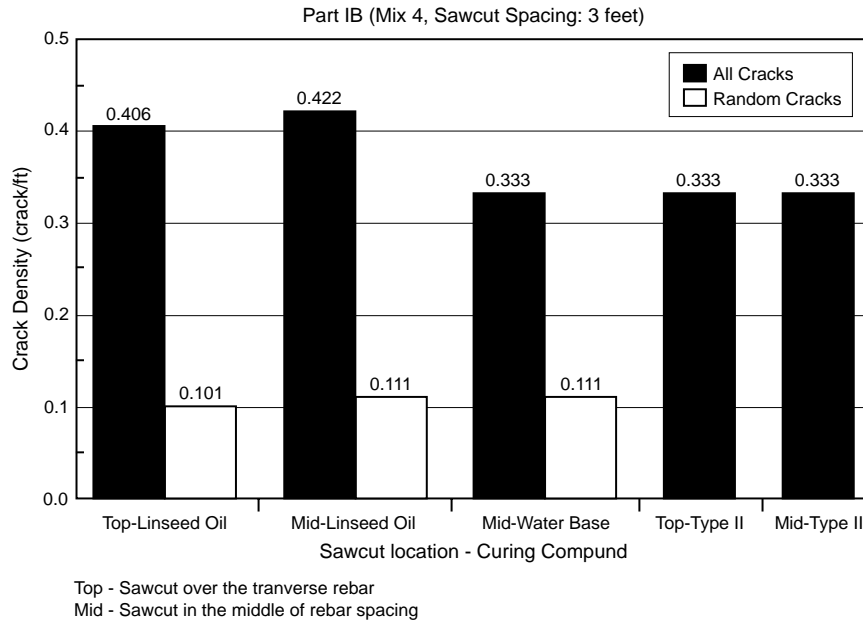


Figure 3.31 Comparison of curing compound performance relative to cracking density

CONCRETE STRENGTH GAIN

A series of field test specimens prepared for the determination of concrete strength shows the flexural strengths of concrete properties as they varied after the construction of the Cypress pavement sections. Table 3.5 shows the four Cypress mix designs. It is clear from the table that the flexural strength of concrete with 100% river gravel as the coarse aggregate is less than that for the others at early ages. At day 28 after paving, the concrete with 100% river gravel had the highest flexural strength among four mix designs.

Table 3.5 Flexural strengths (psi) of concrete for the four mix designs

Concrete Age	Mix 1 100% LS	Mix 2 67% LS 33% RG	Mix 3 67% RG 33% LS	Mix 4 100% RG
1 Day	370.80	369.60	395.85	308.00
3 Days	610.05	610.80	608.64	531.60
7 Days	678.90	682.10	730.43	636.00
14 Days	752.085	737.30	750.43	688.70
28 Days	798.50	818.00	769.00	842.50

This can also be seen clearly in Figure 3.32. Figure 3.33 shows the percentage of cracks at different times for different type aggregates in which the percentage of cracks at day 28 after paving is 100%. Early cracking occurred more frequently in the sections of river gravel concrete than in those of crushed limestone concrete. Cracks occurring at early ages in the concrete consisting of a blend of river gravel and crushed limestone as the coarse aggregate were more numerous than those in the concrete that used only crushed limestone as the coarse aggregate. This is because concrete of crushed limestone has a higher flexural strength than that of concrete of river gravel at early ages. In addition, concrete containing a greater percentage of river gravel as the coarse aggregate developed greater maximum temperatures at early ages than concrete that consisted of a greater percentage of crushed limestone as the coarse aggregate (Figure 3.22).

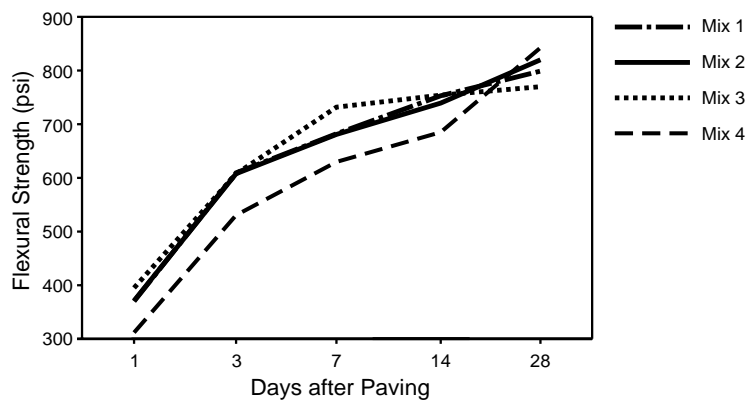


Figure 3.32 Effect of curing method on RH in concrete pavement

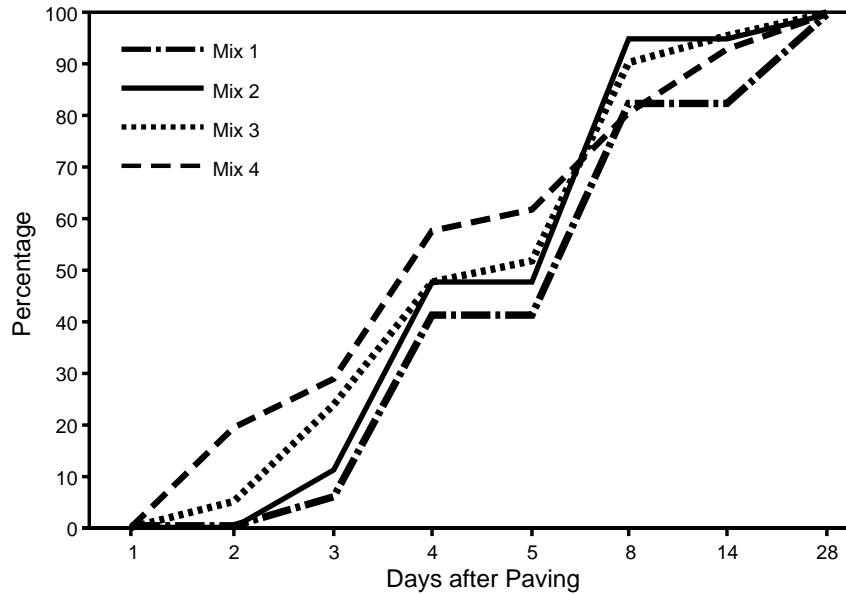


Figure 3.33 Percentage of cracks at different times

3.2 CONCLUSIONS

Based on our experiences with the test sections constructed in Friendswood and Cypress, Texas, the following preliminary conclusions are offered:

1. Early-aged sawcutting in the Cypress test section suggests that surface crack initiation is more efficient than interior crack initiation (i.e., crack inducer and transverse rebar). It is recognized that sawcutting should be performed between initial and final setting of the concrete. Under some conditions, early-aged sawcutting techniques (in combination with the transverse reinforcement location) may be entirely sufficient to control the crack pattern, where under other conditions the use of interior crack inducers may be warranted. The crack control sections also indicated that the design percent of steel was too high for the combination of construction conditions and materials, since the average crack spacing ultimately approached 3 ft (1 m).
2. Control of the crack pattern in CRC pavements can be affected by several factors other than those relative to the technique of crack induction. Good mix design (in terms of workability and crack susceptibility), reinforcement steel design, and

construction practice will ensure that crack intervals will develop as expected. In traditional design analysis of CRC pavement, average crack spacing and crack width are derived as a result of the longitudinal steel design, the tensile strength of the concrete, and the design temperature drop. This approach assumes that when the stress induced by a drop in temperature and drying shrinkage exceeds the tensile strength, a crack forms in concrete pavements. Naturally, a great degree of variation is expected (and does occur as surface defects) in the actual crack patterns, which, if significantly reduced, will result in more economical and longer-lasting CRC pavements.

CHAPTER 4. OBSERVATIONS FROM HOUSTON AND HEMPSTEAD TEST SECTIONS

In this section, observations made from the field experiments are presented. The observations are grouped into the same five performance indicator categories of crack spacing, crack width, randomness index, spalling, and concrete strength variations discussed in Chapter 2.

4.1 CRACK SPACING

To facilitate the discussion of crack spacing, observations are divided into six subcategories: crack development over time, placement season, placement temperature, steel percentage, skewed steel, and aggregate type — all major performance variables considered in the experiment. Typical test sections are selected for these comparisons.

CRACK DEVELOPMENT OVER TIME

The initial cracks develop in CRC pavements very quickly. Figure 4.1 shows the crack spacing distributions at various ages, along with the mean crack spacing at 640 days. The mean crack spacing is slightly greater than the median crack spacing at the same age. Note that the majority of the cracks form during the first year, as found in previous studies. Also note in Figure 4.1 that the crack spacing after 100 days is approaching the last crack spacing recorded for each project that ranges from 2 to 8 years. This confirms previous studies referenced in Chapter 2 that CRC pavements generally reach a stable crack spacing at 100(+) days (Figure 2.1) and remain there until the fatigue life is reached (Ref 15).

This principle is further illustrated in Figure 4.2. Notice that the median crack spacing, as well as the 10th percentile crack spacings, is approaching constant values. The 90th percentile has a more gradual approach to the asymptote. Now consider Figure 4.3, which was also obtained from Section 23E: The percentage of cracks spaced less than 3 ft (0.91 m) apart is increasing, as would be expected, but has begun to stabilize. It is expected that this curve will also approach a constant value in the near future and remain there until the fatigue phase sets in, as shown in Figure 2.1.

PLACEMENT TIME AND SEASON

Figure 4.4 shows the development of the cumulative crack distribution for a section that is similar to section 23E but was placed during the day. The figure shows that the day section experienced crack formation much more quickly than did the section placed at night. The reason for the difference is believed to be related to the daytime higher concrete set temperature. This may be attributed to the fact that the heat produced by hydration of the concrete cannot be dissipated into the atmosphere as rapidly during the day, owing to higher air temperatures (Ref 6). High concrete hydration temperatures lead to greater temperature changes and shrinkage, causing the concrete to crack before it develops sufficient strength to resist the higher thermal stresses.

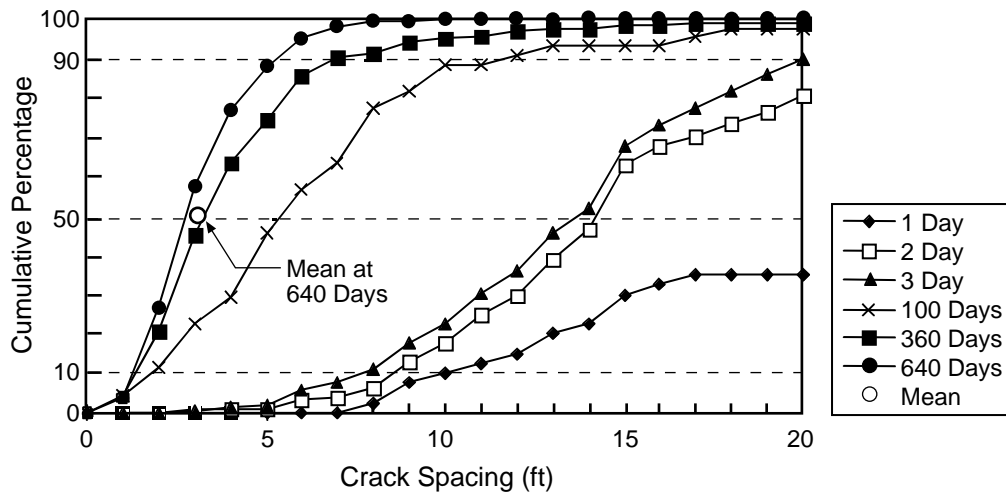


Figure 4.1 Typical formation of the crack distribution over time for an SRG section paved at night (Project 8 — Section 23E) (1 ft = 0.30 m)

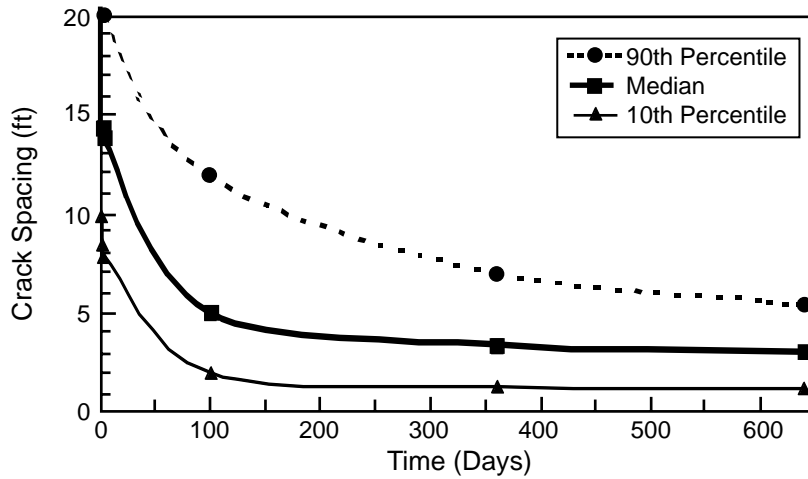


Figure 4.2 Crack spacing for the 10th, 50th, and 90th percentile over time (Project 8 — Section 23E) (1 ft = 0.30 m)

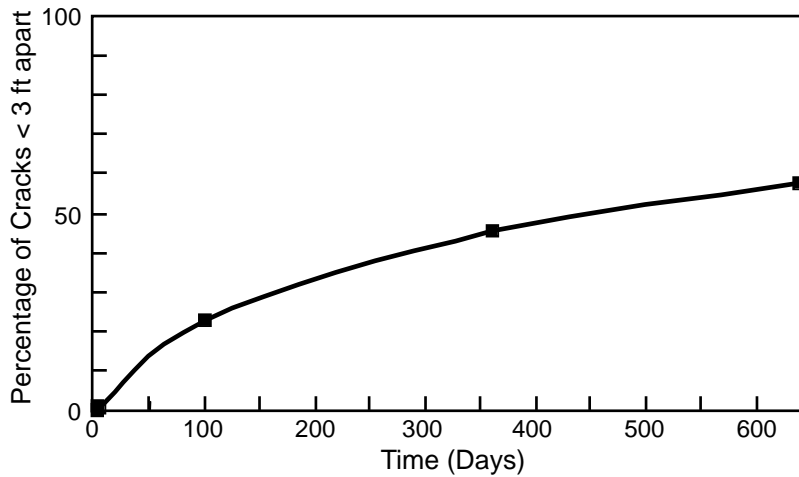


Figure 4.3 Percentage of cracks spaced less than 3 ft (0.91 m) apart over time (Project 8 — Section 23E) (1 ft = 0.30 m)

Using the experiment design in Figure 1.2 and Table 2.1, the crack spacing distributions for the test sections permit a comparison of summer and winter placements. While these may be studied in detail, selected ones have been inserted in this section to demonstrate and discuss trends.

Crack formation is also related to the season during which the pavement is placed. Figures 4.5 and 4.6 show crack spacing distributions over time for similar SRG test sections paved in the winter and summer, respectively. The section placed during the winter did not experience as much cracking over time as did the section placed during the summer; the distributions also show that the winter section stabilized more quickly than did the summer section. Note that the crack distribution at 5 days for the summer placement is poorer than that at 2,600 days for the winter placement. Thus, winter placements of SRG may develop acceptable crack spacing distributions.

Now consider the percentage of cracks less than 3 ft (0.91 m) apart shown in Figure 4.7. This graph is similar to Figure 4.3, except that sections Projects 1 (winter) and 2 (summer) have been added and the period of time shown has been extended. Note that the sections that are 7 and 8 years old have become very stable, and that the winter section stabilized more quickly than did the summer sections. Furthermore, the summer placement sections for both Projects 2 and 8 have similar trends in crack spacing development.

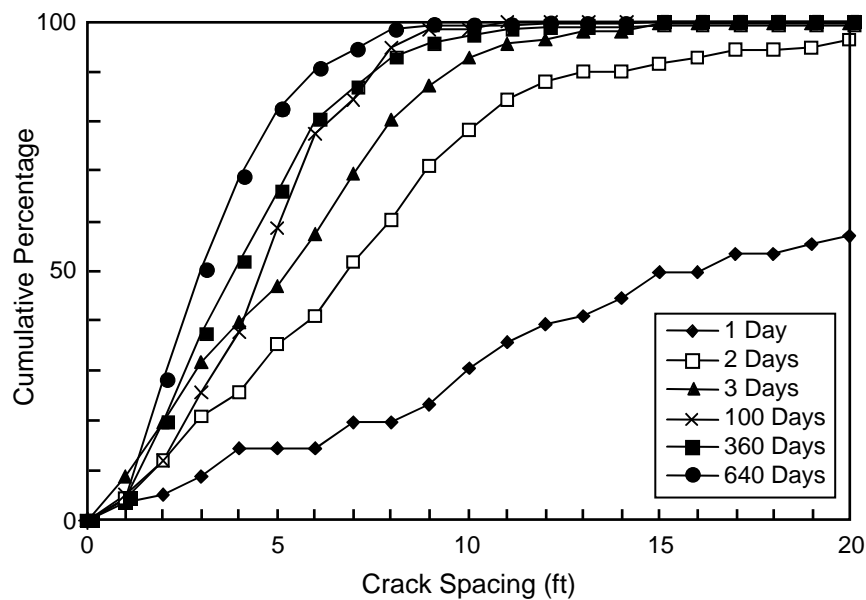


Figure 4.4 Typical formation of the crack distribution over time for an SRG section paved during day (Project 8 — Section 28E) (1 ft = 0.30 m)

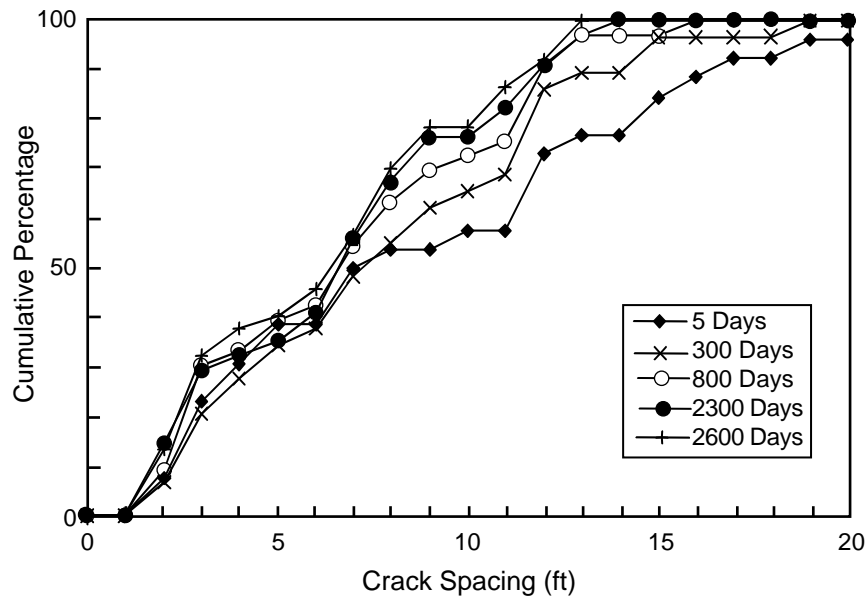


Figure 4.5 Typical formation of the crack distribution over time for an SRG section paved during winter (Project 1 — Section A) (1 ft = 0.30 m)

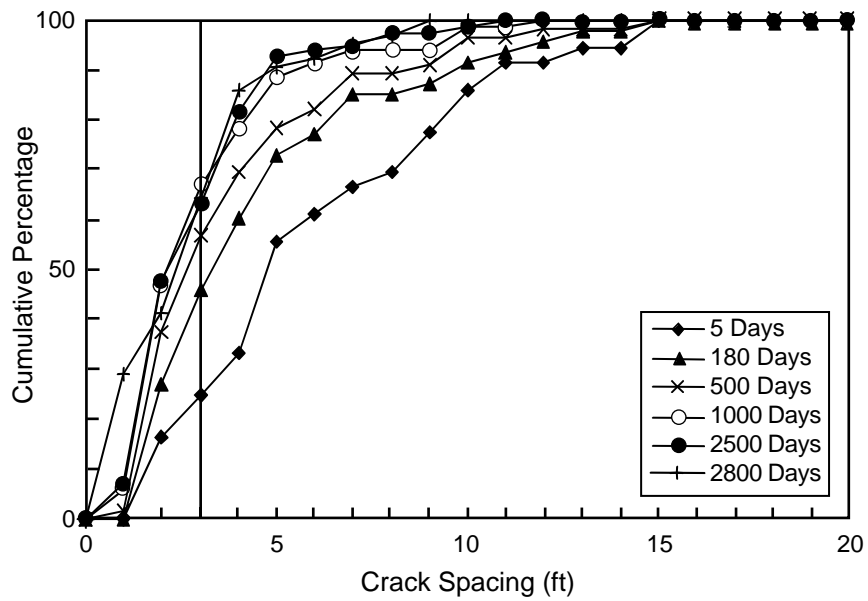


Figure 4.6 Typical formation of the crack distribution over time for an SRG section paved during summer (Project 2 — Section A) (1 ft = 0.30 m)

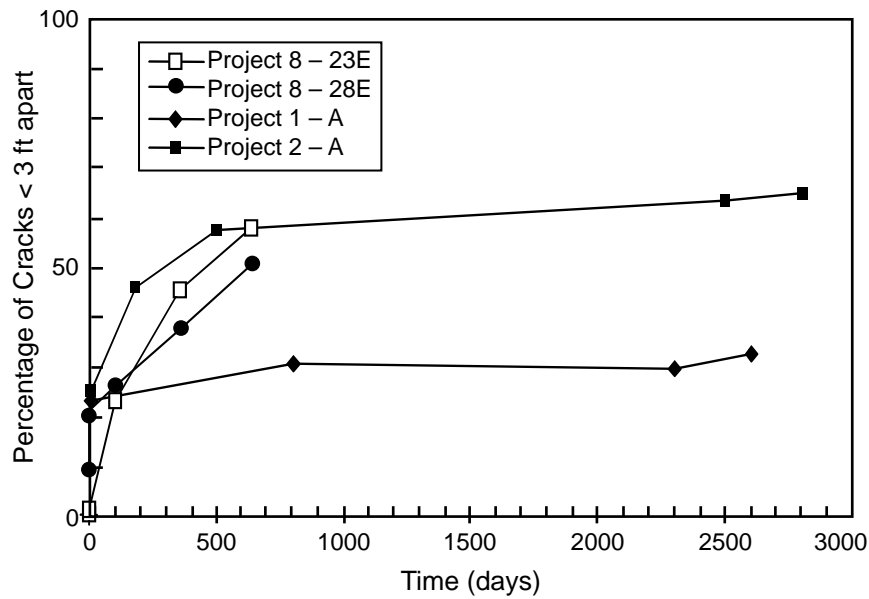


Figure 4.7 Percentage of cracks spaced less than 3 ft (914.4 mm) apart over time (Projects 1, 2, and 8) for the SRG combinations (1 ft = 0.30 m)

Figure 4.8 compares crack spacing in sections that have only two design variables, namely, placement season and aggregate type. Notice that the limestone section placed during the winter has the best crack spacing distribution of all the sections, and that it has fewer than 10% cracks spaced less than 3 ft (0.91 m) apart. On the other hand, the SRG section placed during the summer has the poorest crack spacing distribution, with about 50% of the cracks less than 3 ft (0.91 m) apart.

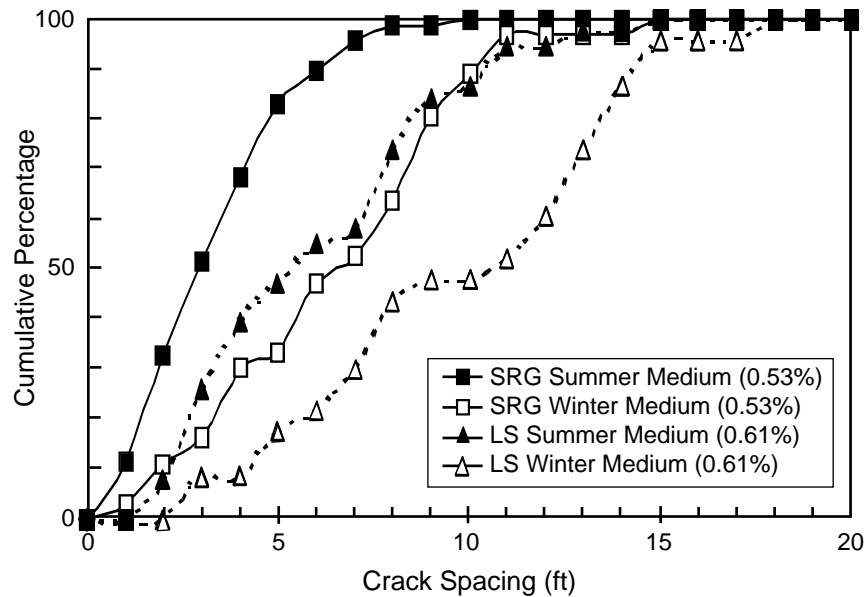


Figure 4.8 Crack distribution for sections with summer and winter paving at ages of 2,600 to 2,800 days (Projects 1 and 2 — Sections B and D) (1 ft = 0.30 m)

Among the summer sections, the limestone section was placed under much more adverse conditions, yet it still performed better than the siliceous river gravel sections. Interestingly, the crack spacing distribution is very similar for the limestone section placed in the summer and the siliceous river gravel section placed during the winter. As previously mentioned, this observation provides a potential solution to performance problems sometimes experienced with SRG. SRG develops a more desirable crack spacing when it is placed in the winter.

PLACEMENT TEMPERATURE

Concrete temperatures associated with the first few days of its placement can also influence crack development and final crack spacing. Concrete temperature is most important in the first few days, during which time the concrete, whose strength is initially very low, may be experiencing very large temperature changes caused by the concrete hydration process. The worst case occurs when the pavement's heat of hydration and the daily air temperature reach their highest point at the same time.

To avoid this worst-case condition, night paving was included in the experiment. The results from the test sections placed for Project 8 were not informative because the temperature was actually warmer in the early evening when the nighttime test sections were paved. Refer to Figure 4.7 for sections placed at night. Note that the percentage of cracks less than 3 ft (0.91 m) apart is greater for night placement. When attempting night paving, it is very important to delay paving until the air temperature is significantly below the high temperature of the day. For example, using a typical daily temperature fluctuation, it would be best to begin paving around midnight and end paving at 8:00 or 9:00 a.m.

STEEL PERCENTAGE

The steel percentage has a strong effect on crack spacing. Generally, as the steel percentage increases, the crack spacing, crack width, and steel stress decrease. That is easily noted in the extreme cases, when reinforced and unreinforced concrete sections are compared. Unreinforced concrete will typically have a much larger crack spacing compared with reinforced concrete. As the steel percentage is increased, cracks begin to form closer together, since the steel restrains cracks from opening when volumetric changes in the pavement occur. Cracks form typically at the weakest locations in the pavement, where the concrete stress is greater than its strength. By extrapolation of this principle, the steel percentage can be adjusted until the appropriate crack spacing is achieved.

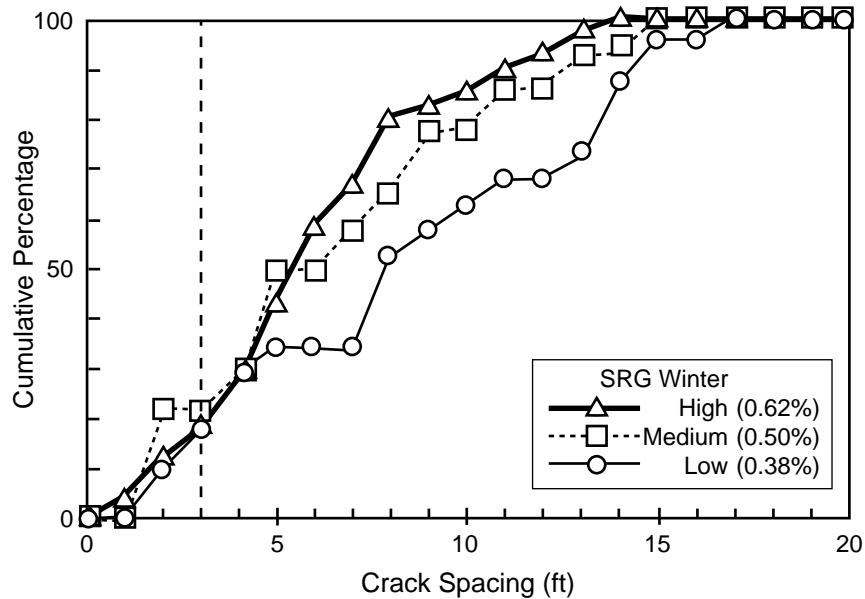


Figure 4.9 Comparison of crack spacing vs. steel percentage at 2,700 days (Project 3 Sections A–C) (1 ft = 0.30 m)

Note in Figure 4.9 that the section having the lowest steel percentage has the largest median and mean crack spacing, as would be expected. Also note that, for winter placement of the SRG, all three steel percentages have acceptable percentages of crack spacing less than 3 ft (0.91 m), with the highest being only 20%. Note that the effect of going from 0.5% to 0.62% is small on the crack spacing distribution. For the lower steel percentages (0.38%), approximately 35% of the cracks are spaced at distances greater than 12 ft (3.65 m), which may be excessive for SRG. The data for all the test sections were compiled to examine the crack spacing distribution in terms of steel percentages for specific aggregate types. A close examination of these graphs again shows that the increase from the medium to the high percent steel has only a minor impact on the crack spacing distribution.

The use of different bar sizes was also investigated. Given a constant steel percentage, the pavement having a larger bar size is expected to have larger crack spacing. This phenomenon occurs because the larger bar has a larger bond slip zone; a larger bond slip zone leads to larger crack widths and to larger mean crack spacing. This hypothesis is verified in Figure 4.10, where we see that the sections having medium steel and a #7 bar have

a larger median crack spacing than the section having medium steel and a #6 bar. The #7 bar also has considerably fewer cracks whose spacings are smaller than 3 ft (0.91 m) (10%–30%). Note that the sections for the project placed in the summer follow this trend, while four of the six section plots based on the winter data do not follow the trend. In most cases, the difference in the crack spacing distribution as a function of bar diameter is small.

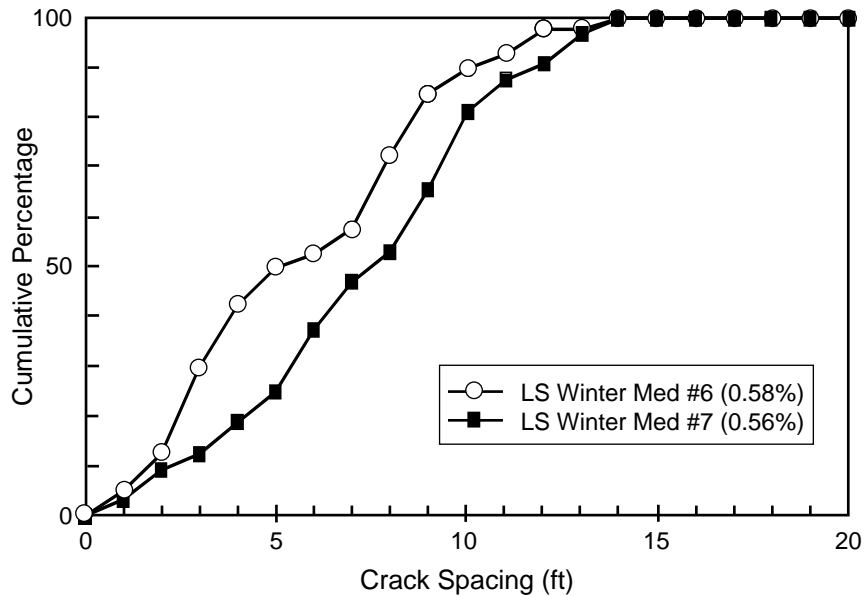


Figure 4.10 Effect of bar size on crack spacing at 2,400 days (Project 4 — Sections E and G) (1 ft = 0.30 m)

SKewed STEEL

Because many transverse cracks appear to occur over transverse steel, the transverse steel was skewed in several of the test sections on Projects 5 and 8. (Skew angles of 30 and 45° were tested.) In Project 8, the skewed steel actually had a worse cracking distribution at 100 days (Figure 4.11). However, after 640 days, the crack spacing was better in the skewed section (Figure 4.12). Notice that the skewed section had only between 8% and 12% more cracks meeting the 3 ft (0.91 m) minimum standard than the normal sections at 2 years. Thus, the effect, while beneficial, is small.

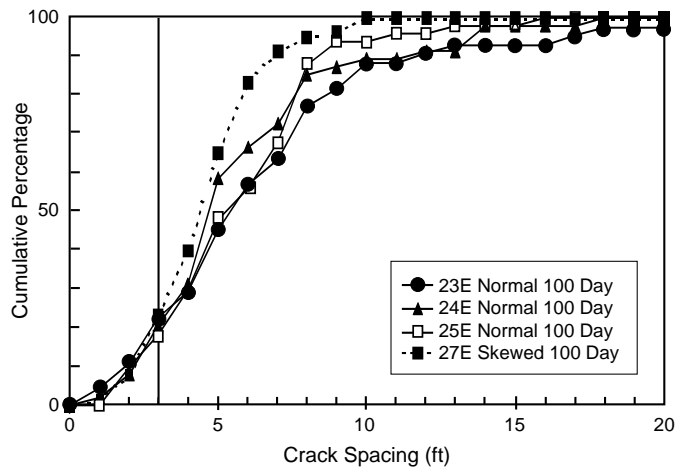


Figure 4.11 Crack spacing comparison for skewed vs. normal transverse steel at 100 days for SRG sections (Project 8) (1 ft = 0.30 m)

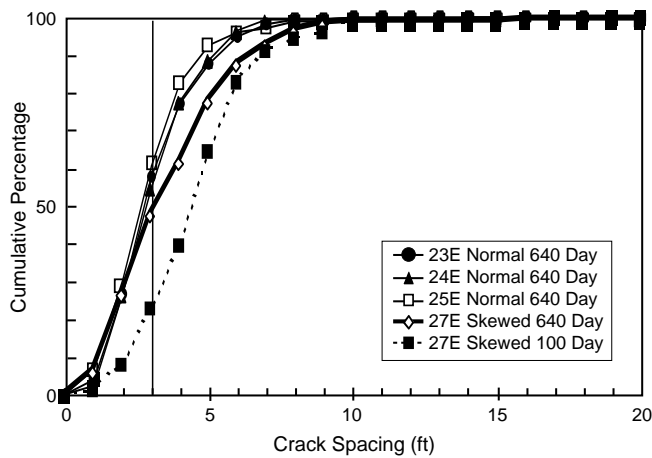


Figure 4.12 Crack spacing comparison for skewed vs. normal transverse steel at 640 days for SRG sections (Project 8) (1 ft = 0.30 m)

AGGREGATE TYPE

The single most important variable in crack development is aggregate type. While many designs and construction techniques have been used to compensate for aggregate-based performance problems, all attempts have yielded only limited success.

Three sections with an SRG coarse aggregate are compared with three sections with an LS coarse aggregate in Figure 4.13, with all sections being from Project 8. Consider a comparison of the test sections based on the percentage of cracks that meets the minimum crack spacing used for design, which is 3 ft (0.91 m); the SRG had only between 42% and 48% of the cracks meeting the design standard, while the LS had between 70% and 90% of the cracks exceeding the design minimum. This is important because significantly greater distress in terms of punchouts is expected in sections having smaller crack spacings. Figure 4.14 shows the percentage of cracks less than 3 ft (0.91 m) apart for Projects 1–4 and Project 8 in terms of SRG and LS. Overall, the LS had considerably fewer cracks less than 3 ft (0.91 m) apart for all conditions. Note that the section with the lowest percentage of cracks less than 3 ft (0.91 m) apart were generally placed in the winter for both aggregate types. An unexpected result was that some of the sections placed in the winter had higher percentages of closely spaced cracks than did other sections placed in the summer using limestone aggregate.

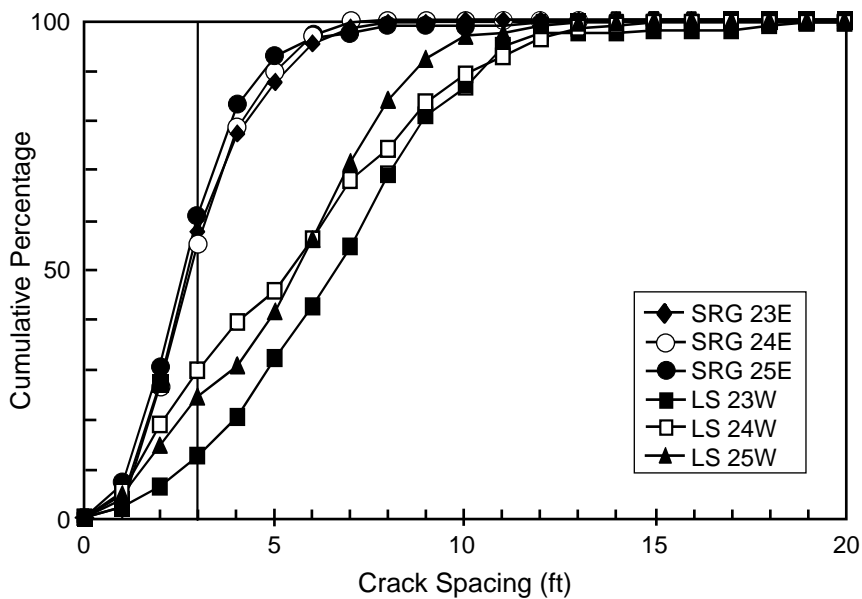


Figure 4.13 Comparison of crack distribution for SRG and LS at 640 days (Project 8) (1 ft = 0.30 m)

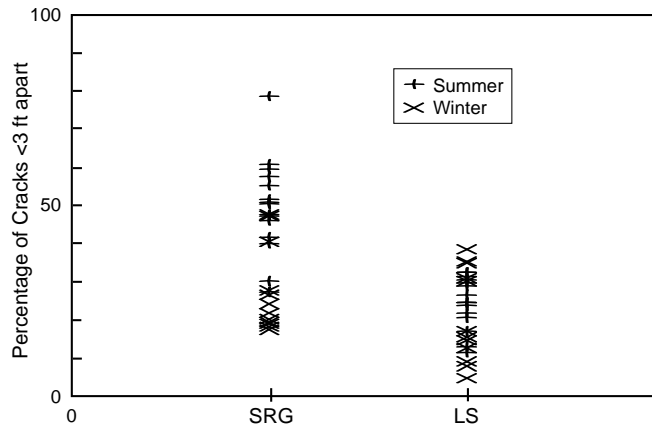


Figure 4.14 Percentage of cracks less than 3 ft (0.91 m) apart (Projects 1–4, and 8)

BLENDED AGGREGATE

A blend of LS and SRG was used for two of the Project 8 test sections. Earlier laboratory testing on blended aggregates showed that the concrete had properties based directly proportioned to the percentage of each aggregate used (Ref 2). Using those results, the test sections placed in Project 8 were expected to have a crack distribution roughly halfway between similar limestone and river gravel sections. Figure 4.15 presents the actual results when the pavement was almost 2 years old. The crack spacing distributions for the SRG and the blended section are nearly identical, while the LS section has a much more desirable crack spacing distribution. This contradicts the field results obtained from Project 7, where there was an approximate line variation as expected (Figures 3.8 and 3.9). The conflict between the laboratory and field results should be resolved through additional testing, since the field tests are not conclusive, given that only two blended test sections were placed.

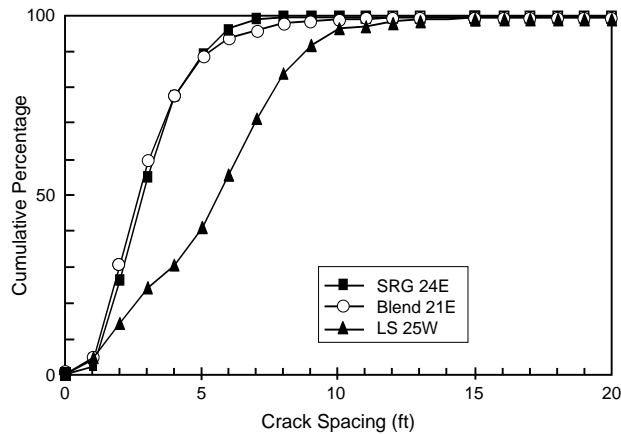


Figure 4.15 Comparison of crack spacing distributions for LS, SRG, and blended coarse aggregate at 640 days (Project 8) (1 ft = 0.30 m)

SUMMARY

The most significant variable in crack spacing is aggregate type. The most successful approach toward improving the crack spacing distribution of CRCP is placement during the winter months. The use of blended aggregates and skewed steel also yield small benefits.

4.2 CRACK WIDTH

A variety of factors affect the width of cracks. As was done previously with crack spacing, the variables that control the crack widths will be subdivided into the six subcategories of early-age cracking, placement season, placement temperature, steel percentage, skewed steel, and aggregate type.

EARLY-AGE CRACKING

Cracks that form within the first few days of a pavement’s life tend to have a larger crack width than cracks that occur later, based on data obtained from Projects 1–4. The difference is small, only about 0.002 in. (0.0508 mm) (Ref 6). The reason for this difference is believed to be owing to the fact that the bond existing between the steel bar and the concrete is weak, compared with its strength at a later age. So the weaker concrete does not develop the stress in the rebar as quickly when a crack occurs. Thus, the bond development

length is larger for new concrete than for older concrete. Since the development length is longer at early ages, cracks formed during early age will have wider openings.

PLACEMENT SEASON

Pavement test sections placed on SH-6 in Houston, Texas (Projects 1 and 2), dramatically show the difference in crack width resulting from the placement season. The average crack widths in sections paved during the winter were much higher, about 2.5 times higher, than crack widths in sections paved during the summer (Ref 6). Little research has been undertaken on the topic to understand the cause of the difference. Part of the difference is related to the crack spacing. The winter sections have cracks that are spaced much farther apart. If a fixed amount of volumetric change occurs in the pavement, the pavement will have either wide cracks spaced far apart, or narrow cracks spaced close together. The difference in crack width may also be related to the bond development, as is the case in early-age cracking. Since the temperatures are lower, the concrete takes longer to develop strength, so the crack's bond development length would also be longer.

REINFORCING STEEL

The percentage of steel in the pavement can affect crack width, just as it can affect the crack spacing. The reinforcing steel can be divided into two categories: (1) steel percentage and (2) bar size.

As the amount of steel increases, the crack width decreases. This is believed to occur because an increased area of steel leads to a decreased average steel stress and, therefore, to less elongation of the steel and a narrower crack. However, the magnitude of the difference between the crack widths for the percentages of steel used in the experiment is not very large (Ref 7). Test sections having steel percentages of greater extremes are needed to verify this hypothesis.

The effect of bar size on crack width is similar to the effect of steel percentage on crack width. If the bar size is increased, the crack width would be expected to increase, given a constant percentage of steel owing to the bond slip between the concrete and steel. This effect was observed in the sections paved in 1989 and 1990, though the effect was very small

(Ref 6). In fact, after 2 years, the SRG sections had crack widths that were contrary to the trend, while the LS sections continued to follow the trend (Ref 7).

AGGREGATE TYPE

One of the most important factors affecting crack width is the coarse aggregate type. The SRG sections have consistently had crack widths larger than those on LS sections in all sections placed under similar conditions. This effect is believed to be based on the thermal coefficient of the aggregate. Since the thermal coefficient of SRG is about 60% higher than the thermal coefficient of LS, the SRG pavement will move much more in response to temperature differentials than would the LS sections (Ref 7). The additional movement in SRG leads to more cracking and larger crack widths, as compared with LS sections.

PAVEMENT THICKNESS

A correlation has also been found between pavement thickness and crack width. The thicker the pavement, the smaller the crack width. This effect could be due to the fact that thicker pavements have a volume-to-surface-area ratio higher than that found in thin pavements. Since thicker pavements have less exposed surface relative to their volumes, the percentage of shrinkage at the time of placement decreases (Ref 7).

SUMMARY

The principal factor affecting crack width is the aggregate type; the reason for its importance with respect to crack width is related to the thermal coefficient of the aggregate. Other factors affecting crack width include the age of the pavement when the crack develops, placement season, steel percentage and bar size, and slab thickness. Of those other factors, placement season is the most significant.

4.3 RANDOMNESS INDEX (RI)

As mentioned in the monitoring section, the randomness index (RI) is a measure of the straightness of a crack. With this index, a value of 5.46 represents a perfectly straight crack, with the value decreasing as the quality of the crack drops (Figure 2.6). Using the RI, the effects of the design and construction variables can be gauged with respect to their

cracking pattern. Straight cracks are ideal because meandering cracks can lead to punchouts as cracks surround all sides of a small section of the slab.

The RI information can be evaluated in several different ways. The RI distribution for the Project 8 test sections in Figure 4.16 shows that SRG sections (28E and 31E) had the lowest values of RI, with 25% of the cracks in the poor RI range, which means that the cracks with the SRG are generally poorer. The sections that had transverse sawcuts had much higher RI values (with most in the excellent range) than did comparable pavements (22E and 26E). The limestone sections were in the middle (25W and 28W), with almost all of the cracks in the “fair” and “good” ranges.

Another useful way to evaluate the RI is to measure the mean value of several cracks. Figure 4.17 shows the mean RI for Projects 1–4 and 8. Note that the sections paved during the winter (Projects 1, 3, and 4) had a higher RI than the sections paved during the summer (Project 2); all these means were in the good range. The Project 8 sections were placed during mild summer conditions. Therefore, the RI values are reasonable compared with the higher RI values for winter sections and the lower RI values for the other summer section. The SRG mean is only in the fair range, whereas the LS and blended means are in the good range. Also note that the transverse sawcuts for the summer placement (Project 8) produced RI values that were higher than those of any of the winter sections. This indicates that the sawcutting is effective in producing straighter cracks if set at values nears those at which the crack spacing will stabilize. The sawcut sections begin with an RI of 5.46 because the sawcuts are straight, but the occurrence of intermediate cracks reduces the average randomness to below 5.46.

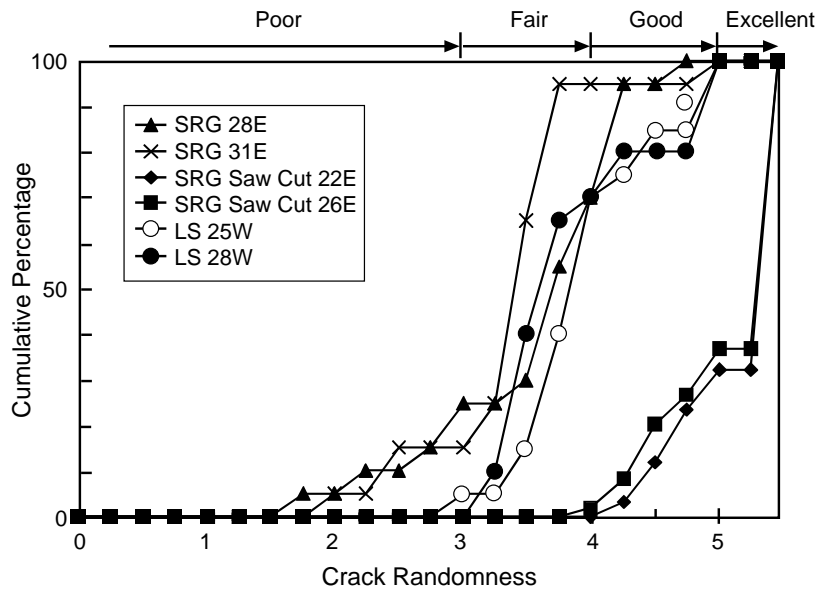


Figure 4.16 Randomness index (RI) distribution by section for the Project 8 test section

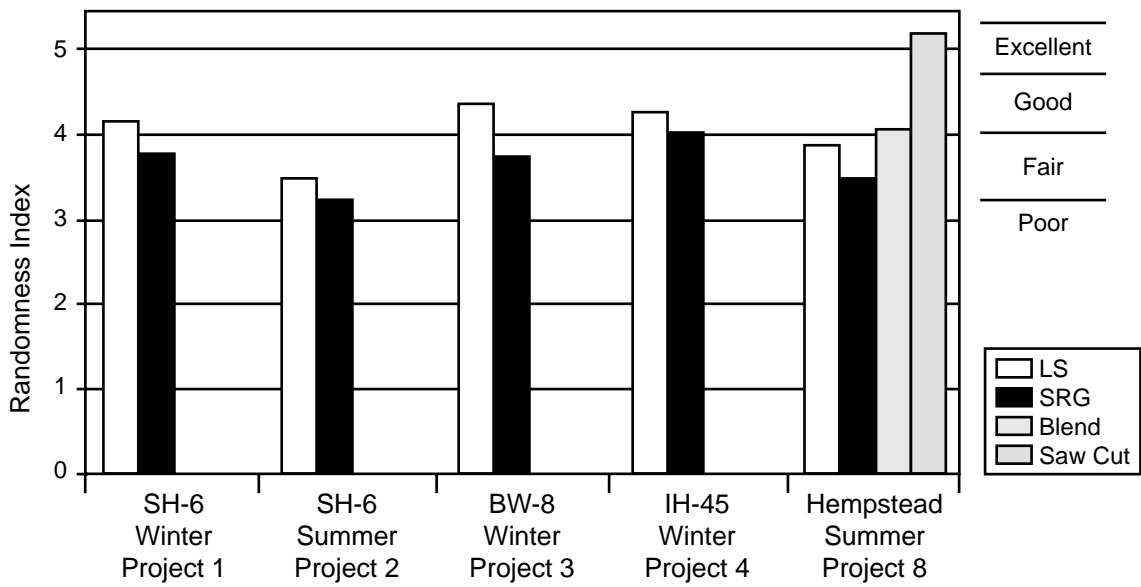


Figure 4.17 Average RI for Projects 1- 4 and 8

4.4 DELAMINATION SPALLING

Spalling is not very severe on any of the Project 8 sections, since only minimal traffic loading has been experienced. Furthermore, it is not expected to become severe because the evaporation rate was unusually low during paving. Cores taken from the pavement did not exhibit any delamination; however, some important observations can be seen from the earlier sections that have experienced spalling. The locations where spalling has been most prevalent are the sections on SH-6, with heaviest spalling occurring in the summer-placement section (Project 2). Some spalling has also been seen on Projects 1, 3, and 4, with most of the spalling occurring in the river gravel sections.

SPALLING OVER TIME

Spalling does not usually manifest itself very early in the pavement life. However, it is believed that the mechanism producing the spall usually occurs around the time the pavement is being placed, though traffic loading must occur before the spall will form to the point of being visible on the surface of the pavement.

PLACEMENT SEASON

Placement season and aggregate type are the two most important variables in spalling development. Comparing the winter and summer placement test sections, the summer sections experienced much more spalling than did the winter sections.

Figure 4.18 shows the four different test sections. The SRG test section placed in the summer is experiencing the most spalling of all the sections. The SRG section placed in the winter is also experiencing spalling, but only minor spalling, even though the pavements have similar designs. The LS sections show little spalling in either the winter or the summer sections.

Also note that the sections placed during the winter are performing much better than the sections placed during the summer. The reason for the large difference is believed to be based on the evaporation rate occurring during the concrete's set time. The evaporation rate for the sections placed in the winter is usually much lower than the evaporation rate for the summer sections.

A high evaporation rate induces a moisture gradient in the pavement. The moisture gradient produces variable stresses within the pavement cross-section that lead to horizontal cracking within the pavement, which, in turn, causes spalling. For that reason, the evaporation rate must be controlled if spalling is to be avoided. If the evaporation rate is low enough, delamination spalling will not occur in pavement placed using either aggregate.

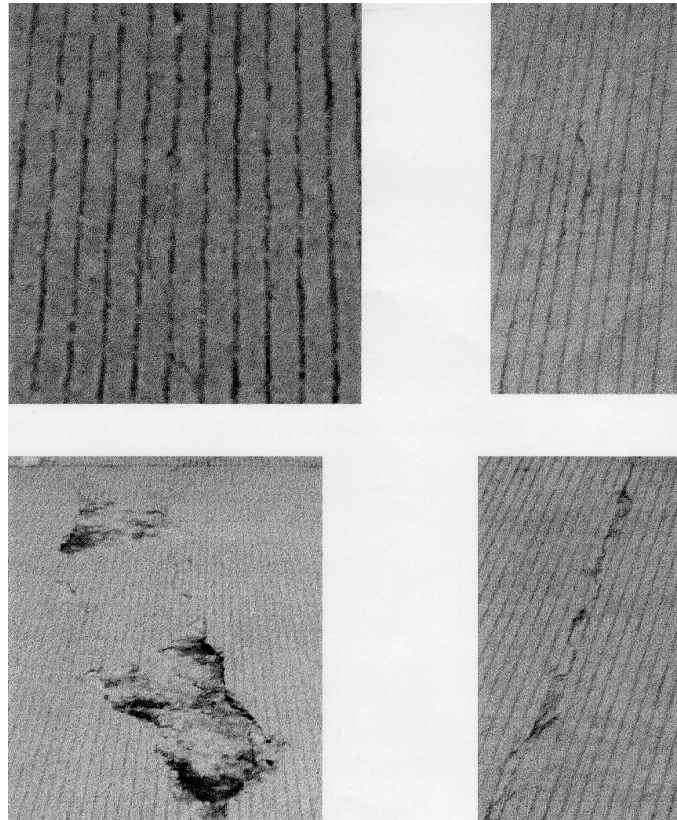


Figure 4.18 Spalling in Projects 1 and 2 (top left — LS summer, top right — LS winter, bottom left — SRG summer, bottom right — SRG winter)

PLACEMENT TIME

Spalling is very strongly correlated to a high evaporation rate. It is, therefore, expected that the placement time will have an effect on spalling, since low evaporation rates usually prevail during nighttime paving. Nighttime paving may even lead to less spalling than the nighttime evaporation rate alone would suggest. However, because the most recent test sections have not yet experienced spalling, proof of the hypothesis is not yet available. It

should be noted that almost any measure taken to reduce the pavement evaporation rate could help reduce spalling.

AGGREGATE TYPE

The other major factor in spall development is aggregate type. Figure 4.18 also compares LS and SRG sections paved during the summer. Notice that the SRG section is experiencing much more severe spalling. There is little doubt that the aggregate type is a factor in the deep spalling noticed in the SRG section. The cause of the difference may be due in part to the angularity of the aggregate, the thermal coefficient of the aggregates, and to the hardness of the aggregate. When designing a pavement using SRG, it is important to avoid conditions that would cause the SRG to have spalling problems. The key factor in preventing spalling is reducing the evaporation rate of the pavement.

ALTERNATE CURING TECHNIQUES

Several methods were attempted to control spalling by decreasing the effective evaporation rate of the pavement in the test sections. The techniques used to decrease the evaporation rate are one coat of standard curing compound, two coats of standard curing compound, one coat of Procrete curing compound, polyethylene sheeting, and cotton mats. While all of these curing techniques attempt to lower the evaporation rate of the pavement, some methods are more effective than others.

Of all the methods used, the cotton mats performed the best. Cotton mats provide a significant decrease in the effective evaporation rate of the section. The polyethylene sheets also work well, though not as well as the cotton mats. The Procrete curing compound is useful when wet sawcutting is going to be used after the curing compound is placed (it does not bind up the blade) (Ref 9). Applying one coat of curing compound can reduce the evaporation rate. Using two coats was attempted, but it has not significantly improved performance of the test sections. Although curing compound can improve pavement performance, it is the least effective way to control evaporation rate of the methods tested.

SUMMARY

The major factors affecting spalling are aggregate type and evaporation rate. The evaporation rate can be decreased by using night paving, winter paving, and better curing

techniques (e.g., cotton mats or polyethylene sheeting). Current research is also investigating the effects of sawcuts on spall development.

4.5 EVAPORATION-INDUCED STRENGTH LOSS

As discussed in Chapter 2, the evaporation rate can affect the strength of concrete. The results from Project 8 and other sources that are presented in the following sections demonstrate this concept.

FIELD DATA

The hypothesis that evaporation produces strength loss in concrete was tested using the cores taken from this project. The first testing step was to cut each core into three horizontal slices. By splitting the core, variations of the concrete strength at different depths could be determined.

The samples were then tested using the split tensile test method. Figure 4.19 shows the distribution of strength for the river gravel sections. The evaporation rates were low in these sections; they were never more than $0.566 \text{ kg/M}^2/\text{hr}$ on the SRG side. Notice that all strengths were fairly similar, but the top is slightly weaker.

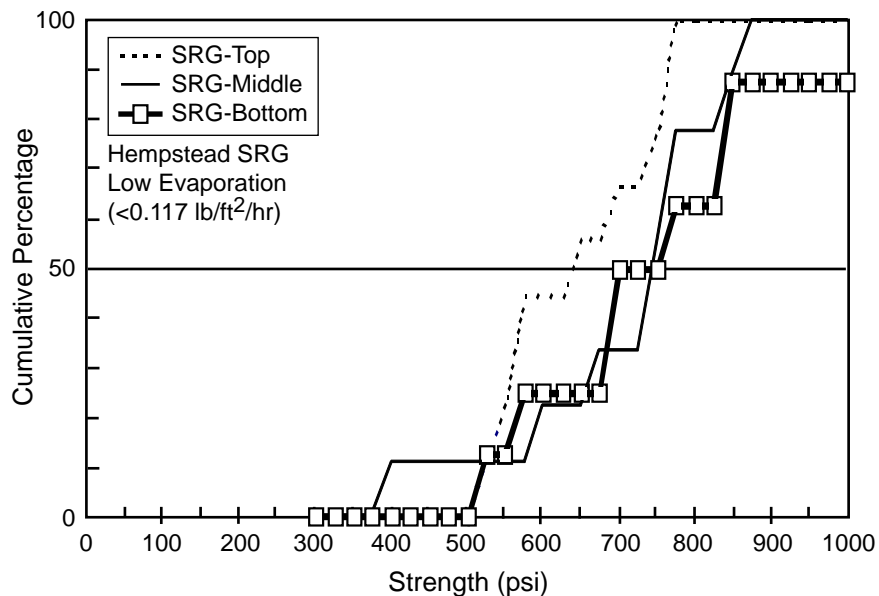


Figure 4.19 Cumulative strength distribution for siliceous river gravel (SRG) aggregate, Project 8

Figure 4.20 shows the distribution for limestone aggregate. The evaporation rate was usually low in these sections, but it was higher than that for the river gravel sections. During one of the days of paving, the evaporation rate reached $1.132 \text{ kg/m}^2/\text{hr}$. However, the evaporation rate stayed above $0.976 \text{ kg/m}^2/\text{hr}$ for a total of only 5 hours during the 6 days that the LS pavement was being placed. Notice that the strength reduction in the top layer of the section is greater than the strength reduction in the river gravel section. The difference between the top and bottom median strength in the SRG sections is about 1,033.5 kPa, while the difference is 1,722.5 kPa in the limestone sections. That difference is consistent with the hypothesis, given that the evaporation rate is somewhat higher in the limestone section.

The data from Project 8 seem to agree with the hypothesis proposed in Section 2.2 of this report. However, the evaporation rates were not high enough to produce lower-level strength reduction. Therefore, data were taken from a pavement that was recently placed at the McLaran Airport in Las Vegas, Nevada. The data show the concrete strength for both high and low evaporation rates.

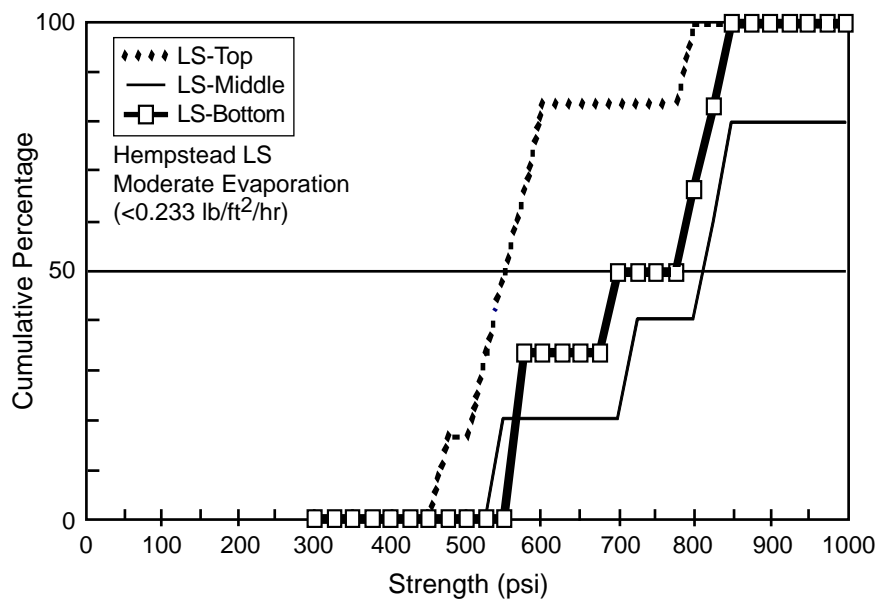


Figure 4.20 Cumulative strength distribution for limestone aggregate, Project 8

Notice in Figure 4.21 that the top strength is much weaker than the bottom strength, and that the maximum difference in median strengths is about 1.55 MPa. The difference is

believed to have occurred because the curing compound was applied approximately 2 hours after concrete placement. The late application of curing compound caused the water to continue to be removed from the upper concrete for an extended amount of time. Because the evaporation rate was low, the lower layers were not affected by the water loss in the upper layers.

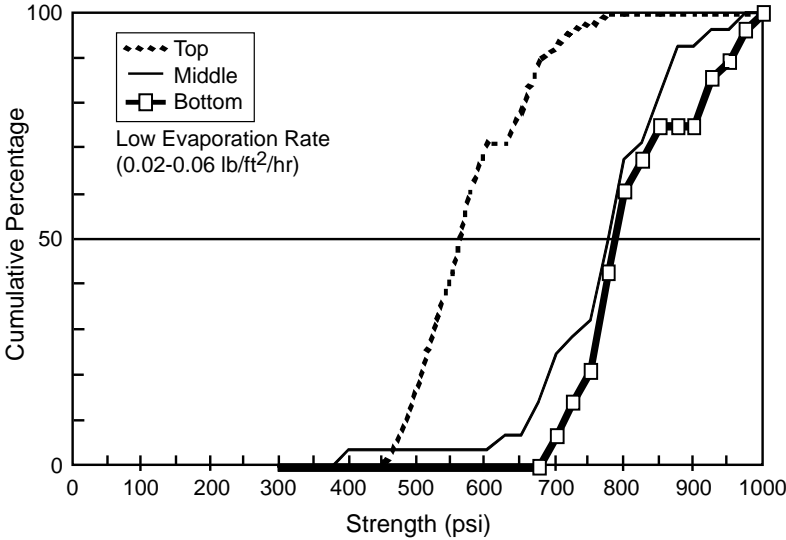


Figure 4.21 Cumulative strength distribution from Las Vegas at low evaporation rates, but delayed application of the curing compound

Figure 4.22 shows the strength distribution for the concrete that was poured with an evaporation rate between 1.708 and 1.757 kg/m²/hr. Notice that all layers of the concrete had low strength. As expected, the strength of the top layer was lowest of all. Since the high evaporation rate led to strength loss in all layers, the difference in median strengths from top to bottom was only 51.7 kPa.

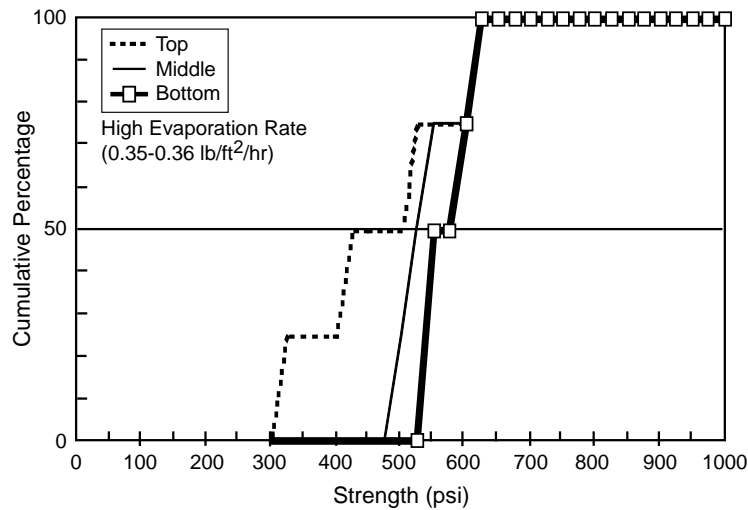


Figure 4.22 Cumulative strength distribution from Las Vegas at high evaporation rate

To clarify the results, the data were separated into top and bottom layers and then plotted. Figure 4.23 shows the strength distribution for the top layers at high and low evaporation rates, while Figure 4.24 shows the same information for the bottom layers. Compare the results with the conceptual results in Figures 2.14 and 2.15. Notice that the strength difference is smaller for the upper layers (41.4 kPa) than for the lower layers (1.37 MPa), indicating the validity of the hypothesis.

These results show the importance of avoiding concrete placement when the evaporation rate is high. The data also show that by controlling the evaporation rate through curing compounds, the concrete tensile strength can be increased.

4.6 SUMMARY

The data presented for Projects 1–4 and 8 indicate that aggregate type and the temperature at placement were the most significant factors affecting the performance of crack spacing, crack width, randomness index, and spalling. Thus, to achieve high performance concrete pavements, these factors must be accounted for by design, specifications, and by construction procedures.

The vertical strength distribution was also a significant finding of this project. Its presence leads to delamination spalling and reduced performance. The following chapter provides an understanding of this mechanism.

Since the significance of aggregate type on performance is primarily due to the thermal coefficient, an understanding is also needed of this parameter. Chapter 6 discusses thermal coefficient in more detail.

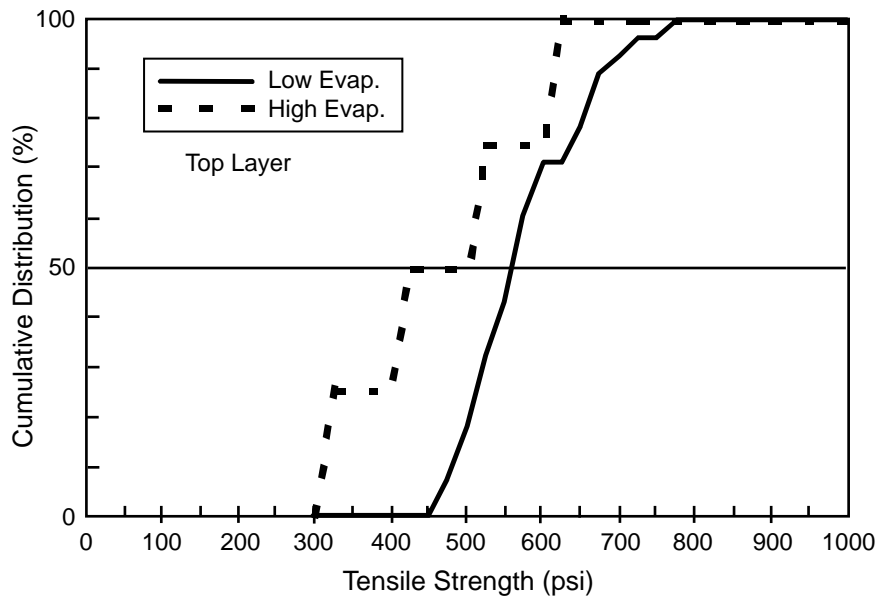


Figure 4.23 Cumulative strength distribution from Las Vegas for the top layers

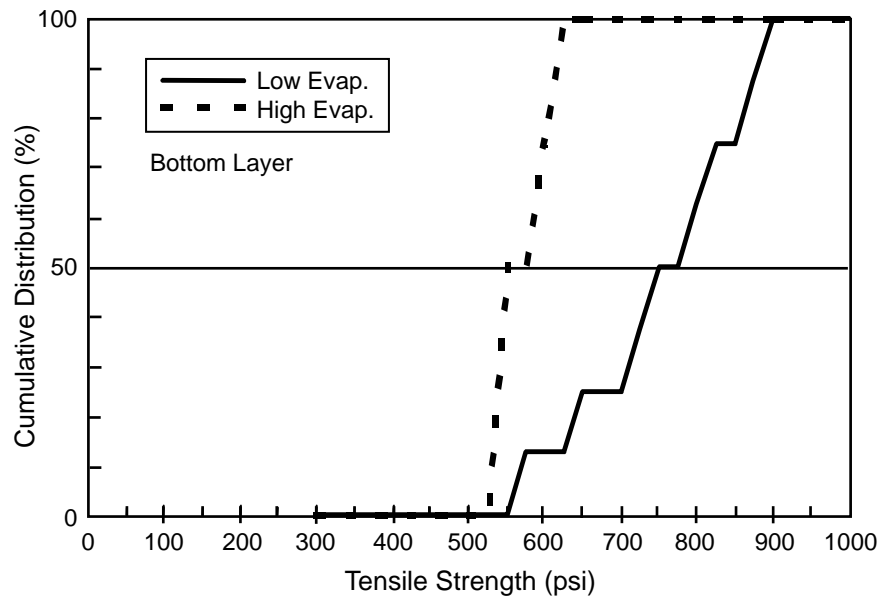


Figure 4.24 Cumulative strength distribution from Las Vegas for the bottom layers

CHAPTER 5. CHARACTERIZATION OF DELAMINATION SPALLING

Spalling is a serious concern in pavement design. As discussed in Chapters 2 and 4, spalling leads to poor ride quality and to other distress. If a mechanistic spalling model could be developed to accurately predict delamination spalling, major improvements could be made in pavement performance by controlling the spalling mechanism. This chapter introduces this spalling mechanism (a more detailed discussion can be found in Appendix E).

5.1 INTRODUCTION

Spalling is a form of distress occurring in concrete pavements. It is defined as the breakdown of the joint of a slab within 6 in. (15 cm) (of the joint (both longitudinal and transverse) or crack. It is often associated with adverse weather conditions and with smooth, rounded aggregates. Since spalling is very costly to repair, an objective of Research Study 7-3925 was to develop a mechanistic spalling model so that spalling could be predicted and, thus, prevented. The spalling model developed has been incorporated into a finite element program to give numeric results that can be easily evaluated; its concepts must now be incorporated into the CRCP model.

5.2 OVERVIEW

Spalling is a concrete pavement distress in which pieces of concrete are dislodged from the surface of the pavement, as illustrated in Figure 5.1. This distress is a consequence of delaminations formed during the early life of concrete pavements as a result primarily of moisture loss from the pavement slab to the environment — a loss that depends on ambient and curing conditions. High tensile and shear stresses develop prior to traffic opening, a result of the pavement being restrained from moving. Accordingly, stresses caused by temperature and moisture variation require further analysis for their potential to surpass the early concrete strength, causing crack development in the zones of higher stress levels. Significant “delamination spalling” is unlikely to occur when the delaminations are not formed. In the event that they are formed, their extension into spalling appears to be by fatigue induced primarily by wheel loads and cyclic temperature fluctuations.

STRESSES DUE TO TEMPERATURE VARIATION

Thermal stresses in pavements hasten spall development once the condition for delamination in the pavement has occurred. However, thermal stresses are usually much smaller than moisture-related stresses in the vertical direction during the early life of the pavement; consequently, thermal stresses were not considered in this research even though the spalling model allows the inclusion of thermal stresses in the input.

STRESSES DUE TO MOISTURE VARIATION

Stresses caused by moisture variation in the vertical direction have often been overlooked in the stress analysis of concrete pavements. However, moisture-induced stresses are usually much larger than thermal stresses. Therefore, the focus of the research was to accurately find concrete moisture contents. In this study, concrete moisture contents have been determined by direct measurements using specially prepared dew point sensors. The relative humidity was then converted to equivalent drying shrinkage to obtain moisture-related stresses.



Figure 5.1 Typical example of spalling

As shown for Project 7, the moisture-related stresses will have significant variation, as demonstrated in Chapter 3. The stresses will depend on the evaporating rate, the type of curing, and the time difference between placement of the concrete and the curing compound. Furthermore, these factors will also affect the distribution of concrete strength vertically through the slab, as shown in the work on Project 8 presented in Chapter 4.

STRESSES DUE TO COMBINED TEMPERATURE AND MOISTURE VARIATION

Since the finite element package used for this study requires input in terms of thermal strains, the inputs of moisture-related strains must be input into the model as an equivalent thermal strain. Therefore, the results can be interpreted as responsible for the combined effect of both thermal and shrinkage strains if both thermal and moisture-related strains are evaluated.

5.3 SPALLING MECHANISM

Recently, field studies in Texas have led to the establishment of a mechanism for the spalling distress characterized with engineering mechanics. Spalling development consists of a step-by-step process. The three steps discussed are: (1) delamination formation, (2) delamination extension, and (3) spall development.

DELAMINATION FORMATION

Delaminations are cracks oriented parallel to the surface of the pavement; they have been noted to initiate early in the pavement life and to be principally located at transverse cracks or joints. These cracks typically occur in depths 1–3 in. (25–75 mm) from the surface. Longer delaminations are observed closer to the pavement surface. Lengths of delaminations may depend on pavement age, but is primarily related to high evaporation rates occurring during construction, and poor bond between the aggregates and mortar.

The formation of the concepts for delamination may be achieved by describing a set of qualitative curing conditions that range from excellent to poor, as shown in Table 5.1. These conditions lead to different rates, quantity, and depth of moisture, leaving the slab as relatively portrayed in Figure 5.2. With excellent curing, very little moisture is lost; thus, the vertical stresses are low, as shown with the conditions to the left on the figure. As the quality

of the curing conditions decreases, the moisture loss increases substantially along with the vertical stress.

Table 5.1 Description of qualitative curing conditions

Curing Condition	Description
Excellent	Low evaporation and/or superior curing method and early application
Poor	Moderate evaporation and/or delayed application of good curing technique
Very poor	High evaporation and/or poor curing techniques or material

Figure 5.3 can be used to illustrate the probability of delamination formation for each curing condition. These conditions will result in a vertical stress distribution through the slab that starts at a high level near the top and decreases with depth. A decrease in the quality of curing results in higher stresses that goes deeper into the slabs. As demonstrated in Chapter 4, the tensile strength (f_t) will be reduced near the surface and the effect will go deeper into the slab with decreased quality of curing. Thus, delaminations will occur that increase in probability and depth with decreased curing quality, as shown on the right. The delamination is created during the initial construction phase, but it is not apparent and its effect does not appear until later.

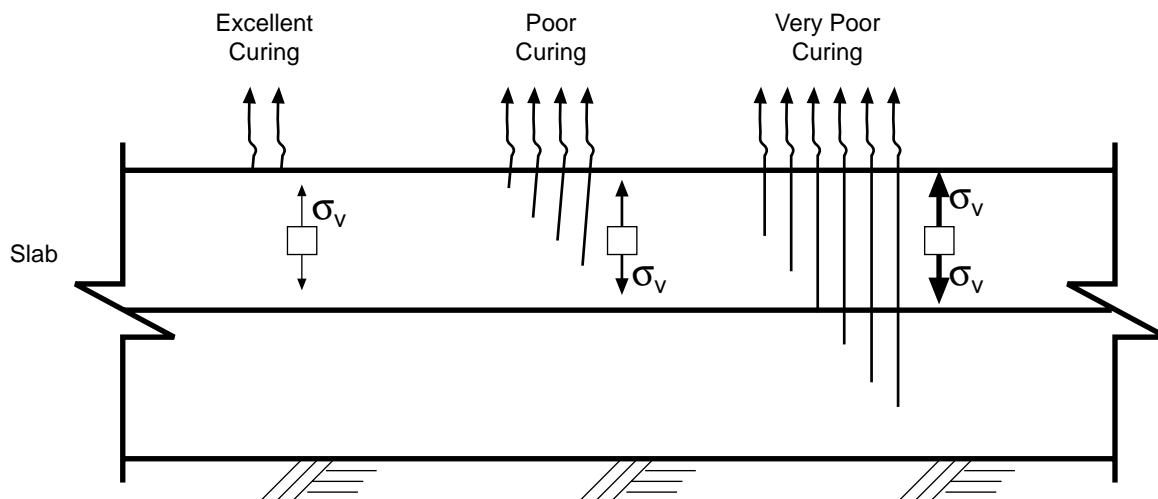


Figure 5.2 Conceptual illustration of relative moisture loss and stresses due to different curing conditions

DELAMINATION EXTENSION

Once the delaminations form, they enlarge primarily as a result of traffic loading. In this study, the traffic-induced stresses were considered by comparing the stresses produced by worst-case scenarios. The direction of delamination extension was based on the highest stress produced near the crack. Other factors, such as variations within the pavement, also influence the direction of delamination extension. However, they were not modeled owing to the lack of data needed to characterize the random nature of such variations.

SPALL DEVELOPMENT

With traffic loadings, the delaminations illustrated in Figure 5.3 will experience vertical fractures. This will produce a loose piece of concrete that will work out with traffic applications. The resulting spalling distress will be as shown in Figure 5.1, with a flat bottom resulting from the delamination plane.

Figure 5.4 was developed from the TxDOT rigid pavement database for low and high evaporation conditions (designated for projects across the state). The approximate date of the construction was known for each test section and the maximum evaporation on the date of placement was computed from the nearest weather station. The age of the pavement at the time of the survey was used as the x -axis. An examination of the graph shows that for a low evaporation rate the spalling starts earlier, but reaches an asymptote. The spalling rate for the high evaporation starts later, but increases more rapidly and does not approach a maximum level. These trends may be explained by the fact that the deeper position of the delamination takes longer for the fatigue from traffic loadings to break out. The greater rate and magnitude of spalling is due to the higher probability.

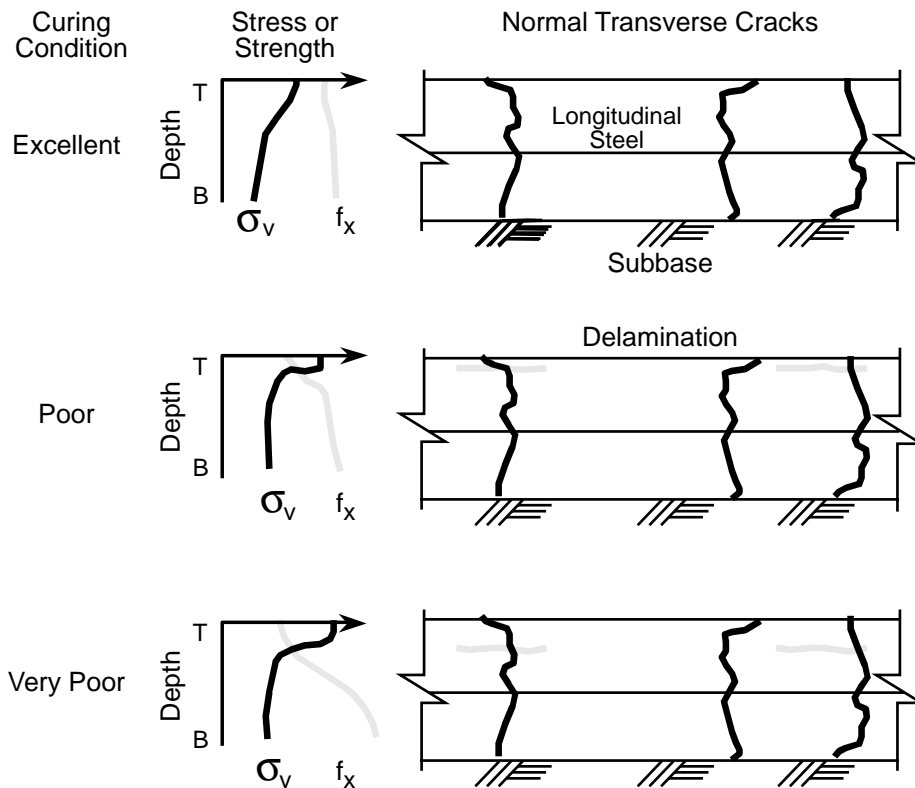


Figure 5.3 Conceptual illustration of the delamination mechanism and the relative impact of different curing conditions

Once a conceptual mechanism for spalling was found, a finite element program was used to determine when spalling is likely to occur, based on the assumption that delaminations grow into spalls as traffic loading is experienced.

SUMMARY

The spalling model developed for this research study uses mechanistic principles combined with a finite element program to give numeric results that model observed field experience. The results of this model are intended for implementation in such pavement design programs as CRCP-8. Using the expected paving conditions, the model would predict the extent to which spalling would likely occur. If spalling is likely, measures can be taken to prevent the distress.

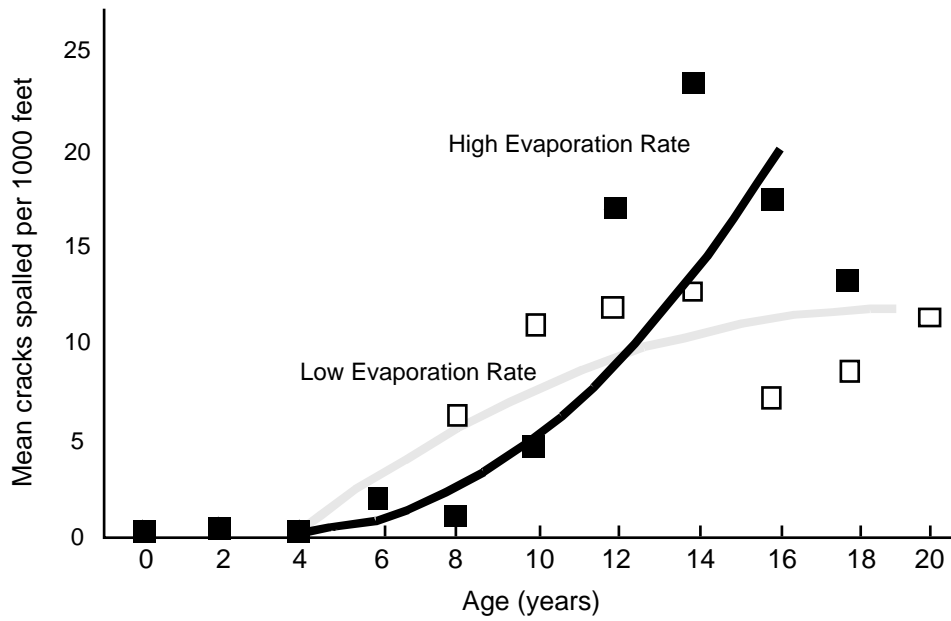


Figure 5.4 Historical development of spalling as a function of evaporation rate

CHAPTER 6. THERMAL COEFFICIENT OF CONCRETE

In Chapters 3 and 4, it was shown that the coarse aggregate has a strong influence on the properties of concrete. A major factor in performance differences found in concrete pavements made with different coarse aggregates is believed to be the coefficient of thermal expansion (CTE) of the aggregates. It is possible to measure the coefficient of thermal expansion using laboratory testing; however, the expense and time required to perform the tests make it impractical to use for design purposes. If a quick, low-cost solution can be found, it would become practical for designers to look at the effects of using a particular aggregate in a proposed concrete mix.

The coarse aggregate studies have, therefore, focused on understanding the factors leading to the CTE of concrete, and finding simple ways to predict it.. Once these tests are simple enough to become commonly used, pavement designers can begin to predict much more accurately the performance of their pavement designs with the help of analysis programs such as CRCP-8.

The following sections summarize the CTE work undertaken in this project. Although the initial CTE developments were initiated on this project, TxDOT has initiated a more detailed study.

6.1 FACTORS AFFECTING CTE

The CTE of concrete is affected by a large number of factors that can be generally grouped into the two major components of concrete: cement paste and aggregate.

CEMENT PASTE

Of the two major components of concrete, the cement paste usually has the largest coefficient of thermal expansion. Typical values of CTE of cement paste are between 9.0×10^{-6} and $21.0 \times 10^{-6} \text{ } ^\circ\text{C}^{-1}$. The CTE of the paste is primarily affected by the moisture content of the paste; thus, it will vary in a significant manner during the hydration process and will stabilize thereafter. Other factors include the fineness, brand of cement, and the age of the concrete.

AGGREGATES

Because aggregates form a large part of concrete by volume, it is logical that the coefficient of thermal expansion of the aggregates would have a large effect on the CTE of the concrete. Aggregates typically have a CTE between 4.0×10^{-6} and $12.0 \times 10^{-6} \text{ } ^\circ\text{C}^{-1}$, although some aggregates shipped from Mexico for use in Texas have a CTE as low as $3.0 \times 10^{-6} \text{ } ^\circ\text{C}^{-1}$. Limestones (LS) typically have the lowest CTE, while siliceous river gravels (SRG) often have some of the highest CTE. Granites and dolomites usually have values between LS and SRG. Figure 6.1 shows actual values of CTE for SRG and LS using a well graded and a gap-graded mix. The maximum aggregate size is also varied. The gap-graded mix generally has the lower CTE. Factors affecting the CTE of aggregates are the type, source, gradation, and chemical composition. Other factors, such as shape, crystalline structure, and degree of orientation, porosity, and degree of absorption, can also affect the CTE of aggregates, though to a lesser degree.

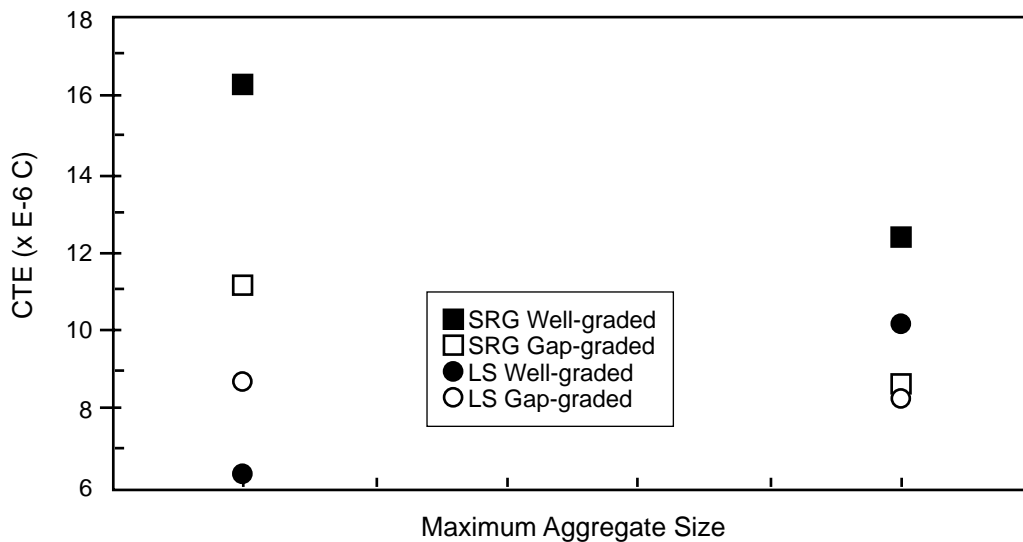


Figure 6.1 CTE for SRG and LS aggregates

6.2 THERMAL COEFFICIENT PREDICTION

Prediction of the CTE has been primarily based on components or based on chemical composition testing.

FROM COMPONENTS

Work has been underway to find a quick, in vitro testing method for determining the coefficient of thermal expansion of concrete based on the thermal coefficient of the components. This method involves placing the aggregates in a water dilatometer. The principle behind this method is that the water will change volume a certain amount for a given change in temperature. If some aggregate is added to the water bath, the CTE of the aggregate can be computed based on the actual volume change compared with the expected volume change of water alone. Once fully operational, this test should prove very easy to use with repeatable results.

FROM CHEMICAL TESTING

The emphasis of the research has been on the CTE of the aggregates because the CTE of the cement remains within a narrow range once it hardens. Since an aggregate's CTE is based primarily on its chemical properties, research has looked at ways to predict the CTE of aggregates based on their properties. The most direct way is by a chemical oxide test. This test can be performed relatively cheaply. Other methods of determining chemical composition are the ICP-AES and SEM-XMA processes. Both of these processes are rather complex and costly. The primary purpose of these tests is to characterize the aggregate properties for preliminary design.

Aggregate properties are primarily determined by an aggregate's chemical constituents, which include sodium (Na), aluminum (Al), magnesium (Mg), silicon (Si), calcium (Ca), and iron (Fe). Oxide residue testing can be used to determine an aggregate's chemical constituents. The primary elemental factors in determining the CTE of aggregates are the percentage of Si and Ca in the aggregate. Figures 6.2 and 6.3 show how the CTE of an aggregate varies by the percentage of each element.

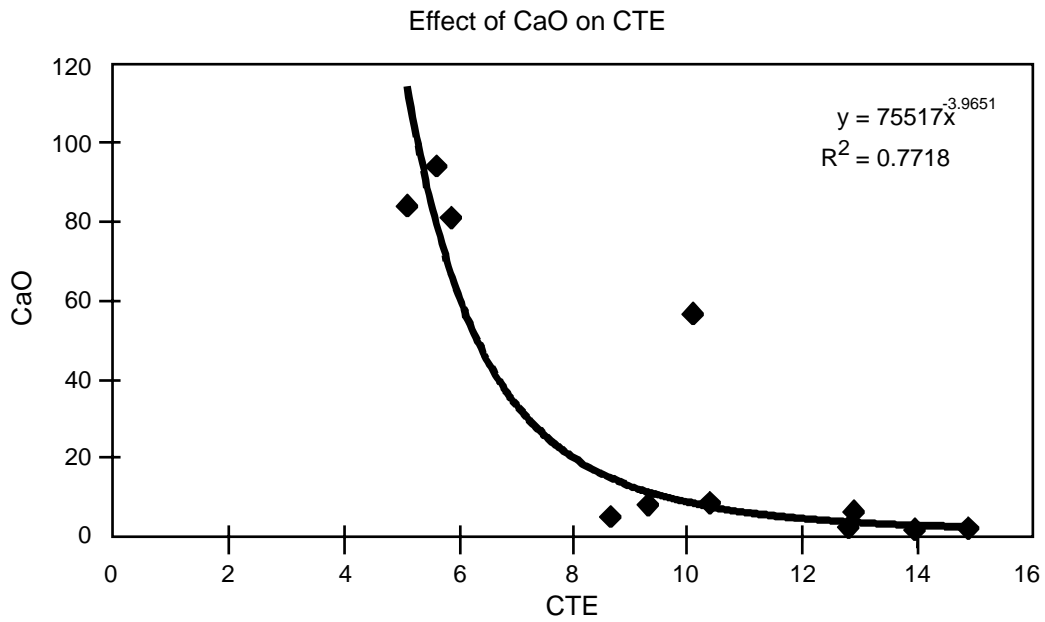


Figure 6.2 Effect of CaO on the CTE of aggregates

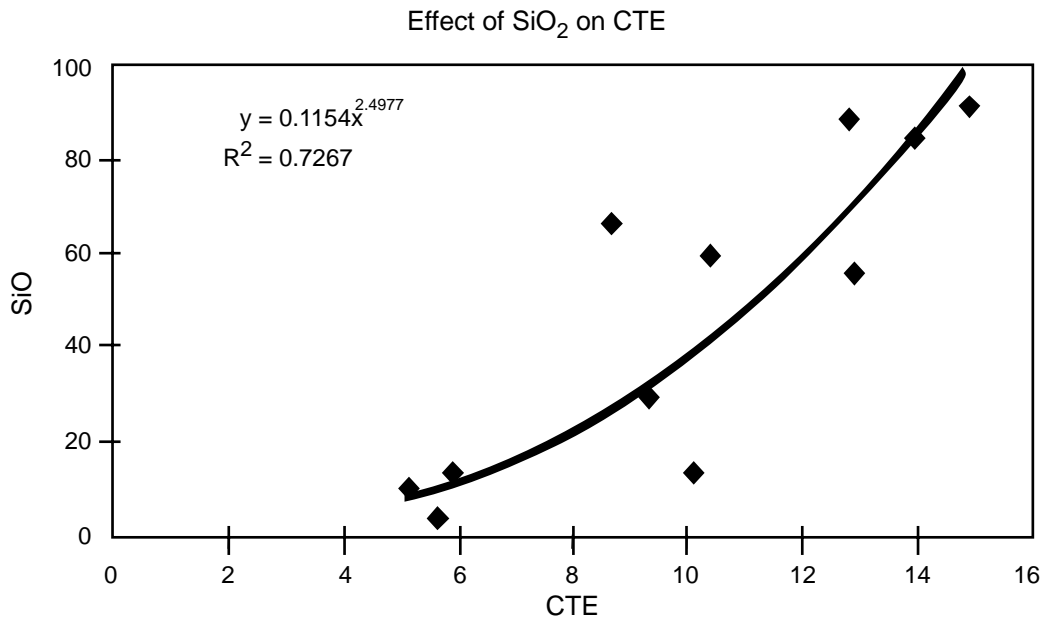


Figure 6.3 Effect of SiO₂ on CTE of aggregates

Based on these findings and on additional research, an equation was developed to determine the CTE based on the chemical composition of aggregates. The final form of Equation 6.1 predicts the CTE of aggregates very well ($R^2 = 0.92$).

$$\text{CTE}_{\text{agg}} = 2.36(\text{Na}) - 0.757(\text{Al}) - 0.109(\text{Ca}) - 0.271(\text{Fe}) + 16.017 \quad (6.1)$$

where:

Na = percent by weight of Na_2O

Al = percent by weight of Al_2O_3

Ca = percent by weight of CaO

Fe = percent by weight of Fe_2O_3

as given in the oxide residue analysis report.

6.3 SUMMARY

The coefficient of thermal expansion of concrete is based primarily on the properties of the cement paste and the aggregate. The CTE of the cement paste and the aggregates are affected by a wide variety of factors. Efforts are underway to find inexpensive ways to determine the CTE of aggregates by using a water bath testing apparatus called a dilatometer.

CHAPTER 7. VALIDATION OF CRCP-8

The pavement analysis computer program CRCP-8 was developed to predict such CRC pavement behavior characteristics as crack spacing, crack width, and steel stress. These factors, along with ESALs, are used to predict performance in terms of punchouts. CRCP-8 prediction models are based on mechanistic or theoretical principles. However, the prediction models have been calibrated by using actual pavement test sections, so that the models are more accurate. CRCP-8 has been calibrated to the point where the predictions produced by the program are reasonably accurate.

The data derived from the Project 8 (Hempstead) test sections surveyed at 640 days have been used to validate the actual crack spacing prediction model under a range of conditions. CRCP-8 was then used to predict crack spacing distributions using the actual environmental conditions and the pavement properties (e.g., steel percentage and coarse aggregate type). The validation of the models with respect to crack spacing distribution and mean crack spacing is discussed below.

7.1 CRACK SPACING

CRCP-8 is designed to predict both the mean crack spacing and the crack spacing distribution once the pavement has stabilized. The results of the program will be compared with actual results to calibrate the program's accuracy.

CRACK DISTRIBUTION

Since CRC pavements are assumed to crack at regular intervals, with a majority of the cracks being between 0.9144 m and 2.6 m, it is useful both for design and analysis to know the distribution of crack spacings in the pavement.

CRCP-8 was developed to predict a crack spacing distribution accurately for any coarse aggregate type and time of placement.

Figure 7.1 shows the actual and predicted distributions for a limestone coarse aggregate that was placed during the day. Note that, in Figure 7.1, the actual crack spacing distribution was slightly less than the predicted crack spacing. In all other figures, the actual crack spacing distribution was greater than the predicted crack spacing distribution, meaning

that CRCP-8 generally predicts the crack spacing distribution conservatively. Figures 7.2 through 7.5 are similar validations of the CRCP-8 program using different aggregate types, placement time, and blended aggregates.

The predicted crack spacing distributions were made using weather data obtained from both a project weather station (during construction) and Weather Bureau records (for subsequent periods). Since no tests were made of the subbase frictional resistance, the resistance was assumed based on previous tests on similar material. The concrete properties and their development with time were derived from general testing on the project and are not site specific. If the actual distribution of tensile strength were known (obviating an *assumed* normal distribution), the predicted crack spacing distributions would probably overlay the actual crack distributions. Even with these assumptions, the fit to the data is very good and would be improved with more site-specific information.

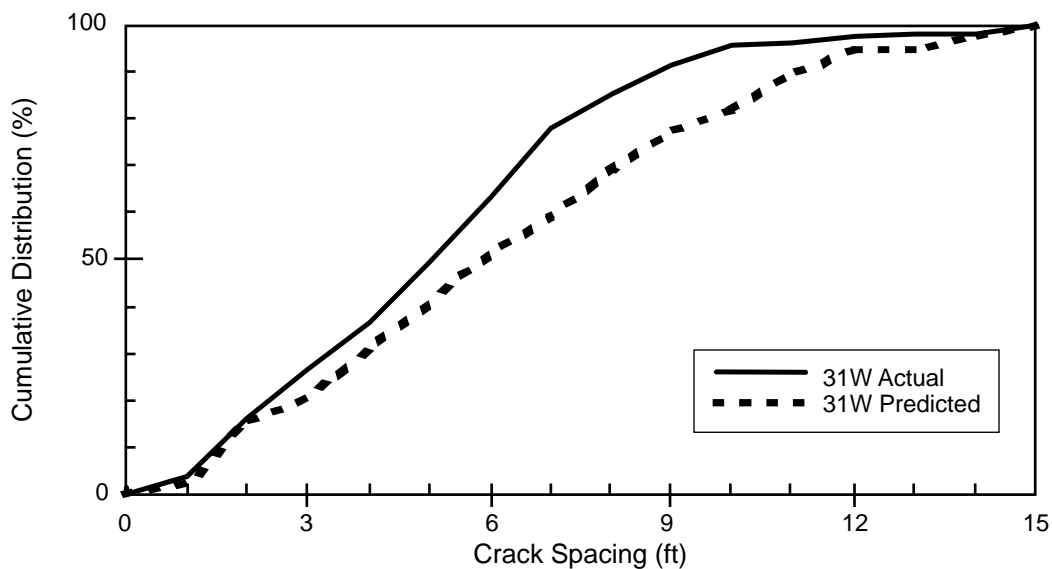


Figure 7.1 Comparison of predicted to actual crackspacing at 640 days for LS Day (Project 8 — Section 31W) (1 ft = 0.30 m)

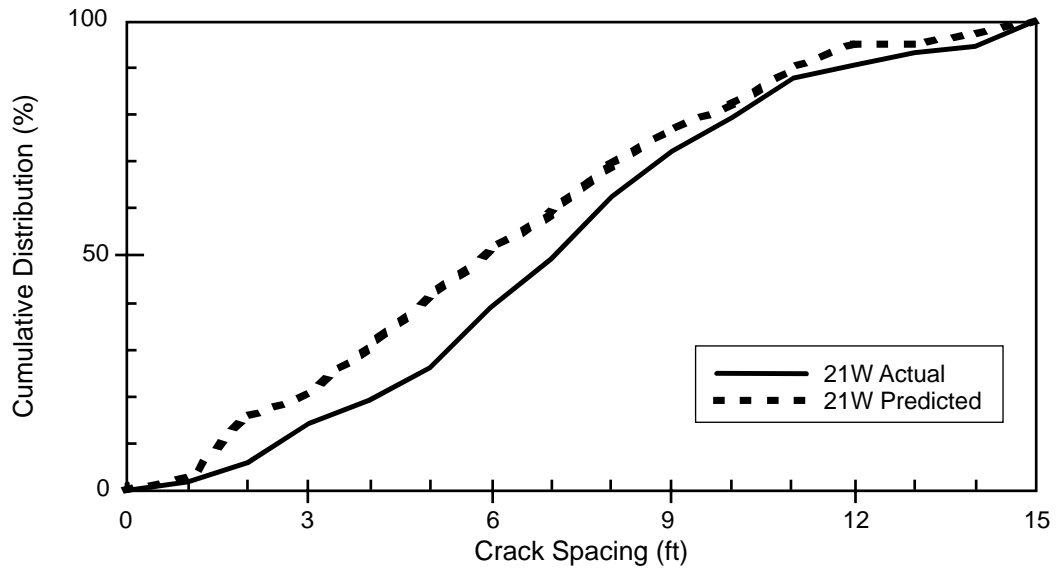


Figure 7.2 Comparison of predicted to actual crack spacing at 640 days for LS Night (Project 8 — Section 21W) (1 ft = 0.30 m)

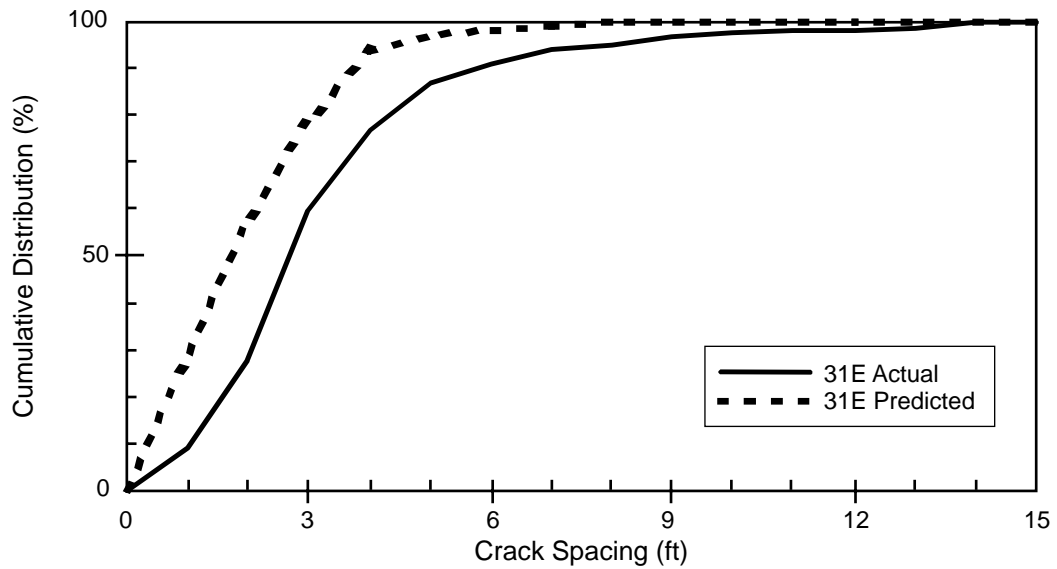


Figure 7.3 Comparison of predicted to actual crack spacing at 640 days for SRG Day (Project 8 — Section 31E) (1 ft = 0.30 m)

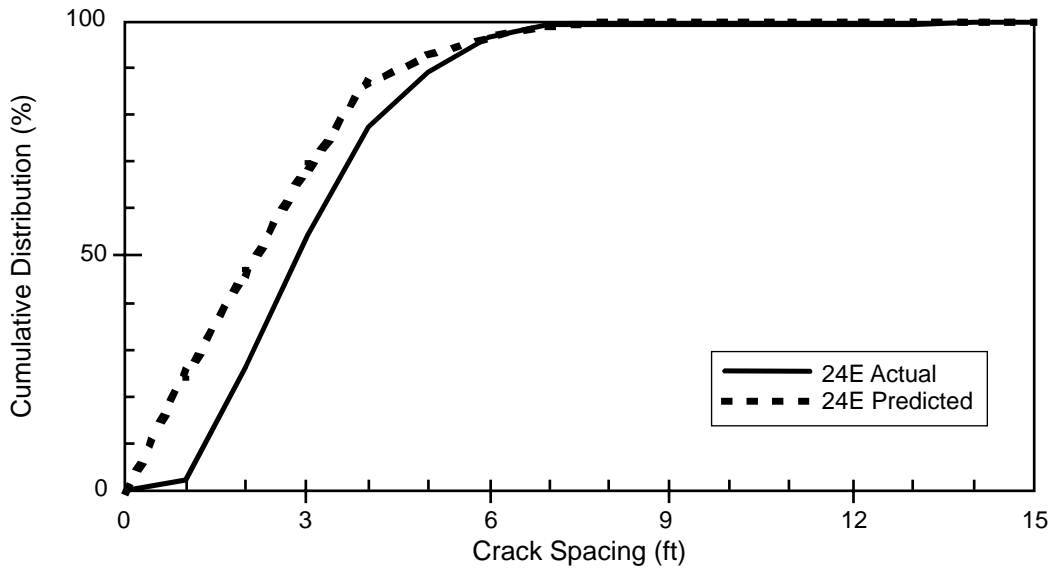


Figure 7.4 Comparison of predicted to actual crack spacing at 640 days for SRG Night (Project 8 — Section 24E) (1 ft = 0.30 m)

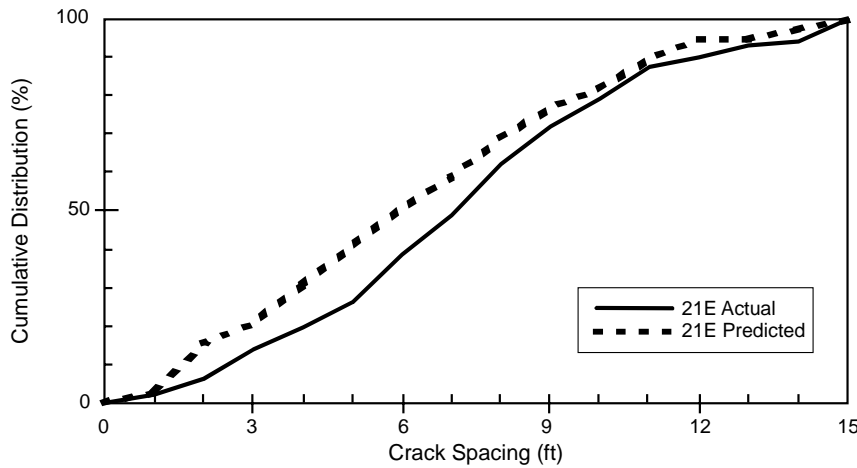


Figure 7.5 Comparison of predicted to actual crack spacing at 640 days for blend Day (Project 8 — Section 21E) (1 ft = 0.30 m)

MEAN CRACK SPACING

Since only selected sections can be shown for crack distribution, the predicted versus actual mean crack spacing is given for all the sections in Projects 1–4 and 8 in Figure 7.6. The predicted mean crack spacing is given on the *y-axis*, while the actual mean crack spacing

is given on the x -axis. Therefore, if the predicted crack spacing were equal to the actual, the point would be plotted along the diagonal line. The predicted mean crack spacings proved to be similar to the actual mean crack spacings. Note the line above the diagonal: It is the regression line for the plot. The regression line of the data is very accurate, considering that most of the concrete properties, and their change with time, were not available.

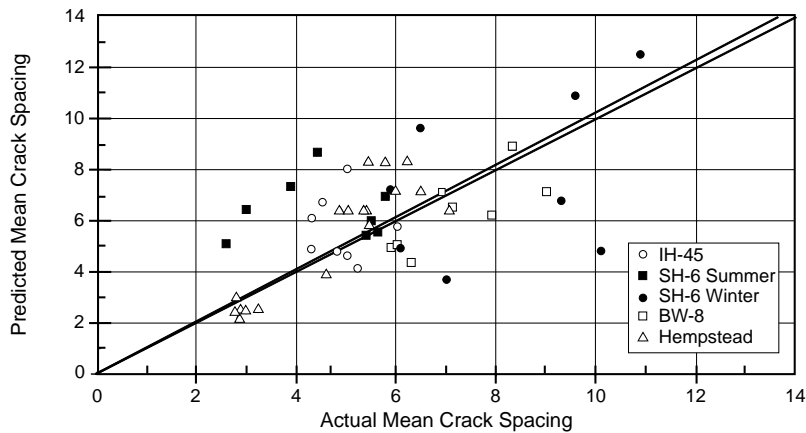


Figure 7.6 Predicted versus actual mean crack spacing ($r^2=0.71$)

7.2 SUMMARY

CRCP-8 is an analysis program that is used to predict the mean crack spacing and the crack spacing distribution of CRC pavements. It has been calibrated by CTR in previous studies using data from test sections placed by TxDOT. The latest test sections were used to validate the models applied to predict crack spacing. Figures 7.1 through 7.6 show that CRCP-8 can predict both the mean crack spacing and the crack spacing distribution very well under a variety of aggregate types and placement times.

CHAPTER 8. IMPLICATIONS OF STUDY

The six report subobjectives enumerated in Chapter 1 may be used as the basis for outlining the study implications. In this chapter, the results presented in Chapters 3–7 are discussed in the following sections vis-à-vis their effect on:

- 8.1 Improving pavement performance
- 8.2 Developing concrete pavement placement guidelines
- 8.3 Developing guidelines for the use of coarse aggregates
- 8.4 Predicting pavement performance
- 8.5 Suggesting future CRCP program developments
- 8.6 Suggesting general PCC pavement developments

When evaluating the recommendations, the reader should remember the scope of performance indicators outlined in the monitoring section of Chapter 2 (i.e., all the key performance indicators with the exception of steel stress and pavement punchouts were considered). Steel stress was not measured on any of the projects, and even the oldest of the projects has not experienced any punchouts. Since even the minimum values of the steel versus cross-sectional area in the slabs were more than adequate, it is doubtful that any significant rankings would have changed even if steel stresses had been measured on the projects. However, a later revisit of the study when the pavements are older may add additional insight to the observations made in the following sections.

8.1 IMPROVING PAVEMENT PERFORMANCE

The observations presented in Chapters 3 and 4 are used to formulate a general discussion regarding how the variables evaluated on these projects may be used to improve pavement performance. Next, a ranking system is used to establish the more significant variables. In addition, the least significant variables are also identified and guidelines are established as to their relative importance in being considered on future projects.

GENERAL DISCUSSION

The purpose of this report was to evaluate the hypotheses developed from previous research that looked at various methods and/or techniques to improve the performance of

concrete pavements. These can be broken into several categories, including aggregate properties, paving conditions, and reinforcement properties.

Since the most significant factor in predicting pavement performance is aggregate type, the designer should characterize the properties of the coarse aggregate that is to be used on the project. Using the CRCP-8 analysis program, a design can be tested using different aggregates to predict the crack spacing distribution, crack width, steel stress, and punchouts that will be based on the climatic conditions expected at the time of paving. If the crack spacing distribution is unacceptable, the results may be changed slightly by altering the design to include sawcutting, skewed steel, or night placement. However, if the crack spacing is not close to the desired crack spacing, the designer may recommend that an alternate coarse aggregate be used.

If the aggregate type cannot be changed, the designer can specify that the pavement be placed only under optimal conditions. The next largest change in crack spacing and spalling can be achieved by changing the placement season. The effect of changing the season represents an order of magnitude equal to changing the coarse aggregate type. However, it is often impractical to change the season in which a pavement is placed, so other environmental changes can be made.

On Project 8, where night and day placements were used, it was found that the performance indicators, i.e., crack spacing, randomness index (RI), etc., were about equal. The placement period was characterized by mild summer temperatures $<90^{\circ}\text{F}$ ($<32.2^{\circ}\text{C}$). By contrast, Project 2, with excessive temperature, experienced poor performance using all of the indicators. Thus, the next most important environmental changes that can be made include changing the placement time during the day and restricting the placement when high evaporation rates and temperatures $>90^{\circ}\text{F}$ ($>32.2^{\circ}\text{C}$) are expected. Although time of day was not significant on Project 8, i.e., night or day owing to a unique set of circumstances, Project 2 shows the possibility that it might be. Thus, the time of placement may be a significant factor in pavement performance when the temperature differentials between day and night are sufficiently large. If placed at night (i.e., while the evaporation rate is low), a pavement can perform significantly better than an identical pavement placed during the day with a high evaporation rate.

The other change that can be made to a pavement involves the reinforcement steel. The percentage of reinforcement steel affects only the performance indicators of crack width and spacing in the pavement. By decreasing the steel percentage, the crack spacing and width will increase, thus reducing the number of cracks less than 3 ft (0.91 m). However, care should be used when attempting this approach, because it can cause the steel to be overstressed and the cracks to open up excessively. A general observation is that once the crack width and steel stress criteria are satisfied, the value of increased steel is minimal.

Skewed steel can increase the crack spacing slightly. The problem associated with skewed steel is an increase in the randomness of cracks. The use of skewed steel may not be significant enough to justify its use. Using these techniques, it is possible to produce a pavement having a more acceptable crack distribution. These techniques may be used in combination if necessary to improve crack spacing distribution.

The curing technique and type studies undertaken on Projects 6, 7, and 8 provided guidance for reducing the effect of rapid water loss from the pavement. The data from Project 7 (Cypress) show that the polyethylene sheet and double layer of the curing compound provide the best curing conditions (i.e., retain slab moisture), whereas the single layer of curing compound had substantial reductions of moisture in the slab. Project 8 revealed that a substantial reduction in strength was experienced in the top of the slab. Furthermore, a late application of a double curing compound (i.e., over 30 minutes) can reduce the strength through the entire depth. In summary, the curing type and placement time must minimize the rate and quantity of moisture loss to ensure an adequate level remains following full cement hydration.

ESTABLISHING SIGNIFICANT FACTORS

After reviewing project results, Table 8.1 was prepared to provide significance levels for the numerous performance indicators and variables. The columns of the table list the primary performance indicators, while the lines represent the primary performance variables considered in the eight projects. On each line, a rating from 0–5 is given, with 5 being very significant and 0 having no significance. Considering all the projects in which the variables were included arrived at these ratings, as subjectively determined by the researchers.

In the far right column, the sum of all the ratings across the various indicators is given for each variable. The higher the number, the greater its significance in affecting the performance of CRCP. The highest in the list are aggregate type, placement season, and placement above ambient temperature of 90°F (32.2°C), and evaporation. The first two are design variables and the latter two are primarily specification items. Thus, for design, the engineer must take into account the aggregate type and placement season. If the designer has no control over these items, then the worst case must be assumed. The specifications should place controls on concrete placements at ambient temperatures above 90°F (32.2°C) and for excessive evaporation levels.

The low scores for the placement variables of crack initiators and skewed transverse steel suggest that these factors have only marginal value.

Based on laboratory tests, it was felt that aggregate blending had potential for reducing the effect of thermal coefficient. Unfortunately, the field test sections for Project 8 revealed (as shown in Chapter 4) that the 50/50 blend produced crack spacings similar to those for SRG. However, the blended aggregates produced crack spacings between the extremes for the LS and SRG in proportion to blending, as expected on Project 7 (Chapter 3).

The impact of steel percent and bar diameter should not be underestimated owing to the low scores. Only small variations were used, and even the low values of steel were in excess of the minimum required. These results invalidate the long-standing assumption that, if you have problems on a particular project, you add more steel to the next project.

The last line provides the sum of ratings vertically across the variables for each performance indicator. In this case, the higher the sum, the more difficult it will be to maintain an acceptable performance level for that indicator. For example, an excellent level can be maintained for the tensile strength distribution vertically, since controlling the placement conditions for evaporation and ambient temperatures above can eliminate 10 of the points 90°F (32.2°C) through the specifications. Controlling the same two items can also minimize delamination spalling. By contrast, the proper control of the other three will cover design, construction, and the specification.

The guidelines established above should be incorporated into operations at the present time to maximize CRCP performance and to minimize cost. Furthermore, these projects

should be revisited in the future (after punchouts have occurred) in order to reevaluate the guidelines.

Table 8.1 Significance ranking of performance indicators and variables studied in Projects 1–8

Performance Variables	Performance Indicators					Σ Ranking
	Crack Spacing Dist.	Crack Width	Crack Randomness	Delam. Spalling	Vertical Dist. Tensile Str.	
Aggregate — Type	5	5	5	5	1	21
Aggregate — Blending	1	1	3	1	0	6
Placement — Season	5	5	5	5	3	23
Placement — Time of Day	3	2	3	3	4	15
Placement — above 32.2°C	5	2	5	5	5	22
Placement — Crack Initiators	1	0	5	1	0	7
Placement — Skewed Transv. Steel	2	0	3	0	0	5
Placement — Evaporation	4	4	4	5	5	22
Percent Steel	3	3	0	0	0	8
Bar Diameter	2	2	0	0	0	6
Σ - Ranking	31	24	34	26	18	133

A ranking of significant (5 — very significant; 0 — no significance)

8.2 CONCRETE PAVEMENT PLACEMENT GUIDELINES

The previous section pointed out that a major improvement in concrete pavement performance could be recognized if the concrete temperature and the moisture evaporation from the surface were monitored and controlled during the construction placement operation. Accordingly, the following subsections discuss the two items in more detail.

CONCRETE TEMPERATURE

The ambient temperature and the concrete temperature should be monitored throughout the entire construction operation, especially during hot weather placement, as

indicated in the previous section. Although there are specification requirements regarding cold weather placement, very little control on hot weather placement — especially when temperatures exceed 90°F (32.2°C) — is exercised. Owing to the problems experienced, we should continuously monitor these two factors. Figure 8.1 shows typical gauges that could be placed in the concrete for measuring the temperature, while Figure 8.2 shows a weather station that provides a continuous record of the ambient temperature.

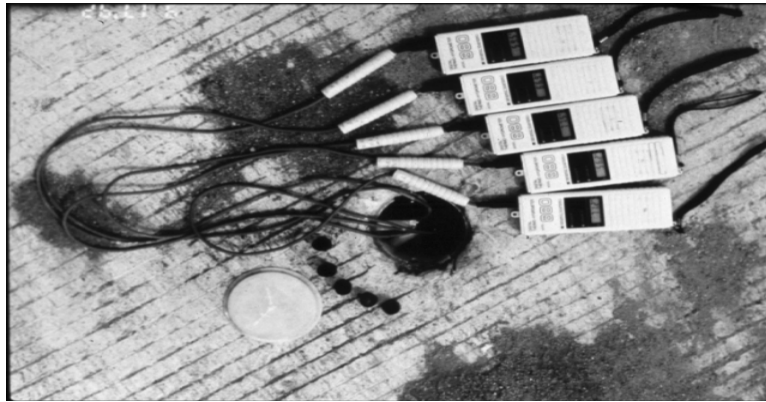


Figure 8.1 Maturity meter (records concrete temperature)

A previous report by Suh et al. (Ref 6) provides information on Projects 1 and 2 that clearly demonstrates the effect of hot weather placement where erratic crack spacings had developed. Suh first presented a graph from another study, as shown in Figure 8.3, that presented the effect of curing temperature on the hydration heat developed by the concrete. As seen in the figure, if the concrete is placed at 41°F (5°C), there is very little heat of hydration. As that temperature is increased, then the heat of hydration builds up at a much higher level much more rapidly. For example, when the curing temperature reaches 140°F (60°C), then the heat of hydration is twice what it would be at 104°F (40°C). The graph explains why ambient temperature is critical: At that point in the example, the air is as warm as the concrete and, thus, the heat transfer is minimized and the concrete pavement becomes a heat sump.



Figure 8.2 *Weather station (records temperature, humidity, and wind speed)*

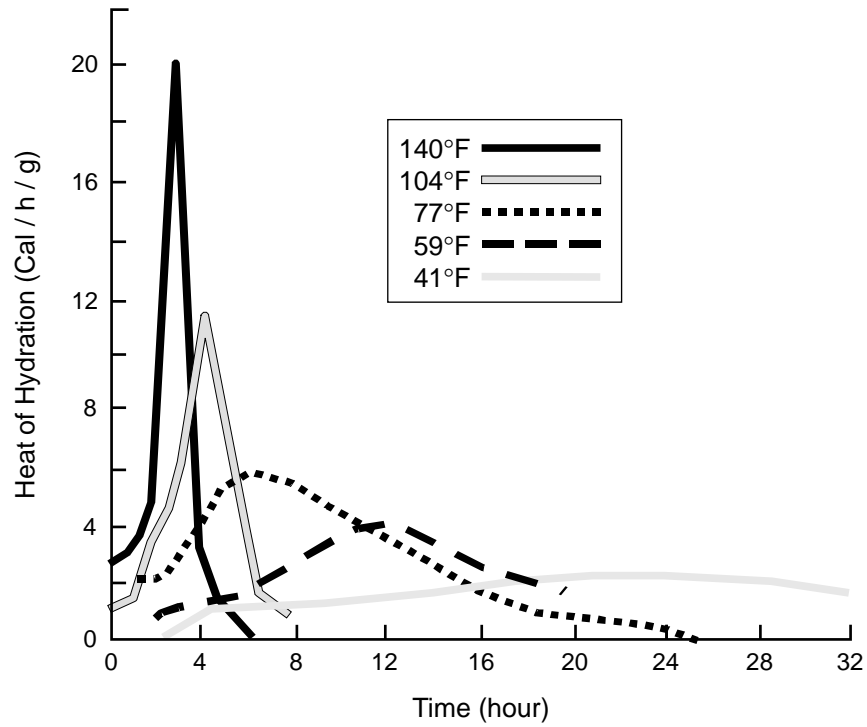


Figure 8.3 *Effect of curing temperature on heat of hydration (140°F = 60°C)*

Figure 8.4 presents a typical plot of the air temperature and the concrete temperature; the left-hand portion of the upper curve represents a typical day when concrete is placed in the early morning hours. As the ambient temperature increases, the concrete temperature also increases, owing to both the ambient temperature and the heat of hydration. At some point, it peaks, then drops off, and eventually, after the curing operation, starts to mirror the ambient temperature relationship. In the lower part of the figure, the concrete stresses are indicated for condition “a,” where the concrete sets; this then is the reference point. As the temperature continues to build up, the slab goes into compression, as indicated at the peak heat condition. Then, as the concrete temperature decreases, the stresses go from compression to tension; at the point where the stress exceeds the tensile strength, it will crack.

Figures 8.5 and 8.6 present the ambient temperature and slab temperature relationships for Projects 1 and 2. For Project 1, it was during a winter condition; as may be noted, the ambient temperature is in the range of 60°F (15.5°C) to approximately 30°F (-1.11°C) at night. With this lower condition, the concrete temperature never builds up much higher than 70°F (21.1°C). By contrast, Figure 8.6 shows a summer day in which the air temperature rises above 90°F (32.2°C) and, owing to the extreme hydration heat as previously shown in Figure 8.3, the slab temperature rises to in excess of 140°F (60°C), approaching 150°F (65.5°C). During the first night, the concrete temperature drops from 140°F(+) [60°C(+)] to approximately 90°F+ [32.2°C(+)], or a differential of approximately 50°F(+) (10+°C) (the slab is less than 24 hours old). Thus, a very high stress is built up as shown in Figure 8.4 as a result of the large temperature differential. For the winter conditions shown in Figure 8.5, the stresses are very small. Hence, with excessive temperature development, very erratic cracking occurs, producing y-cracking, numerous intersections, and narrow crack spacings. Given these conditions, numerous punchouts develop rapidly, the consequence being a reduction in pavement life.

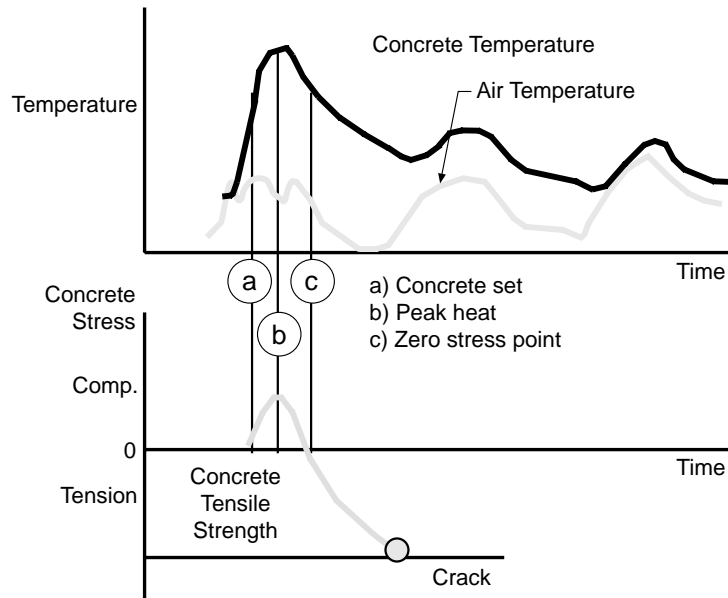
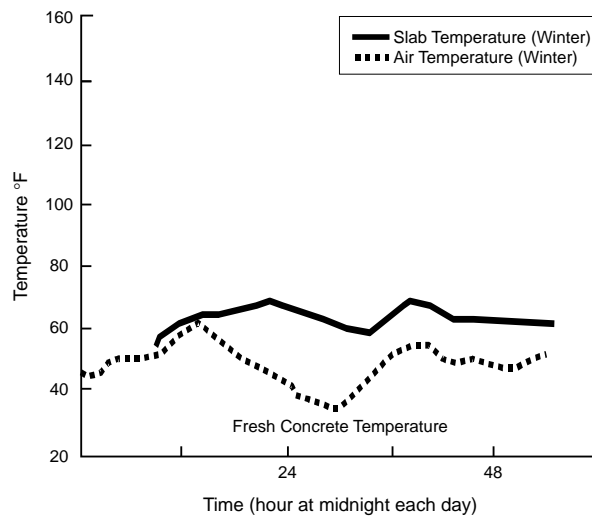


Figure 8.4 Relationship of air and concrete temperatures to stress



**Figure 8.5 Typical air and concrete temperatures during winter placement
 (160°F = 71.1°C)**

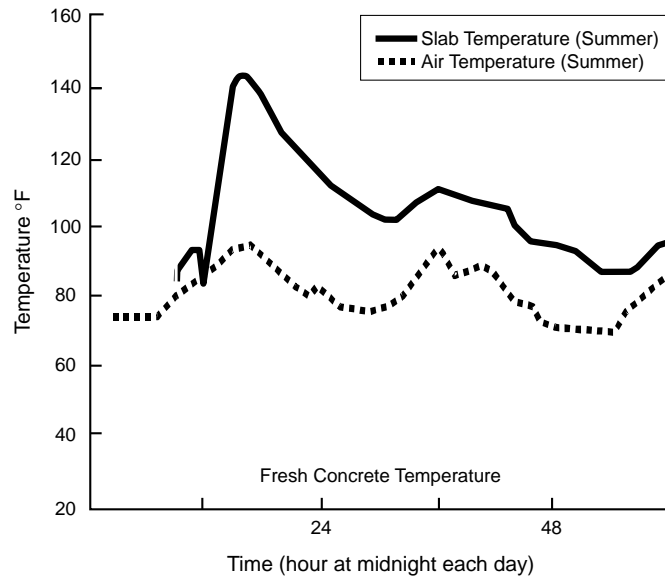


Figure 8.6 Typical air and concrete temperatures during summer placement (160°F = 71.1°C)

Figures 8.7 and 8.8 demonstrate the effect of excessive temperature buildup in terms of longitudinal cracking. The cracking areas shown are areas of longitudinal cracks that occurred before the sawcut was made the next morning. Figure 8.7 involves a high thermal coefficient coarse aggregate, while Figure 8.8 involves a low thermal coefficient. While Figure 8.8 shows less cracking, in both cases the high temperature placement resulted in cracking prior to sawing. Figure 8.9 illustrates the long-term effect of the higher temperatures. The graph shows a percentage of roadway experiencing failure versus various maximum air temperatures experienced during concrete placement on a section of IH-45 south of Huntsville, Texas. This section, overall, demonstrated poor performance over the 14-year period indicated. In particular, the graph shows the effect of concrete placement for those areas of the pavement placed when the air temperature was greater than 90°F (32.2°C): At those temperatures, the failure rate was approximately 3–4 times what it was at cooler temperatures.

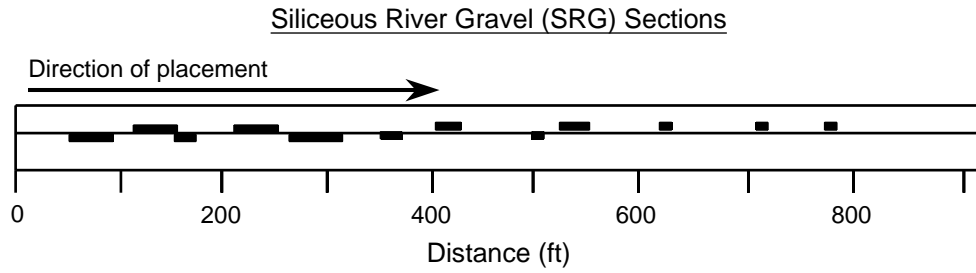


Figure 8.7 Influence of placement time on longitudinal cracking (SRG) (1 ft = 0.30 m)

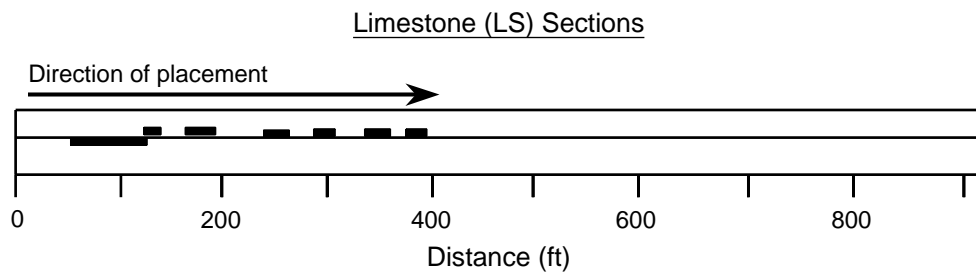


Figure 8.8 Influence of placement time on longitudinal cracking (LS) (1 ft = 0.30 m)

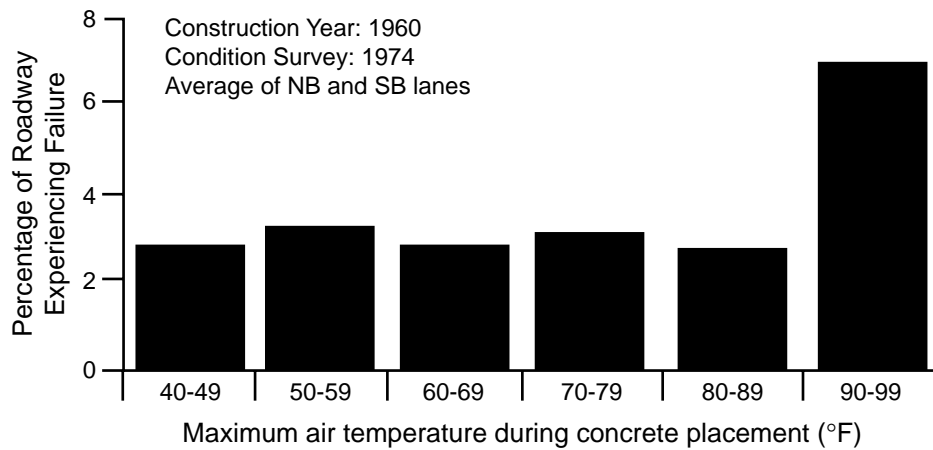


Figure 8.9 Pavement failure as a function of temperature at placement

EVAPORATION

As explained previously, the evaporation of water from the surface of the concrete is highly dependent upon the four factors shown in Figure 8.10, namely, air temperature, concrete temperature, relative humidity, and wind velocity. The higher the temperature and wind velocity and the lower the relative humidity, the greater the evaporation. Since the evaporation is such a key factor in the long-term performance of the pavement, it could be monitored during concrete placement, as conceptually shown in Figure 8.11. When negative conditions occur, double membranes, cotton mats, night placements, and other strategies could be used to minimize the detrimental effects.

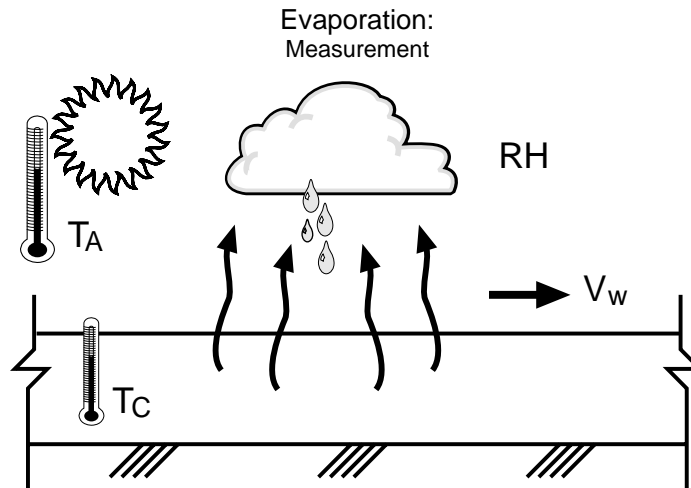


Figure 8.10 Factors influencing evaporation rate

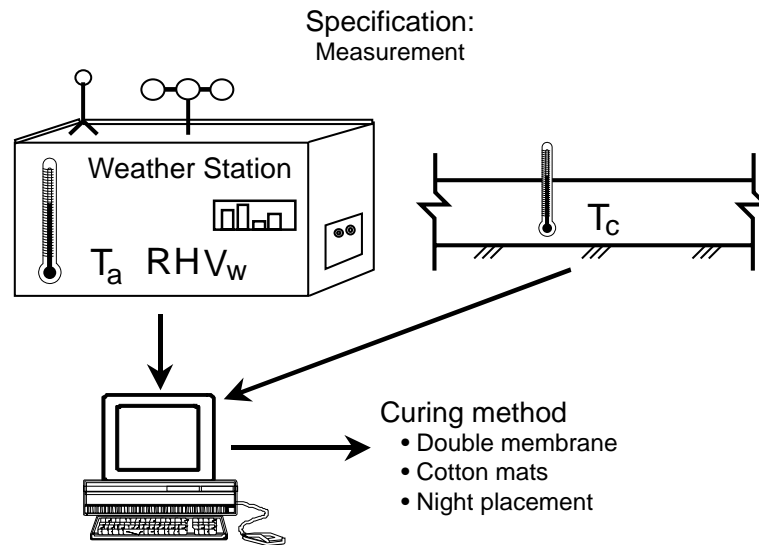


Figure 8.11 Monitoring evaporation to select curing treatment

Figure 8.12, which shows the spalled cracks as a function of the maximum evaporation rate on the day of concrete placement that was experienced on a Beltway 8 project in Houston, demonstrates the impact of evaporation. The data show that as the evaporation rate increases, the amount of spalled cracks increased. It is interesting that the zero condition was for evaporation rates less than the $0.976 \text{ kg/m}^2/\text{hr}$ that has generally been used as the criterion. For the high evaporation rates, very severe spalling was experienced, a situation that required a bonded concrete overlay be placed on a relatively new pavement to offset the detrimental conditions that had developed. Figure 8.13 indicates why the spalling occurred and includes plots very similar to those reported in Chapter 4, only this is for the Beltway 8 project. Note that when subtracting the top minus the bottom, 20% of the area had strengths where the psi tensile strength difference was 2.07 or more. Thus, Figure 8.12 shows the effect on the performance of the concrete pavement and Figure 8.13 presents the results of high evaporation during the concrete placement.

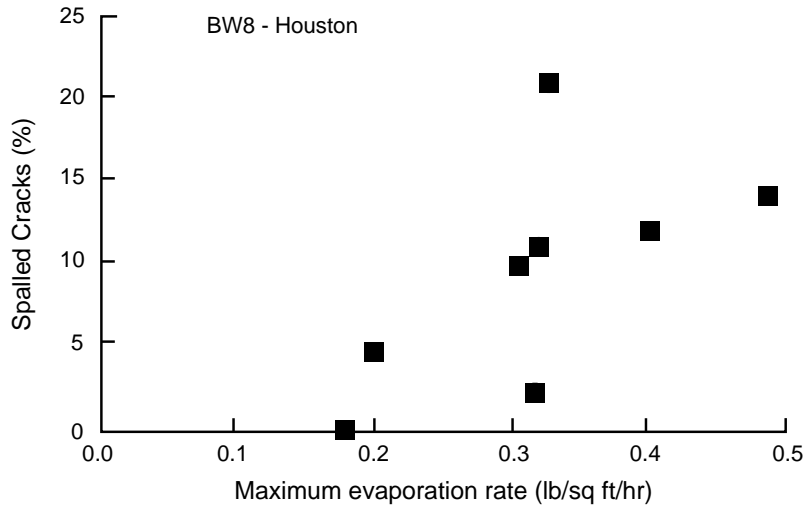


Figure 8.12 Effect of high evaporation rate on spalling development (BW-8)

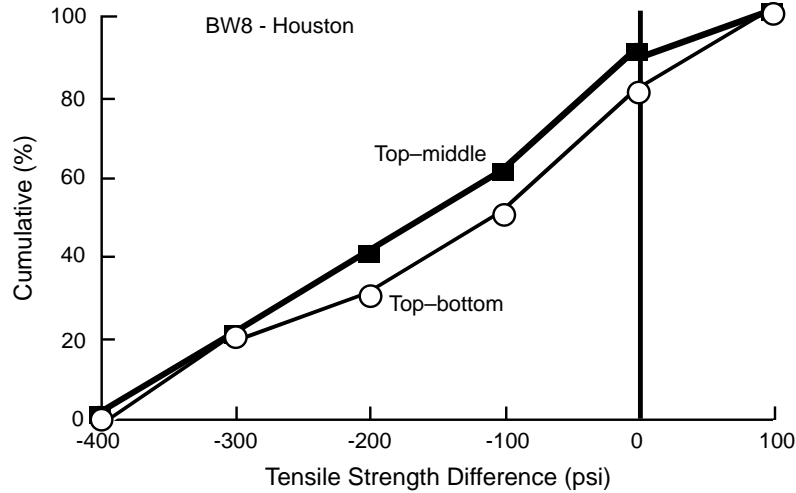


Figure 8.13 Differential tensile strength on BW-8 Project

Corrective measures to offset this high evaporation vary and can be altered using curing methods, concrete temperature controls, and time of placement. With the curing methods, different types of curing can be used: Figure 8.14 illustrates the relative

effectiveness of different types of curing methods. The single membrane is the least effective and the cotton mat is the most effective, with constructability, unfortunately, moving conversely.

Figure 8.15 shows the water loss from a specimen having “no compound,” a “single layer,” and a “double layer” over a 1-week period. The “no compound” obviously loses the most water, which generally happens within the first 24 hours, resulting in the poor performance as noted previously.

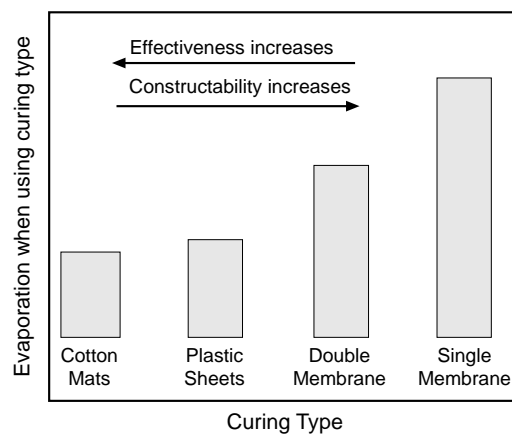


Figure 8.14 Relative effectiveness of curing methods

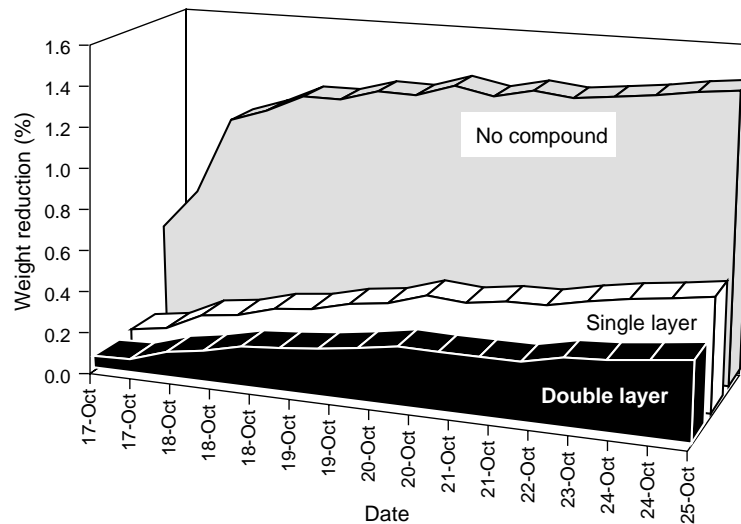


Figure 8.15 Water loss in El Paso

Table 8.2 presents curing recommendations in terms of the evaporation rate. It should be emphasized that when applying the method, the time of placement — also a factor in the equation — must be expedited.

Table 8.2 Recommended evaporation controls

Evaporation (lb/ft/hr)	Require Curing
<0.2 Compound	Single curing @ 180 ft ² /gal
0.2–0.4	Double curing each @ 180 ft ² /gal
>0.4	Cotton Mats?

Thus, the temperature is monitored by a continuously operating project weather system; when it is apparent that the ambient temperatures are going to be 90+°F (32.2°C), then steps should be taken to cool the concrete (e.g., by adding ice, aiding the stockpiles, etc.). This could be anticipated well in advance, such that the negative conditions are avoided. By monitoring the evaporation rate (continuously and in real time), the contractor could become aware of when negative conditions are approaching.

8.3 GUIDELINES FOR COARSE AGGREGATE

This section discusses several important issues related to the use of aggregates in the design and construction of CRC pavement. Recommendations are also provided for pavement engineers seeking to achieve desirable pavement performance while maintaining an equitable market for different coarse aggregate types.

The principle of longitudinal reinforcement design in CRC pavement is to provide an amount of steel sufficient to distribute transverse cracks at a desirable crack spacing 3–8 ft (1-2.44 m) and to keep the cracks tightly closed. The percentage of steel, rebar size and spacing, and aggregate type certainly affect the development of the crack pattern. Consequently, it is highly desirable that the steel percentage be designed considering the coarse aggregate type to be used in the concrete mixture.

GUIDELINE TO ACHIEVE EQUAL PERFORMANCE

In order to make the following discussion clear, two important concepts are introduced. First, there is the concept that a naturally occurring crack pattern is the result of the stresses induced by temperature and moisture changes prior to vehicular loading. A crack pattern that develops in this manner can, and often does when high thermal coefficient aggregates are used under hot weather conditions, develop poor crack patterns that readily lead to spalls and, ultimately, to punchouts. SRG aggregates have low bond strengths and high thermal coefficients of expansion, which inherently make them more sensitive to cracking. This leads to the second concept, which is the fact that concrete made of aggregates manifesting these characteristics may perform either poorly or exceptionally, depending on the construction techniques used. In light of this, the optimum crack pattern is the one that yields the best performing pavement. A goal of pavement construction is to achieve an optimum crack pattern through consideration of rational material properties, steel percentages, and correct construction procedures. Given the category of concrete involved, crack-induction techniques and curing methodologies can minimize undesirable features developing in CRC pavement after construction.

Concrete with 100% SRG is not recommended in summertime paving, when ambient temperature exceed 90°F (32.2°C). For weather conditions of this nature, it is recommended that aggregate blends be considered. Such blends can change the thermal and bonding properties of the concrete so as to elevate the transverse crack spacing into an acceptable range.

Experimental study on the mechanical properties of concrete containing different types and percentages of coarse aggregates shows that the thermal coefficient for river gravel concrete is higher than that for limestone concrete. In field performance and under the same paving conditions, concrete made with 100% limestone aggregates usually demonstrate larger transverse crack spacing than concrete made with river gravel. This indicates that river gravel concrete is more sensitive to changes in ambient temperature. In order to take advantage of these properties and to achieve equal quality of performance when different types of coarse aggregates are available, we suggest using greater percentages of limestone aggregate in concrete mixtures placed during summer, and using greater percentages of river gravel aggregate in concrete mixtures placed during winter; depending on the bond properties

of the concrete containing the aggregate blends, positive crack control measures may need to be implemented (along with specific curing requirements).

QUANTIFICATION OF DESIGN FACTORS

To quantify the effects of aggregate on the properties of concrete, aggregate categories are proposed as follows:

- Category 1. Concrete coefficient of thermal expansion $<6.0 \mu\epsilon$ and fracture toughness at one day $> 2.44 \text{ MPa/cm}$
- Category 2. Concrete coefficient of thermal expansion $>6.0 \mu\epsilon$ but $<8.0 \mu\epsilon$ and fracture toughness at one day $<2.44 \text{ MPa/cm}$ but $>1.9 \text{ MPa/cm}$
- Category 3. Concrete coefficient of thermal expansion $>8.0 \mu\epsilon$ but $< 10.0 \mu\epsilon$ and fracture toughness at one day $<1.9 \text{ MPa/cm}$ but $>1.35 \text{ MPa/cm}$
- Category 4. Concrete coefficient of thermal expansion $>10.0 \mu\epsilon$ and fracture toughness at one day $< 13.5 \text{ MPa/cm}$

Typically, limestone concrete has a large fracture toughness value (2.7 MPa/cm) at early ages and a low thermal coefficient value ($<6.0 \mu\epsilon$). River gravel concrete has a low fracture toughness value (13.5 MPa/cm) at early ages and a high thermal coefficient value ($>10.0 \mu\epsilon$). The larger the fracture toughness value at early ages, the larger the transverse crack spacing. The lower the thermal coefficient of concrete, the less sensitive the concrete is to the ambient temperature change and the larger the transverse crack spacing.

METHOD OF CONSTRUCTION

Transverse rebar in concrete pavement is used (1) to support the longitudinal steel reinforcement at the desired location during the construction process, (2) to maintain the spacing of the longitudinal steel during placing operations, and (3) to keep longitudinal joints and cracks closed. Field investigations show that there are a certain percentage of cracks initiated by transverse reinforcement. It was found that under the same paving conditions, the percentage of cracking initiated by the transverse rebar in the section using river gravel as the coarse aggregate is higher than that in the section using limestone. The percentage of cracking initiated by the transverse rebar in the winter-paved section using river gravel as coarse aggregate is much higher than that in the summer-paved section using the same type

of coarse aggregate. By relocating the transverse rebar away from the location of a notch or crack inducer, the resulting crack pattern can be significantly improved.

Field investigations and theoretical studies indicate that it is possible to control cracks in concrete pavements meeting Category 3 and 4 for certain weather combinations. However, desirable crack patterns cannot be achieved alone through positive crack control. It is also important to ensure that the steel reinforcement is designed in accordance with the thermal and strength properties of the concrete. The percentage of blending is determined based on the paving condition. For example, in summer, one may use a higher percentage of limestone, while in winter, one may use a greater percentage of river gravel. Quantitatively, structural and mix designs can be undertaken based on thermal expansion coefficient and fracture toughness of concrete at early ages. Experience shows that different paving conditions may result in different crack patterns in concrete pavement, which may lead to different behaviors and performances. Wintertime paving may result in better performance than does summertime paving, especially for river gravel concrete. Even in summertime, nighttime paving may provide better results than daytime paving. The effect of ambient conditions on pavement performance can be balanced by choosing different types and percentages of coarse aggregate, as mentioned previously. Moreover, designed sawcut spacing should be changed based on time of paving.

Field investigations show that surface notching (sawcutting) is more efficient than interior crack initiation (i.e., crack inducer or transverse rebar) for summer-paved sections. For partially restrained portions (e.g., a free end close to bridge or a short segment at an intersection), bottom crack induction is strongly suggested.

8.4 PREDICTING PAVEMENT PERFORMANCE

It is essential that a pavement designer have a means of predicting whether a pavement design will need some of the corrective measures outlined above. While many designers use experience to make these judgments, CRCP-8 is ideally suited to supplement a designer's experience and to provide guidelines upon which engineering decisions can be made.

The crack spacing development with time presented in Chapter 4 substantiated the current CRCP-8 approach to calculating the crack spacing development for the first 28 days

and at the end of the first year (and then assuming it remains relatively constant thereafter). Figure 4.1 and Figures 4.4–4.6 show this assumption is a viable one. Figure 4.2 shows that some of the longer crack spacings may be reduced, while the spacings less than the mean remain relatively stable.

The validation of the CRCP-8 models for predicting crack spacing distribution and the mean value leads to an additional criterion that should be used in design. Since the closely spaced cracks (i.e., those less than 3 ft (0.91 m) are the primary factors in punchouts developing before the fatigue phase of the pavement life is reached (Figure 2.1), then an acceptable level should be established. Because the TxDOT rigid pavement database has the crack spacing distribution for most sections, it therefore should be used with the punchout history to establish acceptable guidelines for the small crack spacings.

In the following sections, the steel stress and the crack width are computed for the test sections on Projects 1–4 and 8. There has been sufficient performance history on many of these sections to indicate that these values are not a problem. Thus, if the predicted values are within the current acceptable criteria, a partial validation of the steel stress and crack width models is achieved. In addition, the bond development length for the reinforcing bar is computed in CRCP-8; thus, these values are presented to determine their “reasonableness.”

STEEL STRESS

Steel stress is an important factor in CRC pavement design because it is undesirable that steel bars yield. Figure 8.16 shows the steel stress results for Projects 1–4 and 8. The yield stress for the reinforcement is 413.4 kPa. Note that none of the sections has a predicted yielding of the steel, and that the CRCP-8 steel standard provides a lower steel stress than does the previous design standard. Also note that the sections paved in the winter have a lower steel stress, and that limestone sections have a higher stress owing to their wider crack spacing.

CRACK WIDTH

As previously mentioned, crack width is an important indicator of CRCP performance, given that wide cracks allow water to carry incompressible material into the cracks, which can then lead to possible pavement failures. The crack widths shown in

Figure 8.17 are for temperatures below freezing, i.e., zero degrees; therefore, the desired value of 0.025 in. (0.635 mm) does not apply. If the crack width criterion of 0.025 in. (0.635 mm) was corrected to zero degrees, it would be in the range of 0.043 in. (1.09 mm) to 0.045 in. (1.143 mm). Note that the sections having the widest crack widths (i.e., low level of steel) are not typically used for paving. Since a calibration of the CRCP-8 crack width model was undertaken by Suh (Ref 6), these results indicate that the crack provides “reasonable” answers and serves as a partial validation.

BOND DEVELOPMENT LENGTH

The bond development length is also important because if cracks get closer together than twice the bond development length, pavement continuity is lost and punchouts are likely to result. Figure 8.18 shows the bond development length for Projects 1–4 and 8. Note that the bond development length is similar for both SRG and LS sections. When using twice the bond development lengths shown in Figure 8.18, it may be better to look at the percentage of cracks less than 4 ft (1.22 m) apart instead of 3 ft (0.91 m) apart, since the largest length is about 2 ft (0.60 m). However, the 3 ft (0.91 m) standard is adequate for about half the sections.

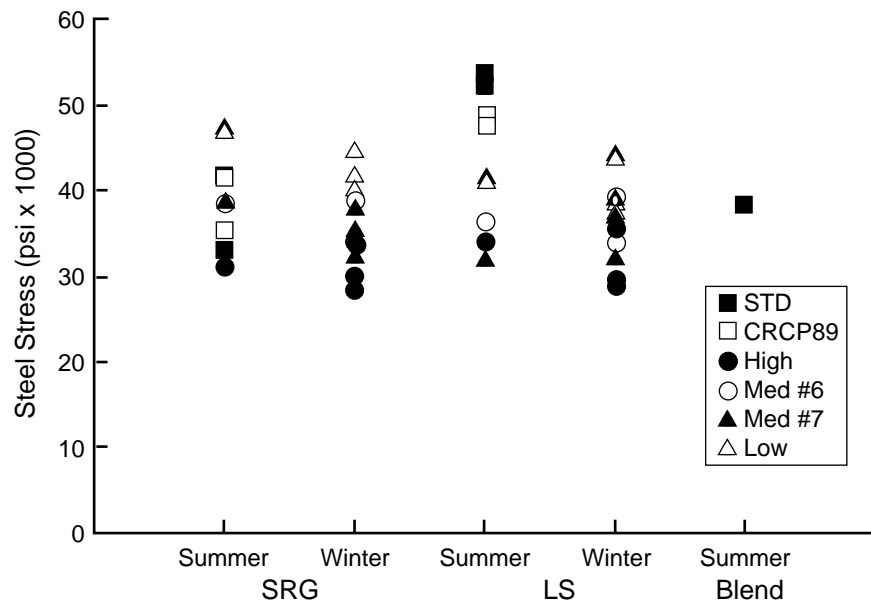


Figure 8.16 Maximum steel stress calculated for Projects 1–4 and 8 (CRCP-8)

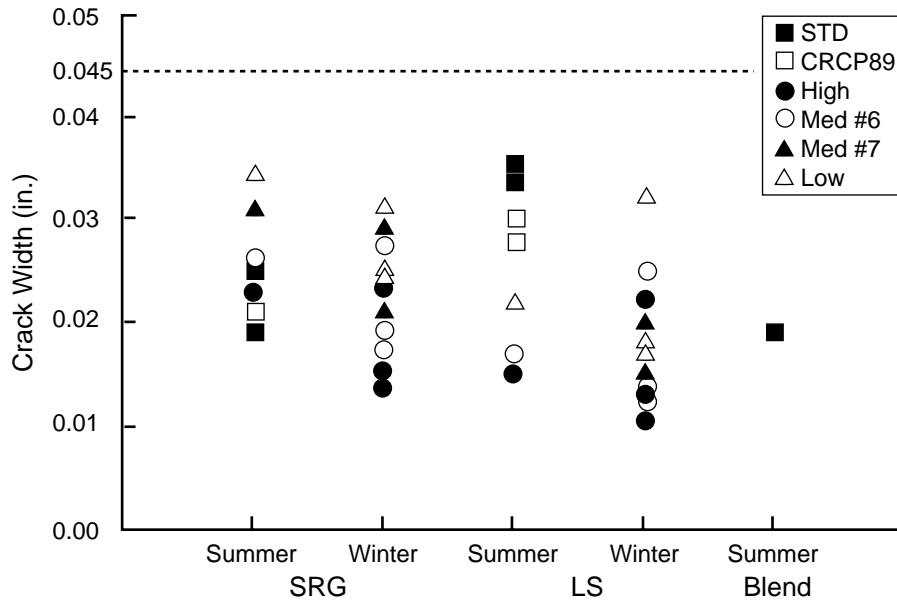


Figure 8.17 Crack width calculated at the minimum design temperature of 20°F using CRCP-8 for Projects 1–4 and 8 (0.01 in. = 0.25 mm)

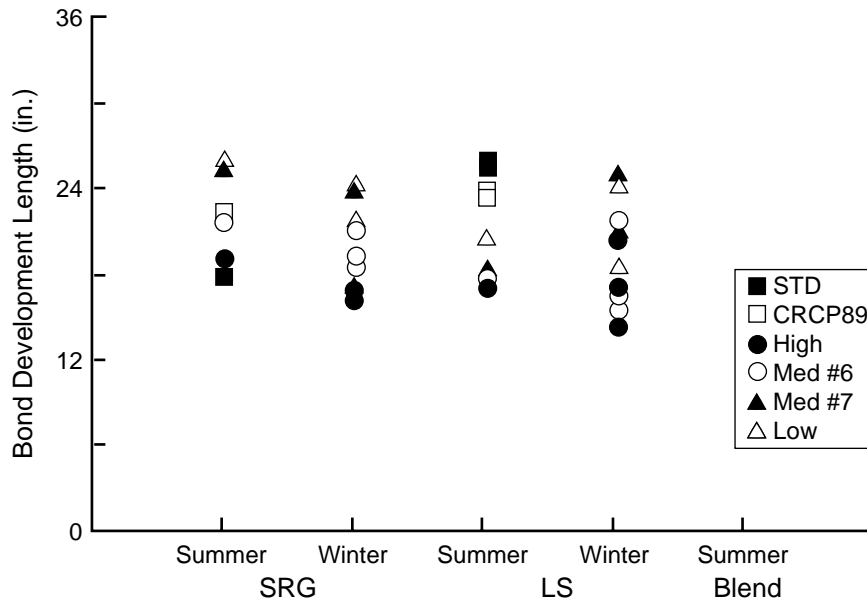


Figure 8.18 Bond development length calculated using CRCP-8 for Projects 1–4 and 8 (0.01 in. = 0.25 mm)

SUMMARY

These results show that CRCP-8 is capable of assisting the designer in producing optimal pavement designs. Since Projects 1–8 are all in the Houston area, the results cannot be applied to all parts of Texas with 100% confidence (though they can be applied more often than most other design procedures). Additional case studies are needed to validate CRCP-8 in all areas of Texas.

8.5 FUTURE PROGRAM DEVELOPMENTS

The CRCP-8 analysis program is one of the most advanced, validated, and documented mechanistic-empirical methods available for the design of pavements. While the CRCP-8 program has evolved over time, there are several enhancements that should be undertaken, based on the results presented herein. The enhancements represent minor changes that could be achieved through minimal effort, though additional development would require additional study.

ENHANCEMENTS

The spalling model conceptually described in Chapter 5 and elaborated on in considerable detail in Appendix E, should be added to the analysis model immediately. Using this model, the designer could select material properties, desired environmental conditions, and curing techniques that would minimize or eliminate spalling. In addition, the impact of the constructed conditions on the occurrence and extent of spalling could be evaluated. Since the difficulties associated with identifying and modeling have been completed, the final step is minimal and short term.

With the addition of the spalling model to the CRCP-8 analysis program, the CRCPAV design program should be revised to reflect the changes.

Figure 8.19 shows the direction of a solution taken by the CRCP-8 analysis program. The user enters all of the design parameters, such as pavement thickness, concrete properties (e.g., strength, modulus, and thermal coefficient), steel reinforcement design, and environmental factors (principally, expected low temperatures). The analysis program then predicts the performance of the pavement in terms of crack spacing, crack width, steel stress,

and, as will soon be added, the onset and severity of spalling. The program also gives an estimate of the rate of punchout development with traffic or time.

The next step is to perform a large number of runs using CRCP-8 according to a predetermined factorial combination of design inputs. The resulting table relating design parameters to cracking, steel stress, and spalling can then be incorporated into a computer program solving in the reverse direction, i.e., finding a design for a specified performance. A simple table look-up process accomplishes this, with some interpolation between the points generated by the repeated CRCP-8 runs to identify a reinforcement solution for the requested performance level. Figure 8.20 illustrates this concept. Note that this process, incorporated in the existing CRCPAV program, generates a range of acceptable solutions for different reinforcement levels and bar sizes.

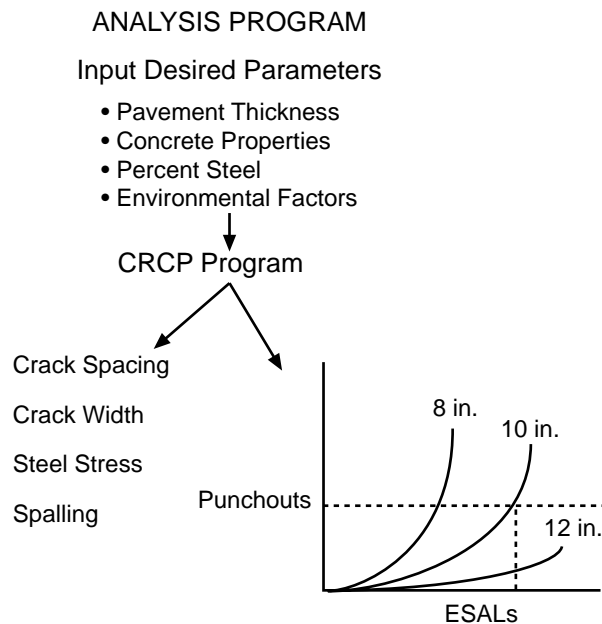


Figure 8.19 Conceptual flow of the analysis program CRCP-8 (1 in. =25.4 mm)

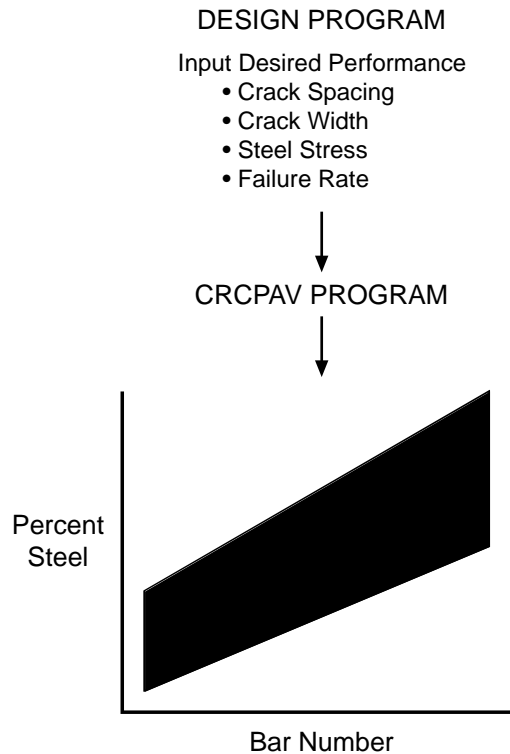


Figure 8.20 Conceptual flow for the CRCPAV (design) program

When the CRCP-8 program is modified to include the latest spalling and thermal coefficient models, it will be necessary to regenerate the solution table driving the CRCPAV design program. Interfacing CTE developments (both component analysis and chemical analysis) with the CRCP-8 analysis program will be straightforward, since CRCP-8 is already linked with the CHEM2 program that predicts thermal coefficient of the concrete from chemical or mineralogical components. Updating the CTE model in the CHEM program will automatically update the CRCP-8 model.

ADDITIONAL PROGRAM DEVELOPMENTS

The original and current CRCP programs incorporate data obtained from the TxDOT rigid pavement database. Most of this work was undertaken when the database contained only 8 in. (203 mm) CRCP. Since that time, a range of pavement thicknesses (15 in., or up to 38.1 cm) has been added. Accordingly, a more sophisticated finite element model for predicting load stresses should be incorporated. This addition would permit an improved

capability for looking at edge conditions, thicker pavements, voids, bonded concrete and asphalt overlays, and multiple steel layers. These models could be calibrated with the improved database.

The predicted steel stresses from the CRCP programs should be calibrated for the thicker pavements. The original models were calibrated from steel stress observations on 8 in. (20.32 cm) CRCP, but zero calibration has occurred to reflect the thicker pavements, subbase resistance, and the stresses during the first 24 hours associated with hot weather concreting.

With the completion of the CRCP model enhancements discussed in the previous section, the JCP/JRCP models should also be revised to reflect these enhancements. This is not a major development, since the jointed concrete models are similar in concept to the CRCP models. Thus, enhancement additions would require only slightly more effort than is required for the CRCP enhancements. These models should be calibrated with the data currently in the rigid pavement database.

Finally, recent work has been undertaken on the CRCP model under TxDOT Project 0-1758, "Development of a Finite Element Program for Continuously Reinforced Concrete Pavements." In this study, finite element analysis was used to develop a mechanistic model similar to the current internal CRCP-8 model, but incorporating additional modeling for temperature and moisture variations throughout the concrete depth, creep effect, and a more realistic bond-slip relationship between the concrete and the longitudinal steel. This work is the beginning of a new mechanistic engine for CRCP behavior that takes into account many factors currently neglected or averaged for simplicity; after more development, the finite element models will eventually replace the existing internal models in CRCP-8.

8.6 GENERAL PCC PAVEMENT DEVELOPMENTS

Based on the results of this study, several general developments for PCC pavements are apparent. First, several items should be added to the rigid pavement database. Next, several items of design criteria are needed that will lead to a full implementation of the design procedures. These items are discussed in the following sections.

DATABASE ADDITIONS

From the information presented for Project 8 in Chapter 4, it is obvious that the evaporation rate on the day of placement should be included in the database. This should be tied to locations on the test sections, in so far as this is possible. This should be done for CRCP and jointed pavements.

At the present time, the crack spacing distribution is recorded for the first 200 ft (60.96 m) of the test section. Since the distribution is more important than the mean, the distribution for the entire section should be recorded, as well as its change with time. As part of this activity, the RI should be recorded for a test section.

A very important but more expensive initial investment would be tensile strength distribution along the test section that is obtained by splitting cores and testing top and bottom.

To further enhance calibration of the spalling model, random samples of spall depth should be obtained and the location recorded. This is an initial investment and would not require later measurements.

Finally, the test sections from Projects 1–8 represent a substantial investment and a wealth of knowledge. Accordingly, they should be included in the rigid pavement database as a special study or as satellite database.

CRITERIA DEVELOPMENT

The database should be analyzed to relate the crack distribution to performance. At the present time, the mean crack spacing is presently used for design, though a more reliable analysis would be to use the distribution, since Chapter 7 has provided validation for the model. Thus, the distributions giving the best performance should be duplicated in design.

With the addition of the tensile strength distribution of a test section-both from the top and bottom of the pavement-acceptable levels could be set for minimizing punchouts and for preventing spalling.

DESIGN DEVELOPMENT

To maximize performance and to minimize cost, the CRCP program (rather than general standards) should be used to design each project. Perhaps some detailed standards reflecting aggregate type, subbase type, climate region, and steel type could be developed.

With such features, the designer could design a project and select the detail closest to the project's specific needs.

PERFORMANCE-RELATED SPECIFICATION DEVELOPMENTS

As the PCC concrete specification is modified to make it more performance oriented, the CRCP model should be used as the basis for establishing the adjustment factor for application to the bid price. The use of the program would permit the adjustment to be based on the following factors (in addition to thickness, tensile strength, and riding quality):

1. Vertical tensile strength distribution
2. Measured crack spacing distribution
3. RI for the cracks

The results presented in the section on significant factors for improving pavement performance emphasize the need in the current QC/QA specification for PCC to ensure that placement above ambient temperatures and the evaporation of water from the slab are closely controlled.

The capability of the moisture meters demonstrated on Project 7 (Cypress) and reported in Chapter 3 offer tremendous potential for future QC/QA activities for rigid pavements. The loss of strength owing to high evaporation (presented in Chapter 4 and conceptually modeled in Chapter 5) suggests that there are problems associated with the maturity method currently used on many projects.

The maturity of concrete is dependent on the summation of concrete temperature and moisture availability over time, as conceptually described by the following equation:

$$\text{Strength} \propto (\Sigma \text{Temp Increase}) \cdot (\text{Available Moisture})$$

With the present maturity approach, the moisture part of the equation is assumed to be equal to 1, i.e., adequate moisture available. Yet the moisture data shown in Chapter 3 and the strength data presented in Chapter 4 reveal that this is not always the case. Thus, in many instances, while the maturity meter may show the pavement strength is adequate, it may be considerably less owing to inadequate moisture. As a consequence, premature failures could be later experienced.

If the capabilities of the moisture meter are fully developed, then the meter could be installed in the pavement during construction. These results could lead to an end result specification in which the specific curing requirements are not specified; rather, the specification would prescribe that the moisture part of the equation be 1. Once the concrete has been placed, the temperature element of the maturity process has been established and little additional control is possible. The ultimate temperature reached by the concrete when it sets will be determined by the interaction of concrete placement temperature, air temperature, use of retarder, etc. However, the contractor can still monitor relative humidity in the pavement at various depths, adding curing compound or wetting cotton mats as needed to keep the humidity high and achieve the maximum possible strength gain within the temperature conditions available.

To illustrate how sensitive concrete strength gain is to curing humidity, consider Equation 8.1, the maturity equation. PCC strength gain can be measured in degree-hours, strongly correlated to tensile and compressive strength. In the equation, the gain in maturity (degree hours) is multiplied by B_{rh} , the humidity factor. As long as B_{rh} is 1, the maximum possible gain in strength is achieved. If, for example, B_{rh} was instead, 0.9, only 90% of the possible strength gain would be realized during that time period.

$$dM = (\beta_{rh})\beta_T dt; M = (\beta_{rh})\sum \frac{T - T_0}{T - T_r} \Delta t \quad (8.1)$$

But, as shown in Eq 8.2, B_{rh} is an exponential function, varying with the fourth power of humidity. Very small changes in relative humidity result in large reductions in B_{rh} , ultimately reducing strength gain severely during periods of low relative humidity.

$$B_{rh} = [1 + (7.5 - 7.5 \times rh)^4]^{-1} \quad (8.2)$$

Figure 8.21 illustrates graphically the steepness of the B_{rh} curve. For example, it can be seen in the figure that allowing the relative humidity to decrease to just 90% results in a 25% reduction of strength gain during the period in question.

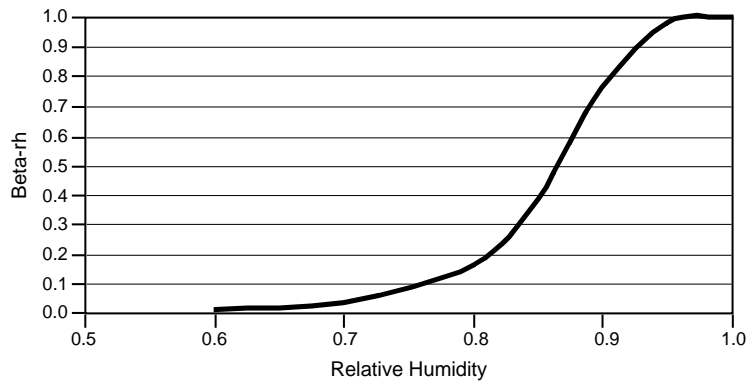


Figure 8.21 Exponential effect of humidity in maturity equation

CHAPTER 9. CONCLUSIONS AND RECOMMENDATIONS

9.1 INTRODUCTION

The observations and recommendations developed as a part of the PCC pavement coarse aggregate studies conducted by CTR, TTI, and TxDOT's development program for a QC/QA specification for PCC pavements provide an excellent starting point for an improvement program. Using this information, a plan is organized for developing a high-performance concrete pavement (HPCP) in Texas that encompasses design, construction, specifications, and testing. The objective of this program is to eliminate or minimize the instances in which PCC pavement failures cause CRCP pavement sections to fall far short of their predicted life. Thus, the program will result in PCC pavement that serves for 25 to 40 years on high-volume facilities and that requires minimum maintenance.

For the work plan, an improvement program is presented in five basic areas as follows:

- (1) Improving pavement performance
- (2) Guidelines for selecting PCC coarse aggregate
- (3) Developing concrete pavement placement guidelines
- (4) Improving and refining CRCP design models
- (5) General PCC pavement developments

In the following sections, conclusions and recommendations are presented for a continuous improvement program in each of these areas. These are followed by a series of action items that may be achieved over the next five years. The intent is to avoid moving too rapidly (i.e., in a way that invites controversy and minimizes acceptance). What we envision is a series of progressive steps that will lead to an incremental evolution toward HPCP.

9.2 IMPROVING PAVEMENT PERFORMANCE

1. The field data from the eight projects manifest that the most important variables affecting PCC pavement performance are aggregate type, placement season, placement above ambient temperature of 90°F (32.2°C), and surface moisture evaporation. Thus, these factors should be reflected in the design and construction of PCC pavement as follows:

- a) Aggregate type and placement season are design variables and may be taken into consideration in the design process. The effect of aggregate type on performance is due primarily to the PCC thermal concrete coefficient, and, owing to the aggregate volume, it is primarily controlled by the coarse aggregate thermal coefficient.

Specific Recommendations:

- (1) Design standards should be developed for various regions of the state, for various aggregate types, and for the various construction seasons.*
 - (2) A testing manual should include test method for thermal coefficient of concrete and aggregates for reference in the specifications. Also include/develop a test for 12-hour aggregate bond strength.*
- b) The factors of placing above ambient temperatures of 90°F (32.2°C) and surface moisture evaporation are basically construction/specification items. For placements above 90°F (32.2°C), special precautions should be taken to minimize the excess buildup of the heat of hydration of the concrete. The evaporation should be monitored and managed to maintain stress levels to acceptable levels, and with critical situations of excessive evaporation special steps should be taken to minimize moisture loss (e.g., the process of applying curing compound should be expedited, special curing techniques utilized, and monomolecular film used).

Specific Recommendations:

- (1) The specifications should encompass hot weather concreting, i.e., ambient temperatures >90°F (>32.2°C), with controls on the concrete temperature, curing effectiveness, and techniques during construction for reducing the temperature (e.g., adding ice, cooling stockpiles, wet cotton mats, etc.).*
- (2) The effectiveness of all curing membranes and specifically monomolecular film in maintaining acceptable stress levels should be evaluated by testing in the lab and in the field.*
- (3) If the monomolecular film performs satisfactorily, then its use should be incorporated into the specifications.*
- (4) Testing techniques should be added to the manual for measuring concrete temperature and for acceptance of the monomolecular film.*
- (5) The use of a weather station for measuring the water evaporation from the surface should be included in the specifications with limits and corrective techniques for various levels of evaporation.*

- (6) *Testing techniques for measuring evaporation should be included in the test manual.*
- c) The vertical loss of strength from top to bottom owing to excessive moisture leaving the slab and the delamination (spalling) may be controlled by preventing excessive moisture from being lost from the slab as a result of evaporation. This must be handled through various techniques during the placement and curing of the concrete.
- (1) *A technique for cutting a core into segments (two to three levels) and testing them should be developed and included in the testing manual.*
- (2) *The RPDP and previous QC/QA test sections should be used to develop a correlation between vertical distribution of strength and spalling.*
- (3) *Small test slabs should be instrumented for maturity using moisture and temperature gauges, and cored for testing. The small slabs should include various effective curing thickness and moisture losses, curing types, etc. The information should be used to develop a relationship between the strength loss moisture-based maturity and the parameters investigated.*
2. At the present time, the acceptance testing of PCC is based on flexural testing of specimens made at the side of the road, cured in water at a constant temperature, and aged to 7 days. Since concrete fails in tension, splitting tensile strength testing should be used for acceptance testing. Furthermore, the QC/QA development work and basic strength mechanics have demonstrated the viability of the splitting tensile test.
- a) The use of splitting tensile testing for the official TxDOT tool for the planning, design, and construction of PCC pavements should evolve over time.

Specific Recommendations:

- (1) *A testing program on cores and cylinders from small slabs should be used to investigate the relation between in situ cores and cylinders cured with simulated field conditions, etc.*
- (2) *The testing program in Item 1 should also reflect the effect of reinforcement.*
- (3) *An acceptable strength level for use in design and acceptance testing should be established using previous QC/QA experience and the evaluation of in-service pavements selected from the TxDOT RPDB.*
- (4) *The test method should be included in the testing manual.*

3. Several techniques of marginal value relative to Items 1 and 2 should be investigated further.
 - a) The crack initiators and skewed placement of the transverse steel were the least effective in controlling the pavement performance under hot weather placement conditions.

Specific Recommendation:

Consider techniques for developing design standards for hot weather conditions.

- b) The blending of aggregates of high thermal coefficient and high bond strength showed promise, with success on Project 7 (Cypress).

Specific Recommendation:

Consider additional projects to further evaluate hot weather conditions.

- c) The longitudinal steel percentage and the bar diameter had only a small effect on the projects where it was considered. This probably indicates that the range used was small (0.19%) and that we have more than an adequate amount of steel in the present designs.

9.3 GUIDELINES FOR SELECTING PCC COARSE AGGREGATE

1. Utilization of coarse aggregates in concrete paving should be made in light of specific engineering properties that affect pavement performance and crack development. The width of transverse cracks and the degree of load transfer govern CRCP performance. The aggregate bond strength, the method of construction (curing practice and degree of crack control), and the weather conditions prevailing during paving influence the initial crack pattern. The final crack pattern is largely influenced by the thermal coefficient of expansion (CTE) of the concrete and the steel design, which also influence transverse crack opening.
2. It is important to recognize the utilization of coarse aggregate involves the selection of curing methodology, the degree of cracking control, and steel design. In light of these conditions, it is clear that the characterization of coarse aggregate CTE and bond strength dictate certain construction and curing practices. Aggregate CTE serves as an indicator of the CTE of concrete, while the concrete fracture toughness serves as an indicator of the aggregate bond strength.

Specific Recommendations:

- (1) *Develop the design approach for CRCP systems to maintain a sufficient balance between stress buildup and strength gain with time to achieve a specific crack pattern for a given steel design and aggregate type. The development of stress should account for curing, crack control, and shrinkage effects, while strength development will need to accurately account for moisture and bond effects in addition to the other factors currently taken into account.*
- (2) *Complement Item (1) above with a CTE model for concrete based on the CTE of the aggregate and other relevant properties. Further develop the test procedure for both the aggregate CTE and bond strength so that a laboratory procedure can be adopted by TxDOT to determine these important properties.*

9.4 CONCRETE PAVEMENT PLACEMENT GUIDELINES

The ambient temperature and evaporation were two important parameters affecting the performance of the pavement. The following are conclusions, implementation, and recommendations pertaining to both items.

1. The revisions of the construction process and the specifications should encompass several areas.
 - a) The ambient and the concrete temperature should be continuously monitored, since summer placement generally involves conditions that are more problematic, and especially since ambient air temperatures above 90°F (32.2°C), are critical. Steps should be taken during the critical placement to ensure that the heat of hydration does not become excessive; such steps include using ice, cooling the aggregate stockpiles, and restricting placement during the heat of the day.

Specific Recommendations:

- (1) *Further studies are needed to develop an improved mathematical model correlating the relation between heat of hydration and concrete set temperature relative to the ambient temperatures, cement chemistry, wind speeds, concrete temperature at placement, subbase condition, curing type, and effectiveness, etc. The HIPERPAV Model developed by the FHWA can be used as a starting point.*

- (2) *The model developed from Item 1 should be used to develop construction guidelines and specification requirements (i.e., ice, time of placement, etc.).*
 - (3) *The model should be incorporated in the CRCP Computer Model as part of Section D.*
- b) Low thermal coefficient and high bond strength concrete mixtures are suitable for all placement times and seasons; suitable placing conditions for high coefficient and low bond strength concrete mixtures must be established by appropriate computer simulation and analysis, but may be appropriate only for summer placement unless special precautions are taken.

Specific Recommendations:

- (1) *The existing CRCP-8 program should be used to develop specific initial criteria for high ambient temperatures using high thermal coefficient aggregates.*
 - (2) *When the improved version of CRCP is developed in Section D that encompasses the heat of hydration model developed in Section C-1. -a. - (3), a recomputation of Item (1) should be developed.*
2. The evaporation of surface moisture during concrete placement conditions should be continuously monitored as follows:
- a) Excessive evaporation rates (i.e., greater than 0.976 kg/m²/hr) correspond to low curing effectiveness and may lead to detrimental conditions of strength loss (vertically from the top to the bottom of the slab), delamination, and, consequently, spalling.

Specific Recommendations:

- (1) *The strength loss model developed in Section A, 2, b, (3) should be used to determine the acceptable/unacceptable evaporation rate and quantity to minimize the vertical strength loss.*
 - (2) *The information developed from Item 1 should be used for developing criteria to eliminate or minimize delamination spalling. These criteria should be incorporated into the revised CRCP model developed in Section D.*
- b) During the excessive evaporation periods, several operational techniques should be considered for inclusion in the specifications or in a manual on PCC pavement placement.

Specific Recommendations:

- (1) Cease concrete placement or place during the day when conditions are more favorable.*
- (2) Immediately after the PCC surface strike-off operations, place a molecular material that prevents evaporation and that does not interfere with the finishing operations.*
- (3) Apply two separate coats of curing compound as soon after the finishing operation as possible and consider appropriate levels of curing effectiveness to control the balance between stress development and strength gain with time.*

9.5 IMPROVING AND REFINING CRCP DESIGN MODELS

1. The CRCP-8 program, a mechanistic-empirical design procedure, was calibrated and validated in previous studies using the data from the various experimental projects considered.
 - a) The application of the program to the test section data demonstrated that crack spacing distribution and crack width could be predicted very reliably with the CRCP-8 model. The field studies also revealed the predicted crack spacing distribution should be studied by the design engineer and used as criteria in lieu of the average crack spacing. Furthermore, crack spacings below 3 ft (0.91 m) have a significant effect on reducing pavement life.

Specific Recommendations:

- (1) The crack spacing distributions and the pavement performance data from the RPDP may be used to establish acceptable limits as the crack spacing distribution.*
- (2) The maximum allowable crack width based on water infiltration, joint stiffness, and spalling developed in previous TxDOT and NCHRP studies should be further studied using laboratory test slabs. The data may be used to reference the present criteria.*
- (3) Full-scale field slabs should be tested using the Mobile Load Simulator (MLS) to further refine Item 2.*
- (4) Include the effects of crack control in Items 1, 2, and 3 above to determine the range of the balance between strength gain and stress development suitable for selected aggregate types and concrete mixtures to achieve the best crack pattern.*

- b) Since the steel stress was not measured as part of recent projects, the steel stress algorithm in the CRCP-8 program could not be validated, but the predicted results for the various projects appeared to be logical and in line.

Specific Recommendations:

- (1) Several future projects should incorporate strain gauges on the steel to measure the steel stress variation with time.*
 - (2) The projects selected for Item (1) should encompass both Grade 60 and 70 steels.*
 - (3) The measured and predicted steel stresses from projects included in Items 1 and 2 should be compared. The models should be updated periodically.*
- c) The CRCP-8 computer program provides an excellent design or diagnostic tool that may be used for site-specific studies.

Specific Recommendations:

- (1) As new projects are added to the rigid pavement database, their actual performance should be compared with the predicted performance, thus, providing a continuous calibration and validation program. The validation should be more precise with time, since the evolutionary specifications will result in properties required in the model to be collected during the construction operations.*
 - (2) If Item 1 identifies areas where the computer model needs to be improved, steps should be taken to develop submodels that will improve the model precision.*
- d) In lieu of developing a pavement standard that is general and very conservative for the entire state, the program may be used to develop designs for a specific project, as previously discussed in Section A, 1, a), (1).
2. The CRCP-8 program has evolved over time. Based on the results presented herein, the following enhancements and additional developments are recommended:
- a) The improved finite element model for predicting stresses owing to wheel load developed in Project 0-1758 should be inserted into the program to permit a more accurate calculation of stresses for the thicker pavements.

Specific Recommendations:

- (1) *Since pavement thickness and subbase type are variables in the rigid pavement database, the predicted and actual performances should be calibrated.*
 - (2) *New projects added to the rigid pavement database should be used for validation.*
- b) As a part of this study, the spalling mechanism has been characterized and modeled; thus, the program should be revised to cover the spalling.

Specific Recommendations:

- (1) *The spalling model should be added to the CRCP program.*
- (2) *Sensitivity studies using the spalling should be conducted to check the program logic.*
- (3) *The rigid pavement database should be used to compare predicted and measured per performance for calibration purposes.*

9.6 GENERAL PCC PAVEMENT DEVELOPMENTS

The following are a number of conclusions and recommendations relative to the general area of PCC pavement development:

1. For the rigid pavement database that has been maintained since 1974, a number of pavement performance factors should be added to the database. Those requiring minimal effort should be added immediately and those requiring more effort should be added over a period of time.
 - a) Within the next year, the following items could be added to the rigid pavement database as a part of an existing project:
 - (1) *The evaporation rate (relative to curing effectiveness) at the time of the PCC placement for the test section.*
 - (2) *As part of the survey the spall depth should be recorded, since the results from this study indicate that the depth of the spall is related to the evaporation rate and is tied to the amount of water leaving the pavement during the curing period.*
 - (3) *The test sections on Projects 1–8 reported herein should be included in the rigid pavement database, since significant information is available on the initial stages of the pavement and for a number of years thereafter. Thus, after a period of time, these sites could be revisited to ascertain the effect of the parameters on punchout formation and spalling.*

- b) The following items will require more effort and could be added in subsequent years for the rigid pavement database project:
 - (1) *At the present time the crack spacing distribution is recorded for only the first 200 ft (60.96 m) of a test section; based on its importance, we recommend it be kept for the entire 1,000 ft (304.8 m).*
 - (2) *The vertical distribution of the tensile strength has been identified as an important factor affecting the concrete pavement performance, especially in the spalling area; thus, it is recommended that the tensile strength distribution vertically be determined for a subsection of the rigid pavement database in order to determine what is an acceptable range.*
 - c) The results of this study indicate that several areas of criteria need to be developed for use in the design and construction of PCC:
 - (1) *The rigid pavement database should be used to identify the acceptable level of cracking less than 3 ft (0.91 m). Since the information is currently in the database (along with performance information), the criteria may be developed by analyzing the data.*
 - (2) *Once the vertical strength distribution is ascertained from the additions to the database described in Item 1, an acceptable level of difference between top and bottom may be established by examining the pavement's performance at various levels.*
2. Performance-based specifications for PCC pavement should be developed using these studies, since significant information has been derived and may be used to improve the overall level of rigid pavement performance in Texas. The specification should be developed incrementally by adding only those concepts that have been verified.
- a) Factors that should be included as special provisions to the PCC pavement specification on an immediate basis are as follows:
 - (1) *Control should be placed on the pavement for concrete placement with ambient air temperature greater than 90°F (32.2°C) to ensure this concrete does not develop excessive hydration temperatures.*
 - (2) *The evaporation rate on every project should be monitored in real time and for use by the contractor to adjust the curing conditions of placed pavements to ensure a desirable set of conditions are realized.*
 - (3) *The thermal coefficient of the portland cement concrete and, specifically, the coarse aggregate should be included in the specification so that various design levels (and in some instances crack control) may be established by the designer for various conditions experienced in the field.*

- b) Concepts that should be added at later stages include the following:
- (1) *The CRCP-8 program should be used, along with the present technique, to develop the pavement factor adjustment, since it can generate the distribution for cracks, the measured crack spacing distribution, and the vertical strength distribution.*
 - (2) *The desire is to develop an NDT for measuring in situ strength. This project has demonstrated that, in addition to a temperature history, the moisture in the pavement is a very important factor affecting the strength of portland cement concrete. Of course, the importance of concrete density is well known. Therefore, to ensure that proper concrete conditions are achieved so as to provide acceptable portland cement concrete pavement in place, an equation with tensile strength as a function of temperature, moisture, and density should be developed. At the present time, only temperature is used in a maturity equation; but in order to ensure the in situ strength is adequate, the moisture and density should be considered. The technology for achieving these factors is now presently available.*

REFERENCES

1. Dossey, Terry, and B. F. McCullough, "Updating and Maintaining the Rigid Pavement Database," Research Report 1342-3F, Center for Transportation Research, The University of Texas at Austin, November 1994.
2. Dossey, Terry, B. F. McCullough, and Abigail Dumas, "Effects of Aggregate Blends on the Properties of Portland Cement Concrete Pavements," Research Report 1244-8F, Center for Transportation Research, The University of Texas at Austin, August 1994.
3. Allison, Brent, Technical Memorandum 1244-74b, Center for Transportation Research, The University of Texas at Austin, November 1991.
4. Won, Moonchoel, Kenneth Hankins, and B. F. McCullough, "Mechanistic Analysis of Continuously Reinforced Concrete Pavements Considering Material Characteristics, Variability, and Fatigue," Research Report 1169-2, Center for Transportation Research, The University of Texas at Austin, March 1991.
5. Suh, Young-Chan, Technical Memorandum 1244-34, Center for Transportation Research, The University of Texas at Austin, May 1991.
6. Suh, Young-Chan, Ken Hankins, and B. F. McCullough, "Early-Age Behavior of Continuously Reinforced Concrete Pavement and Calibration of the Failure Prediction Model in the CRCP-7 Program," Research Report 1244-3, Center for Transportation Research, The University of Texas at Austin, March 1992.
7. Otero-Jimenez, Miguel Angel, B. F. McCullough, and Ken Hankins, "Monitoring of Siliceous River Gravel and Limestone Continuously Reinforced Concrete Pavement Test Sections in Houston 2 Years after Placement, and Development of a Crack Width Model for the CRCP-7 Program," Research Report 1244-4, Center for Transportation Research, The University of Texas at Austin, March 1992.
8. Green, William J., Ramon L. Carrasquillo, and B. F. McCullough, "Coarse Aggregate for PCC — Pilot Study Evaluation," Research Report 422-1, Center for Transportation Research, The University of Texas at Austin, September 1987.
9. McCullough, B. F., Dan Zollinger, and Brent T. Allison, "Preliminary Research Findings on the Effect of Coarse Aggregate on the Performance of Portland Cement Concrete Paving, Research Report 1244-5, Center for Transportation Research, The University of Texas at Austin, October 1993.

10. Suh, Young-Chan, B. F. McCullough, and Ken Hankins, "Development and Application of Randomness Index for Continuously Reinforced Concrete Pavement," *Transportation Research Record* 1307, January 1991.
11. McCullough, B. F., and Pieter Strauss, "Performance Survey of Continuously Reinforced Concrete Pavements in Texas," Research Report 21-1F, Center for Transportation Research, The University of Texas at Austin, November 1974.
12. Aslam, Mohammad F., and C. L. Saraf, "Design Recommendations for Steel Reinforcement of CRCP," Research Report 422-2, Center for Transportation Research, The University of Texas at Austin, November 1987.
13. Hankins, Kenneth, and Young Chan Suh, "Field Evaluation of Coarse Aggregate Types: Criteria for Test Sections," Research Report 1244-1, Center for Transportation Research, The University of Texas at Austin, November 1974.
14. Dossey, Terry, and B. F. McCullough, "Effects of Aggregate Blends on the Properties of Portland Cement Concrete Pavements," Research Report 1244-8, Center for Transportation Research, The University of Texas at Austin, August 1994.
15. McCullough, B. F., and Terry Dossey, "Case Study of Overlay Performance of Continuously Reinforced Concrete Pavement (CRCP) Located on IH-35, Bowie County, Texas," Research Report 1342-1, Center for Transportation Research, The University of Texas at Austin, February 1994.
16. Chiang, Chypin, and B. F. McCullough, "Sensitivity Analysis of Continuously Reinforced Concrete Pavement Model CRCP-1 for Highways," Research Report 177-2, Center for Transportation Research, The University of Texas at Austin, August 1975.
17. Mindess, Sidney, and J. Francis Young, *Concrete*, Prentice-Hall, Inc., Englewood Cliffs, 1981.
18. Carmichael, Frank, and B. F. McCullough, "Modification and Implementation of the Rigid Pavement Design System," Research Report 123-26, Center for Transportation Research, The University of Texas at Austin, January 1975.
19. Trevino, Manuel, N. J. Delatte, S. Gräter, and B. F. McCullough, "Partial Construction Report of a Bonded Concrete Overlay on IH-10, El Paso, and Guide for Expedited BCO Design and Construction," Research Report 2911-5F, Center for Transportation Research, The University of Texas at Austin, December 1996.

20. Bradbury, R.D. (1938). Reinforced concrete pavements. Wire reinforcement Institute, Washington, D.C.
21. Bauant, Z.P. and Xu, K. (1991). "Size Effect in Fracture of Ceramics and Its Use to Determine Fracture Energy and Effective Process Zone Length," *Journal of American Ceramic Society*, 73(7), 1841-1853.
22. Hibbitt, H.D., Karlsson, B., and Sorensen, E. P. (1994). *ABAQUS User's Manual*. Hibbit, Karlsson, and Sorenson Inc., Pawtucket, R.I.
23. Huang, Y.H. (1993). *Pavement Analysis and Design*. Prentice Hall, Englewood Cliffs, NJ.
24. Senadheera, S.P. (1995). "Spalling in Concrete Pavements: Its Relationship to Coarse Aggregate in Concrete and a Framework for Design." Ph.D. Dissertation, Texas A&M University, College Station, TX.
25. Hillerborg, A., Modeer, M., and Peterson, P.E. (1976). "Analysis of Crack Formation and Crack Growth in Concrete by Means of Fracture Mechanics and Finite Elements." *Cement and Concrete Research*, 6(6), 773-782.
26. Hoshino, M. (1989). "Relationship Between Bleeding, Coarse Aggregate, and Specimen Height of Concrete." *ACI Materials Journal*, 86(2), 185-190.
27. Mohamed, A.R. and Hansen, W. (1997). "Effect of Nonlinear Temperature Gradient on Curling Stresses in Concrete Pavements." *Transportation Research Record* 1568, 65-71.
28. Wittman, F.H., Mihashi, H., and Nomura, N. (1990). "Size Effect on Fracture Energy of Concrete." *Engineering Fracture Mechanics*, 35(1), 107-115.
29. Allen, D.H., Jones, R.H., and Boyd, J.G. (1994). "Micromechanical Analysis of a Continuous Fiber Metal Matrix Composite Including the Effects of Matrix Viscoplasticity and Evolving Damage." *Journal of Mechanics and Physics of Solids*, 42(3), 505-529.
30. Cook, R. (1981). *Concepts and Applications of Finite Element Analysis*. 2nd Edition, John Wiley & Sons, New York, NY.
31. Texas Department of Transportation (1997). Houston District, personal communication.
32. Tielking, J.T., and Roberts, F.L. (1987). "Tire Contact Pressure and Its Effect on Pavement Strain." *Journal of Transportation Engineering*, ASCE, 113(1), 56-71.

33. Tielking, J.T. (1991). "Pavement Shear Forces Produced by Truck Tires." Memorandum,, February, Texas A&M University, Department of Civil Engineering, College Station, TX.
34. Yang, S. (1996). "A Temperature Prediction Model in New Concrete Pavement and a New Test Method for Concrete Fracture Parameters." Ph.D. Dissertation, Texas A&M University, College Station, TX.
35. Westergaard, H.M. (1926). "Analysis of Stresses in Concrete Pavements Due to Variations of Temperature." Highway Research Board Proceedings, 6, 201-215.
36. Zollinger, Dan G., Sanjaya P. Senadheera, and Tianxi Tang, "Spalling of Continuously Reinforced Concrete Pavements," Vol. 120 No.3, ASCE Journal of Transportation Engineering, May/June 1994, pp.394-411.

APPENDIX A

Crack Distribution over Time for Projects 1–4 and 8

Project 1 — SH6 at Patterson

Project 2 — SH6 at Huffmeister

Project 3 — BW8

Project 4 — 1H 45

Project 8 — Hempstead

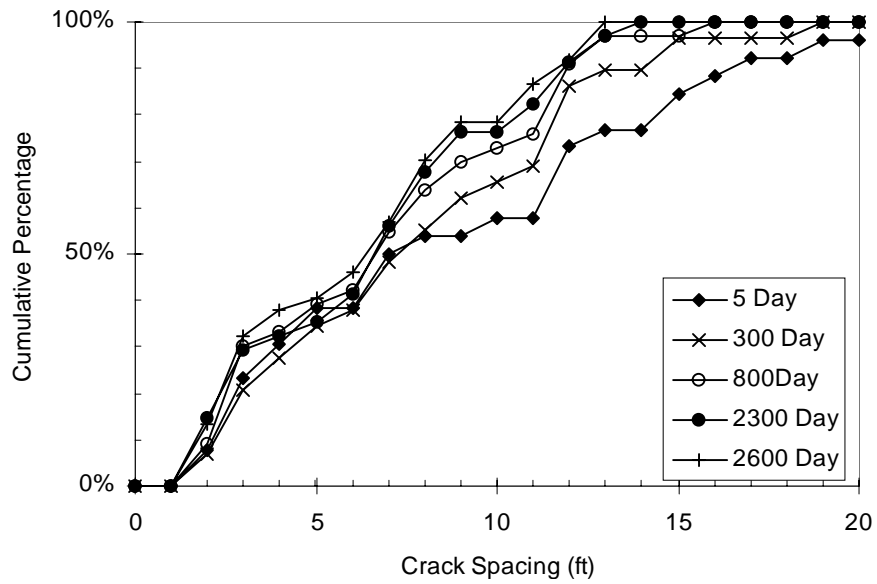


Figure A1 Crack formation over time for Project 1 - Section A (SRG, Winter, 0.63% Steel)

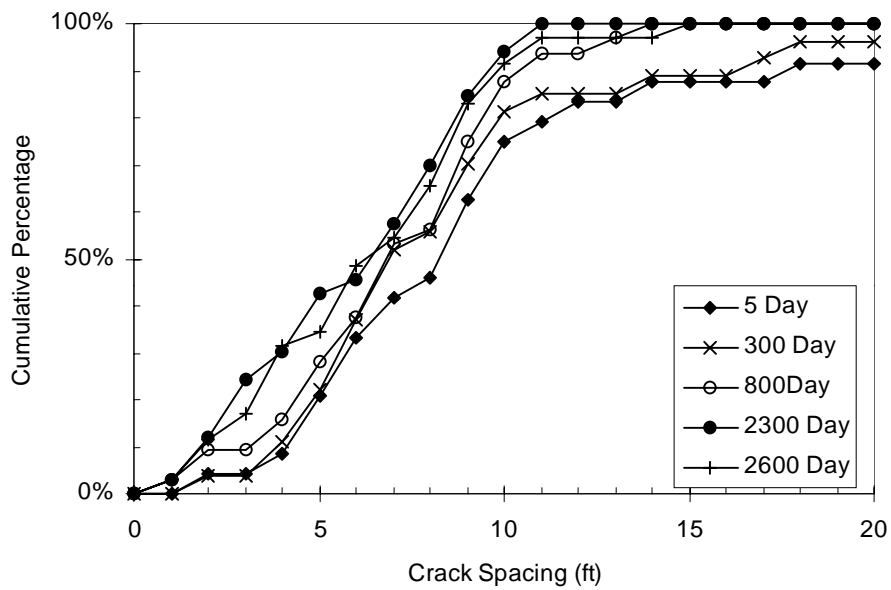


Figure A2 Crack formation over time for Project 1 - Section B (SRG, Winter, 0.53% Steel)

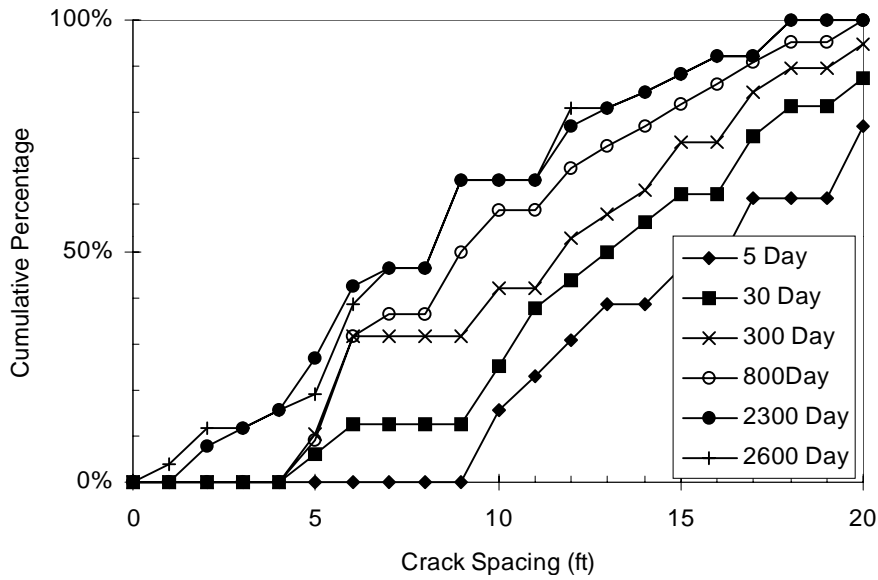


Figure A3 Crack formation over time for Project 1 - Section C (SRG, Winter, 0.42% Steel)

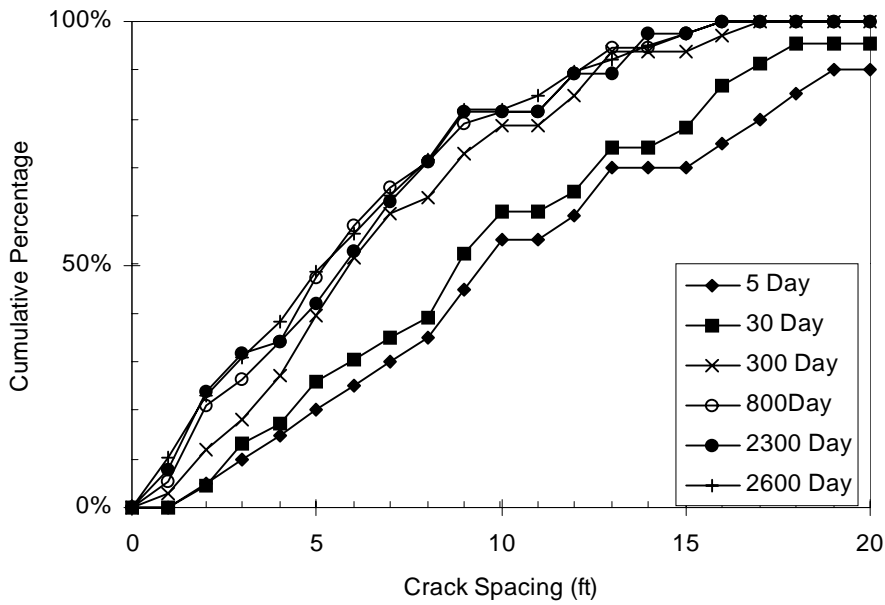


Figure A4 Crack formation over time for Project 1 - Section D (SRG, Winter, 0.53% Steel)

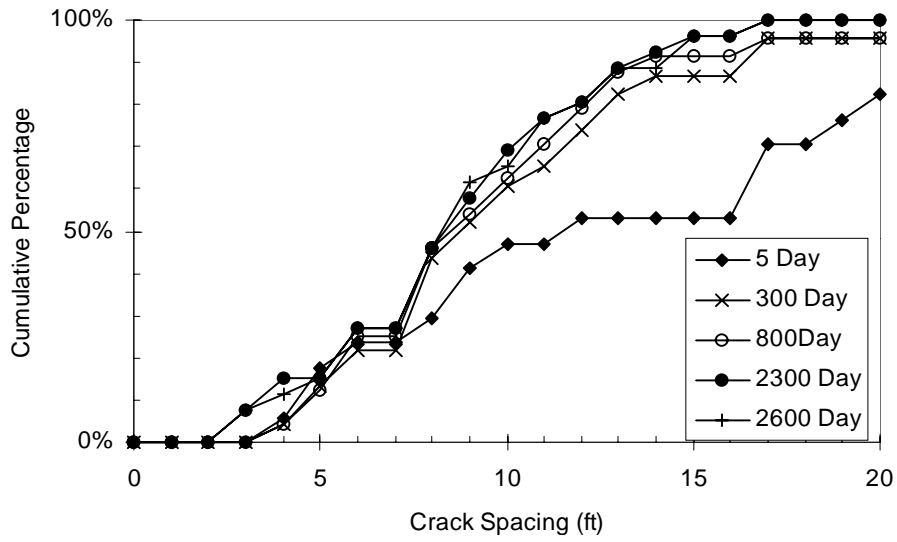


Figure A5 Crack formation over time for Project 1 - Section E (LS, Winter, 0.63% Steel)

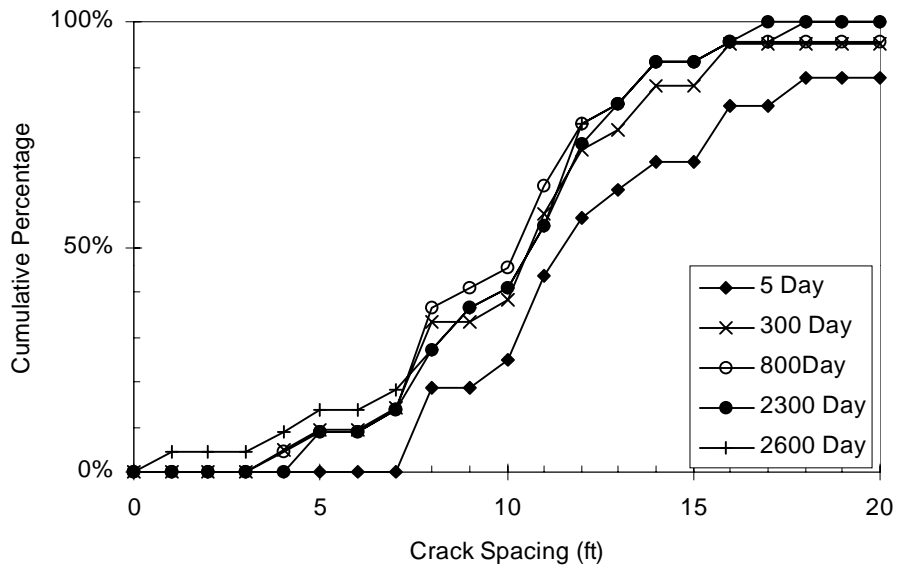


Figure A6 Crack formation over time for Project 1 - Section F (LS, Winter, 0.52% Steel)

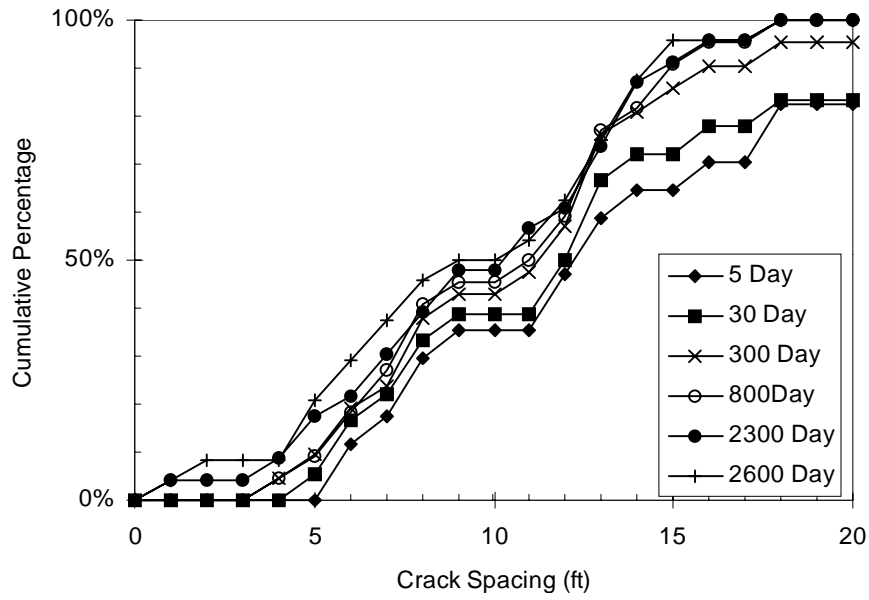


Figure A7 Crack formation over time for Project 1 - Section G (LS, Winter, 0.61% Steel)

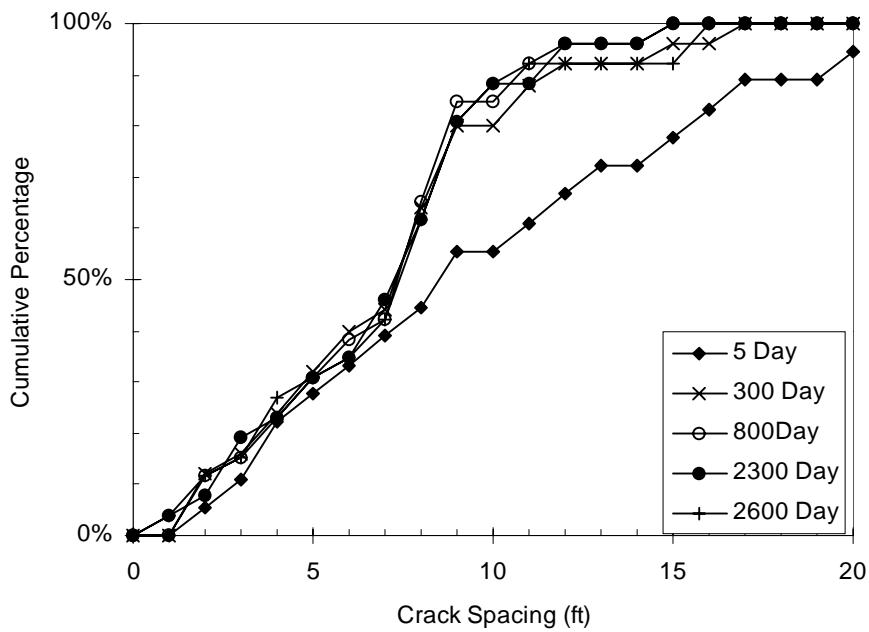


Figure A8 Crack formation over time for Project 1 - Section H (LS, Winter, 0.68% Steel)

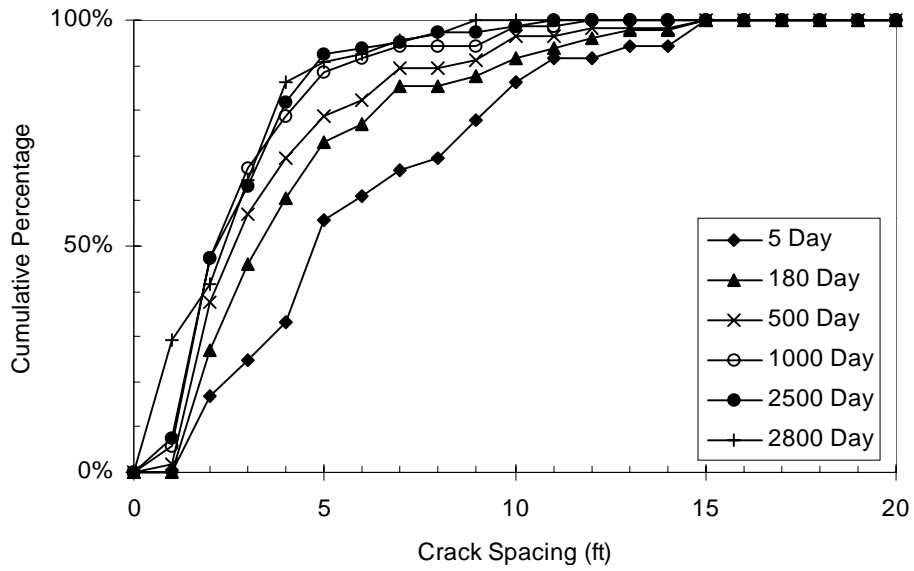


Figure A9 Crack formation over time for Project 2 - Section A (SRG, Summer, 0.63% Steel)

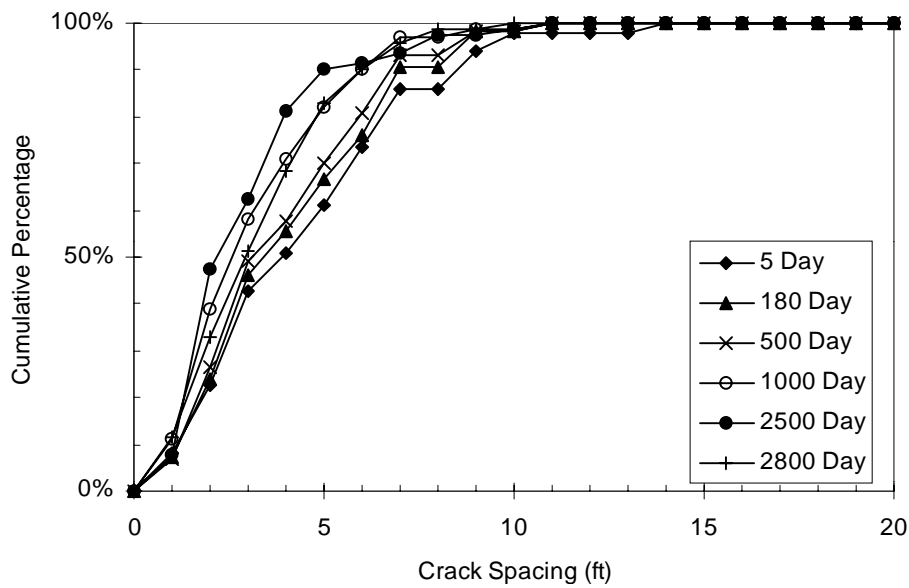


Figure A10 Crack formation over time for Project 2 - Section B (SRG, Summer, 0.53% Steel)

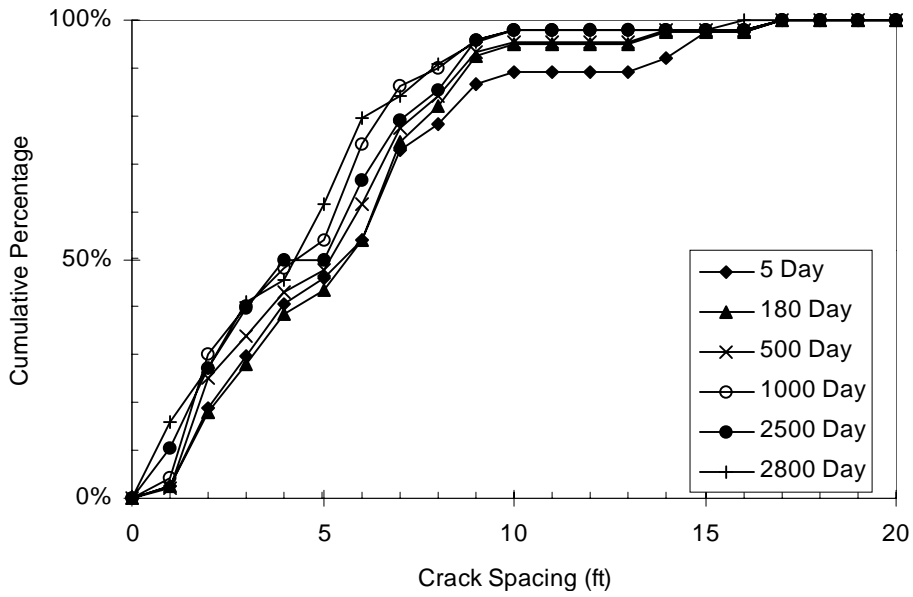


Figure A11 Crack formation over time for Project 2 - Section C (SRG, Summer, 0.42% Steel)

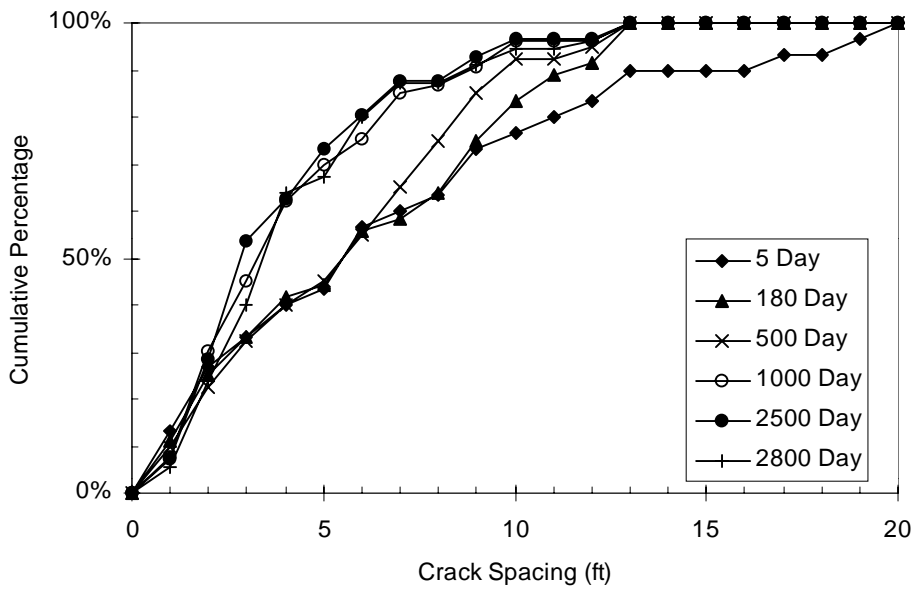


Figure A12 Crack formation over time for Project 2 - Section D (SRG, Summer, 0.53% Steel)

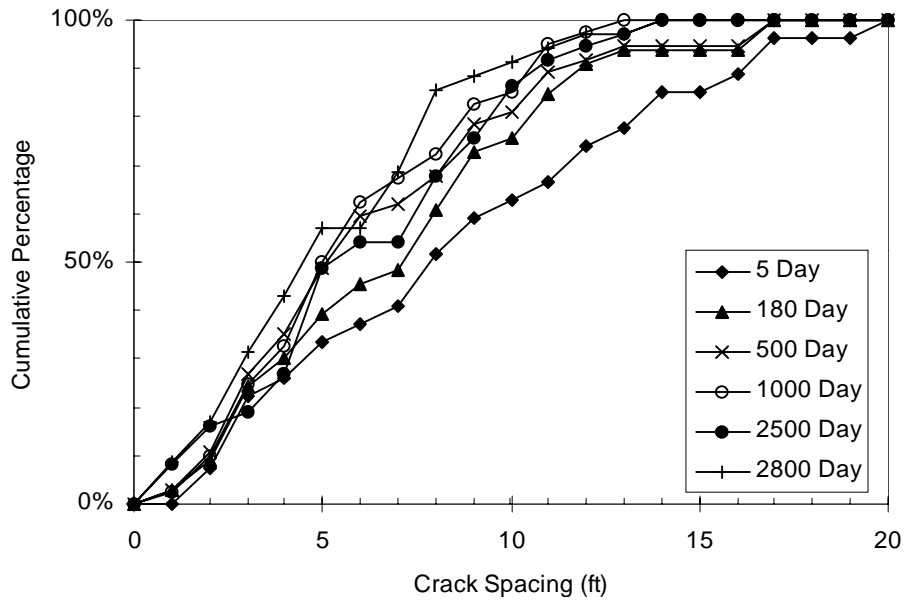


Figure A13 Crack formation over time for Project 2 - Section E (LS, Summer, 0.63% Steel)

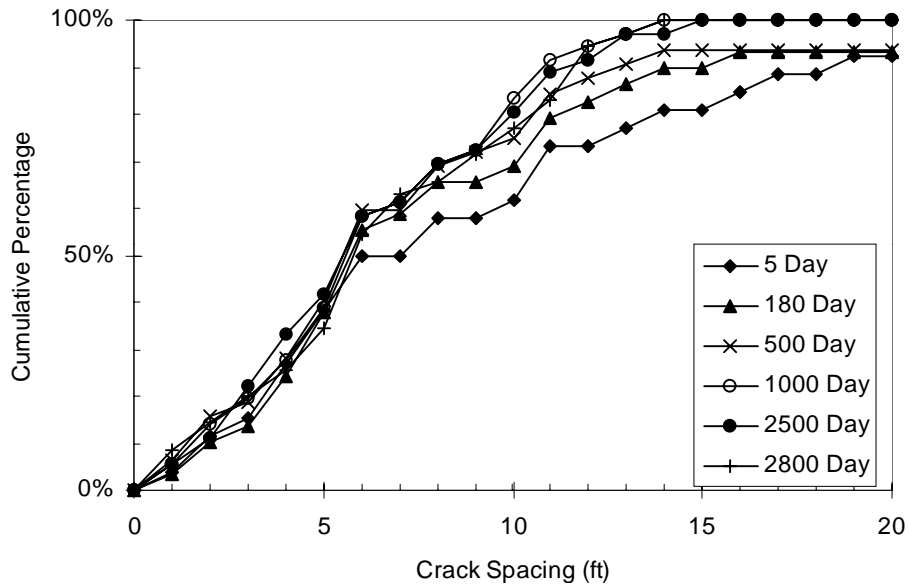


Figure A14 Crack formation over time for Project 2 - Section F (LS, Summer, 0.52% Steel)

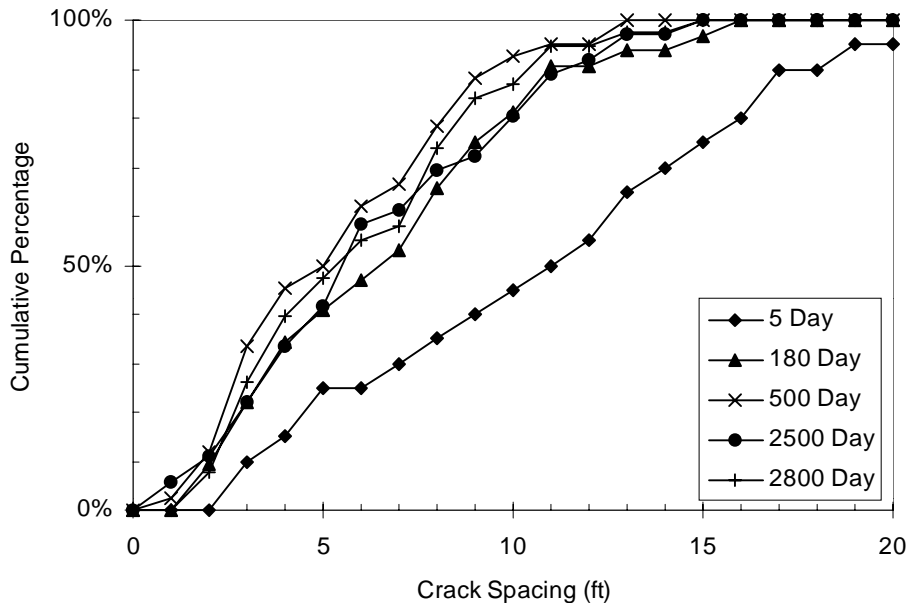


Figure A15 Crack formation over time for Project 2 - Section G (LS, Summer, 0.61% Steel)

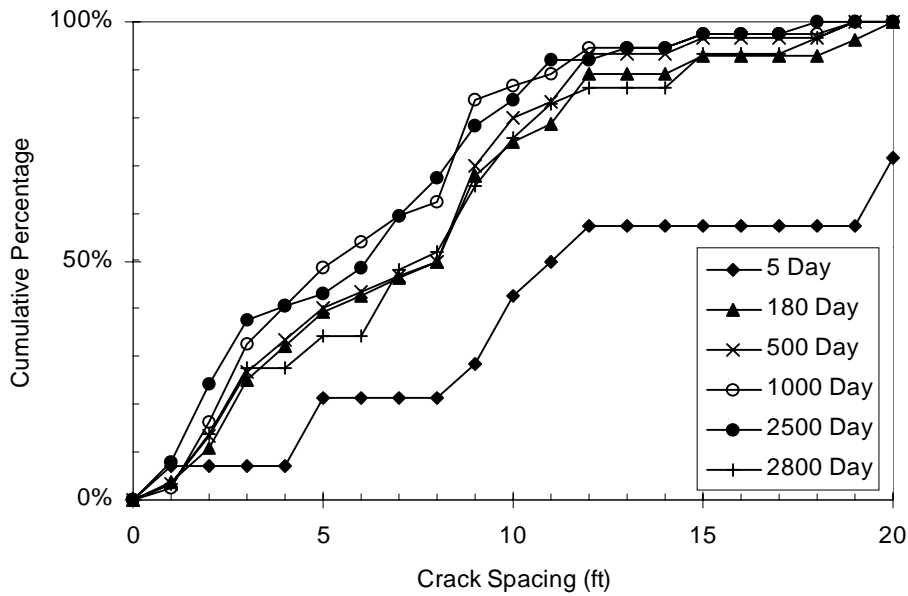


Figure A16 Crack formation over time for Project 2 - Section H (LS, Summer, 0.68% Steel)

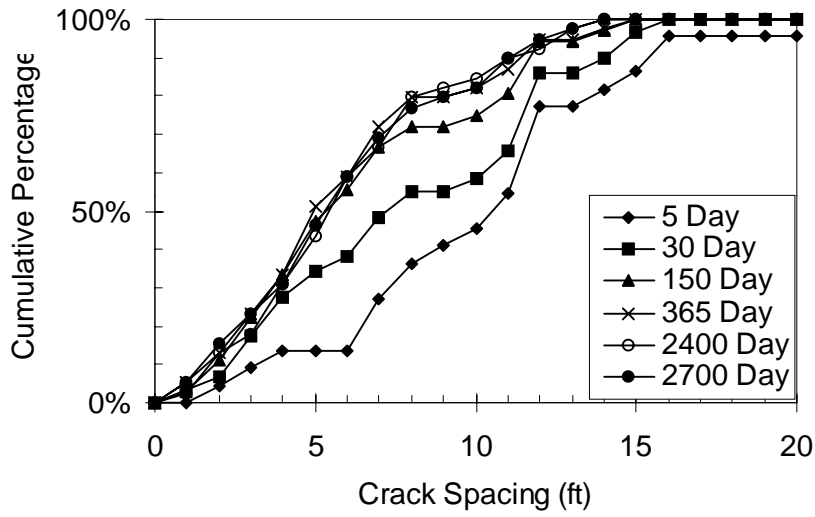


Figure A17 Crack formation over time for Project 3 - Section A (SRG, Winter, 0.62% Steel)

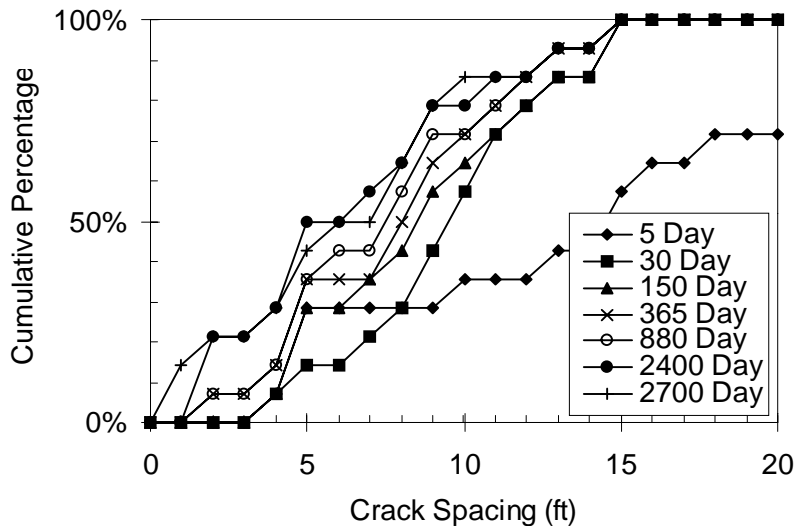


Figure A18 Crack formation over time for Project 3 - Section B (SRG, Winter, 0.50% Steel)

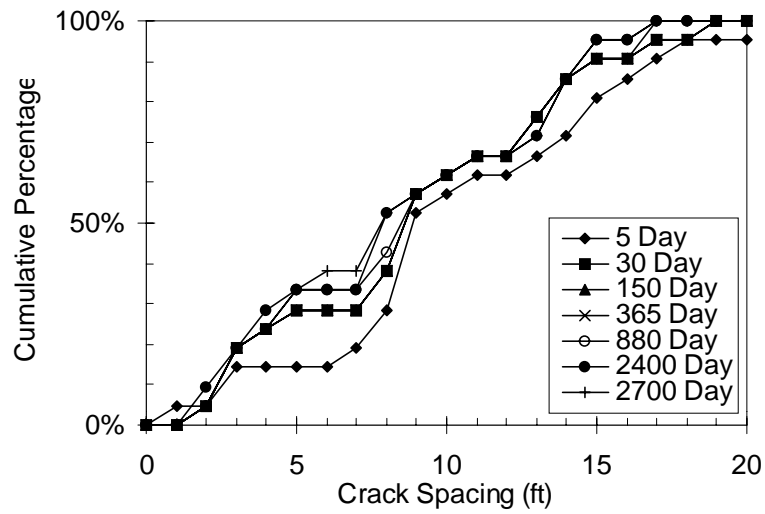


Figure A19 Crack formation over time for Project 3 - Section C (SRG, Winter, 0.38% Steel)

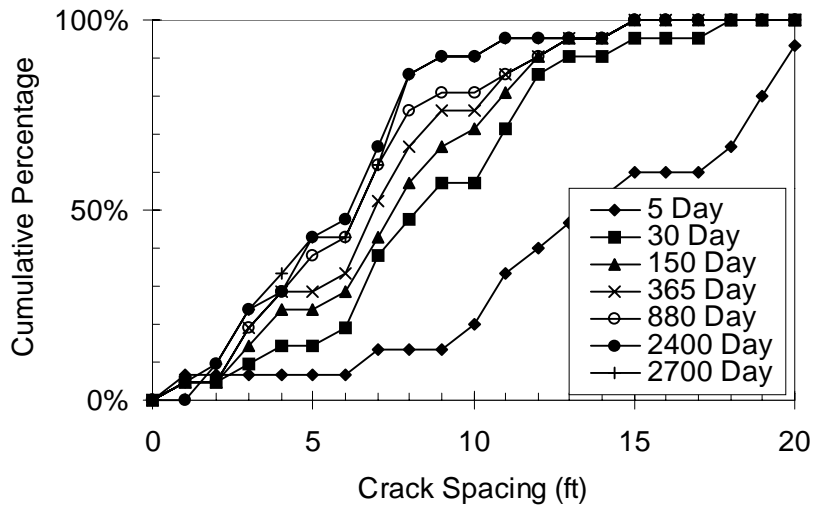


Figure A20 Crack formation over time for Project 3 - Section D (SRG, Winter, 0.48% Steel)

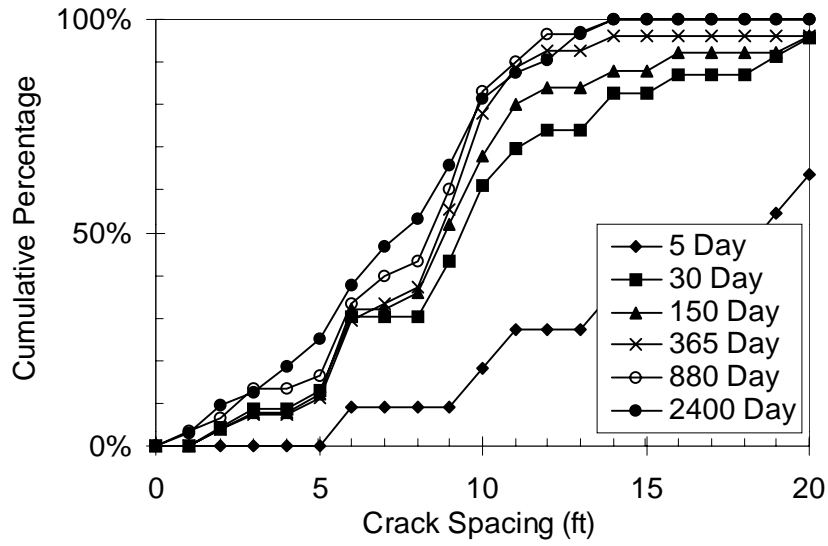


Figure A21 Crack formation over time for Project 3 - Section E (LS, Winter, 0.56% Steel)

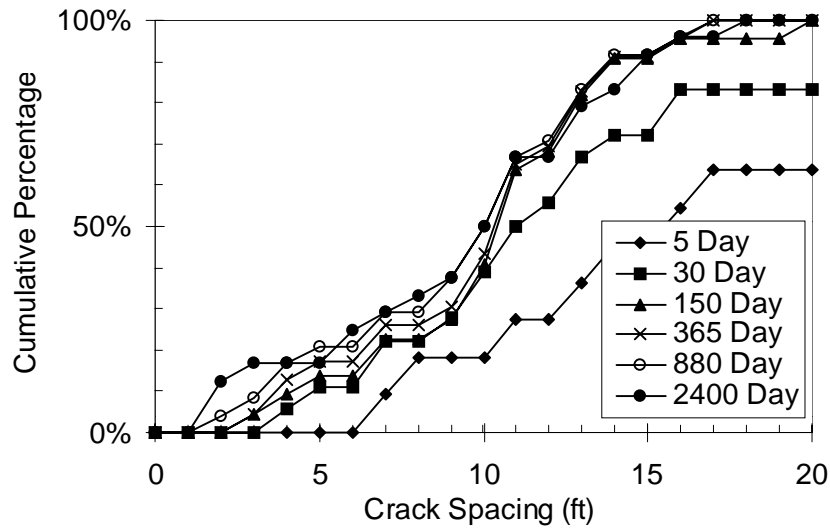


Figure A22 Crack formation over time for Project 3 - Section F (LS, Winter, 0.45% Steel)

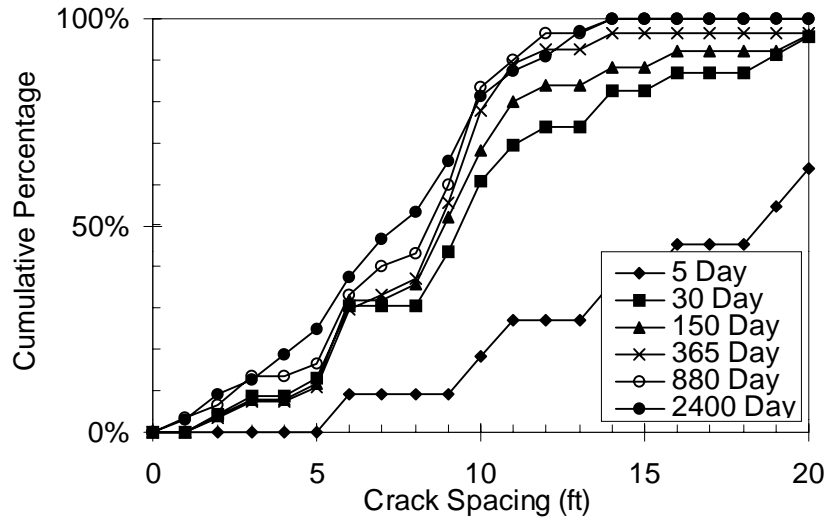


Figure A23 Crack formation over time for Project 3 - Section G (LS, Winter, 0.58% Steel)

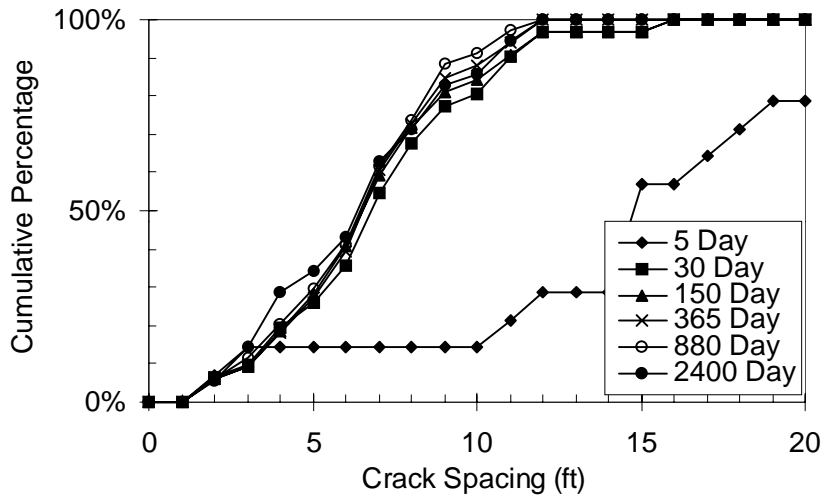


Figure A24 Crack formation over time for Project 3 - Section H (LS, Winter, 0.67% Steel)

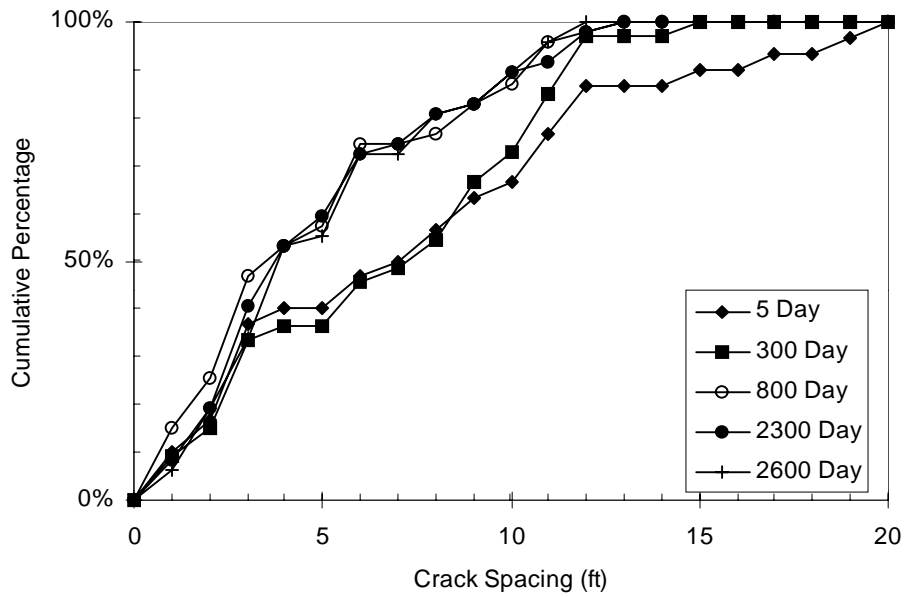


Figure A25 Crack formation over time for Project 4 - Section A (SRG, Winter, 0.67% Steel)

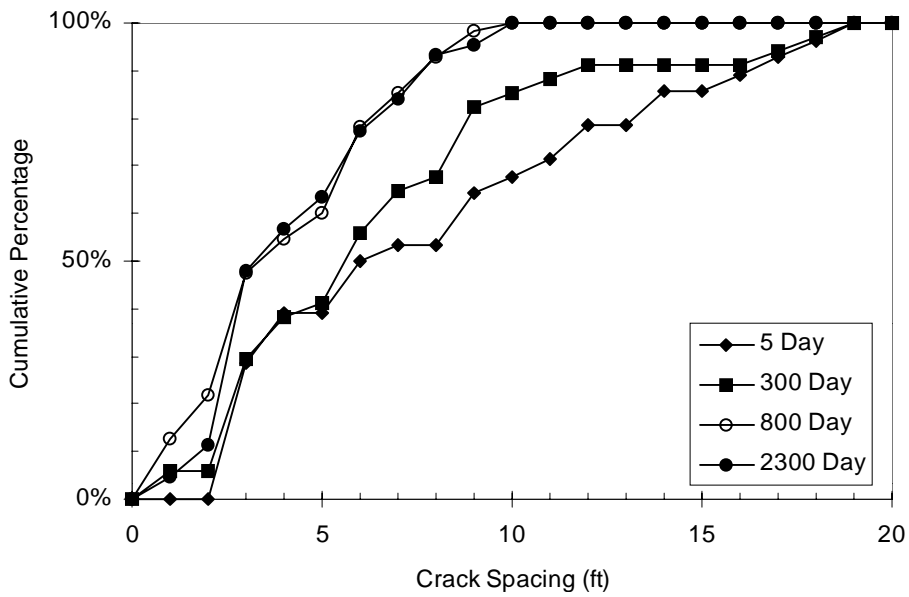


Figure A26 Crack formation over time for Project 4 - Section B (SRG, Winter, 0.55% Steel)

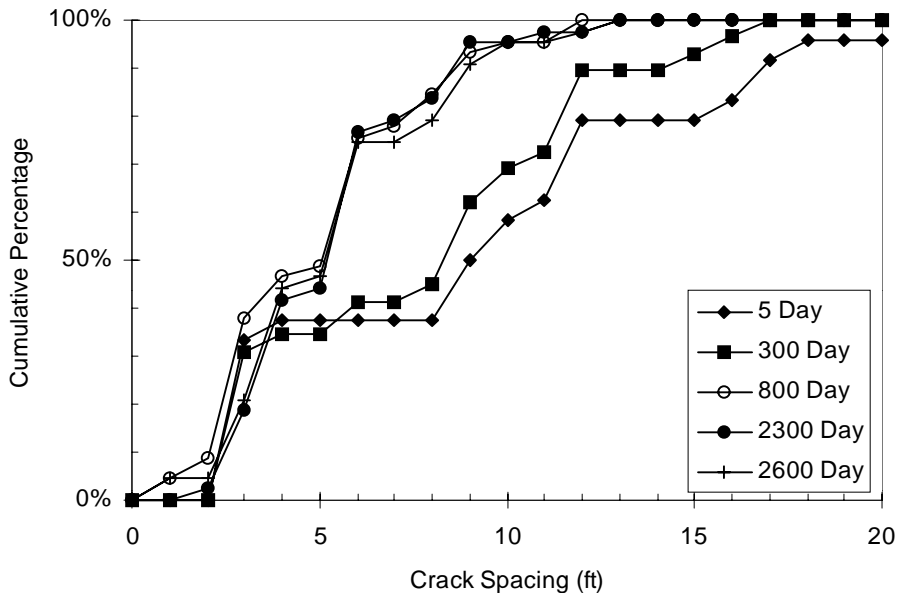


Figure A27 Crack formation over time for Project 4 - Section C (SRG, Winter, 0.65% Steel)

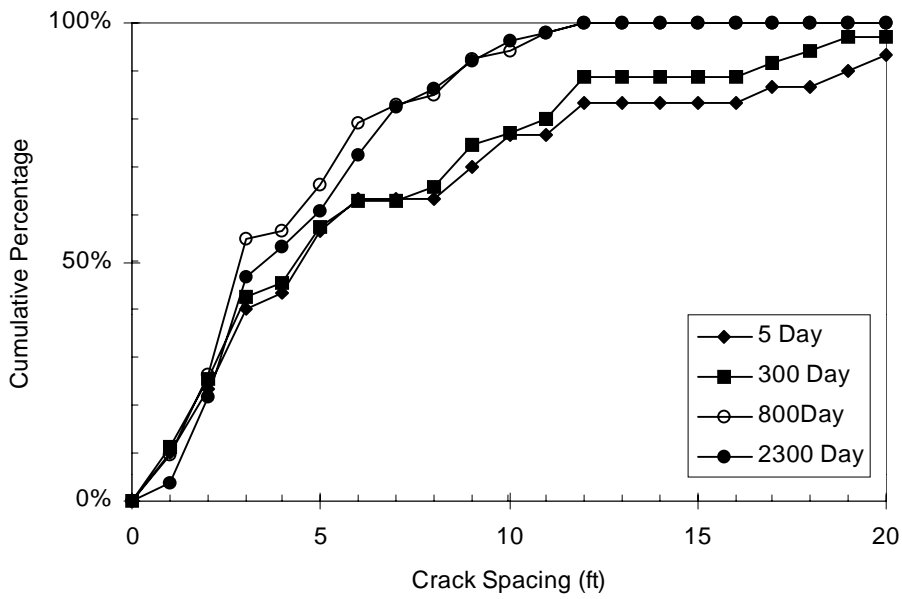


Figure A28 Crack formation over time for Project 4 - Section D (SRG, Winter, 0.76% Steel)

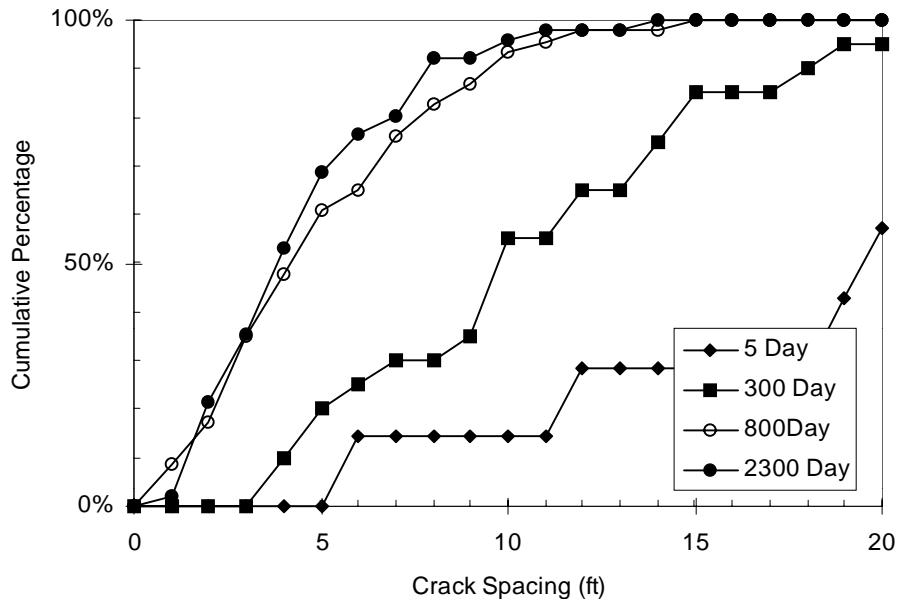


Figure A29 Crack formation over time for Project 4 - Section E (LS, Winter, 0.84% Steel)

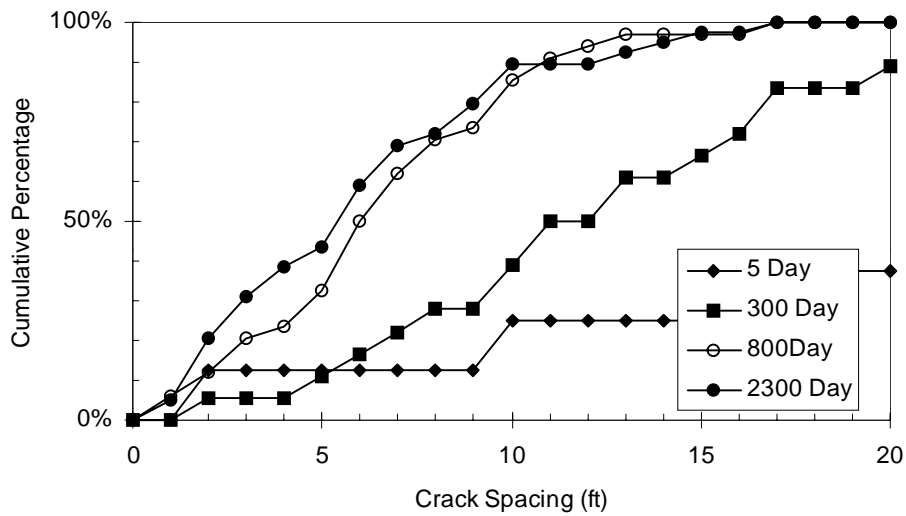


Figure A30 Crack formation over time for Project 4 - Section F (LS, Winter, 0.74% Steel)

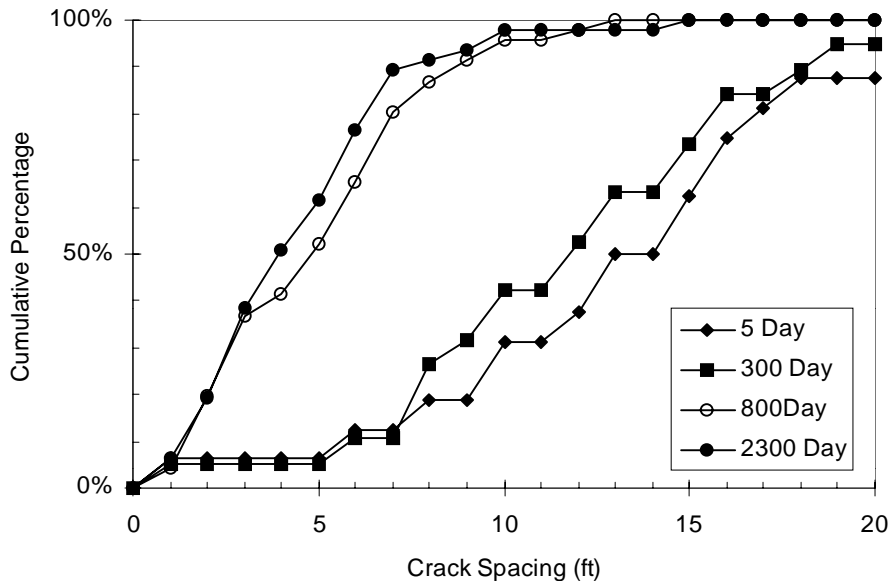


Figure A31 Crack formation over time for Project 4 - Section G (LS, Winter, 0.63% Steel)

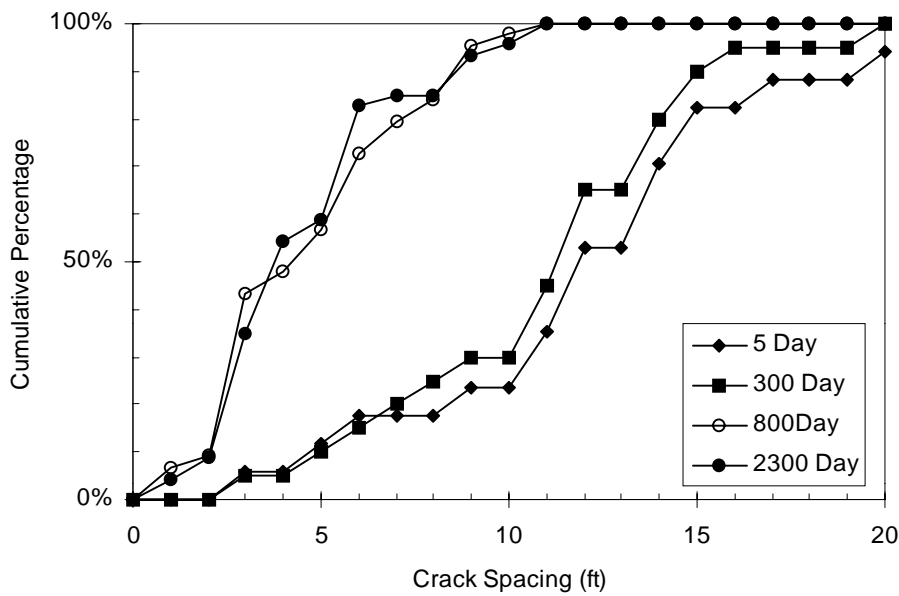


Figure A32 Crack formation over time for Project 4 - Section H (LS, Winter, 0.75% Steel)

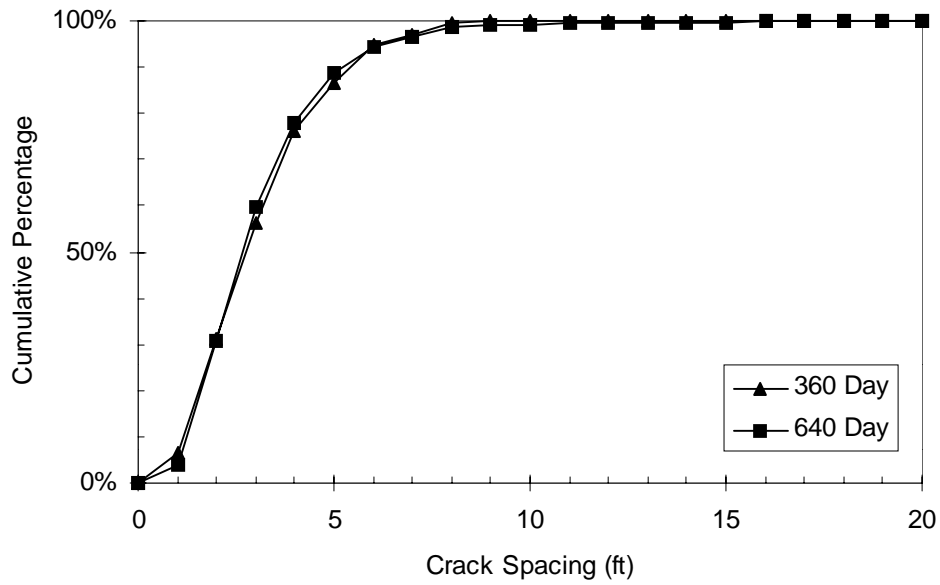


Figure A33 Crack formation over time for Project 8 - Section 21E (SRG/LS, Summer, 0.52% Steel)

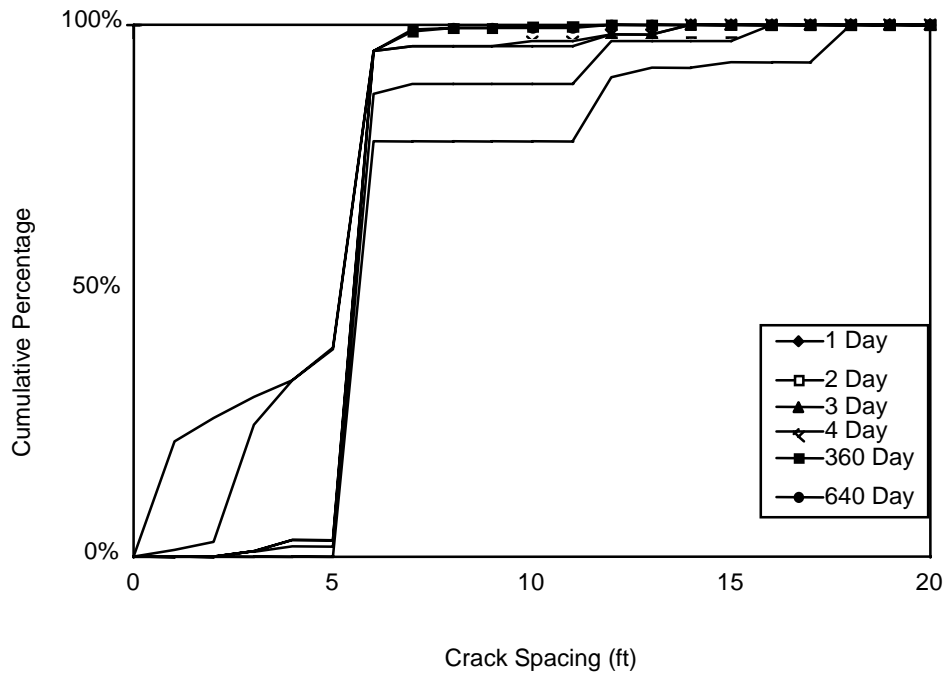


Figure A34 Crack formation over time for Project 8 - Section 22E (SRG/LS, Summer, 0.52% Steel, Transverse sawcuts)

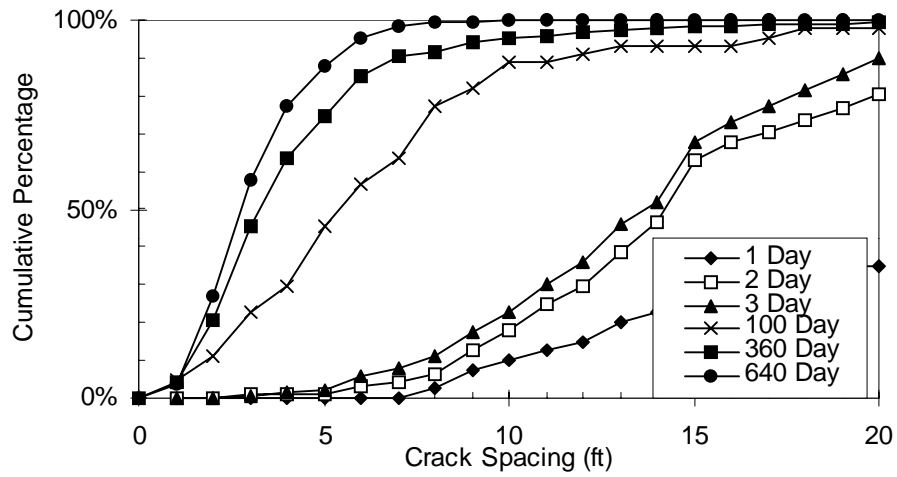


Figure A35 Crack formation over time for Project 8 - Section 23E (SRG, Summer, 0.52% Steel)

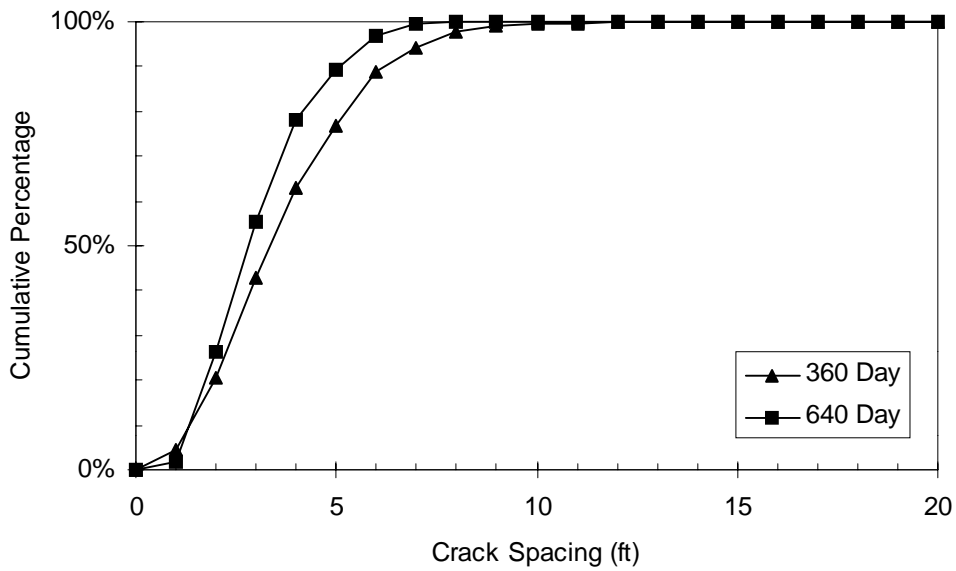


Figure A36 Crack formation over time for Project 8 - Section 24E (SRG, Summer, 0.52% Steel)

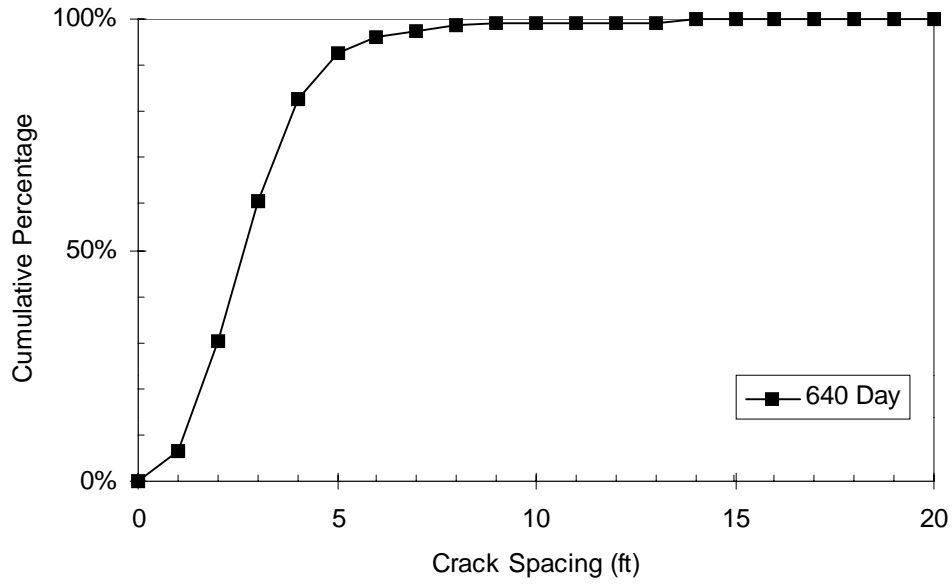


Figure A37 Crack formation over time for Project 8 - Section 25E (SRG, Summer, 0.52% Steel)

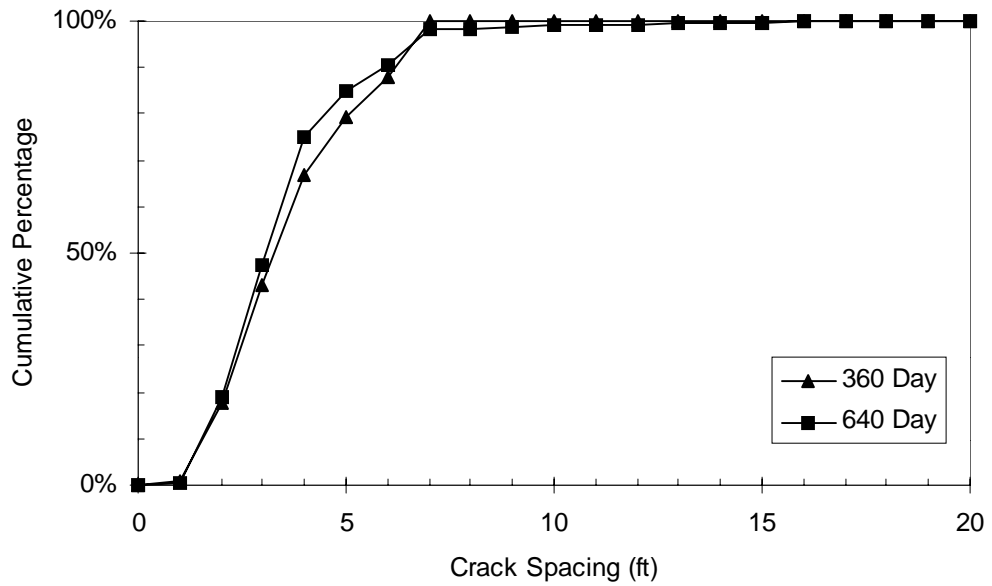


Figure A38 Crack formation over time for Project 8 - Section 26E (SRG, Summer, 0.52% Steel, Transverse sawcuts)

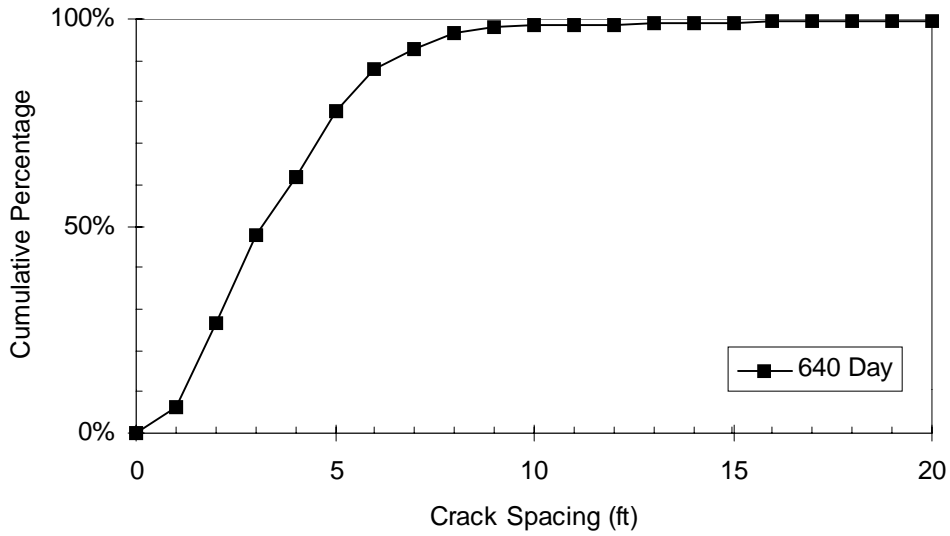


Figure A39 Crack formation over time for Project 8 - Section 27E (SRG, Summer, 0.52% Steel)

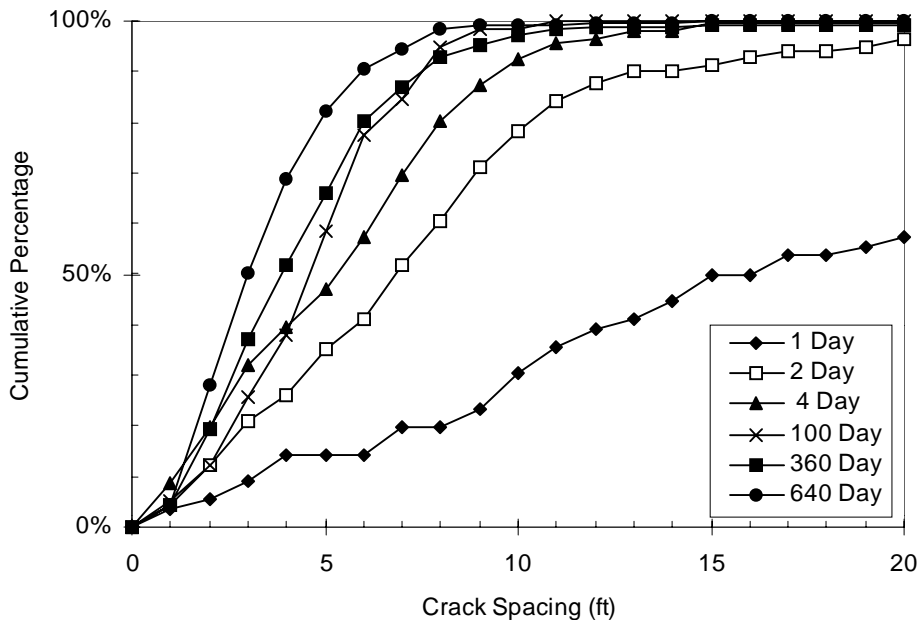


Figure A40 Crack formation over time for Project 8 - Section 28E (SRG, Summer, 0.49% Steel)

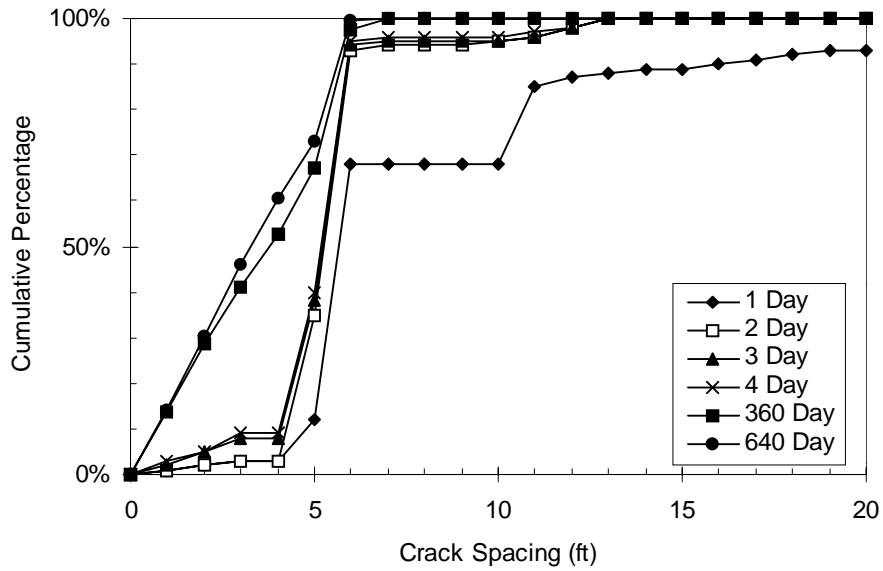


Figure A41 Crack formation over time for Project 8 - Section 29E (SRG, Summer, 0.49% Steel, Transverse sawcuts)

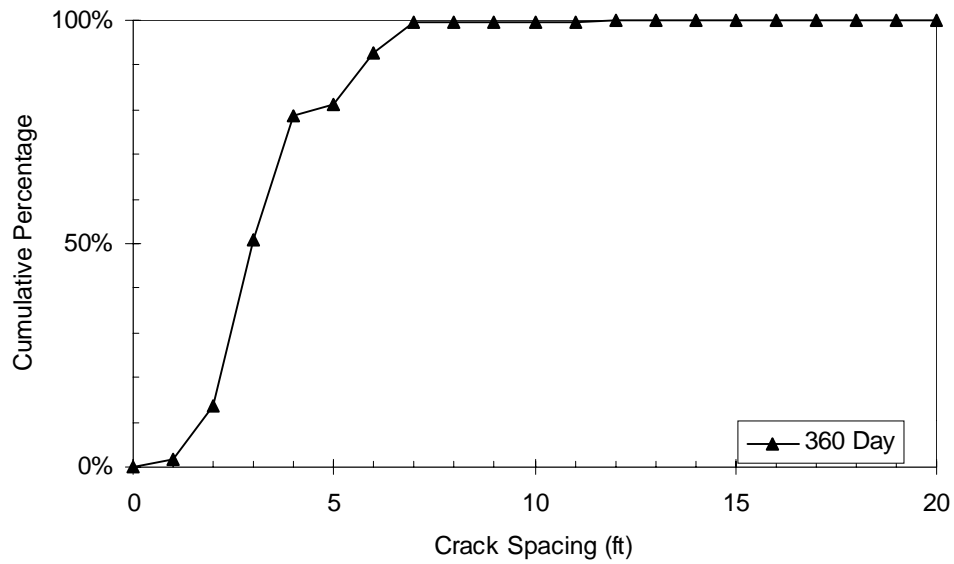


Figure A42 Crack formation over time for Project 8 - Section 30E (SRG, Summer, 0.49% Steel)

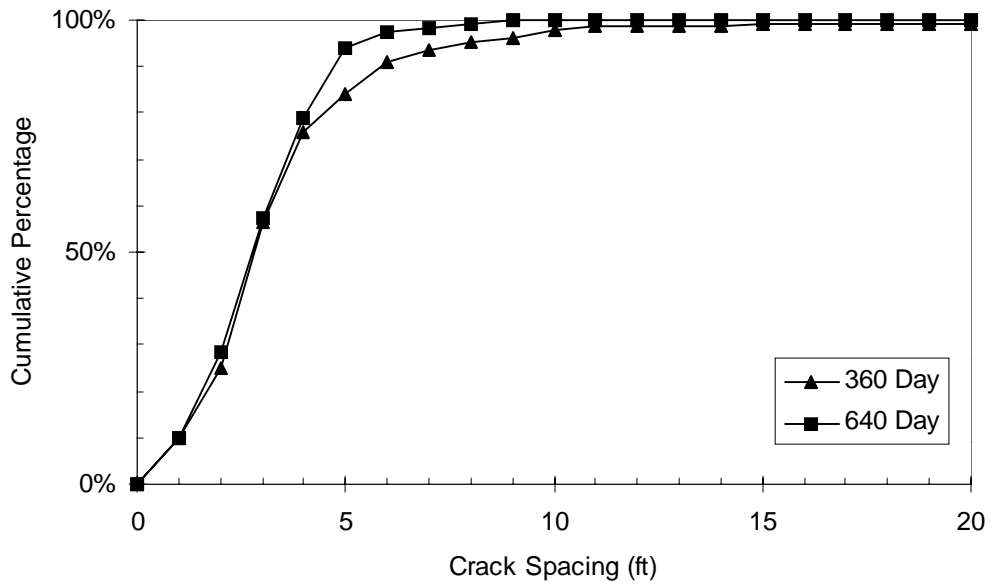


Figure A43 Crack formation over time for Project 8 - Section 31E (SRG, Summer, 0.49% Steel)

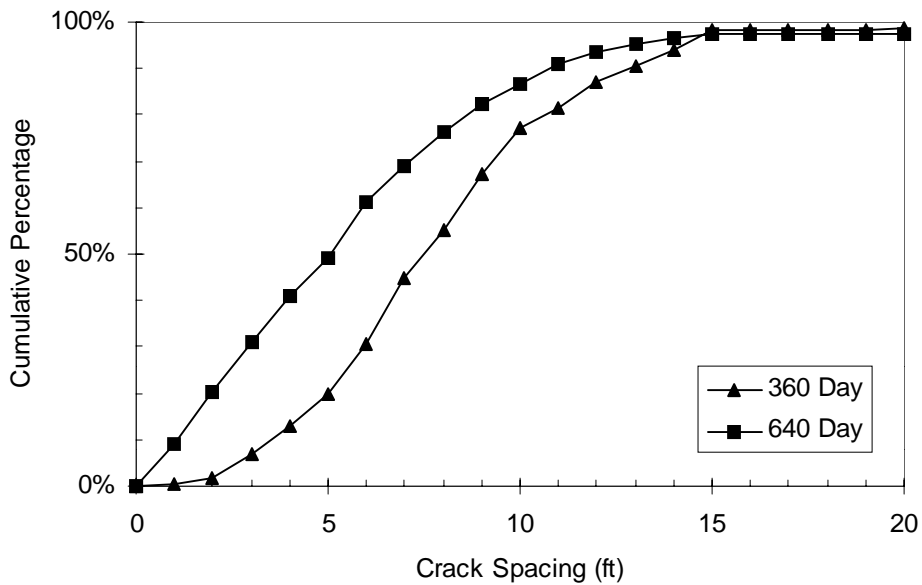


Figure A44 Crack formation over time for Project 8 - Section 21W (LS, Summer, 0.52% Steel)

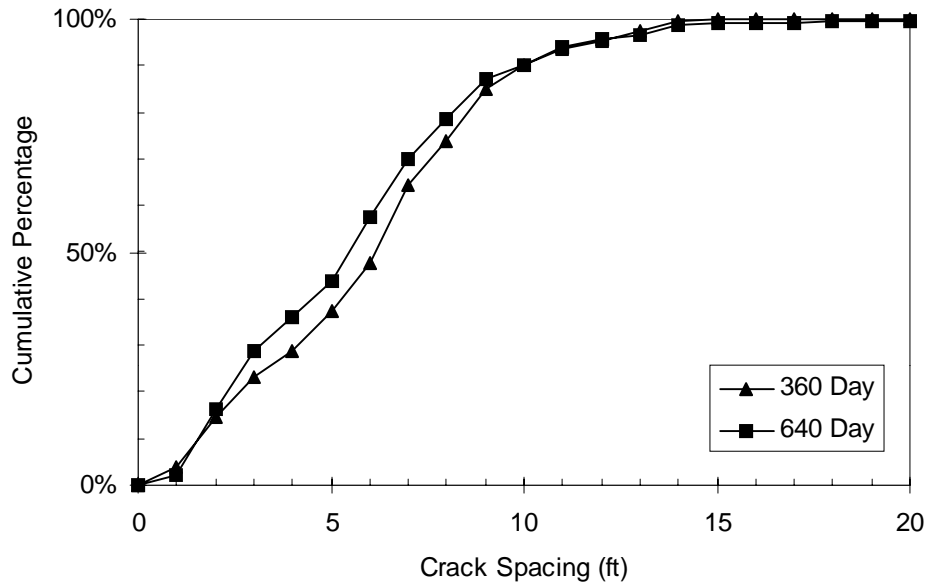


Figure A45 Crack formation over time for Project 8 - Section 22W (LS, Summer, 0.52% Steel)

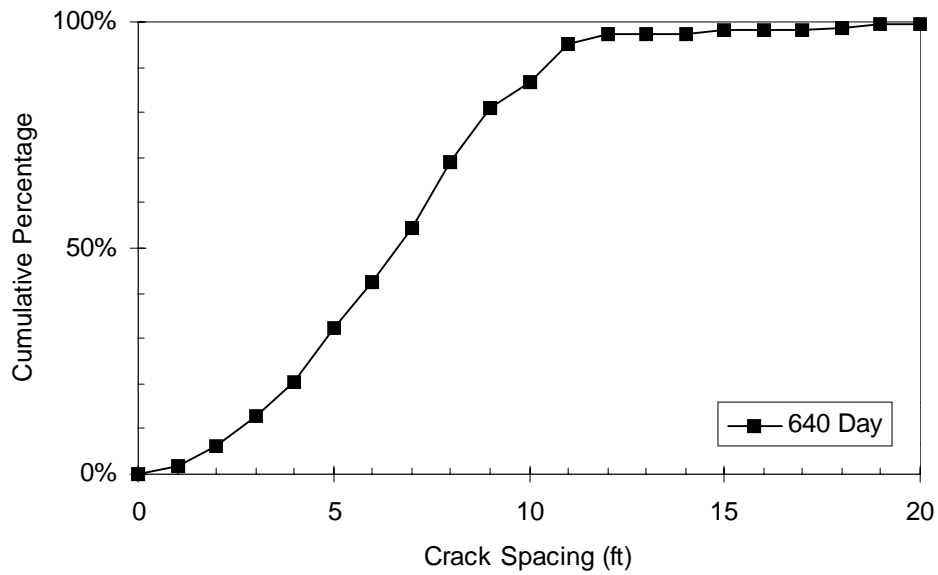


Figure A46 Crack formation over time for Project 8 - Section 23W (LS, Summer, 0.52% Steel)

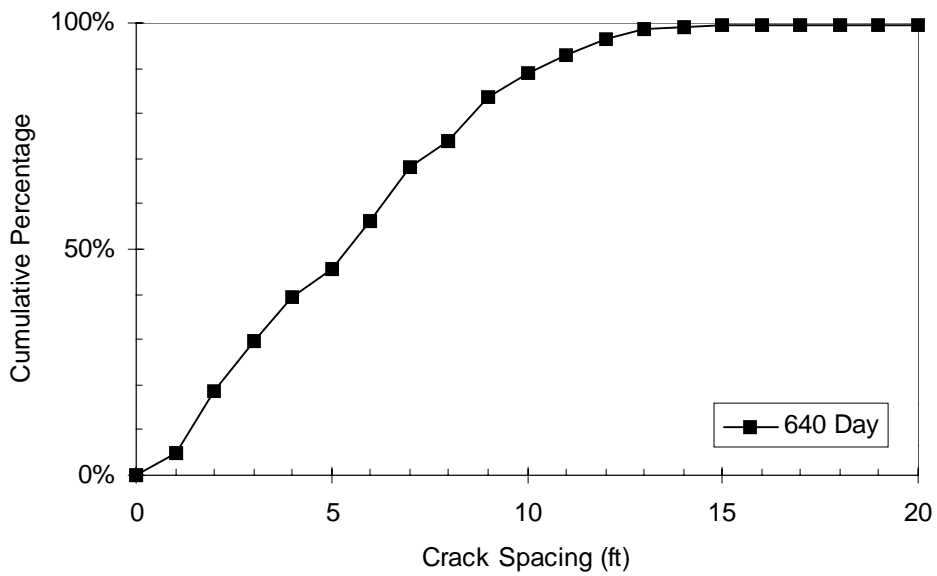


Figure A47 Crack formation over time for Project 8 - Section 24W (LS, Summer, 0.52% Steel)

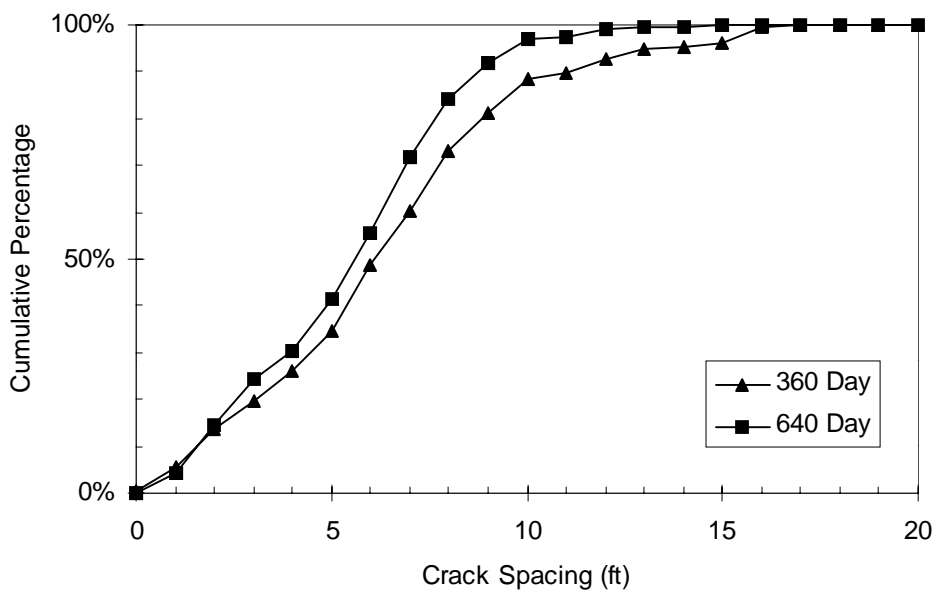


Figure A48 Crack formation over time for Project 8 - Section 25W (LS, Summer, 0.52% Steel)

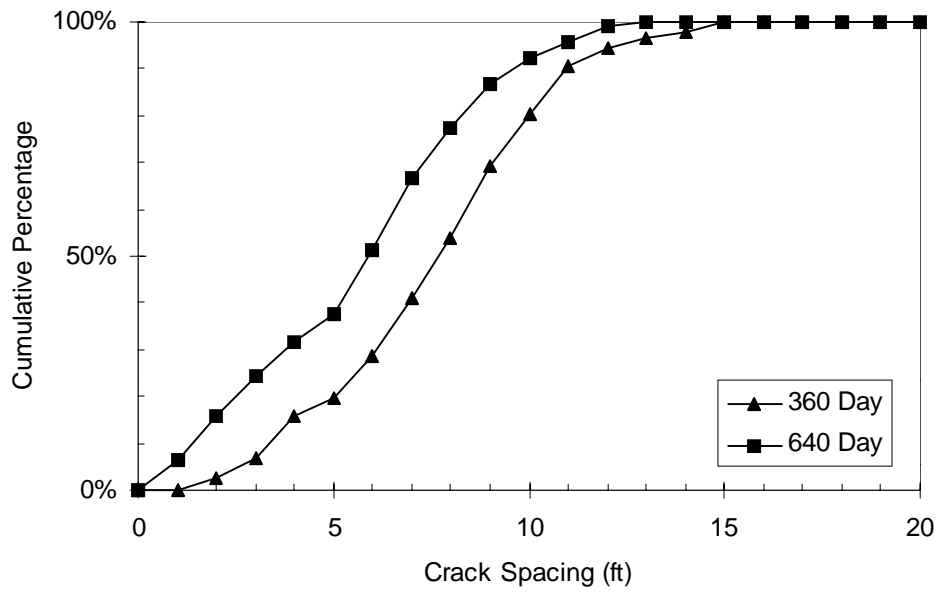


Figure A49 Crack formation over time for Project 8 - Section 26W (LS, Summer, 0.52% Steel)

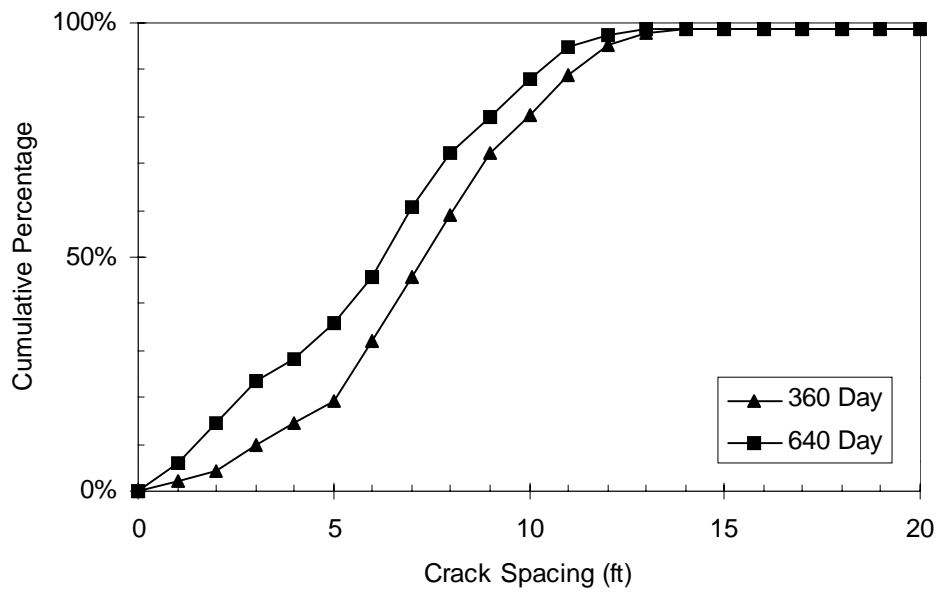


Figure A50 Crack formation over time for Project 8 - Section 27W (LS, Summer, 0.52% Steel)

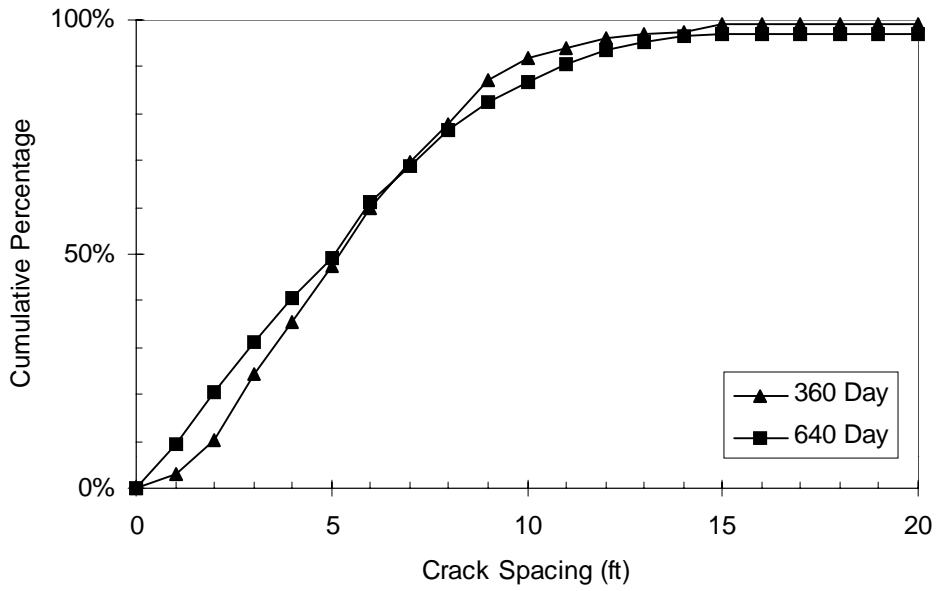


Figure A51 Crack formation over time for Project 8 - Section 28W (LS, Summer, 0.59% Steel)

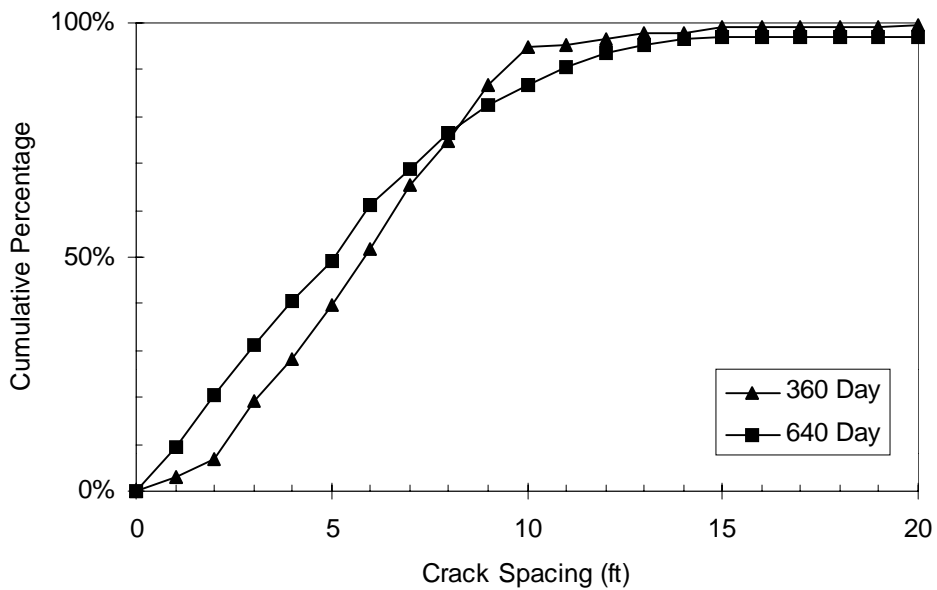


Figure A52 Crack formation over time for Project 8 - Section 29W (LS, Summer, 0.59% Steel)

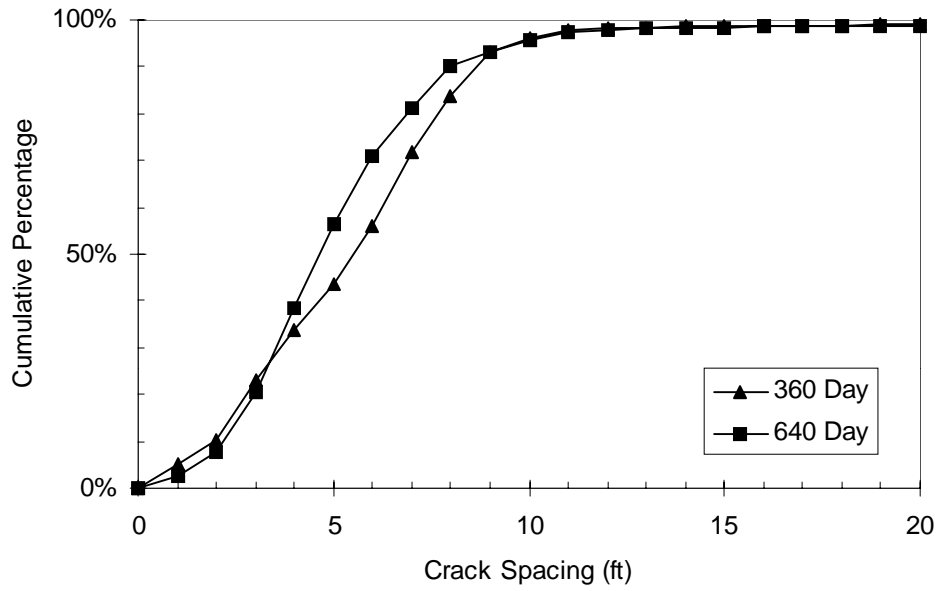


Figure A53 Crack formation over time for Project 8 - Section 30W (LS, Summer, 0.59% Steel)

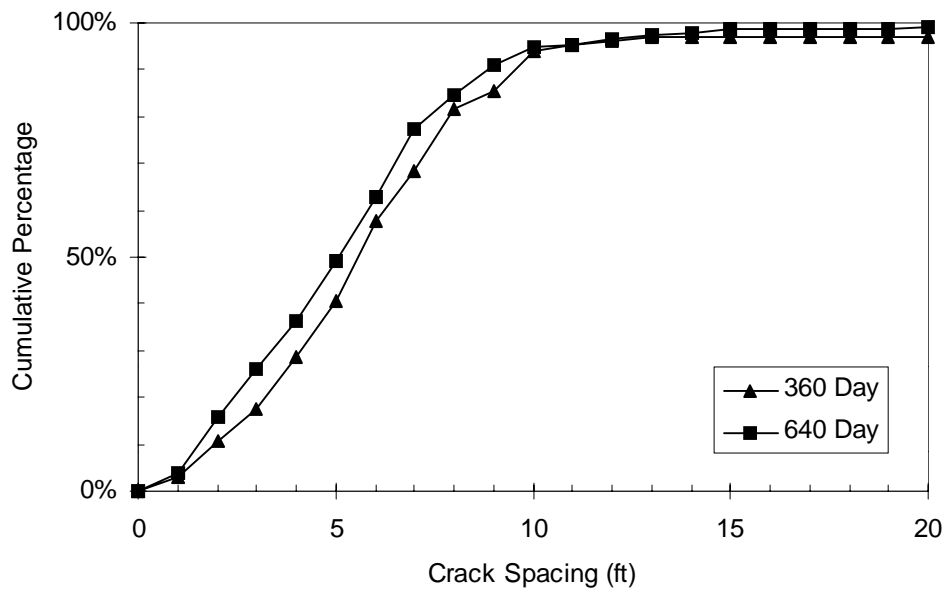


Figure A54 Crack formation over time for Project 8 - Section 31W (LS, Summer, 0.59% Steel)

APPENDIX B

Comparison of Crack Distribution for Test Sections with Variable Steel Percentage for

Projects 1–4

- Project 1 — SH6 at Patterson**
- Project 2 — SH6 at Huffmeister**
- Project 3 — BW8**
- Project 4 — IH 45**

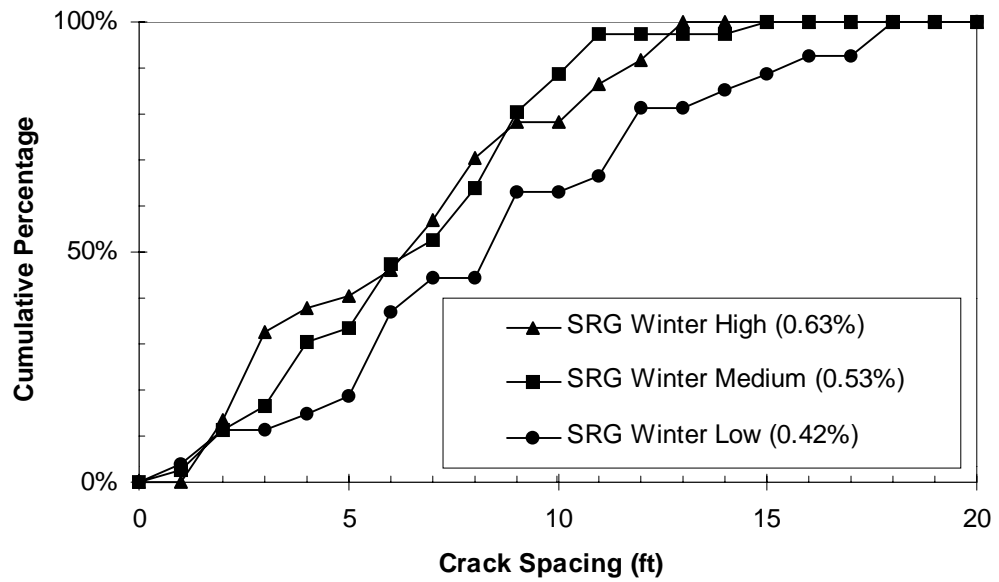


Figure B1 Comparison of cumulative crack distributions with different steel percentages Project 1 (2300 Day)

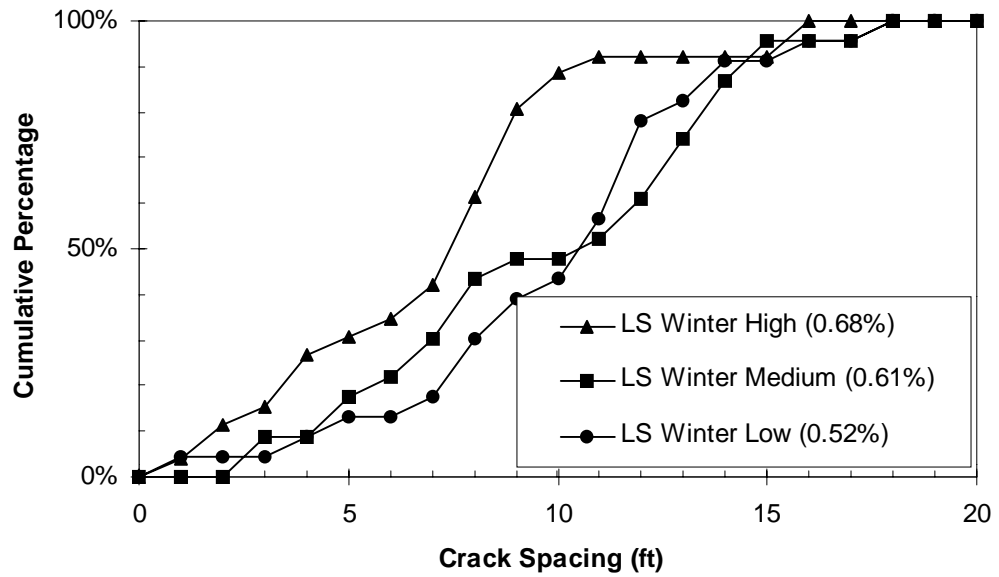


Figure B2 Comparison of cumulative crack distributions with different steel percentages for Project 1 (2300 Day)

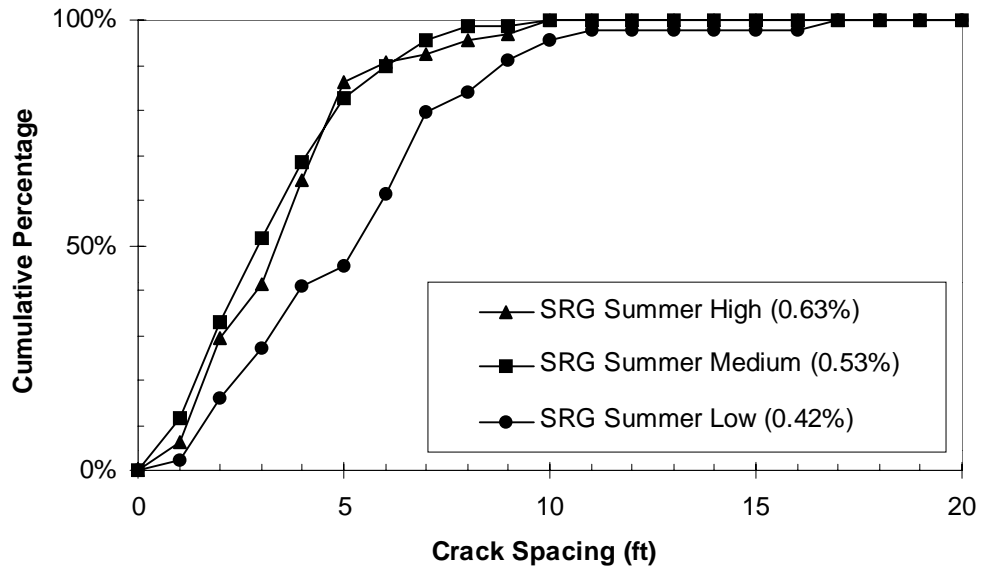


Figure B3 Comparison of cumulative crack distributions with different steel percentages for Project 2 (2500 Day)

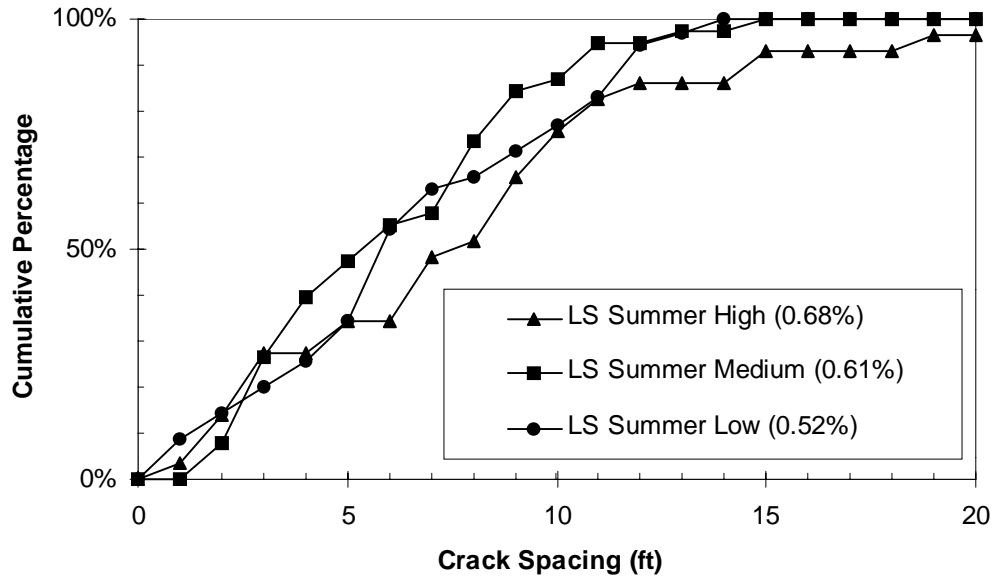


Figure B4 Comparison of cumulative crack distributions with different steel percentages for Project 2 (2500 Day)

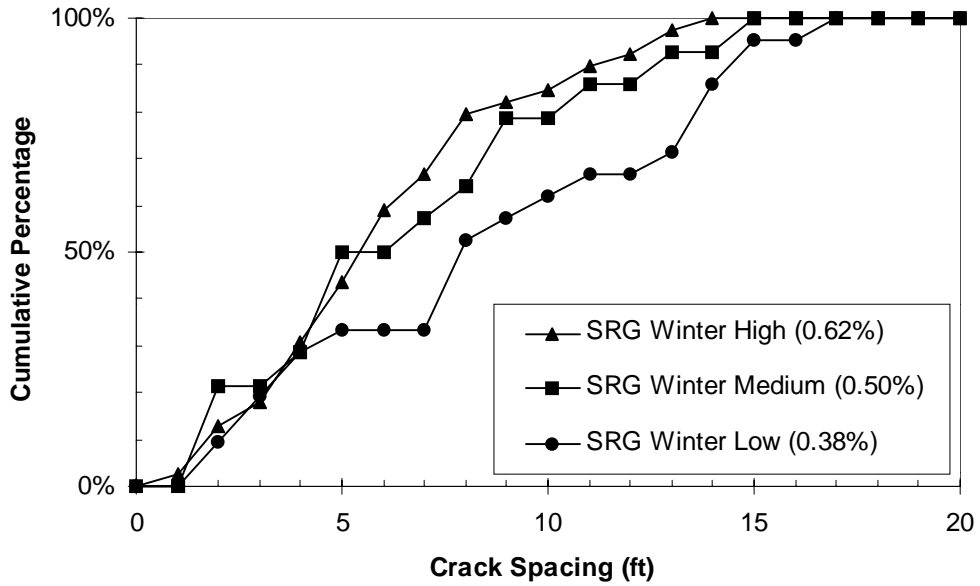


Figure B5 Comparison of cumulative crack distributions with different steel percentages for Project 3 (2400 Day)

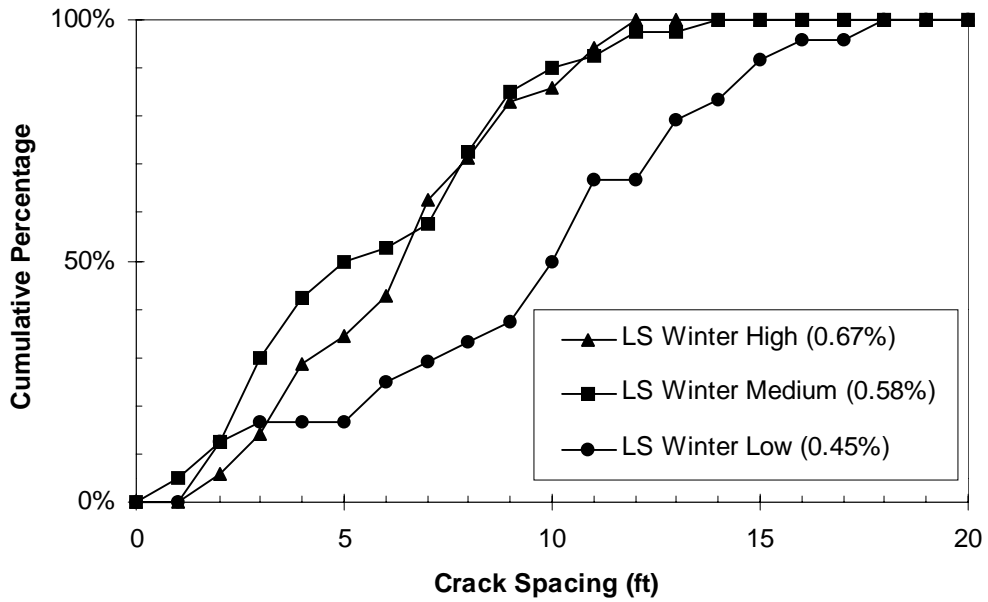


Figure B6 Comparison of cumulative crack distributions with different steel percentages for Project 3 (2400 Day)

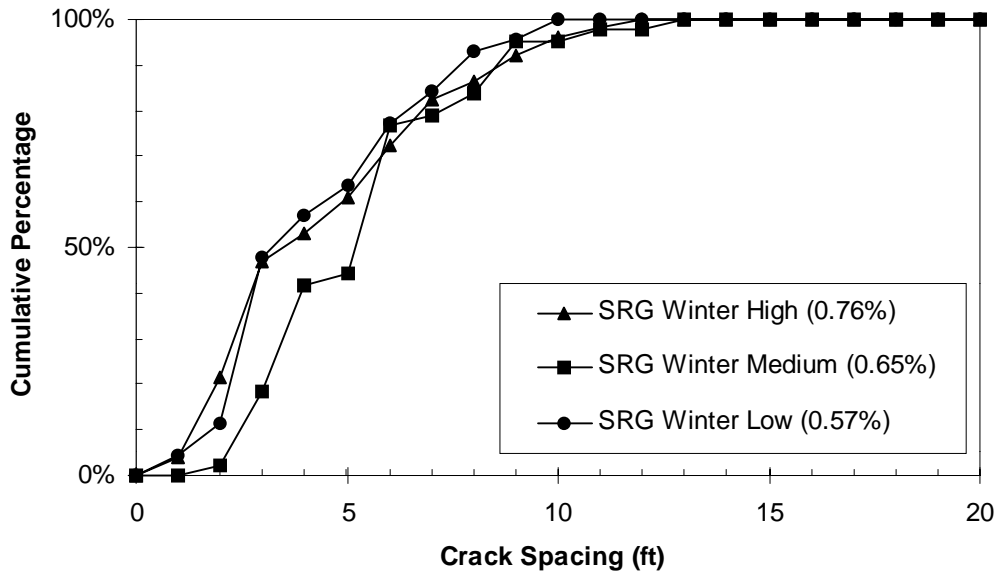


Figure B7 Comparison of cumulative crack distributions with different steel percentages for Project 4 (2300 Day)

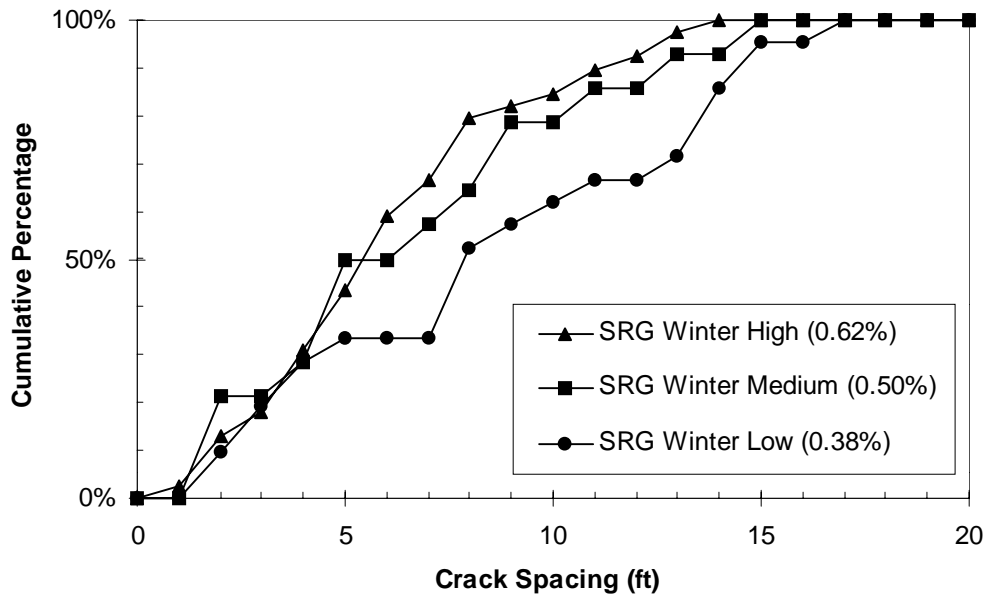


Figure B8 Comparison of cumulative crack distributions with different steel percentages for Project 4 (2300 Day)

APPENDIX C

Comparison of Crack Distribution for Test Sections with Varied Reinforcement Bars Diameters for Projects 1–4

**Project 1 — SH6 at Patterson
Project 2 — SH6 at Huffmeister
Project 3 — BW8
Project 4 — IH 45**

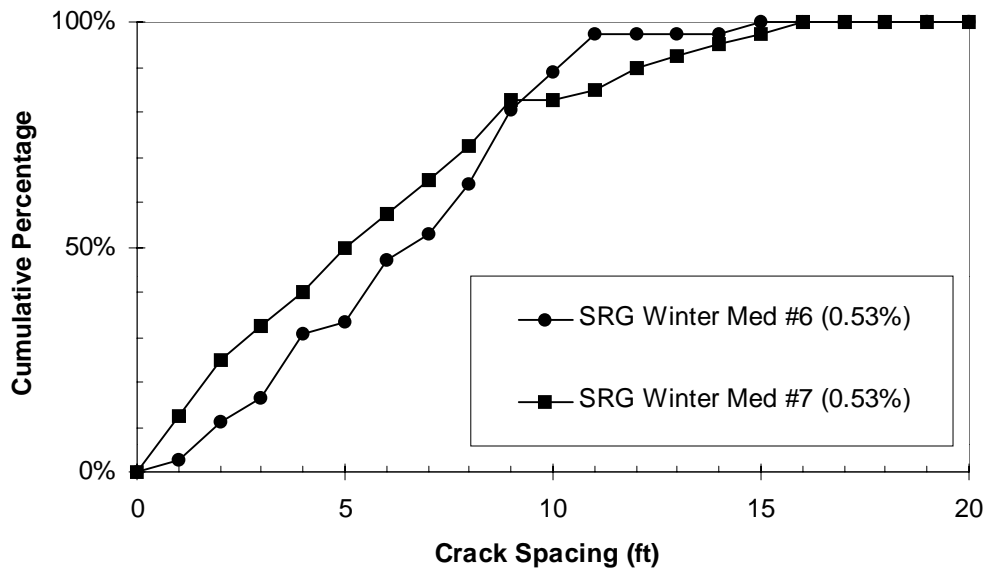


Figure C1 Comparison of cumulative crack distributions with different reinforcement bar diameters for Project 1 (2300 Day)

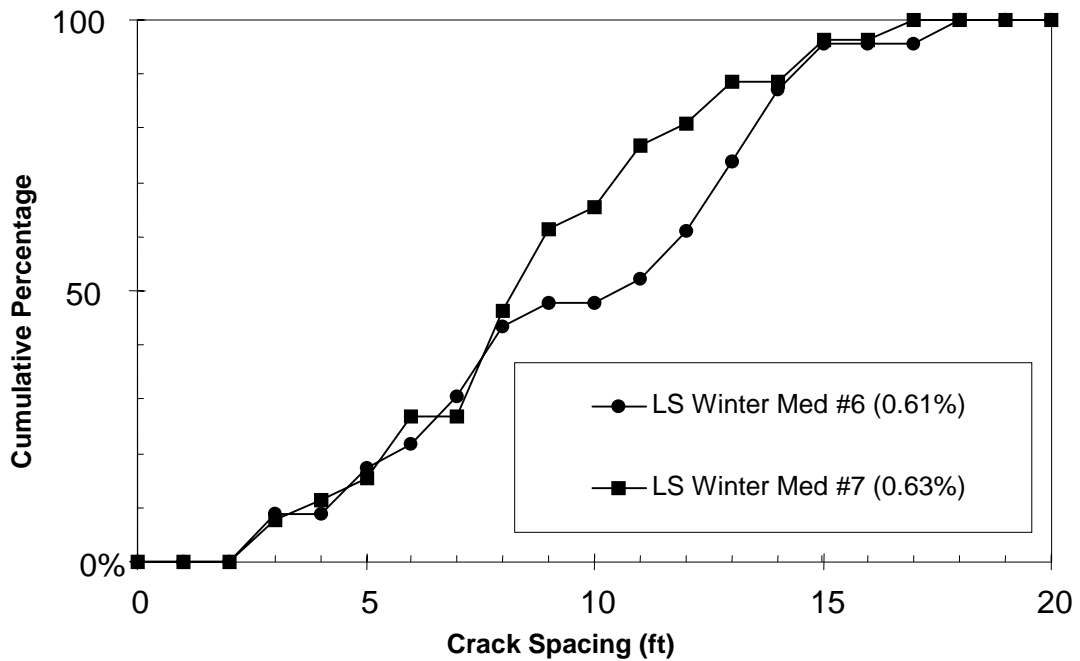


Figure C2 Comparison of cumulative crack distributions with different reinforcement bar diameters for Project 1 (2300 Day)

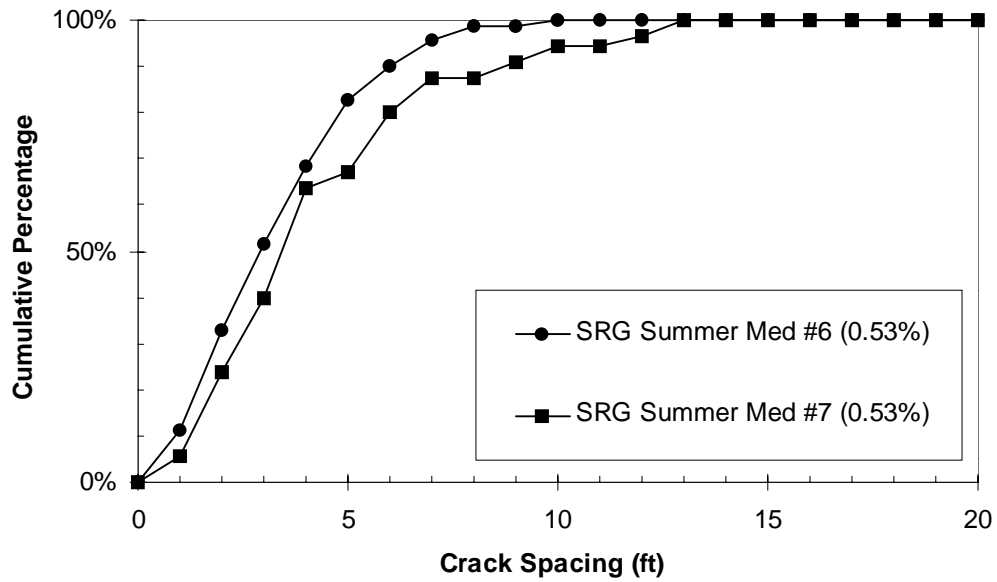


Figure C3 Comparison of cumulative crack distributions with different reinforcement bar diameters for Project 2 (2500 Day)

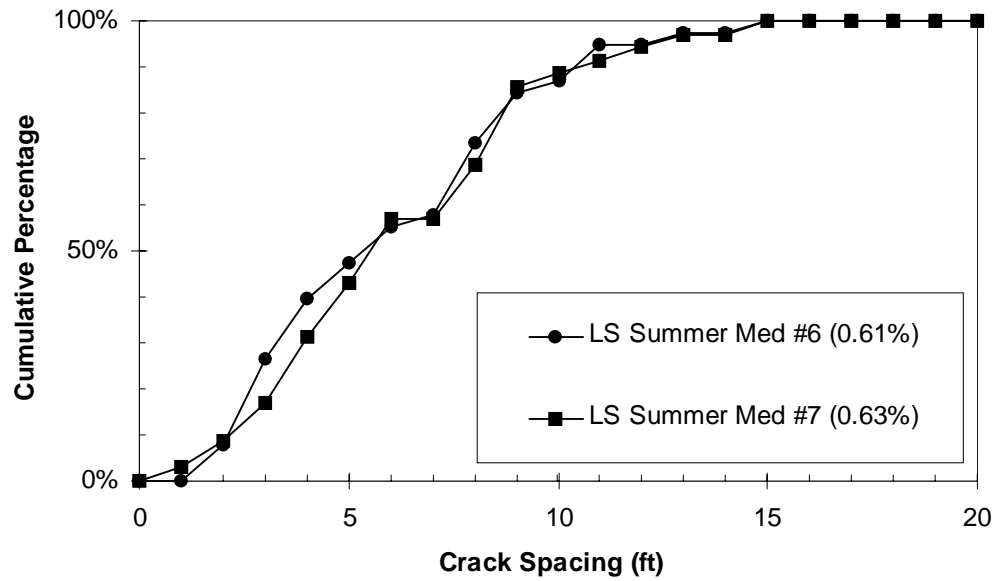


Figure C4 Comparison of cumulative crack distributions with different reinforcement bar diameters for Project 2 (2500 Day)

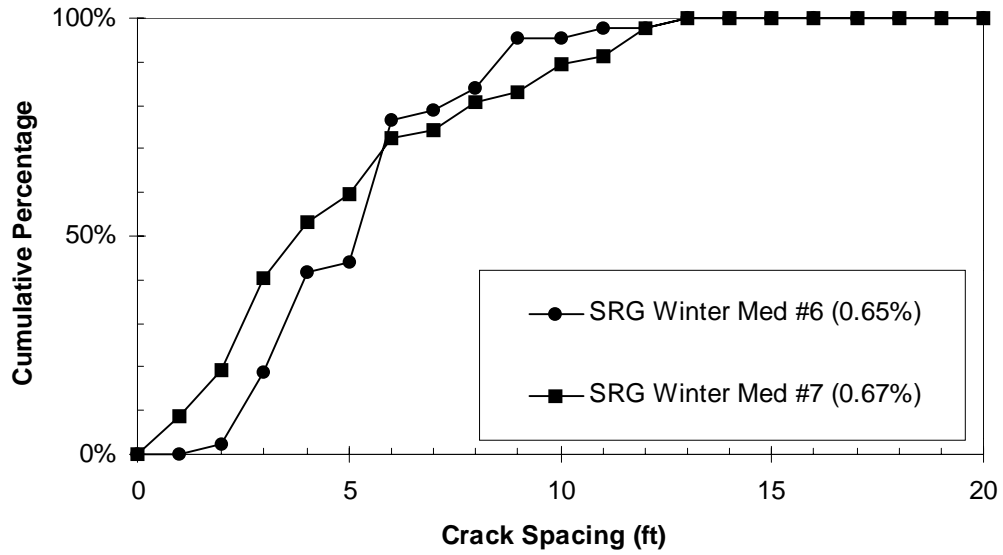


Figure C5 Comparison of cumulative crack distributions with different reinforcement bar diameters for Project 3 (2400 Day)

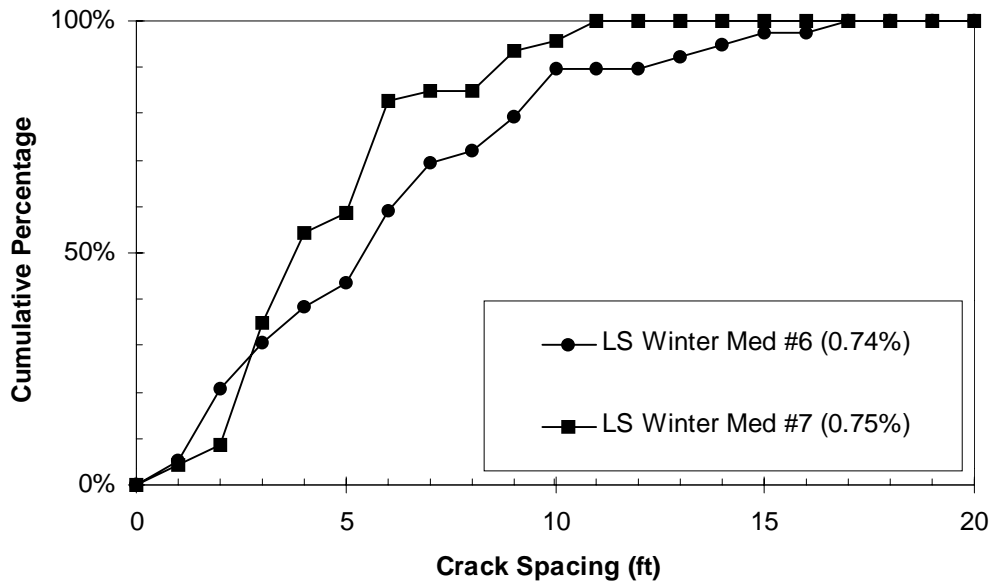


Figure C6 Comparison of cumulative crack distributions with different reinforcement bar diameters for Project 3 (2400 Day)

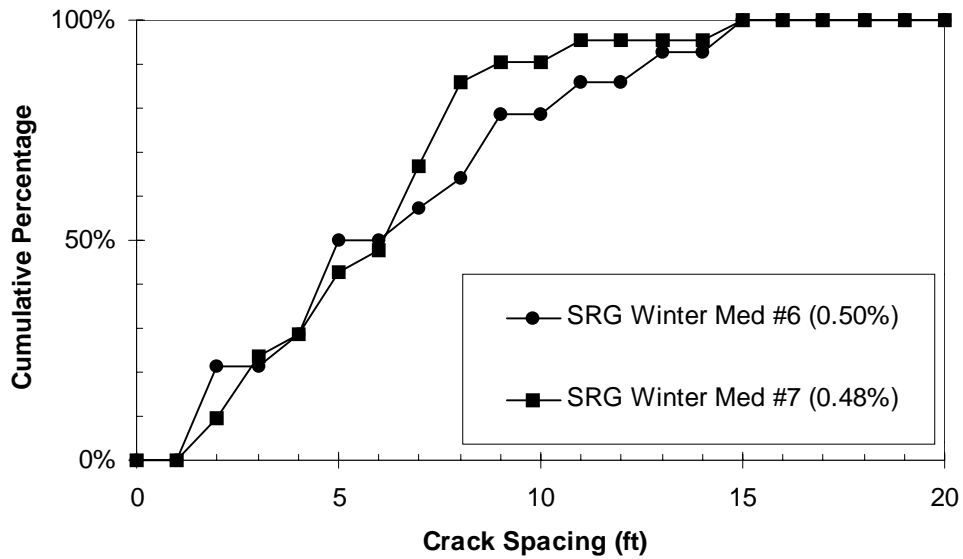


Figure C7 Comparison of cumulative crack distributions with different reinforcement bar diameters for Project 4 (2300 Day)

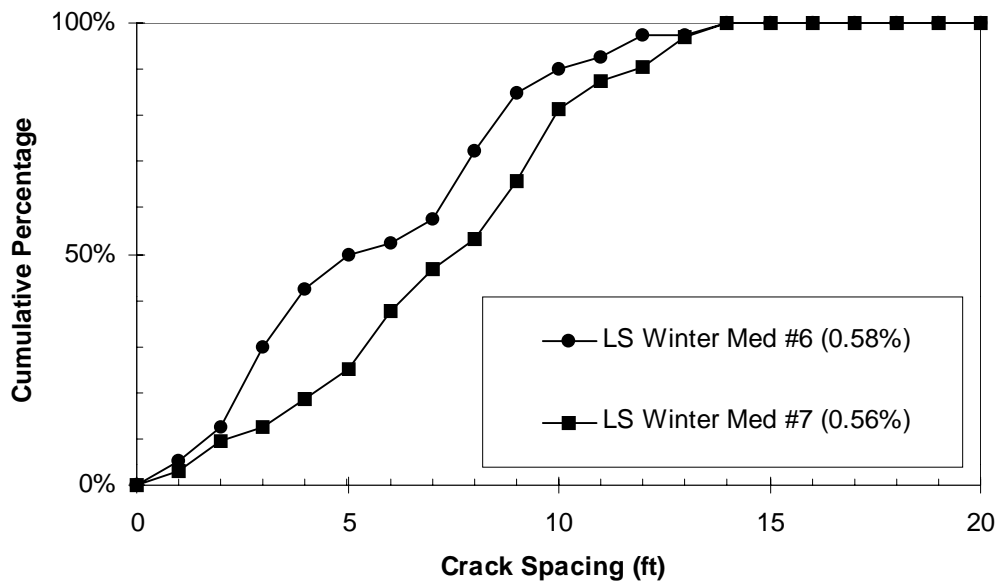


Figure C8 Comparison of cumulative crack distributions with different reinforcement bar diameters for Project 4 (2300 Day)

APPENDIX D

Comparison of Crack Distribution for Test Sections with Different Placement Seasons:

Projects 1-4

- Project 1 — SH6 at Patterson**
- Project 2 — SH6 at Huffmeister**
- Project 3 — BW8**
- Project 4 — IH 45**

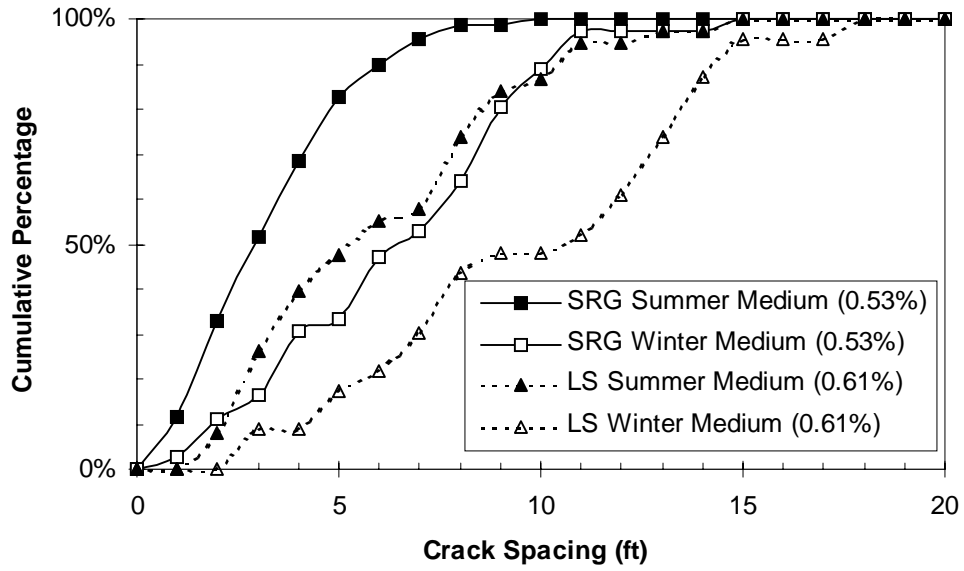


Figure D1 Comparison of cumulative crack distributions for sections placed in the winter and summer (2300 - 2400 Day)

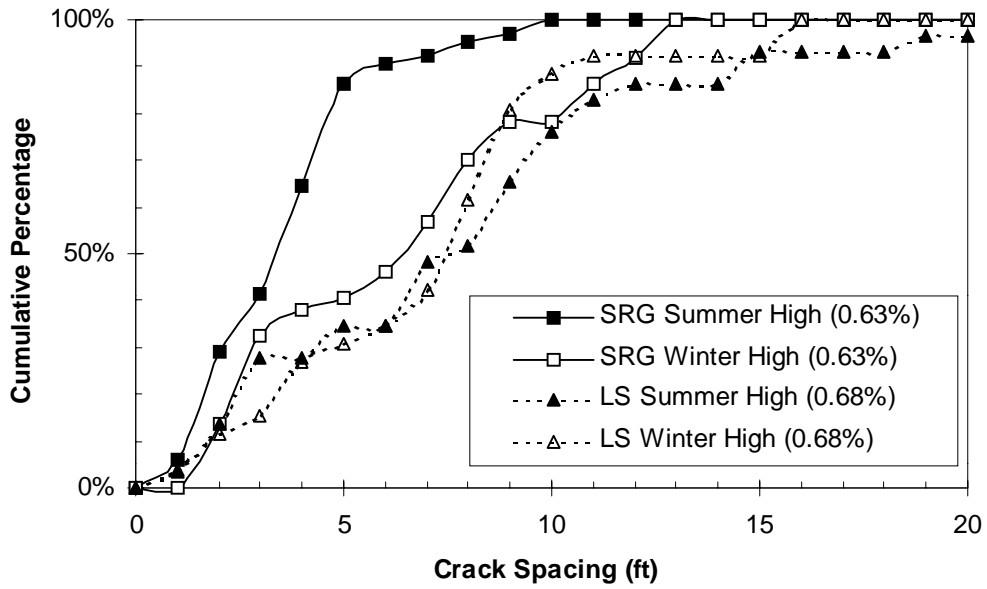


Figure D2 Comparison of cumulative crack distributions for sections placed in the winter and summer (2300 - 2400 Day)

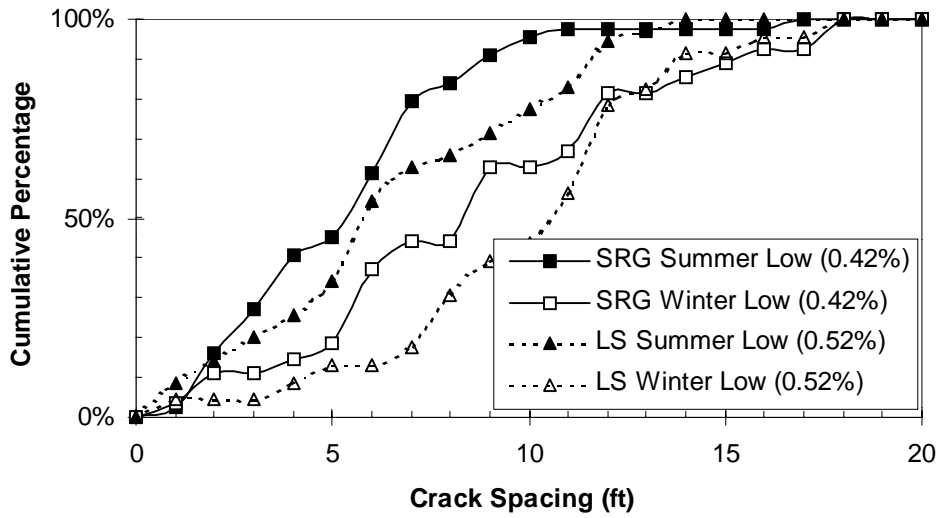


Figure D3 Comparison of cumulative crack distributions for sections placed in the winter and summer (2300 - 2400 Day)

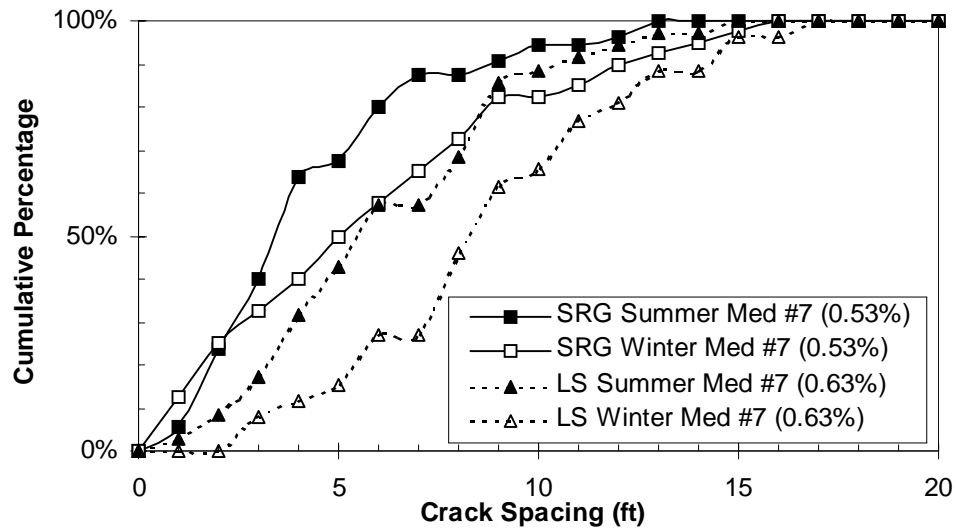


Figure D4 Comparison of cumulative crack distributions for sections placed in the winter and summer (2300 - 2400 Day)

APPENDIX E

Mechanistic Evaluation of Spalling Distress

INTRODUCTION

Spalling, a form of concrete pavement distress is defined as the breakdown of the joint of a slab within 6 in. (15 cm) of the joint or crack, with such distress occurring at both longitudinal and transverse joints. It has been suggested that this distress is exacerbated by excessive compressive stresses at the joint or crack face resulting from infiltration of incompressible or slab bending under traffic loading (Refs 23, 24)*. Most performance models for spalling have been empirical in nature and, consequently, have been devoid of any semblance of a distress mechanism. Recently, efforts have been underway at Texas A&M University to formulate mechanistic spalling models derived from the processes related to spall development.

Extensive field studies in Texas have led to the establishment of a spalling mechanism consisting of a step-by-step process that can be characterized through engineering mechanics. Recent findings have indicated that spalling is the result of damage initiated in the form of a delamination that is oriented parallel to and at various depths below the surface of the pavement. Conditions necessary for formation of the delaminations include low interfacial strength between the aggregate and mortar, and ambient conditions that cause sufficient moisture evaporation from the pavement resulting in differential drying shrinkage near the pavement surface. Temperature variation is also a factor in the development of high stresses close to the pavement surface, although such stresses are not as large as the stresses resulting from moisture variation (unless large temperature drops occur). Delaminations have been noted to initiate early in the life of the pavement and, once formed, extend later into spalls as a result of incompressible, freeze-thaw cycles, and traffic loading, to name a few factors.

In this chapter, delamination formation and subsequent spalling development are investigated in light of fracture mechanics. Stresses resulting from temperature and moisture variation are considered within the scope of the formation of the delamination fracturing. Tensile and shear stresses are determined numerically based on finite element analysis using simulated pavement moisture data. A finite element program is developed to allow for a

* References appear at the end of this appendix.

variety of input of temperature and moisture values through the slab thickness. When the stresses are found to be sufficiently large to form the delaminations, a fracture mechanics analysis of the crack evolution based on the cohesive zone model (Ref 25) is undertaken.

BACKGROUND

Spalling is a concrete pavement distress in which pieces of concrete are dislodged from the surface of the pavement, as illustrated in Figure E1. This distress, which can impair ride quality, is a consequence of delaminations formed during the early life of concrete pavement, primarily as a result of moisture loss from the pavement slab to the environment, depending on ambient and curing conditions. High tensile and shear stresses develop prior to traffic opening, given that the pavement is restrained from moving. Therefore, stresses caused by temperature and moisture variation require further analysis for their potential to surpass the early concrete strength, causing crack development in the zones of higher stress levels. Significant spalling is unlikely to occur when the delaminations are not formed. In the event that they are formed, their extension into spalling appears to be by fatigue owing primarily to wheel loads and to temperature fluctuations.



Figure E1 Typical spalling of a pavement

STRESSES CAUSED BY TEMPERATURE VARIATION

The so-called curling stresses or thermal stresses in concrete pavements, caused by pavement expansion and contraction, occur only because pavements are typically restrained by friction, slab weight, and/or tied adjoining lanes. These stresses vary with the temperature distribution across the slab thickness. The simpler approach to model temperature distribution in a slab is to assume the temperature varies linearly from the top to the bottom of the slab. Stresses induced by a linear temperature gradient have been analyzed by Westergaard and Bradbury (Refs 35, 20). The actual distribution of temperature in a concrete slab has been found to be highly nonlinear (Refs 23, 27). Sophisticated models for the prediction of temperature distribution in a concrete slab that considers both ambient conditions and chemical reactions associated with the hydration of portland concrete cement has been developed.

Yang (Ref 34) developed a numerical model for the prediction of concrete temperature that utilizes the general differential equation for heat transfer in two dimensions, assuming constant thermal conductivities, k_x and k_y :

$$k_x \frac{d^2 T}{dx^2} + k_y \frac{d^2 T}{dy^2} + Q_h(t, T) = \rho C_p \frac{dT}{dt} \quad (\text{E.1})$$

where C_p and ρ are the concrete's specific heat and density, respectively, and Q_h is the generated heat from the hydration of cement. The thermal diffusivity (D), given by the ratio of thermal conductivity to the product between specific heat and density ($k_x/[C_p \rho]$ and $k_y/[C_p \rho]$), has a low value in concrete that results in slow temperature changes. This slow temperature change is the reason stresses caused by temperature variation is of significant magnitude only in the presence of large temperature drops. The generated heat from hydration of cement (Q_h) can be determined from laboratory measurements. It can also be obtained empirically from the concentrations of cement components, particularly the tricalcium silicate (C_3S) and tricalcium aluminate (C_3A). Yang's model also considers environmental conditions by accounting for the heat energy transferred between the concrete surface and the environment through convection, irradiation, and solar absorption.

Figure E2(a) shows a typical temperature variation in a concrete pavement slab. Note that in the two-dimensional space, the temperature distribution is assumed independent of x and a function of the distance from the slab surface only, i.e., $T(x_1, y) = T(x_2, y)$.

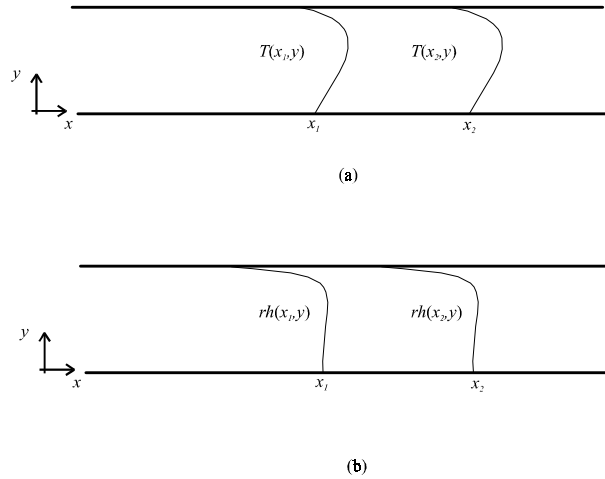


Figure E2 Typical temperature variation in a concrete pavement slab

In order to predict stresses caused by temperature variation in concrete pavements, this study utilizes temperature distributions as they vary with the slab distance from the surface and time since placement. Since the cement hydration process in concrete is a function of time, any prediction of stresses owing to temperature variation caused by hydration should be given as a function of time. To obtain the stresses resulting from a nonlinear temperature distribution, one can use the approach discussed by Mohamed and Hansen, in which an equivalent linear temperature gradient is used as input to the existing closed-form solutions by Westergaard and Bradbury.

Another approach, which was taken in the present investigation, was to evaluate the stresses owing to nonlinear temperature distribution numerically with the finite element method. The stress-strain relation is given by the Hooke's law as $\{\sigma\} = [C] \{\epsilon_e\}$, which can also be written in its inverted form as $\{\epsilon_e\} = [C]^{-1} \{\sigma\} = [D] \{\sigma\}$. The subscript e on ϵ indicates elastic deformation. The matrices $[C]$ and $[D]$ represent the material stiffness matrix and the material flexibility matrix, respectively. For homogeneous and isotropic materials, only two coefficients, Young's modulus E and Poisson's ratio ν , are necessary to express all

coefficients in Hooke's law. Nonuniform temperature distributions affect the above stress-strain relation.

In the case in which initial strains exist, the total strain in an elastic solid is described by a mechanical component, dependent on the stress state, plus the initial strain. The total strain is given in the form:

$$\{\boldsymbol{\varepsilon}\} = \{\boldsymbol{\varepsilon}_e\} + \{\boldsymbol{\varepsilon}_o\} = [D]\{\boldsymbol{\sigma}\} + \{\boldsymbol{\varepsilon}_o\} \quad (\text{E.2})$$

where $\{\boldsymbol{\varepsilon}_o\}$ is the vector of initial strain. When there is thermal expansion (or contraction), Equation E.2 is valid if $\{\boldsymbol{\varepsilon}_o\}$ is replaced by the thermal strain vector, which is given in two dimensions by $\{\boldsymbol{\varepsilon}_x, \boldsymbol{\varepsilon}_y, \boldsymbol{\gamma}_{xy}\}^T = \{\alpha(T-T_o), \alpha(T-T_o), 0\}^T$ for plane stress and $\{\alpha_t(1+\nu)(T-T_o), \alpha_t(1+\nu)(T-T_o), 0\}^T$ for plane strain, α_t being the coefficient of thermal expansion, T the material temperature as a function of the x - y coordinates, and T_o a reference temperature for the unstrained state of the solid (that can be taken as the temperature of concrete at final setting time). The superscript T above indicates the transpose of a row vector, i.e., a column vector. Noting again that $[C]=[D]^{-1}$, the total stresses in the solid including thermal effects is obtained from Equation E.2 as:

$$\{\boldsymbol{\sigma}\} = [C]\{\boldsymbol{\varepsilon}_e\} - [C]\{\boldsymbol{\varepsilon}_o\} \quad (\text{E.3})$$

Thermal effects are incorporated in DELAM, a finite element code developed in this study for analyzing stresses in concrete pavements resulting from temperature effects. Assuming the temperature distribution to vary in space only vertically across the slab thickness as indicated in Figure E2(a), once the distribution is obtained by field data or prediction models such as the one by Yang (1996), the temperature variation ($T-T_o$) can be input in the program for each element row in a finite element mesh of a pavement slab.

STRESSES CAUSED BY MOISTURE VARIATION

Stresses caused by moisture variation are often overlooked in the stress analysis of concrete pavements. Field data on moisture measurements across a concrete pavement slab have shown that the drying process occurs vertically with a nonlinear profile (Buch and Zollinger 1993). A typical relative humidity (rh) profile for a pavement slab is shown in

Figure E2(b). Note that the relative humidity distribution is assumed independent of x and a function of the distance from the slab surface only, i.e., $rh(x_1, y) = rh(x_2, y)$. The representation of moisture distribution across a slab may require sophisticated finite element or finite difference models. Zollinger et al. (1993) provided a simplified approach in which a linear moisture distribution was assumed at the top portion of the slab above an arbitrary depth, H , while a constant moisture distribution was assumed below H .

Moisture quantities in concrete have been determined from direct measurements using specially prepared dewpoint sensors. The diffusion of moisture through the concrete is faster at early ages and slower in later ages (i.e., when the concrete has hardened). The present study utilizes an available model that predicts relative humidity in a concrete pavement based on ambient conditions and on material-related moisture properties (permeability, diffusivity, slope of moisture isotherm). These properties, along with laboratory tests to determine them, are discussed by McCullough et al. (1994).

Once the relative humidity in a concrete pavement slab is obtained, a concrete shrinkage model can be used to predict strains caused by drying shrinkage. According to this model, concrete shrinkage is described by the following function:

$$\varepsilon^{sh} = \varepsilon^{sh\infty} (1 - rh^3) \quad (E.4)$$

where rh is the relative humidity in the concrete, and $\varepsilon^{sh\infty}$ (microstrain) is the ultimate concrete shrinkage at the reference rh of 50% and is considered a material property. Such a property can be calculated from concrete mixture quantities according to the following formulation:

$$z = 0.381\sqrt{f'_{28}} \left[1.25 \left(\frac{a}{c} \right)^{1/2} + 0.5 \left(\frac{g}{s} \right)^2 \left\{ \frac{1 + \frac{s}{c}}{\frac{w}{c}} \right\}^{1/3} \right] - 12 \quad (E.5)$$

where

- a/c = total aggregate/cement ratio,
- g/s = coarse aggregate/fine aggregate ratio,
- s/c = fine aggregate/cement ratio,
- w/c = water/cement ratio, and
- f'_{28} = 28-day cylinder compressive strength (psi).

It should be clear that, as in the case for temperature, the moisture (relative humidity) in concrete and consequent shrinkage stresses vary as concrete ages. Therefore, any prediction of shrinkage stresses needs to be performed as a function of time.

STRESSES CAUSED BY COMBINED TEMPERATURE AND MOISTURE VARIATION

In order to account for the combined effect of stresses caused by both temperature and moisture variation, Equation E.3 can be used with a total initial strain vector $\{\epsilon_0\}$ caused by both thermal and shrinkage strains. From Equation E.5, the shrinkage strains are given by the relative humidity at various distances below the slab surface. These strains can be transformed to an equivalent thermal strain caused by a temperature variation in such a way that $\epsilon^{sh}_{\infty} = \alpha_t dT$. Adding the equivalent dT to the actual temperature variation $(T-T_0)$ responsible for the thermal stresses, one obtains a final temperature variation DT that can be interpreted as responsible for the combined effect of both thermal and shrinkage strains. This combined effect can be conveniently implemented in a finite element program using a single strain vector $\{\epsilon_x, \epsilon_y, \gamma_{xy}\}^T = \{\alpha_t(DT), \alpha_t(DT), 0\}^T$ or $\{\alpha_t(1+\nu)(DT), \alpha_t(1+\nu)(DT), 0\}^T$ for plane strain or plane stress, respectively. This approach is used in this investigation.

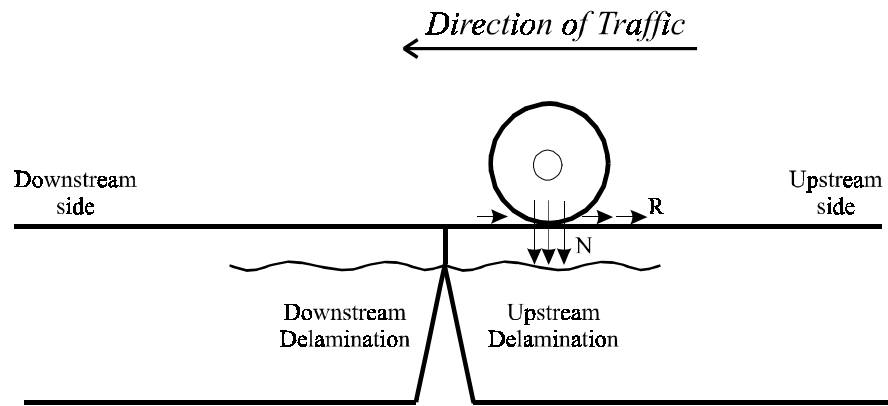
In summary, this study makes use of available prediction models of temperature and moisture (relative humidity) distribution in time across a concrete pavement slab. The combined thermal and shrinkage strain profile is assumed to vary with time and with distance from the slab surface, and to be constant in the horizontal plane. The stresses caused by combined temperature and moisture variation are obtained from two-dimensional finite element calculations (with the program DELAM) by entering an equivalent temperature

variation DT for each element row across the slab depth for different times. This process is elaborated on later.

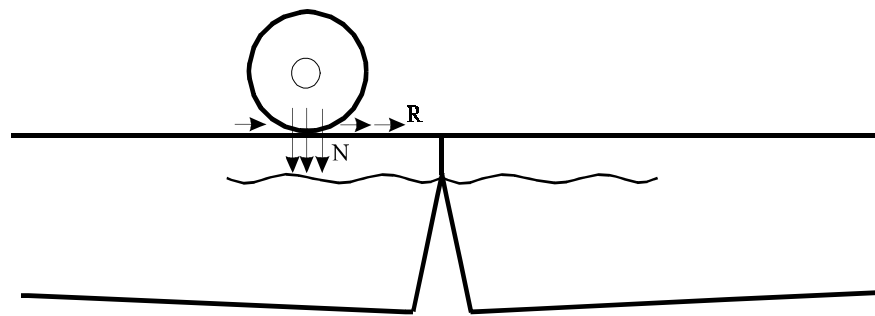
SPALLING MECHANISM

Recently, field studies in Texas have led to the establishment of a mechanism for the spalling distress characterized through engineering mechanics. Spalling development consists of a step-by-step process (Ref 24). The three steps discussed next are: (1) delamination formation, (2) delamination extension, and (3) spall development.

Delaminations are cracks oriented parallel to the surface of the pavement that have been noted to initiate early in the pavement life and to be principally located at the transverse crack, as shown in Figure E3. These cracks typically occur in depths 1 to 3 in. (25 to 75 mm) from the surface (Ref 24). Longer delaminations are observed closer to the pavement surface. At a depth of 1 in. (25 mm), delaminations as long as 5 in. (125 mm) can be found, while at a depth of 3 in. (75 mm), delaminations on the order of 1 in. (25 mm) in length are more likely. Lengths of delaminations have been observed to depend on pavement age.



(a)



(b)

Figure E3 Delamination formation in pavements

DELAMINATION FORMATION

Senadheera (Ref 24) points out two primary factors for the formation of delaminations: (1) weak interfacial bonding between aggregate and mortar, and (2) bleeding of the concrete, which is defined as the settlement of solids and expulsion of water within fresh concrete (Ref 17). The debonding cracks between aggregates and mortar eventually bridge together forming a longer delamination. Aggregate size and mineralogy are believed to affect the interfacial resistance to cracking. The mortar-aggregate interfacial toughness can be evaluated by a new test procedure developed in this project. Bleeding, which affects

concrete strength, is more pronounced in spherical and siliceous aggregates (Ref 26). The negative effect of bleeding water on concrete strength suggests that the concrete close to the pavement surface may have a lower strength than that found elsewhere.

Besides mortar-aggregate interfacial debonding and bleeding of concrete, the analysis performed in this project indicates that high shear and tensile stresses develop close to the surface of a concrete pavement slab. Once debonding has initiated, it may grow in various ways in the presence of load-induced stresses. The energy available from thermal and shrinkage forces to open a delamination is much greater near the slab surface, since this is where greater moisture variation is found to occur, as illustrated in Figure E2(b). Therefore, even if small debonding cracks are assumed at different pavement depths, they are more likely to become large delaminations near the pavement surface where most of the moisture loss in concrete occurs.

FRACTURE ENERGY APPROACH TO DELAMINATION EXTENSION

An approach to determine the extension of the delamination in fatigue is based on the cohesive zone model (Ref 25). Since the formulation presented for this model couples the normal (opening) and tangential (shearing) behavior through the nondimensional parameter λ , mixed mode fracture can be considered. One advantage of this approach is that no remeshing is necessary in finite element calculations.

To analyze the direction of delamination extension, one can determine the fracture energy for different directions, as illustrated in Figure E4. The analysis can assume different wheel load positions. It is important to note that delamination extension depends on several factors: One factor is the existence of other flaws as the delamination grows in such a way that crack bridging or kinking may occur; another is the presence of aggregates or abnormal porous zones in the crack growth path. These factors play a critical role in determining the direction of crack growth. Since they cannot all be accounted for, it is assumed that the crack grows in the direction of the largest fracture energy caused by wheel loads.

No work is performed on the crack surfaces, since they are stress-free zones. The work of fracture (or fracture energy) is therefore equivalent to the energy absorbed in the region near the crack tip (cohesive zone). For a given delamination length, if the fracture energy resulting from wheel loads is higher for the upward direction in Figure E4, it can be

assumed that for several load repetitions the crack extends in that direction. It is important to note that a single wheel load pass creates only a very small fracture energy — much less than the critical fracture energy of the concrete. Therefore, unstable crack propagation is not likely to occur. It is stressed again that delamination extension is a fatigue process. The accumulation of load repetitions causes the crack to grow.

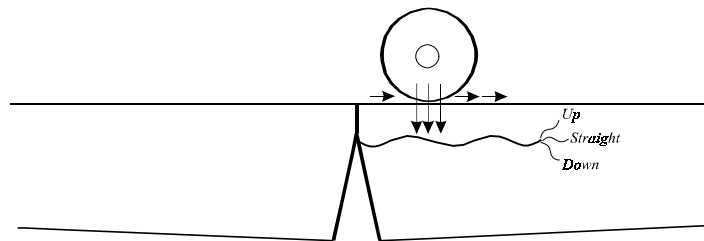


Figure E4 Fracture energy for different directions

SPALLING DEVELOPMENT CAUSED BY FATIGUE

In order to model numerically delamination extension caused by fatigue, the properties of the cohesive zone (CZ) need to change with the number of wheel load repetitions so as to simulate a decrease in resistance to crack propagation. Two options can be considered: (1) to decrease the maximum concrete tensile strength f_t and (2) to increase the maximum opening displacement w_c . For the first option, Mindess and Young (Ref 17) indicate that at 107 cycles the concrete strength (in compression, tension, and flexure) is approximately 55% of the static strength. For the second option, Xu (Ref 21) concluded from a fatigue study that the size of the fracture process zone is greatly enlarged by cyclic loading. A multiplication factor of 10 for the fracture process zone size growth fitted the fatigue data well. Given that the critical opening displacement is proportional to the fracture process zone

(Ref 28), it is assumed that w_c grows to $10w_c$ with an increasing number of load repetitions. Since crack opening occurs prior to strength failure, the decrease in tensile strength of concrete specimens reported by Mindess and Young (Ref 17) is likely to be due to an increase in the maximum crack opening displacement, and not the other way around. Therefore, the second option is preferred.

CONSIDERATIONS FOR NUMERICAL SIMULATION OF SPALLING DEVELOPMENT

To simulate numerically the spalling development owing to fatigue by changing the cohesive zone properties as discussed above, one needs to determine the number of wheel load repetitions necessary for a delamination to grow into a spall. This requires calibration from field performance data that makes the numerical prediction phenomenological in nature. In a finite element code, the requirement is translated into the number of runs (and respective time increments) necessary before the delamination grows into a spall. This leads to restrictions related to computation time. Given that the model is phenomenological, one approach is to consider a minimum desired number of runs, associating each run with a certain number of wheel load repetitions. This approach taken in this study uses the finite element code FATIGUE developed to analyze delamination extension. This program utilizes the cohesive zone elements implemented in the program SADISTIC, developed by Allen (Ref 29).

Once the numerical simulation is performed, it is necessary to translate the information obtained in such a way that it can be used as a concrete pavement analysis tool. The amount of spalling used as a criterion in mechanistic concrete pavement design procedures may be given as: (1) a percentage of spalled pavement sections in relation to the total number of pavement sections surveyed, or (2) the number of spalls per mile of pavement. Thus, a model needs to relate delamination extension into a spall to the amount of spalls (percentage or number) developed in a concrete pavement given a certain amount of load repetitions.

The approach taken in this investigation is to assume the growth of the percentage of spalls to be proportional to the growth of the delamination. A critical delamination length is assumed (a_f). As the delamination length, a , grows from zero to a_f with the number of wheel

load repetitions, the spalled/surveyed sections ratio is assumed to grow from 0% to 100%. This is equivalent to the damage ratio (D_r) typically used in pavement design schemes (Ref 23). This number, which ranges from 0 to 1, is the ratio between predicted and allowable number of repetitions.

In the numerical simulation of spalling development, each run corresponds only to a single wheel load repetition. Therefore, the delamination length a does not grow to the critical value a_f unless the cohesive zone properties are changed in such a way that it is no longer active (equivalent to a break in the cohesive zone elements). This approach is not appealing, since it is equivalent to assuming a priori the a/a_f curve that circumvents the objective of this effort. Instead, the approach taken is to assume that the ratio a/a_f is directly proportional to the ratio of the fracture energy created by a single wheel load to the critical fracture energy, G/G_F . The fracture energy owing to a wheel load is constant in time, while the critical fracture energy increases in time owing to the increasing fracture process zone size.

SPALLING MODEL

By simulating how a delamination grows with wheel load repetitions, one can obtain the necessary input for a mechanistic design, i.e., the percentage of spalled sections. In order to obtain this input, the approach discussed next is proposed.

- (2) The objective is to translate a curve of delamination extension (a/a_f) with load repetitions to a curve of percentage of spalled sections with load repetitions. Mathematically, a mapping is required from a function $f(x)$ to a function $g(x)$, where $f(x)$ is the function corresponding to a/a_f , and $g(x)$ is the function corresponding to the percentage of spalled sections. The variable x represents the number of load repetitions.

Both $f(x)$ and $g(x)$ are continuous functions, as shown in Figure E5(a)–(b), where $f_i(x)$ and $g_i(x)$ are schematically illustrated for three different delamination lengths (indicated by the subscript i). It is important to note that $f_i(0)$ is not zero for the cases where an initial delamination (a_0) is considered [$f_2(0)$ and $f_3(0) \neq 0$]. On the other hand, $g_i(0)$ is always zero. Therefore, special attention is required when considering an initial delamination length, i.e., $f_i(0) \neq 0$. In this case, even though the delamination has a nonzero initial length a_0 , no growth has occurred owing to fatigue. Therefore, the corresponding initial percentage of spalled sections, $g_i(0)$, should still have a zero value. It should be obvious from Figure E5(a) that higher

$f_i(0)$ values lead to higher $f_i(x)$ values for each x . Moreover, longer initial delamination lengths (higher $f_i[0]$) causes a/a_f to increase at a large rate, which means the curve $f_i(x)$ is smoother (has less curvature) than $f_2(x)$, which is smoother than $f_3(x)$.

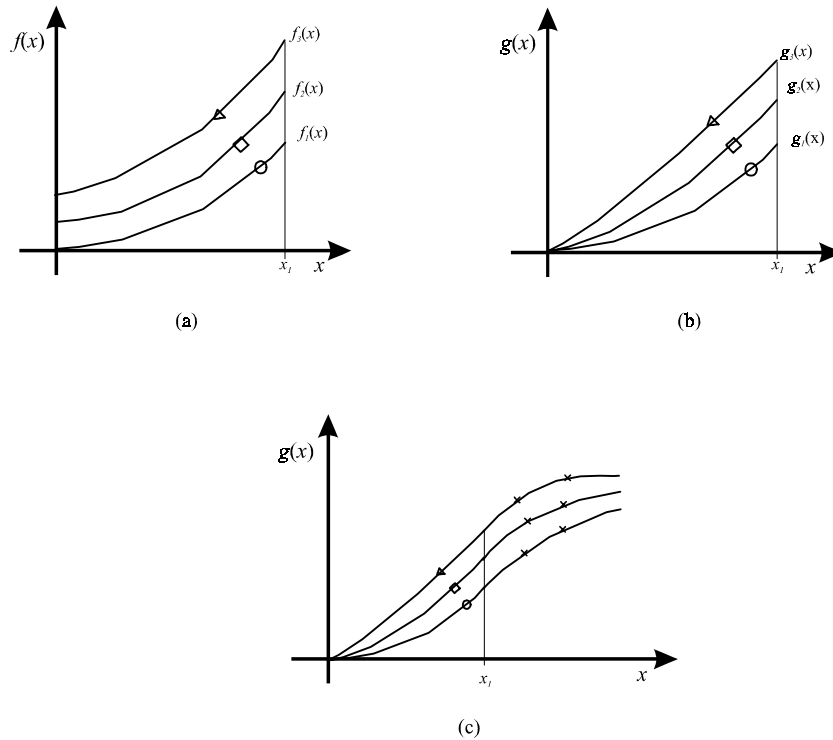


Figure E5 Delamination growth through wheel load repetitions

(2) Assumptions of the model:

- The number of load repetitions corresponding to spall development is equal to the number of load repetitions to extend a delamination (x in both situations).
- For each delamination depth, the percentage of spalled sections is linearly proportional to the delamination extension, i.e., $g_i(x) = A_i x f_i(x) + B_i$, where the subscript i indicates different initial delamination lengths.

(3) B_i is determined from the boundary condition $g_i(x = 0) = 0$, which means that the percentage of spalled sections for zero load repetitions is zero.

Therefore, $B_i = -A_i x f_i(0)$. The equation above reduces to:

$$g_i(x) = A_i x [f_i(x) - f_i(0)] \quad (\text{E.6})$$

From Equation E.6, $g_i(x)$ can be determined for x values (load repetitions) for which $f_i(x)$ was numerically determined ($x \leq x_1$), and where x_1 is the maximum number of load repetitions assumed in the numerical determination of $f_i(x)$ (see Figures E5 [a] – [b]).

- (4) To obtain $g_i(x)$ for $x \geq x_1$, field performance data of the percentage of spalled sections for a certain number of load repetitions should be used, as shown in Figure E5(c). For predictions of the amount of spalling in a pavement, as few as two data points corresponding to $x \geq x_1$ may be gathered from similar pavements at the location where predictions are desired. The following function can then be used to fit the combined numerical ($x \leq x_1$) and performance ($x \geq x_1$) data points:

$$g_i(x) = a_e^{-[(bx)^c]} \quad (\text{E.7})$$

where a , b , c are regression coefficients assumed to be functions of material properties and local weather conditions.

The factors in the model discussed above need to be calibrated with field performance data. An example of the utilization of the model is presented later. Delamination extension can be investigated for different depths that give valuable indication of the percentage of spalled sections when delaminations are found in those respective depths.

ANALYSIS OF SPALLING DEVELOPMENT PROCESS

Next, an analysis of the spalling process is performed, starting with the development of high stresses resulting from nonlinear temperature and moisture profiles. Once it is determined that such stresses are sufficiently large to surpass the early concrete strength and to create delaminations, the potential directions of delamination growth are investigated. Finally, the utilization of a model for spalling development caused by fatigue failure owing to wheel load repetitions is presented.

DELAMINATION FORMATION

A finite element program developed at the Texas Transportation Institute (Ref 34) is used to obtain typical temperature and moisture (relative humidity) profiles for concrete pavement slabs at different times after paving (12 hours, 72 hours, and 120 hours are included in this analysis). This program, which simulates temperature and moisture profiles

at desired time increments for concrete pavements, is always the starting point for the analysis to be presented in the remaining of this chapter. The program can handle different environmental conditions (temperature, relative humidity, and wind velocity obtained from weather stations) and different concrete properties.

Temperature and moisture (*rh*) profiles that can be used in this analysis, as they vary within the pavement slab, are illustrated in Figures E6(a) and E6(b), respectively. A 12 in. (304.8 mm) thick slab is assumed. Both profiles, for all three times analyzed, show greater variation close to the pavement surface. Different temperature profiles are obtained at different times of the day, with the profile shape shown in Figure E6(a) changing accordingly. During certain times of the day, when the temperature is lower closer to the pavement surface, stresses owing to temperature variation may add to the moisture-related stresses (shrinkage stresses). However, as previously mentioned, thermal stresses are high only when large temperature drops occur. The moisture profile was found to always be approximately that of the shape shown in Figure E6(b), since the greater moisture loss is always through the pavement surface. Again, as previously mentioned, the moisture profile is the factor primarily responsible for the high shear and tensile stresses that develop close to the pavement surface. Since the moisture profile has a consistent shape, as illustrated in Figure E.6(b), and since it also has a greater effect on the total stress result of a combination of both thermal and shrinkage strains, only shrinkage stresses are considered in this analysis.

As discussed in the previous section, the finite element program DELAM developed for this investigation uses concrete mixture information (*a/c*, *g/s*, *s/c*, *w/c*, and f'_{28}) and the temperature and relative humidity output from Yang's program; it then combines them to obtain an equivalent temperature differential *DT* responsible for the total strain. If stresses owing to temperature variation are not considered, a zero temperature profile can be output from Yang's program. In a finite element analysis of a pavement slab in two-dimensional space, *DT* is obtained for each element row. This information, along with the concrete properties (i.e., *E*, *v*, and α_t) and their variation in time are used by DELAM to determine the total stresses in the pavement slab as they vary with time. This procedure is outlined in Figure E7.

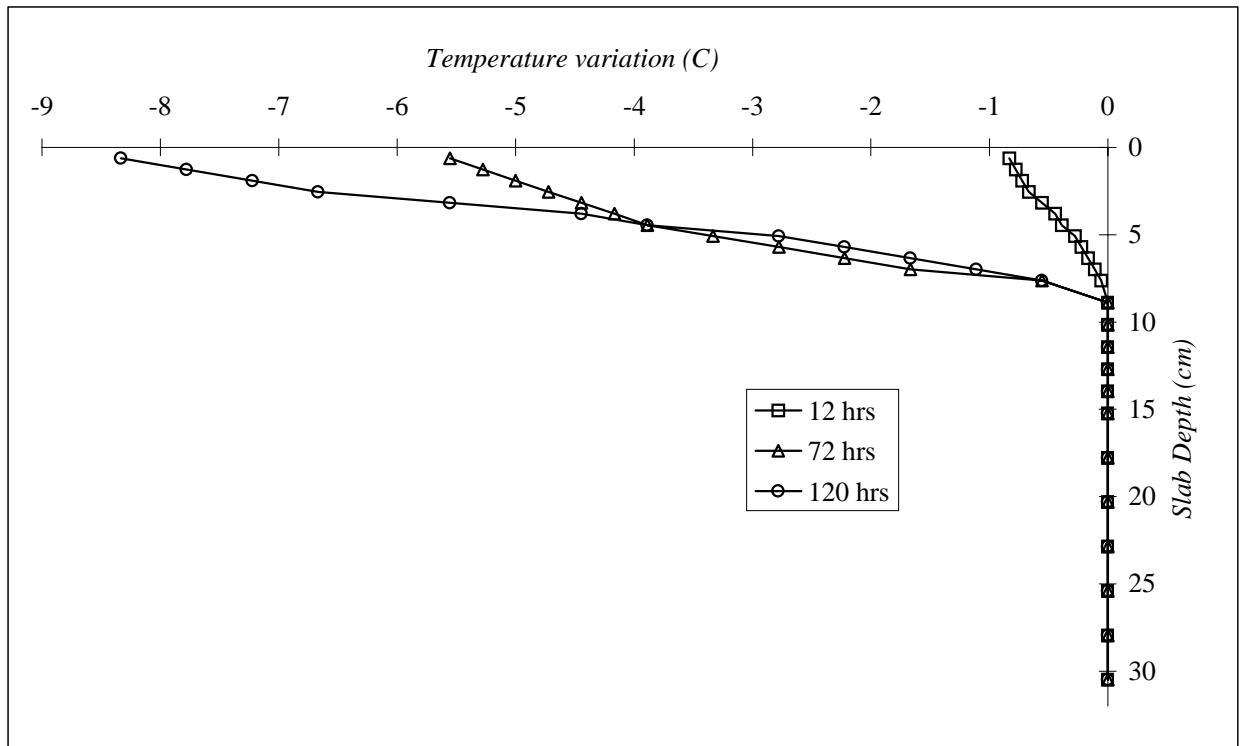


Figure E6(a) Temperature and moisture profiles

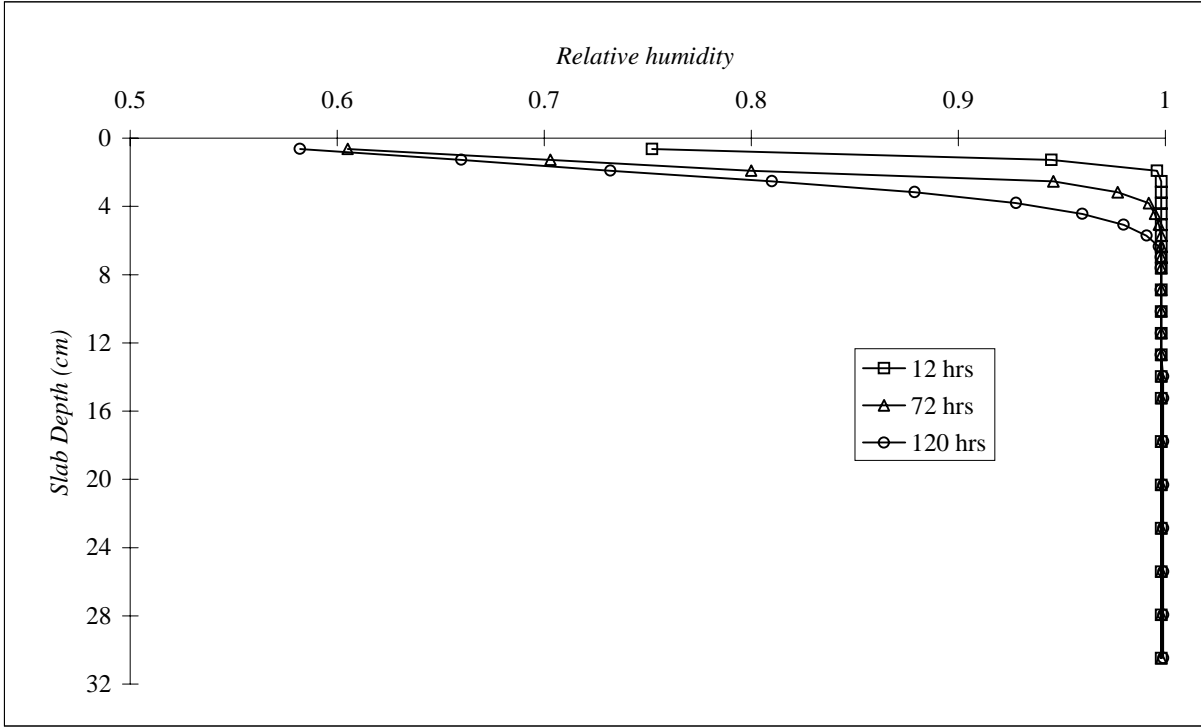


Figure E6(b) Temperature and moisture profiles

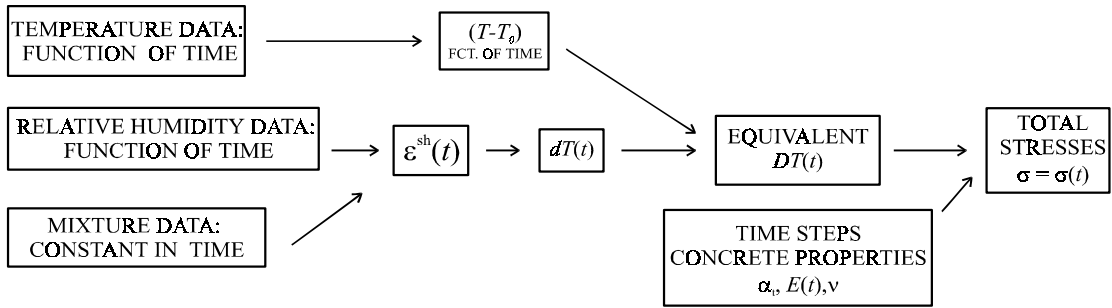


Figure E7 DELAM procedure to determine total stresses

Table E1 indicates the values assumed in this analysis. The coefficient of thermal expansion is typical for concrete using river gravel as the coarse aggregate. Young's modulus $E = E(t)$ is assumed to be 10,345 MPa (1.5×10^6 psi), 15,860 MPa (23×10^6 psi), and 20,690 MPa (3.0×10^6 psi) for 12, 72, and 120 hours, respectively. Note that lower stresses will occur at earlier hours owing to the lower Young's modulus.

Table E1 Input values assumed for stress analysis

Constant Values	
Compressive strength at 28 days (f'_{28})	27.6 MPa
Total aggregate/cement ratio (a/c)	5.56
Coarse aggregate/fine aggregate ratio (g/s)	1.66
Fine aggregate/cement ratio (s/c)	2.09
Water/cement ratio (w/c)	0.42
Poisson's ratio (ν)	0.15
Concrete coefficient of thermal expansion (α_t)	$10.8 \times 10^{-6}/^\circ\text{C}$

$$1 \text{ MPa} = 145 \text{ psi}, T(^{\circ}\text{C}) = [T(\text{F}) - 32] / 1.8$$

The equivalent DT for different slab thicknesses and times is determined from the rh profile in Figure E6(b) and Equation E.5 from the relation $DT = \varepsilon^{sh\infty} / \alpha_t$. The finite element mesh (with 1,200 nodes and 2,286 elements) used for the calculations is shown in Figure E8. A finer mesh is used closer to the pavement slab surface, since that is the region of maximum strain.

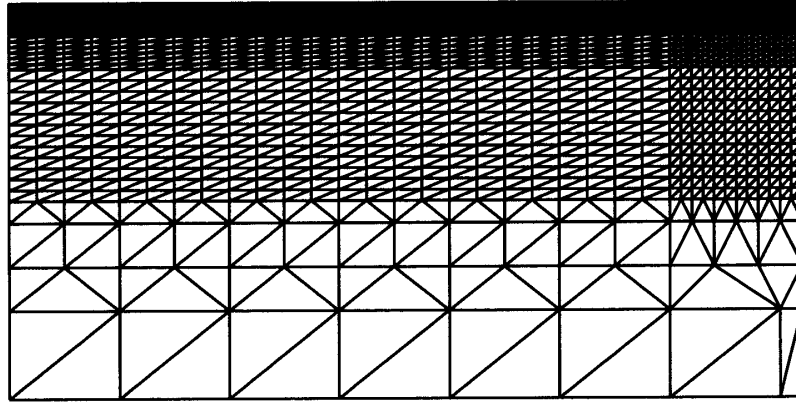


Figure E8 Finite element mesh

Figures E9(a)–(f), which are used for qualitative purposes, give an indication of the location of maximum stresses at the three different times analyzed. Eight-node isoparametric elements were used with the finite element program ABAQUS (Ref 22) to obtain the stress results. The figures present amplified views of tensile (σ_{yy}) and shear stresses (τ_{xy}) near a transverse joint. It is seen that the stresses are symmetric with respect to the joint and are functions of the x - y coordinates. The finer mesh on the top represents the first 3 in. (76.2 mm) of the slab thickness — the zone of highest energy owing to the greatest moisture loss.

Table E.2 presents the times, slab depth ranges where maximum stresses occur, and respective maximum stress values. The maximum tensile stresses are observed close to the joint surface, whereas the maximum shear stresses are approximately 1 in. (25.4 mm) away from the joint, as indicated in Figures E9(a)–(f). It is interesting to observe that, for each time, the maximum tensile stresses are found at the depth at which the relative humidity has a sudden change to 100% and becomes approximately constant, as shown in Figure E.9(b). The maximum shear stresses are at approximately half the depth of the maximum tensile stresses. This is more clearly seen in Figures E10(a)–(b), which contain the variation of σ_{yy} and τ_{xy} , respectively, with slab depth.

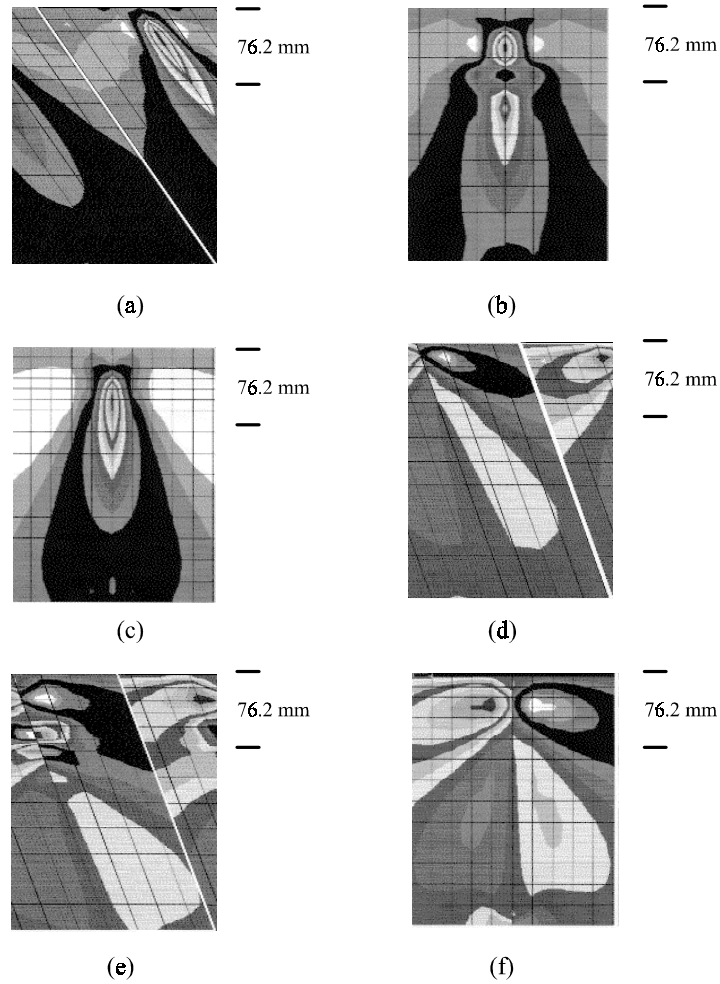


Figure E9(a)-(f) Locations of maximum stresses for the three times analyzed

Table E2 Maximum shear and tensile stresses caused by moisture loss

Time (hours)	Depth of Max or σ_{yy}	σ_{yy} (MPa)	Depth of Max or σ_{yy} (mm)	σ_{yy} (MPa)
12	25.4–38.1	0.38	12.7–19.1	0.59
72	38.1–44.5	1.68	19.1–31.8	1.76
120	57.2–69.9	3.69	25.4–44.5	2.97

1 MPa = 145 psi
1 mm = 0.04 inch

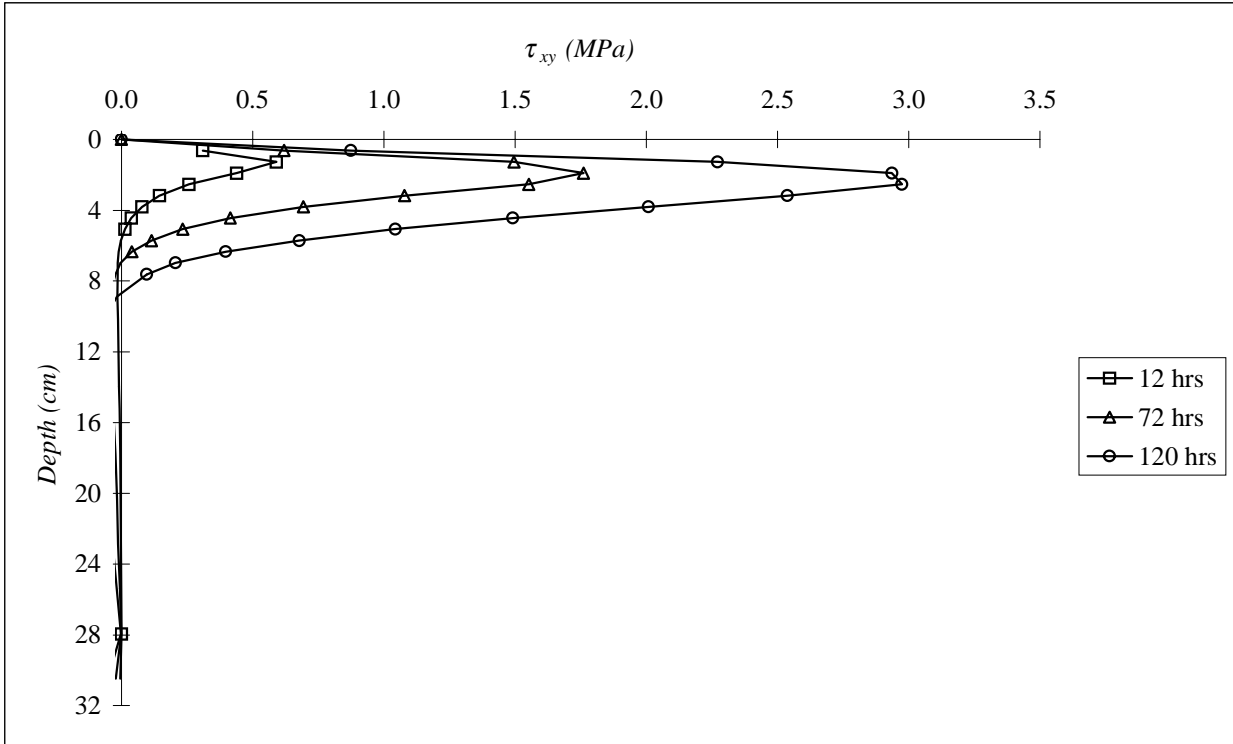


Figure E10(a) Variation of σ_{yy} and τ_{xy} , respectively, with slab depth

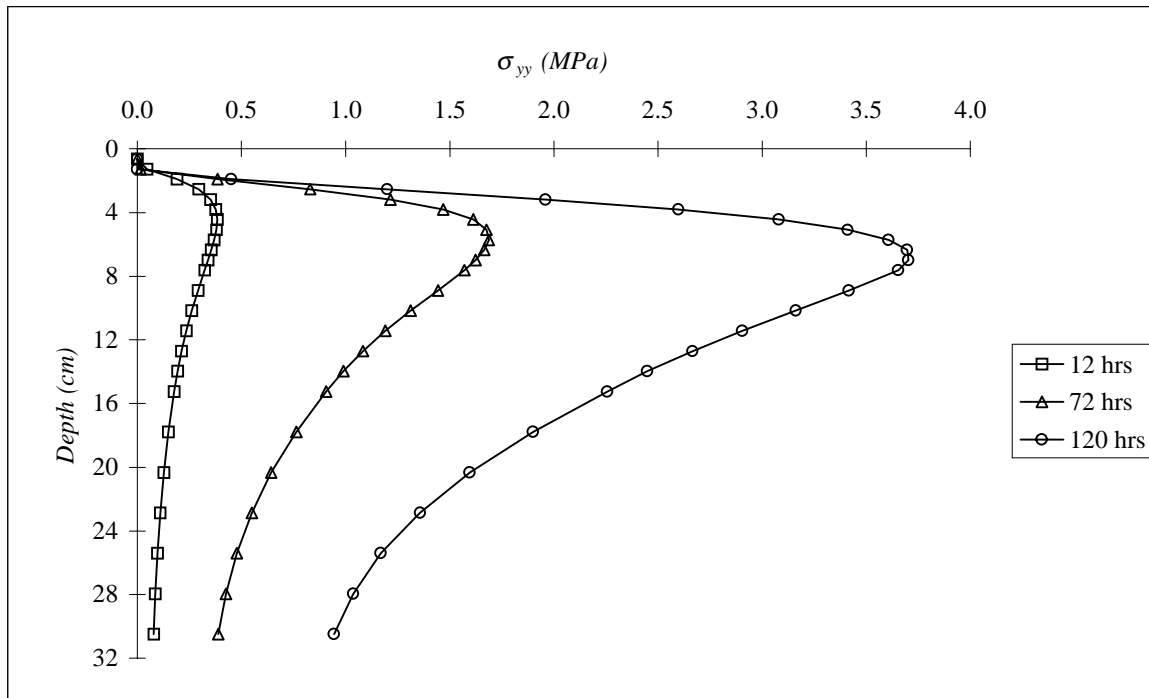


Figure E10(b) Variation of σ_{yy} and τ_{xy} , with slab depth

In summary, it is important to observe that high tensile and shear stresses develop owing to moisture loss (evaluated from the highly nonlinear distribution of relative humidity across the slab thickness). The zones of maximum tensile and shear stresses, as indicated in Figure E11, are precisely where delaminations in concrete pavements have typically been found in field surveys (Ref 24). This strongly suggests that minor flaws caused by mortar-aggregate interface debonding may grow into larger cracks owing to the presence of such high stresses. Given the *rh* profile in Figure E6(b), the results clearly indicate that special attention needs to be given to the stresses developed at early ages, since they may eventually lead to delamination formation and subsequent spalling. Although remedies for this situation are not discussed in this section, it is clear that moisture loss needs to be minimized in order to obtain a moisture profile that is not as drastically nonlinear as the one indicated in Figure E6(b). The analysis performed in this section can be performed with the program DELAM for any desired moisture profile (temperature profile may also be included) and concrete properties.

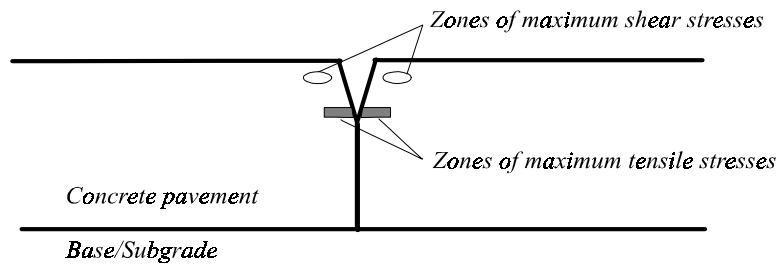


Figure E11 Zones of maximum tensile and shear stresses

DELAMINATION EXTENSION

The potential for delaminations to develop can be determined from the analysis performed in the previous section. However, it is of interest to investigate the direction in which a particular delamination grows once it is formed. For this analysis, three different delamination depths are investigated, namely, 1, 2, and 3 in. (25.4, 50.8, and 76.2 mm). For depths of 1 in. (25.4 mm) and 2 in. (50.8 mm), three initial delamination lengths (a_0) are assumed. For the deeper 3 in. (76.2 mm) delamination, only a 1 in. (25.4 mm) initial delamination is considered, since at this depth very short delaminations are encountered.

The fracture energy is determined for each case. As indicated in Figure E5, the direction of delamination extension (up, straight, or down) is selected as the one that has the largest fracture energy owing to a wheel load.

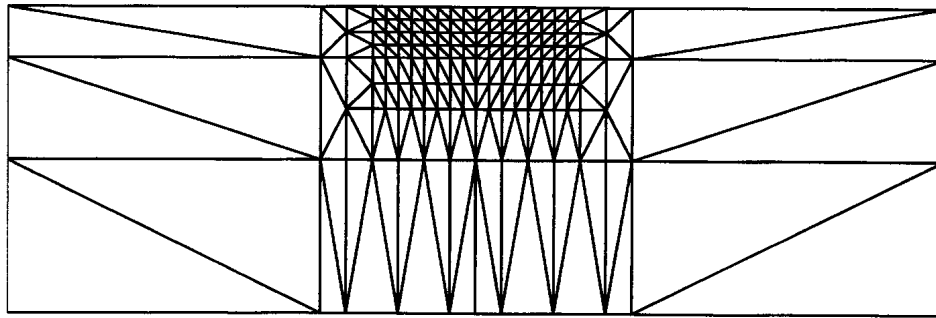
The mesh illustrated in Figure E12(a), which contains 175 nodes and 282 elements, is used in the numerical analysis performed. Note that a finer mesh is placed on the top surface close to the joint and along the delamination length. A penalty constraint method described by Cook (Ref 30) and implemented by Allen (Ref 29) is used to connect the elements at the joint in order to avoid interpenetration. Three constitutive relations are used for the different interface (cohesive zone) elements utilized in the analysis, as shown in Figure E12(b).

(1) At the joint, elements are connected by interface elements with a constant shear stiffness (vertical direction). These interface elements cannot take any tension since the joints should be able to separate freely. Recall that the interpenetration of the elements is avoided through penalty constraints.

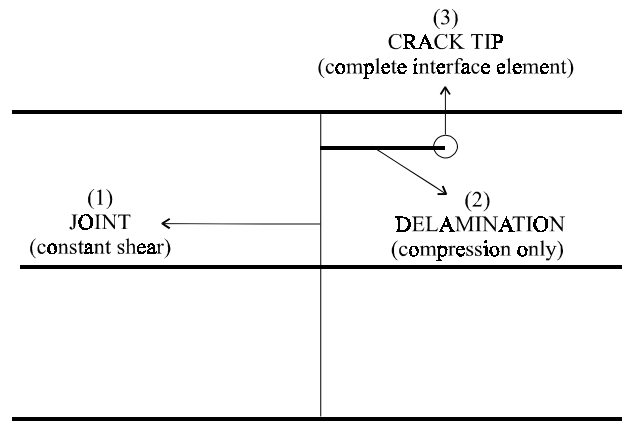
(2) At the delamination surfaces, interface elements with zero stiffness for opening displacements are used in such a way that the delamination is free to open. However, if the displacement is such that the delamination surfaces move toward each other, which is often the case owing to the compression caused by the wheel load, a high stiffness is added to avoid element interpenetration. No shear stiffness is considered for these elements.

(3) At the crack tip, an interface element is used (complete interface element). It has both normal and tangential stiffness function of coupled normal and tangential displacements. Depending on the direction assumed for delamination extension, this element is put on a certain inclination: 45° for a delamination growing upward, 0° for a delamination growing straight, and -45° for a delamination growing downward.

The values in Table E3 are assumed for the analysis. The load used corresponds to 100 psi (0.69 MPa) normal pressure and 25 psi (0.17 MPa) of horizontal pressure owing to friction forces, as indicated by Senadheera (Ref 24), Tielking and Roberts (Ref 32), and Tielking (Ref 33). The load spreads through a 8 in. (203.2 mm) length, as recommended by Huang (Ref 23). As indicated in Figures E13(a)–(c), the three wheel load positions considered are: (1) on the downstream side just before the transverse joint; (2) centralized on the transverse joint with half the load on the downstream and half on the upstream side; and (3) on the upstream side just after the transverse joint. Analysis has indicated that these three positions are the three worst scenarios. No other load position farther away from the transverse joint, either upstream or downstream, generates higher fracture energy than the load positions considered.



(a)



(b)

Figure E12(a)–(b) Mesh and constitutive relations used in the numerical analysis

Table E3 Input values for the analysis of delamination extension

Cohesive Zone		Cohesive Zone		Base/Subgrade	
f_t (MPa)	3.45	E_{concrete} (MPa)	32,750	E_{base} (MPa)	3,450
w_c (mm)	0.015	V_{concrete}	0.15	V_{base}	0.30
α	10				

1 MPa = 145 psi
1 mm = 0.04 inch

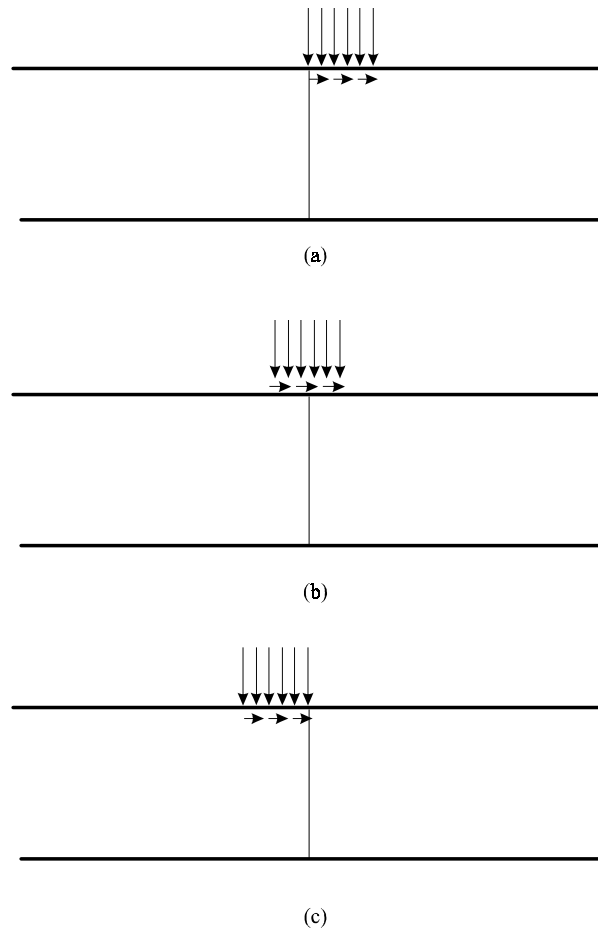


Figure E13(a)–(c) Three wheel load positions

In the discussion that follows, it is said that there is a “tendency” for the delamination to grow in the direction of highest fracture energy. The following is observed from the results:

(1) For 1 in. (25.4 mm) deep delaminations: The tendency of a 1 in. (25.4 mm) long delamination is to grow downward owing to the highest fracture energy at the downstream load position. The fracture energy is also high for a straight extension for a centered load position. A 3 in. (76.2 mm) long delamination tends to grow straight given the highest fracture energy at the centered load position. The tendency to grow downward is approximately the same as the tendency to grow upward for the centered and downstream load positions. Finally, for a 5 in. (127.0 mm) long delamination, the tendency of extension is either upward for a centered load position or straight for a downstream load position. It is interesting to observe that delaminations of different lengths have tendencies to grow in

different directions. Particularly interesting is the fact that the tendency changes from extending downward or straight for shorter delaminations to extending upward for longer delamination. This is in agreement with the observed tendency of delaminations to develop into spalls at approximately 5 to 6 in. (127.0 to 152.4 mm) from the joint (Ref 24).

(2) For 2 in. (50.8 mm) deep delaminations: The tendency of a 1 in. (25.4 mm) long delamination is to grow straight owing to the highest fracture energy at the upstream load position. The fracture energy is also high for a downward extension. A 3 in. (76.2 mm) long delamination tends to grow down or straight given the high fracture energy at the centered and upstream load positions, respectively. The tendency to grow upwards is smaller for these first two delamination lengths. Finally, for a 5 in. (127.0 mm) long delamination, the tendency of extension is to grow straight for a centered load position. It is noted that there is a great increase in the fracture energy for a straight extension owing to the increase in delamination length.

(3) For 3 in. (76.2 mm) deep delaminations: The tendency of the 1 in. (25.4 mm) long delamination analyzed is to grow straight owing to the highest fracture energy at the upstream load position. However, high fracture energy is also found for the other two directions of extension at the same load position.

The results of the discussion above are summarized in Table E4.

The fact that high fracture energies were found when considering downward extension (that is not observed in the field) for shorter delamination lengths indicate that delaminations may grow to be greater than 5 in. (127 mm) even before traffic starts.

For the two deeper delaminations, the results indicating that the delaminations have a tendency to grow straight are in agreement with field observations that show that deeper delaminations oftentimes do not develop into spalls, despite the fact that they are formed. As previously mentioned, other factors besides the wheel load may determine the direction of extension of delaminations at different depths. Even concrete characteristics may be different at the different depths where delaminations are typically found. As mentioned before, bleeding may cause the top portion of a concrete slab to have lower strength. Nevertheless, the analysis performed indicates that the wheel load alone may determine the direction of delamination extension, since the results are in agreement with field survey observations. The importance of the results lies in the fact that if delaminations cannot be avoided, engineers should at least try to keep them from developing too close to the pavement surface. Further discussion on this matter is addressed in a section devoted to remedies for spalling development.

Table E4 Summary of delamination extension direction

Depth (mm)	Length (mm)		
	25.4	25.4	50.8
25.4	Downward	Straight	Straight or Up
50.8	Straight	Down or Straight	Straight
76.2	Straight	-	-

1 mm = 0.04 inch

SPALLING DEVELOPMENT CAUSED BY FATIGUE

The final part of the analysis considers the delamination extension to a critical value (a_f) associated with spall development. This critical value is taken as 5.5 in. (139.7 mm), since the majority of spalls observed in the field are within 5 to 6 in. (127.0 to 152.4 mm) of the transverse crack (Ref 24). As previously mentioned, the ratio of the delamination length to the critical value (a/a_f) is assumed directly proportional to the ratio of the fracture energy owing to a wheel load repetition to the critical fracture energy (G/G_F). The delamination length (a) varies with the number of wheel load repetitions.

For the numerical analysis, the same mesh and interface elements considered in the previous section and illustrated in Figures E12(a)–(b) are used. The difference in the fatigue analysis is that the interface elements at the delamination are inactive only when the delamination surfaces are moving toward each other. This is the case only for the portion considered as initial delamination (a_0), as indicated in Figure E14. The remaining portion up to the critical value a_f , i.e., the cohesive zone, contains complete interface elements with both normal and shear stiffness; it is therefore able to resist opening and shear displacements.

The properties in Table E5 and the same load values (0.69 MPa for normal pressure and 0.17 MPa for horizontal pressure) are assumed for the fatigue analysis. The downstream load position is considered since it is believed to be the one causing the most damage to the downstream delamination. The same three depths are analyzed. Table E5 indicates the three initial delamination lengths (a_0) for each depth. Note that longer initial delaminations are assumed for delaminations closer to the pavement surface, as has been observed in field surveys.

The maximum number of load repetitions for which a/a_f is 100% is assumed to be 1 million ESALs (equivalent single axle loads), i.e., $x_I = 1 \times 10^6$ as shown in Figure E5(c). This is for a 2.5 in. (63.5 mm) initial delamination length at a depth of 1 in. (25.4 mm) that is considered the condition having greater potential for spall development. The a/a_f values for all other situations are determined considering this worst-case scenario as a reference.

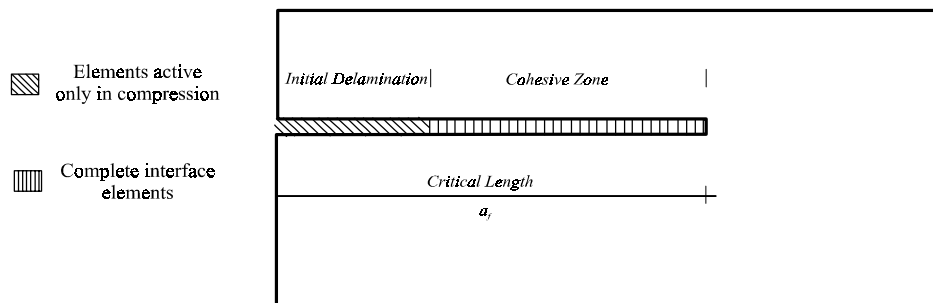


Figure E14 Initial delamination

The results of the analysis are presented in Figures E15(a)–(c) for the three different depths. The plots show the variation of a/a_f with the number of load repetitions ($x \leq x_I$) for different initial delamination lengths, i.e., $f_i(x)$. Longer initial delaminations, i.e., higher $f_i(0)$, have higher $f_i(x)$ for each x . A quadratic polynomial is fitted through regression on the numerical results, and they are included in the plots for each different depth and initial delamination length. For depths of 1 and 2 in. (25.4 and 50.8 mm), note that the rate at which a/a_f increases with the number of load repetitions increases for longer initial delamination lengths. This is indicated by the coefficients of the regression equations for these two delamination depths. For the 3 in. (76.2 mm) deep delamination, this rate is the same for the three initial delamination lengths assumed. It should be noted that not only the delamination depth affects this rate, but also the fact that smaller delamination lengths are considered for the larger depths.

Table E5 Initial delamination lengths for the three depths analyzed

Initial Delamination Length (mm)		
At depth = 25.4 mm	At depth = 50.8 mm	At depth = 76.2 mm
0.0	0.0	0.0
38.1	19.1	6.4
63.5	38.1	19.1

1 mm = 0.04 inch

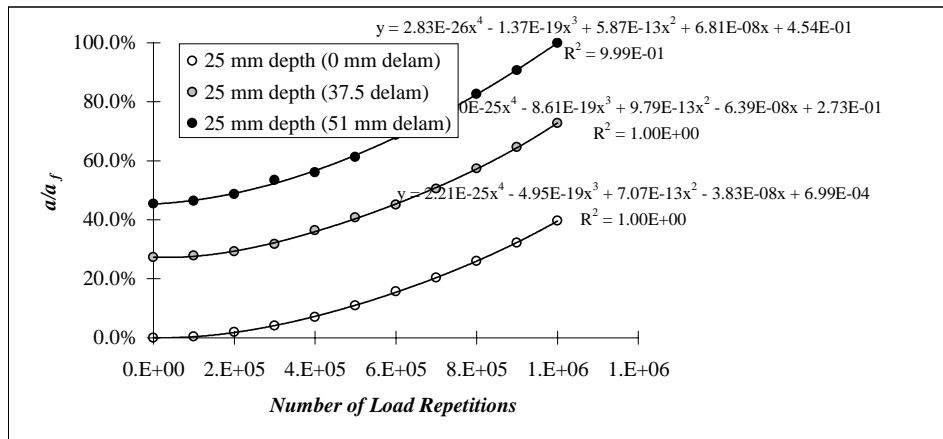


Figure E15(a) Variation of a/a_f with the number of load repetitions ($x \leq x_1$) for different initial delamination lengths

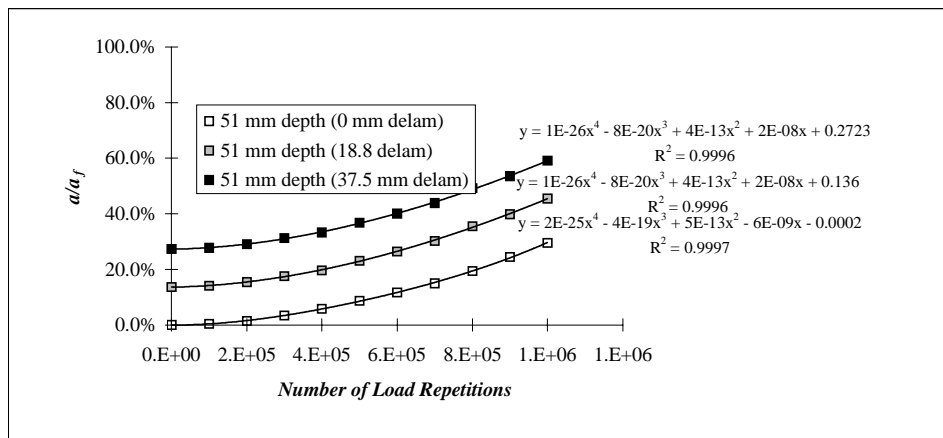


Figure E15(b) Variation of a/a_f with the number of load repetitions ($x \leq x_1$) for different initial delamination lengths

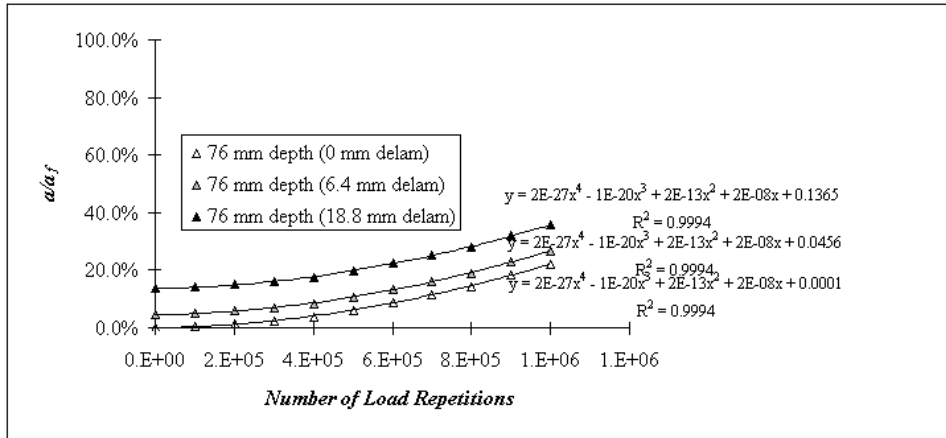


Figure E15(c) Variation of a/a_f with the number of load repetitions ($x \leq x_1$) for different initial delamination lengths

In order to translate the information on Figures E15 (a)–(c) in such a way that it can be used in a concrete pavement design procedure, the spalling model discussed earlier in this chapter is used. Recall that the function $f_i(x)$ represents the growth of a/a_f and the function $g_i(x)$ represents the growth of the percentage of spalled sections with the same number of load repetitions x . Both functions vary with initial delamination length (indicated by the subscript i) and also with delamination depth.

To obtain function $g_i(x)$ for $0 \leq x \leq N_f$ (N_f being the number of loads to failure) at each delamination depth, the following procedure can be used:

(1) Fixed inputs:

- x_1 : number of load repetitions at which the delamination a grows to its critical value a_f , i.e., $a/a_f = 100\%$. Since this number varies for different initial delamination lengths $f_i(0)$, x_1 , is assumed to be 1 million ESALs, corresponding to the worst-case scenario;
- $g_i(x = 0) = 0$, which means that the percentage of spalled sections for zero load repetitions (ESALs) is zero;
- $f_i(x)$: the explicit functions obtained from regression analysis of the numerical results. They give a/a_f according to the number load repetitions. This is obtained from Figures E16(a)–(c) for different initial delamination lengths. Both $f_i(x_1)$ and $f_i(0)$ are also obtained from Figures E15(a)–(c).

(2) Inputs from field performance data:

- x_j and $g_i(x_j)$: number of load repetitions (x_j) for which the percentage of spalled sections $g_i(x_j)$ is known. Field performance data in Texas (Ref 31) indicate that Highway 6 in Bryan, where river gravel was used as the coarse aggregate, demonstrated 69% spalled sections after 3.0 million ESALs; and Beltway 8 West in Houston, also constructed with river gravel as the coarse aggregate, demonstrated 75% spalled sections after 3.65 million ESALs. This information is assumed to be for a 1 in. (25.4 mm) deep delamination.

(3) Procedure:

- From the fixed inputs based on the numerical determination of $f_i(x)$, $g_i(x)$ for $x \leq x_1$, can be obtained for different initial delaminations and different delamination depths. Figures E16(a)–(c) show these results.

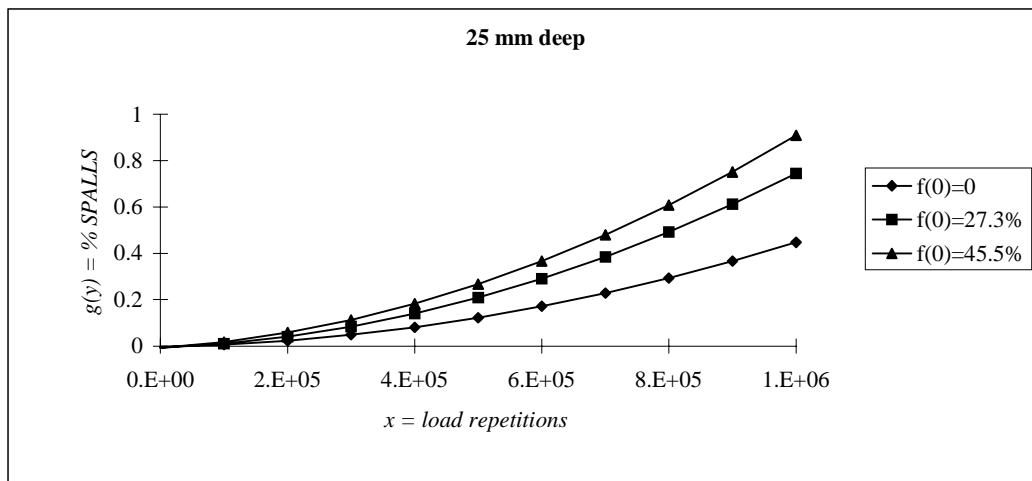


Figure E16(a) Results from the fixed inputs based on the numerical determination $f_i(x)$, $g_i(x)$ for $x \leq x_1$ for different initial delaminations and different delamination depths

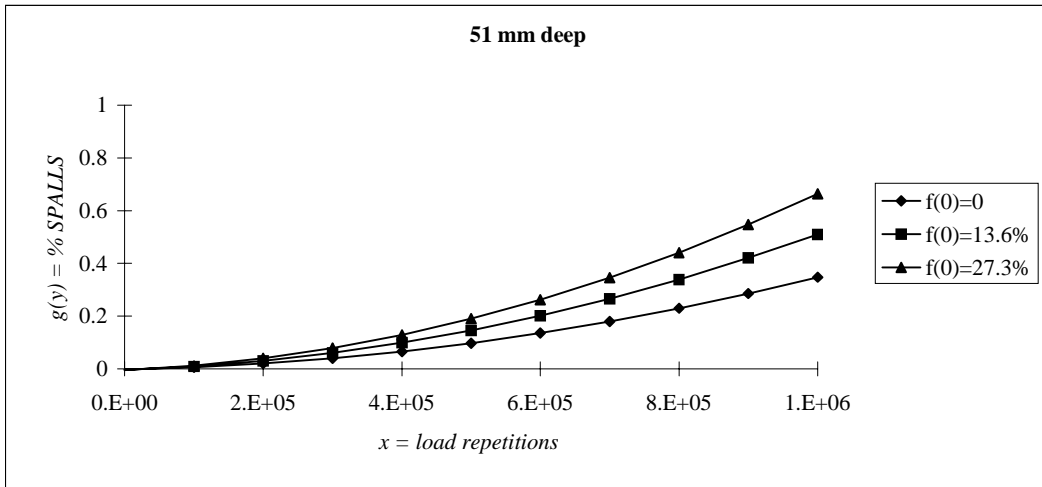


Figure E16(b) Results from the fixed inputs based on the numerical determination $f_i(x)$, $g_i(x)$ for $x \leq x_1$ for different initial delaminations and different delamination depths

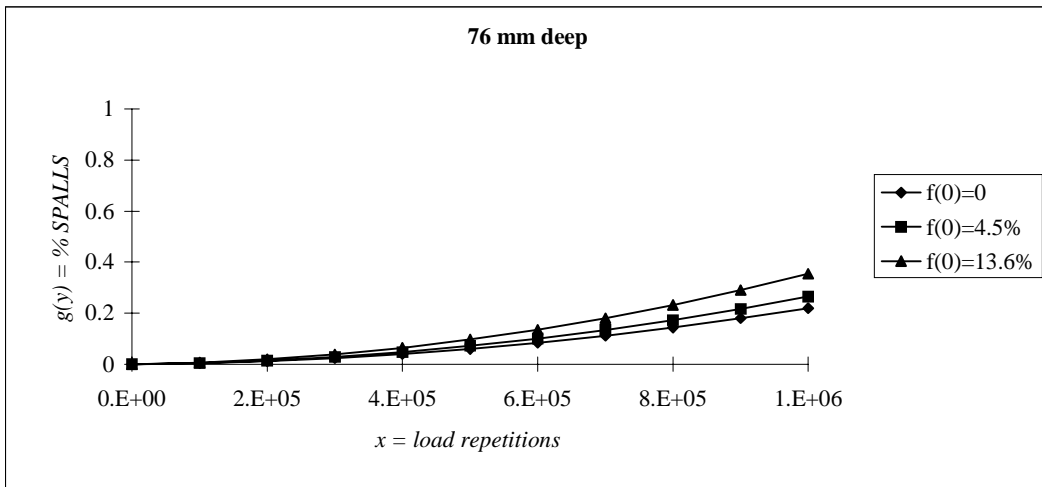


Figure E16(c) Results from the fixed inputs based on the numerical determination $f_i(x)$, $g_i(x)$ for $x \leq x_1$ for different initial delaminations and different delamination depths

Note that larger initial delaminations develop faster into spans than smaller or zero initial delaminations. Also, shallower delaminations develop faster into spans than deeper delaminations. The following is suggested based on the results for $g_i(x \leq x_1)$: (1) Although initial delamination lengths were found to have an effect on the percentage of spalled sections, an average curve may be used. This

recommendation is based on the fact that delamination length measurements have great variability and it is difficult to represent a set of pavement sections by a single delamination length value. Therefore, a single curve (the one for an intermediate initial delamination length) for each plot at Figure E16 will be assumed. (2) Delamination depth was found to be a more important factor than initial delamination length; accordingly, it should be considered when collecting field performance data related to the spalling distress. Also, delamination depth is believed to be more consistent for a given set of pavement sections.

- Based on $g_i(x)$ for $x \leq x_l$, and the two field performance data points ($x \geq x_l$) for a 1 in. (25.4 mm) deep and 1 in. (25.4 mm) long delamination, a complete $g_i(x)$ function can be plotted as show in Figure E17(a). The a , b , c regression coefficients in (14) can be obtained. For the case analyzed the coefficients are: $a = 0.832$, $b = 1.262$, and $c = -1.395$. The curve fits the combined numerical and performance data points with an R^2 of 0.99. From Figure E17(a) it is seen that the $g_i(x)$ function found tends to 80% spalled sections corresponding to a number of load repetitions of 8.5 million ESALs. This is assumed to be the number of loads to failure (N_f).
- With N_f found, the percentage of spalled sections, $g_i(x)$, with damage ratio typically used in design practice, can be obtained. The damage ratio was previously defined as $D_r = N/N_f = \text{number of load repetitions/number of loads to failure}$ as shown in Figure E17(b). This curve has the same form as that shown in Figure E17(a).

The spalling model proposed is calibrated with two performance data points at 3.0 and 3.65 million ESALs for a particular location. As more data become available, the model should be further refined and checked for accuracy. Only through data collection can appropriate relations and factors in the model be found.

REMEDIES FOR THE SPALLING PROBLEM

Preventive approaches to the spalling distress can be related (1) to delamination formation and (2) to spalling development. The first tries to prevent the initial problem of delamination in order to avoid the major problem of spalling. As previously mentioned, spalling development has been observed only where delaminations have been found. The second approach considers that delaminations do occur and, therefore, measures should be taken to prevent those delaminations from developing into spans.

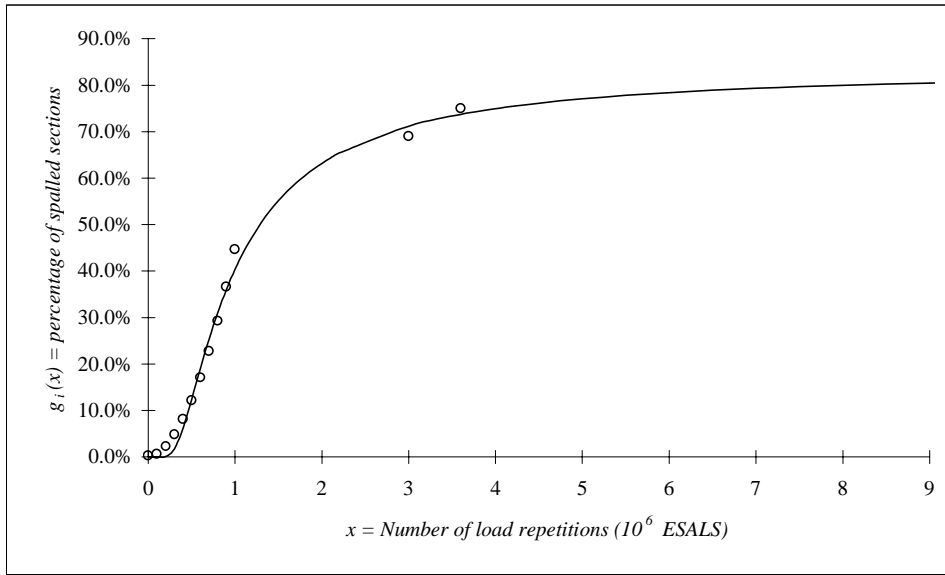


Figure E17(a) Percentage of spalled sections

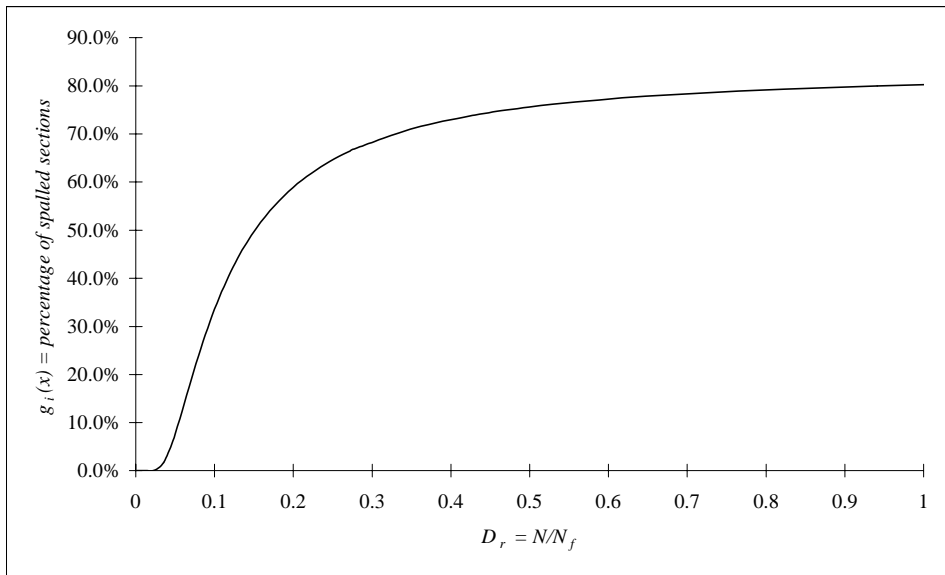


Figure E17(b) Percentage of spalled sections

DELAMINATION FORMATION

- (1) It was shown that delamination may start from mortar-aggregate interface debonding prior to traffic.
- (2) When debonding occurs, it was shown that it is likely to grow owing to large stresses that develop close to the pavement surface caused by both temperature and moisture variation. To avoid drastic nonlinear moisture profiles, more effective curing methods should be used. Special attention should be given to the zones of very high ambient temperatures or low air relative humidity, since they increase the susceptibility of great moisture loss through the pavement surface. As for temperature fluctuations, in the zones where large temperature drops occur, coarse aggregates with lower coefficient of thermal expansion should be preferred.

DELAMINATION DEVELOPING INTO SPALLING

In the event that delaminations are formed, as previously mentioned, an effort should be made to lower the acting point of the resultant forces transmitted through the transverse joint. Creating an artificial groove on the pavement surface can change the pressure distribution. The groove can be filled with low-modulus sealant such that most of the compression will be transmitted by the concrete beneath the sealant, as shown in Figure E18. If the force acting point is sufficiently lowered, the stress intensity factors K_I and K_{II} may attenuate. Consequently, the delamination extension angle becomes negative, which means that the delamination will have a tendency to propagate downwards, thus avoiding spall development.

CONCLUSION

A mechanistic model for spalling was proposed in this appendix. The model consists of delamination formation and extension with subsequent spall development. A finite element program was developed to analyze the stresses that develop in concrete pavements owing to nonlinear distribution of moisture and temperature. The two effects were combined by transforming the shrinkage strains to an equivalent thermal strain caused by a temperature variation. This equivalent temperature variation was added to the actual temperature variation and the summation is assumed to be responsible for the combined effect of both thermal and shrinkage strains. Preventive actions to avoid the development of high stresses were

discussed. When delaminations occur, a model was presented to determine the percentage of spalled sections with number of load repetitions. Percentage of spalled sections was assumed to be proportional to the delamination growth to a critical value. The critical delamination value is associated with observed spall distances from the pavement transverse crack. It was also shown how the model can be calibrated with field performance data to obtain the complete curve of the percentage of spalled sections with number of load repetitions.

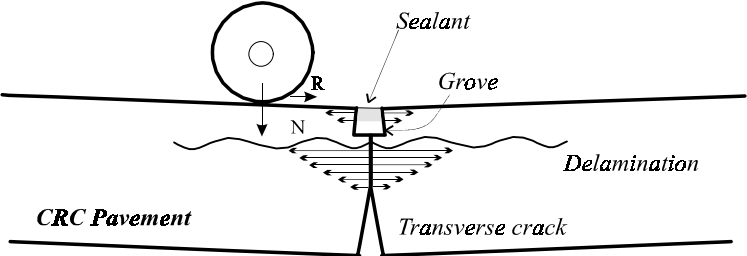


Figure E18 Artificial groove used to change pressure distribution